

Development of the Impact Attenuation Standard for Public Order Helmets

DAWBER, William

Available from the Sheffield Hallam University Research Archive (SHURA) at:

https://shura.shu.ac.uk/36293/

A Sheffield Hallam University thesis

This thesis is protected by copyright which belongs to the author.

The content must not be changed in any way or sold commercially in any format or medium without the formal permission of the author.

When referring to this work, full bibliographic details including the author, title, awarding institution and date of the thesis must be given.

Please visit https://shura.shu.ac.uk/36293/ and http://shura.shu.ac.uk/information.html for further details about copyright and re-use permissions.

Development of the Impact Atte	enuation Standard for Public Order Helmets
V	Villiam Dawber

A thesis submitted in partial fulfilment of the requirements of Sheffield Hallam University

For the degree of Doctor of Philosophy

Candidate Declaration

I hereby declare that:

- I have not been enrolled for another award of the University, or other academic or professional organisation, whilst undertaking my research degree.
- 2. None of the material contained in the thesis has been used in any other submission for an academic award.
- 3. I certify that this thesis is my own work. The use of all published or other sources of material consulted have been properly and fully acknowledged.
- 4. The work undertaken towards the thesis has been conducted in accordance with the SHU Principles of Integrity in Research and the SHU Research Ethics Policy, and ethics approval has been granted for all research studies in the thesis.
- 5. The word count of the thesis is 56,816.

Name William Dawber

Award PhD

Date of Submission January 2025

Research Institute Health Research Institute

Director(s) of Studies Dr John Hart

Abstract

Public Order (PO) events, such as riots, expose officers to significant head injury risk. Helmets in the UK conform to the Home Office standard 'PSDB 21/04', although head injuries remain common, and helmet designs have seen little innovation since the 1970s. This research aimed to improve situational and injury representation in helmet testing standards to better scrutinise helmet efficacy.

There is little knowledge of the specific causes of head injury in PO conditions. Analysis of footage identified prevalent threats associated with, projectile bricks and stones (37% of weapon events), flat-faced wooden beams (24.5%), and circular metallic poles (16.3%). Falls from height, particularly involving mounted officers, were also a significant risk. Representative experiments quantified the mechanics of these scenarios, showing peak linear accelerations of 126–771 g, angular accelerations of 1.3–24.5 krad/s², and pulse durations under 5 ms. A test system was developed to recreate these with more repeatable methodology, such as is required in standard procedure.

Testing revealed that a cradled headform without a neckform, as per current standard procedure, most accurately replicated realistic dynamics. Flat anvils, which are not a current requirement of the standard, produced significantly higher peak kinematics compared to curved surfaces (P = 0.03). These also exceeded the 250 g failure threshold at lower impact energies (-48 J). In addition, angular velocity-based metrics, such as BrIC, predicted lower injury severity compared to angular acceleration-based metrics.

Key recommendations for adaptations to the standard include that although the current 120 J energy drop test is representative of severe loading mechanics in PO activity, incorporation of flat anvils and angular-based failure thresholds would better scrutinise headgear efficacy. Suggested thresholds are 250 g for linear acceleration and 6 krad/s² for angular acceleration, however further validation is needed to finalise these. This work provides a foundation for improved helmet efficacy in PO activity and therefore long-term potential for a reduction in sustained neurotraumatic injuries.

Acknowledgements

I would like to express my deepest thanks to my supervisors, Dr. John Hart, Dr. Leon Foster, and Mr. Terry Senior, for their invaluable guidance throughout this project. I have learned much from your expertise, and your insights were crucial at every stage of this work. My acknowledgments also go to Dr. Tom Allen and Professor Andrew Alderson, who have been incredible mentors throughout my academic journey. Your advice and belief were key to shaping my aspirations and led to me pursuing a career in research.

A special thanks is owed to the Sports Engineering Internship students who supported the data collection in this project. In particular, I am grateful to Loni Nickel, Chris Nealon, and Mario Contarino for their dedication, contributions, and positivity.

To my amazing family, I cannot thank you enough. To my mother, father, and Auntie Deb, your unwavering encouragement and support gave me confidence to pursue my passions and a career that I truly enjoy. Your love and support have shaped who I am today and who I hope to become.

Finally, to Anna, who has lived every day of this project with me. Thank you for your endless love, encouragement, and patience. Your ability to calm the moments of stress and bring perspective to the challenges has been invaluable. I look forward to our wedding and all the adventures that follow.

Personal Bibliography

Conference Proceedings

Dawber, W., Foster, L., Senior, T., & Hart, J. Traumatic Brain Injury Predictions Amid Equestrian Activity with Realistic Biomechanical Constraints. *IRCOBI Conference Proceedings* (pp. 637-638), 2023.

Dawber, W., Foster, L., Senior, T., Hart, J. Design Development of a Repeatable
Helmet Test System for Public Order Threat Recreations. In: Design Tools and
Methods in Industrial Engineering III. Special session on design for Sports
Engineering at ADM 2023 International Conference, Florence. Lecture Notes in
Mechanical Engineering. Springer, 2024. https://doi.org/10.1007/978-3-031-58094-9 20

Dawber, W., Foster, L., Senior, T., Hart, J. Sports Engineering Practices Applied to Public Brain Injury Prevention. ISEA 2024: The Engineering of Sport 15, Conference Proceedings. Loughborough University, 2024.

Contents

1	. Introduction	1
	1.1 Motivation for Research	1
	1.2 Aims and Objectives	3
	1.3 Thesis Structure	3
2	Literature Review	5
	2.1 Introduction	5
	2.2 Head Trauma in Public Order Activity	6
	2.2.1 Injury Prevalence and Causes	6
	2.2.2 Head Injury Pathologies	6
	2.2.3 Section Summary	9
	2.3 Quantifying Head Impacts	10
	2.3.1 Fundamentals of Head Impact Mechanics	10
	2.3.2 Linear Kinematics	12
	2.3.3 Angular Kinematics	13
	2.3.4 Finite Element Methods	15
	2.3.5 Injury Criteria	16
	2.3.6 Section Summary	19
	2.4 Head and Helmet Impact Testing	19
	2.4.1 Test Setup and Systems	19
	2.4.2 Bio-realism	22
	2.4.3 Public Order Helmet Testing	23
	2.4.4 Impact Monitoring and Instrumentation	27
	2.4.5 Section Summary	29
	2.5 Helmet Design	29
	2.5.1 Helmet Energy Attenuation Mechanics	29
	2.5.2 Helmet Design	30
	2.5.3 Public Order Helmets	31
	2.5.4 Section Summary	33
	2.6 Chapter Summary	34
3	. Causes of Head Injury in Public Order Conditions	35
	3.1 Introduction	35
	3.1.1 Head Impact Monitoring	35
	3.2 Method	37
	3.2.1 Data Acquisition	37
	3.2.2 Data Analysis	38

	3.3 Results	40
	3.4 Discussion	43
	3.5 Chapter Conclusion	46
4.	. Injury due to Wielded Blunt Implements	47
	4.1 Introduction	47
	4.1.1 Methods for Recreating PO Conditions	48
	4.1.2 Injury Risk for Wielded Blunt Weapons	50
	4.2 Method	51
	4.2.1 Experimental Arrangement	51
	4.2.2 Swung Implements	52
	4.2.3 Tracking of Swung Implements	54
	4.2.4 Kinematic Measurement & Analysis	55
	4.3 Results	57
	4.4 Discussion	68
	4.5 Chapter Conclusion	71
5.	. Injury due to Falling from Horseback	72
	5.1 Introduction	72
	5.2 Method	75
	5.2.1 Experimental Arrangement	75
	5.2.2 Kinematic Measurement & Data Capture	76
	5.3 Results	. 77
	5.4 Discussion	81
	5.4.1 Head impact location	. 82
	5.4.2 Head impact velocity	. 83
	5.5 Chapter Conclusion	85
6.	. Development of a Helmet Impact Test System	87
	6.1 Introduction	87
	6.1.1 Rationale	87
	6.1.2 Objectives	88
	6.2 Background	. 89
	6.2.1 Impact Methods	89
	6.2.2 Head Impact Constraints	89
	6.3 Design Definition and Methodology	91
	6.3.1 System Requirements	91
	6.3.2 Key Design Features	93
	6.4 Final Design	97
	6.4.1 Summary	97

	6.4.2 Optimising Bearing Separation	98
	6.4.3 Refining Drop Plate Mass	.100
	6.4 Implementation	.102
	6.4.1 Installation Compromises	.102
	6.4.2 Added Features	.103
	6.4.3 Operating Procedure	.104
	6.4.4 Cost	.105
	6.4.5 Implementation Challenges	.105
	6.5 Discussion	.107
	6.5.1 Design Review	.107
	6.5.2 Further Improvements	.108
	6.7 Chapter Conclusion	.109
7	. Injury due to Projectile Bricks	.110
	7.1 Introduction	.110
	7.2 Quantifying Thrown Brick Mechanics	.111
	7.2.1 Brick Characteristics	.111
	7.2.2 Throw Mechanics	.112
	7.3 Head Impact Recreation Methodology	.114
	7.3.1 Experimental Arrangement	.114
	7.3.2 Head Impact Assessment	.116
	7.4 Results	.118
	7.4.1 Peak Headform Kinematics	.118
	7.4.2 Predicting Larger Impact Velocities	.122
	7.5 Discussion	.127
	7.5.1 Impact Location Effects	.127
	7.5.2 Impact Velocity Effects	.128
	7.5.3 Indicators for Injury Predicting	.129
	7.5.4 Method and Limitations	.130
	7.6 Chapter Conclusion	.131
8	. Recreating Public Order Impacts with a Drop Rig	.133
	8.1 Introduction	.133
	8.2 Comparison of Head Injury Mechanics Across Dangerous PO Conditions	.133
	8.2.1 Quantification of Typical Head Impact Mechanics	.133
	8.2.2 Assessing the Representativity of Drop Rig Setups	.138
	8.2.3 Determining Drop Rig Setup Parameters for Recreating PO Conditions	
	8.3 Method	.141

		8.3.1 Experimental Arrangement	141
		8.3.2 Data Capture	144
		8.3.3 Data Analysis	145
	8.	.4 Results	146
		8.4.1 Drop Rig Setup Repeatability	146
		8.4.2 Drop Rig Peaks Compared to Representative PO Limits	146
		8.4.3 Comparing Between Drop Rig and Situationally Representative	
		Conditions	
		8.4.4 Differences Between Cradling the Headform and Affixing a Neckform	
	8.	5 Discussion	
		8.5.1 Comparison to Representative Kinematics	
		8.5.2 Comparison of Acceleration-Time Histories	154
		8.5.3 The Influence of a Neckform on Head Impact Biomechanics	156
		8.5.3 Drop Rig Setup Recommendations from Current Understandings	
	8.	.6 Chapter Conclusion	159
9.	. P	O Helmet Impact Attenuation Performance	161
	9.	1 Introduction	
		9.1.1 PO Helmet Design Features	161
		9.1.2 Helmet Impact Attenuation Mechanics	162
	9.	2 Method	163
		9.2.1 Experimental Arrangement	163
		9.2.2 Head Impact Analysis	165
	9.	3 Results	168
		9.3.1 Peak Headform Kinematic when Helmeted	168
		9.3.2 Energy Attenuation Performance	169
		9.3.3 Helmet Wear and Damage	170
	9.	.4 Discussion	172
		9.4.1 Effects of Drop Rig Setup on Helmet Performance	172
		9.4.2 Helmet Wear and Damage	173
		9.4.3 Limitations and Further Work	174
	9.	.5 Chapter Conclusion	175
1	0.	Injury Metrics for PO Helmet Testing	177
	10	0.1 Introduction	177
		10.1.1 Injury Thresholds	178
	10	0.2 Method	183
		10.2.1 Impact Data	183
		10.2.2 Data Processing	184

10.4.3 Statistical Analysis	185
10.3 Results	185
10.3.1 Severity Predictions	185
10.3.2 Impact Location Effects	187
10.4 Discussion	188
10.4.1 Ranking Injury Metrics	188
10.4.2 Thresholds Values	189
10.4.3 Limitations	190
10.5 Chapter Conclusion	192
11. Discussion	193
11.1 Introduction	193
11.2 Review of Research Objectives	194
11.2.1 Identification of Injurious Events	194
11.2.2 Quantification of Head Impact Loading Conditions	196
11.2.3 Recreation of Impacts with Repeatable Methodology	199
11.2.4 Recommendations for a Revised Public Order Helmet Test	Standard 202
11.3 Contribution to Knowledge	204
11.3.1 Understanding PO Injury Risk	204
11.3.2 Advising Helmet Test Methodology	205
11.3.3 Implications for Other Head Impact Applications	206
11.3.4 Enabling Computational Research Methods	206
11.4 Limitations	207
11.4.1 Injury Prediction	207
11.4.2 Drop Test Conditions	208
11.5 Future Research	209
11.6 Project Conclusion	211
References	212
Appendix	251

List of Tables

Table 2.1, The Abbreviated Injury Score (AIS) range from 1-5 for non-fatal brain
injuries [62] 8
Table 2.2, Popular kinematic Injury Criteria (IC). $t = time$, $t_0 = initial time$, $a = linear$
acceleration, α = angular acceleration, ω = angular velocity, β = IC specific
constants, δ = brain displacement calculated from viscoelastic mechanics.
Subscripts: x, y, z = headform axes, $i = each$ subsequent of x, y, z, $c = critical$
constants. Superscripts: n, m, s = 2, \star = normalised by a critical value [72],
[141], [149], [150]
Table 2.3, Review of systems for laboratory head impact testing with descriptions
of their key features and advantages/disadvantages [190]
Table 3.1, Search engine phrases to source video data of violent riot conditions
from the public domain 38
Table 3.2, Occurrences of events that can be linked to head injury likelihood from
footage of riot conditions
Table 3.3, Prevalent objects used as weaponry in public order conditions with
description of their common characteristics
Table 4.1, Characteristic properties of implements for the study of wielded blunt
weapon head impact conditions [349]53
Table 4.2, Mean (± one standard deviation) angles for wooden and metallic
implements at the point of impact, taken relative to the longitudinal axis of
the headform 59
Table 6.1, Decisions and rationale for key components of the guided drop system,
made to advise design ideations
Table 6.2, Density and elastic moduli of materials used in the simulation and the
components they were applied to [190]102
Table 7.1, Dimensional and mass properties of clay bricks used in the preliminary
study to quantify achievable throw velocities113
Table 7.2, Mean throw velocities (± one standard deviation) at the moment of
release for 2.5 and 3.5 kg clay bricks113
Table 7.3, Regression parameters between headform data and impact velocity at

each head impact location. A and B denote coefficients for a power law
relationship, Equation 7.2. Predicted values for 8.7 and 10.6 m/s represent
expected measures at human throw-like impact energies 122
Table 8.1, Range of expected magnitudes for PLA, PAA, and pulse durations in PO
conditions. These are equal to the greatest/lowest mean ±one standard
deviation, shown in Figure 8.1134
Table 8.2, Injury severity hierarchy (most to least) of each PO condition relative to
linear and angular tolerance curves [109], [120]. Difference refers to the
vertical distance from each respective tolerance13
Table 8.3, Setup conditions for recreating experimented PO conditions with a
guided drop rig. Impact angles are relative to the longitudinal axis of the
headform. Each condition was repeated five times142
Table 8.4, Power law coefficients for change in peak headform kinematics with
respect to impact velocity for oblique (back, front, and side) and radial
(crown) experimented conditions. PLA has a lower error relationship with
the radial load, although both are low, whereas PAA has high error with
radial conditions14
Table 8.5, Impact velocity ranges to represent PLA of injurious PO conditions with
radial and oblique loading setups. Values are specific to the neckform
affixed system in this study159
Table 10.1, Brain injury metrics and their corresponding 80 % likelihoods of AIS 2+
and 4+ injury thresholds179
Table 10.2, Summary of mean (standard deviation) injury metric scores for 5 m/s
flat surfaced impacts with a PO helmeted headform. Means include impact
locations across the back, crown, front, and side of the headform, hence
relatively large standard deviations
Table 11.1, Current energy attenuation test criteria in PSDB 21/04 and the
recommended conditions for improving Public Order injury representation.
200

List of Figures
Figure 1.1, Examples of helmets worn by UK officers during Public Order activity:
the 'Defender' (left) [1] and 'Defender Hybrid' (right) [2]
Figure 2.1, A proposed research cycle for reducing the burden of TBI in society by
addressing the specific situational needs of the application [30] 5
Figure 2.2, A simplified summary of blunt trauma induced head injuries and their
respective categories, taken from Zheng et al., 2022 [46]. Open/closed refer
to whether penetration of the skull occurs
Figure 2.3, Radial (A) and oblique (B) force vectors as a result of blunt trauma head
impact [70]. Radial refers to a vector in-line with the centre of mass
whereas oblique incur both linear and angular motion
Figure 2.4, Representative groupings for head injurious events in literature, based
on peak magnitudes of linear and angular acceleration as well as their
duration [109]
Figure 2.5, Wayne State Tolerance Curve (WSTC) depicting the brains time-
dependent tolerance to linear acceleration, where a measure above the line
is considered a danger to life [120]
Figure 2.6, Threshold curve depicting the brains time-dependent tolerance to
angular acceleration where above the line is considered the occurrence of
mTBI [109]
Figure 2.7, Examples of pendulum and pneumatic ram systems for laboratory head
impact recreations [188]
Figure 2.8, Common 50 th percentile male headforms used in head impact research
and helmet standards. A) NOCSAE, B) EN 960, C) Hybrid III [198], [199],
[200], [201]
Figure 2.9, Schematic of the PSDB 21/04 standard procedure for assessing helmet
energy attenuation [13] 24
Figure 2.10, Impact anvils used in the PSDB 21/04 standard representing the
corner of a brick and a curved hand wielded weapon [13]
Figure 2.11, Headform polarity according to the recommended practice for
instrumentation of headforms (SAE J211) [28], [244]27
Figure 2.12, Compressive loading of cellular foams demonstrating strain energy
absorption per unit volume (W) [274]

Figure 2.13, 'Defender Hybrid' PO helmet (MLA Ltd) imaged from the exterior and
interior to highlight key features [2], [294]
Figure 3.1, Snapshot of a Public Order training session at the Metropolitan Police
Specialist Training Centre, taken May 2022. Here, officers can be seen
helmeted and armed with shields and batons. Officers in the foreground are
armed with projectile flammables and wooden bricks to simulate 'rioters'.
Figure 3.2, Screenshots from videos in the content analysis of riot scenarios.
Highlighted are example weapons that were identified as likely to cause
severe blunt trauma head injury [311], [312]
Figure 3.3, Categorised occurrences of prevalent blunt objects used in PO that are
a danger of causing head injuries. Numbers are the accumulative
occurrences taken from five hours of riot footage 41
Figure 4.1, Example of rioters wielding blunt weaponry, taken from video footage of
riots on Youtube.com [311]48
Figure 4.2, Hybrid III ATD setup for measuring head impacts due to swung
weaponry. In this scenario, implements were swung along a vertical plane
by a participant, the ATD was rotated around the longitudinal axis to vary
head impact location 52
Figure 4.3, An adaptation of the PSDB 21/04 reference image to show all headform
target locations in this study of threat recreations using swung implements.
1. 'Back', 2. 'Crown', 3. 'Front', and 4. 'Side' [13] 54
Figure 4.4, Swing paths of wooden (A) and metallic (B) implements for frontal
impact recreations. Frames are taken from a side-view high-speed camera.
Dashed plots are the positional coordinates of marker centroids, only the
marker closest to impact was tracked for each trial 55
Figure 4.5, Impact velocity comparisons of all wooden and metallic swung
implement trials (n = 96). Median values for each group are labelled, as well
as the only outlier of the dataset (Wooden, Side Impact, Trial 5) 57
Figure 4.6, Example of relative angle between headform and swung implement at
contact (Trial 1. Wood Crown)

rigule 4.7, 1137 frames indicating variations in impact tocation on the headlotting	^
and B: Wooden, Back, trials 1 and 2) and swung implement (C and D:	
Metallic, Crown, trials 11 and 3).	59
Figure 4.8, Peak resultant headform kinematics (PLA and PAA) for swung weapon	
impacts to the back, crown, front, and side locations (coloured). Error bar	s
indicate one standard deviation	60
Figure 4.9, Mean headform linear acceleration (x, y, z, and resultant) vs time for	
wooden and metallic swung weaponry trials impacting the back, crown,	
front, and side of the headform. Red dashed line shows the 120 J impact	
pass threshold outlined in PSDB 21/04 [13].	62
Figure 4.10, Visualisation of mean reaction linear acceleration vectors at each	
instance of peak resultant for impacts to the back, crown, front, and side	of
the headform. Vector lengths are normalised by the greatest PLA (metallic)
crown) with length demonstrating magnitude and the directions calculate	
using the pythagorean resultant of orthogonal data. Red concentric rings	
represent scale of 100, 300, and 500 g magnitude	64
Figure 4.11, Common post-impact dynamics of wooden and metallic implement	s.
Images show wooden implement rebound with an increasing gap betweer	า
headform and wooden implement over 10 ms after impact (Time (T) = 0 ms	s)
and little headform movement (see reference line in contact with the apex	(
of the chin at contact). The rebound effect did not happen for metallic	
implements where contact with the headform was maintained and more	
headform motion was visible (more chin visible under reference line) 6	35
Figure 4.12, Headform angular acceleration (x, y, z, and resultant) vs time for	
wooden and metallic swung weaponry trials impacting the back, crown,	
and front of the headform. Red dashed line shows an example angular	
acceleration pass threshold (6 krad/s2) for American Football helmets	
[15]	66

Figure	4. 13, Headform angular acceleration (x, y, z, and resultant) vs time for
	wooden and metallic swung weaponry trials impacting the Side of the
	headform. Red dashed line shows an example angular acceleration pass
	threshold (6 krad/s2) for American Football helmets [15] 67
Figure	5.1, Screenshot of UK officers mounted on horseback during PO conditions
	[360]
Figure	5.2, Setup for recreating falls from a stationary horse using a Hybrid III ATD
	[380]
Figure	5.3, HSV frames at the point of impact between the ATD and floor for trials
	10 (A) and 12 (B) when simulating falls from horseback. Red dashed lines
	show the headform marker trajectory from entering frame until impact 78
Figure	5.4, Mean headform linear and angular acceleration (x, y, z, and resultant) vs
	time curves for horseback fall scenarios. Red dashed lines indicate
	proposed 80 % likelihood of mTBI thresholds for equestrian falls by Clark et
	al (2020) [320]
Figure	5.5, Z (superior/inferior) acceleration for trial 5 of horseback fall recreations.
	The impact is synchronised with HSV frames to show simultaneous neck
	compression across 3 cyclic loading peaks. L is the distance between
	neckform pin joint and torso, normalised by the distance at contact T = 0
	ms. Note that both neck compression and head kinematics stay ≈ 0
	between 6 and 7 ms (D and E)
Figure	5.6, Relative angle change between the headform and torso at contact ($T=0$
	ms) and 50.5 ms. Change in angle ($\theta 2 - \theta 1$) = -45.4°
Figure	6.1, Different brick orientations at the point of contact with the helmeted
	headform. This demonstrates variation in brick impact conditions for free
	fall drop simulations, leading to inconsistent head impact measurements
	[190]
Figure	6.2, PSDB 21/04 standard schematic for assessing helmet energy
	attenuation using a guided drop system [13]
Figure	6.3, Examples of guided drop rigs using Hybrid III head and neckforms in
	research. A) Head Impact Testing Facility, Portland Biomechanics Lab, USA
	[192]. B) University of Canterbury, New Zealand [105]

Figure 6.4, An example of steel guide cables deforming at impact (nightighted in
red), thus reducing motion in the head/neckform [390]9
Figure 6.5, Diagram of HIWIN linear guideway HG series rails and bearings used fo
guiding the decent of drop assembly [393]9
Figure 6.6, Initial concept for an aluminium 'drop plate' to act as a rigid componen
between the affixation of neckform or cradle and guide rails 9
Figure 6.7, Initial sketch of the drop plate lifting and release mechanism. The
operator pulls down on the rope above pulley to lift the drop assembly with
mechanical advantage 9
Figure 6.8, 3D CAD model of the designed guided drop system in configurations fo
affixing headforms with a representative neck or cradling without further
support9
Figure 6.9, Forces and moments considered in calculating the effective bearing
reaction forces (P _e) across varying vertical (V) and horizontal (D) separation
between 0.1 and 0.7 m 9
Figure 6.10, Original and refined drop plate designs following the removal of
unnecessary mass using Finite Element Analysis. The final design was a 43
% mass reduction10
Figure 6.11, Modelled geometry for identifying and removing regions of low
structural support on the drop plate. A) initial plate half geometry, B) final
plate half geometry, C) Side cross-sectional view of plate, ATD components
and impact anvil [190]10
Figure 6.12, The guided drop system installed at the laboratory. A) Impact rig
showing the lower portion of drop tower height, B) HIII ATD head and neck
components affixed to the drop plate, C) Inverted HIII ATD components wit
temporary steel bracket between neckform and drop plate, D) Temporary
cradle for dropping an unconstrained headform or simulating projectile
bricks10
Figure 7.1, Bricks remaining on the floor in the aftermath of a PO event, after the
public used them as projectile weaponry [400]11
Figure 7.2, The relationship between achievable throw velocity and resultant
kinetic energy for mass in the range expected of traditional clay bricks (1.2

3 kg). k = 12.8 and 14.3 are constants representing realistic average and
extreme throw capabilities114
Figure 7.3, Experimental arrangement for simulating cradled brick impacts to the
head using a drop rig. Bricks were cradled and dropped from a known
height. The neckform constraint was rotated to permit different impact
locations on the headform115
Figure 7.4, PLA for all headform locations with brick impact velocities of 3, 5, and
6.5 m/s. Error bars indicate one standard deviation colours represent
impact velocity118
Figure 7.5, PAA for all headform locations with brick impact velocities of 3, 5, and
6.5 m/s. Error bars indicate one standard deviation. Y axis is shown as
logarithmic to accommodate the difference in magnitude between back
impacts and other locations119
Figure 7.6, High-speed video frames at 0, 4, 8, and 12 ms after impact for trials to
the back and front at 6.5 m/s. Frames show how the brick bounces from the
headform for back conditions though not for front, and how rotation of the
headform is greater for back impacts120
Figure 7.7, Visualisation of power law regression plots for headform data over
impact velocities 2 - 12 m/s. Markers show measured kineamtics at 3, 5,
and 6.5 m/s with predicted values at 8.7 and 10.6 m/s124
Figure 7.8, Mean headform resultant linear acceleration vs time curves for tested
(3, 5, and 6.5 m/s) and predicted (8.7 and 10.6 m/s) impact velocities.
Predicted curves are formed as a half sine wave from Equation 7.3 and
Table 7.3. Red dashed lines indicate the high energy impact pass threshold
in PSDB 21/04 [13]125
Figure 7.9, Mean headform resultant angular acceleration vs time curves for tested
(3, 5, and 6.5 m/s) and predicted (8.7 and 10.6 m/s) impact velocities.
Predicted curves are formed as a half sine wave from Equation 7.3 and
Table 7.3. Red dashed lines show the angular acceleration pass threshold
(6 krad/s²) for American Football helmets [15]126
Figure 8.1, Mean PLA, PAA, and respective durations for experimented PO
scenarios. Predicted brick data refers to 10.6 m/s conditions from non-
linear regression (Chapter 7) The Post et al (2015) example shows the

۲	octential increase in FAA for moving noise conditions. Word and noshizaki
e	et al (2017) curves demonstrate thresholds for life-threatening and mTBI
i	njury, respectively [109], [120]134
Figure 8	.2, Transient resultant linear headform acceleration curves for all
e	experimented PO conditions at each head impact location (Back, Crown,
F	Front, and Side)139
Figure 8	.3, Transient resultant angular headform acceleration curves for all
e	experimented PO conditions at each head impact location (Back, Crown,
F	Front, and Side)140
Figure 8	.4, Experimental setup for dropping a neck affixed and cradled headform
C	onto representative anvils. The headform was rotated in its constraint to
a	achieve different impact locations. Impact velocity was defined by varying
c	drop height. Impact surfaces were set to replicate weapons identified in PO
a	activity (Chapter 2)144
Figure 8	.5, Scatter plots for PLA, PAA, and respective pulse durations across all
C	drop rig tested conditions with a neckform. Grey limits represent the
r	maximum and minimum region expected for PO conditions, Table 8.1146
Figure 9	.1, 'Defender Hybrid' PO helmet (MLA Ltd) imaged from the exterior and
i	nterior with annotated key features [2], [294]162
Figure 9	.2, Experimental setup for helmet impacts when dropping the neckform
a	affixed headform onto representative metallic and wooden anvils (top row),
c	dropping a clay brick (bottom left), and dropping an unconstrained cradled
h	neadform (bottom right)165
Figure 9	.3, Helmet sections, in-line with the anatomical mid-sagittal and coronal
p	planes, for assessing internal wear and damage167
Figure 9	.4, Mean peak linear (PLA) and angular acceleration (PAA) for helmeted
r	neadforms at each drop rig setup condition. Standard deviations are large
b	pecause means include all head impact locations168
Figure 9	.5, Change in linear and angular acceleration between helmeted and bare
r	neadforms to assess the protective performance of PO headgear. Figure
t	iles represent the setup condition, and each setup is separated by impact
L	ocation. There was no hare brick data to compare angular measurements

	to and crown impacts were radial, thus irrelevant for angular comparisons
	in this analysis169
Figure 9	9.6, Differences in mean PLA and PAA between new and used (anything
	greater than one impact) PO helmets. * Indicates significant P < 0.05
	difference between new and used headgear170
Figure 9	9.7, Internal and external damage of PO helmets following three repeated
	impacts to each of the back, crown, front, and side impact locations. Rows
	represent damage after repeated trials with a metallic cylindrical anvil,
	such as the current requirement of PSDB 21/04, and a flat surfaced wooden
	anvil171
Figure ¹	10.1, Mean injury metric scores, Table 10.2, normalised by their
	corresponding 80 % likelihood of AIS 2+ and 4+ thresholds, Table 10.1. Bars
	are coloured according to their proximity to the threshold, where a greater
	relative score suggests a greater severity of injury186
Figure	10.2, Mean injury scores for each impact location, normalised by their
	corresponding AIS 4+ threshold

Nomenclature

Abbreviations

6DOF Six Degrees of Freedom

AIS Abbreviated Injury Score

ANOVA Analysis of Variance

ASTM American Society for Testing and Materials

ATD Anthropomorphic Test Device

BrlC Brain Injury Criterion

BSI British Standard Institute

CEN European Committee for Standardisation

CFC Channel Frequency Class

CoM Centre of Mass

CP Probability of Concussion

CSDM Cumulative Strain Density Measure

DAI Diffuse Axonal Injury

DAMAGE Diffuse Axonal, Multi-Axis, General Evaluation

DOF Degrees of Freedom

EAL Energy Absorbing Liner

EPP Expanded Polypropylene

EPS Expanded Polystyrene

EPU Expanded Polyurethane

FE Finite Element

FEA Finite Element Analysis

FFT Fast Fourier Transform

GAMBIT Generalised Acceleration Model for Brain Injury Threshold

GFRP Glass Fibre Reinforced Polymer

HAE Head Acceleration Event

HBM Human Body Model

HIC Head Injury Criterion

HIII Hybrid III

HIP Head Impact Power

HIT Head Impact Telemetry System

HSV High Speed Video

IC Injury Criteria

ICP Intracranial Pressure

iMG Instrumented mouthguard

IMU Inertial Measurement Unit

IRC Injury Risk Curve

KLC Kleiven's Linear Combination

LOC Loss of Consciousness

MPPPG Metropolitan Police Personal Protective Group

MPS Maximum Principal Strain

mTBI Mild Traumatic Brain Injury

NAP Nine Accelerometer Package

NIJ National Institute of Justice

NOCSAE National Operating Committee on Standards for Athletic

Equipment

PAA Peak Angular Acceleration

PAV Peak Angular Velocity

PCA Principal Component Analysis

PCS Post-Concussive Syndrome

PCS Principal Component Score

PDS Product Design Specification

PLA Peak Linear Acceleration

PO Public Order

PPE Personal Protective Equipment

PRHIC Power Rotational Head Injury Criterion

PSDB Police Scientific Development Branch

PU Polyurethane

RIC Rotational Injury Criterion

RVCI Rotational Velocity Change Index

SAE Society of Automobile Engineers

SI Severity Index

sTBI Severe Traumatic Brain Injury

TBI Traumatic Brain Injury

UBRIC Universal Brain Injury Criterion

VN Vinyl-Nitrile

WHO World Health Organisation

WSTC Wayne State Tolerance Curve

Symbols

F Force

t Time

m mass

v Velocity

kE Kinetic Energy

Δ Change in (Difference)

g Gravitational Acceleration (= 9.81 m/s)

a Linear Acceleration

α Angular Acceleration

ω Angular Velocity

δ Displacement

κ Cohen's Kappa Statistic

CV% Coefficient of Variation

C Individual Specific Swing Constant

I Moment of Inertia

L Length

σ Material Stress

ε Material Strain

W Strain Energy per Unit Volume

n Cumulative Count

R² Coefficient of Determination

d Distance

E Modulus of Elasticity

w Width

V Vertical Separation

D Horizontal Separation

P Reaction Force

K Offset Planar Distance

H Offset Normal Distance

k Person-specific throw constant

A Linear constant for power law regression

θ Headform angular orientation

Scripts

0 Initial

X Head Sagittal Axis

Y Head Frontal Axis

Z Head Longitudinal Axis

i Each subsequent x, y, and z.

c Critical

* Normalised

d Distance

a Axial

r Radial

e Effective

n Exponent for throw velocity regression

B Exponent for power law regression

1. Introduction

This thesis documents a programme of work to encourage the design innovation of helmets (Figure 1.1) worn by Police Officers undertaking Public Order (PO) activity, often called 'Riot Police', by advancing current helmet testing policy. The process included identification of the unique protective requirements for this application and advising how standardised legislation can best ensure they are effective in their use. This can lead to long term improvements in helmet quality with transferable implications across broad personal protective equipment (PPE) applications. The following highlights the motivation for research, including the existing limitations within PO headgear and injury knowledge, and outlines the aim, objectives, and structure of the thesis.



Figure 1.1, Example helmets worn by UK officers during Public Order activity: the 'Defender' (left) [1] and 'Defender Hybrid' (right) [2].

1.1 Motivation for Research

Traumatic brain injuries (TBI) are a leading cause of death and have been identified as a prominent health problem by the World Health Organisation (WHO) [3], [4], [5]. They are estimated to affect sixty-nine million (95% CI 64–74 million) people per annum, with an associated healthcare cost of \$2.9 billion [5], [6], [7]. Since the mid-20th century, increased knowledge of brain injury biomechanics has resulted in significant advancements of protective headwear design [8], [9], [10]. Whilst these have predominantly benefitted the sports and automotive industries [10], [11], [12], high-risk occupations such as Policing, Construction, or Fire Safety have

seen relatively less attention. Scientific advancements in these fields can benefit public health on a global scale, given their international prevalence in society.

The propensity for head injuries in PO activity was brought to attention by the Metropolitan Police Personal Protective Group (MPPPG, United Kingdom), who have supported this work with their advice, anecdotal evidence, and provision of helmets. Their concern was in regard to serving officers being injured, despite being equipped with headgear certified to the current standard, PSDB 21/04 [13]. This legislation, provided by the Home Office and last revised in 2004, received British Standard Institute (BSI) administration in the form of a Product Approval Specification (PAS017) in 1995. While it directly implies blunt trauma risks in the form of 'non-edged' wielded weapons and bricks, there is no publicly available rationale for the methods of this standard. Similarly, the standard lacks validation as to if it appropriately scrutinises the in-situ efficacy of helmet designs. Therefore, study of the typical injury causes and how they compare to the test standard addresses an important gap in knowledge for this application, which could also identify areas for improving helmet design.

Improving representation within test standards has been applied in multiple sports over recent decades and is often followed by substantial headgear innovation [9], [14], [15], [16], [17], [18], [19]. Helmets for use in American Football are an example of this; recent designs have transitioned from foam padding to polymeric structure-based systems, or 'metamaterials', which have forced older designs out of use [20], [21], [22], [23], [24]. This coincides with advancements in American Football headgear testing [12], [25], [26], [27], [28], [29]. The sports industry benefits from being a consumer market, where manufacturers continuously evolve their designs to maintain a competitive advantage and protect high-value asset players. There is also a growing awareness of TBI within sport and an ever-growing user space demanding greater protection from their equipment. Within the PO market, there is significantly less competition due to the limited number of manufacturers offering product, thus incentive to innovate is almost entirely reliant on test standard requirements. As a result, the current energy absorbing liner (EAL) structure in PO helmets remains unchanged since at least the 1980's. Therefore, targeting the test standard was believed the best method for forcing

design innovation, which could result in a long-term reduction of Police Officers sustaining neurotraumatic injuries.

1.2 Aims and Objectives

The aim of this work was to improve injury and situational representation in the Public Order helmet test standard, which can better ascertain if designs are fit for purpose. This was achieved through completion of the following objectives.

- Identification of events leading to head and brain injuries in Public Order conditions.
- Quantification of blunt trauma head impacts with Public Order representative loading conditions.
- 3. Demonstration for how Public Order representative impacts can be recreated with repeatable helmet impact test methodology.
- Recommendation for how the Public Order helmet test standard can improve situational injury representation and encourage more protective headgear.

1.3 Thesis Structure

This work is presented as a traditional thesis with eleven chapters:

- Chapter 2 provides critical review of the literature for head and brain injury biomechanics, Police specific injury risks, and helmet impact testing.
- Chapter 3 details the identification of injurious conditions leading to head injuries in Public Order activity. This includes documenting the causes of head impact events and any relevant weaponry being used to harm officers.
- Chapter 4 quantifies head impact mechanics attributable to contact with wielded blunt weaponry. This includes experimental recreation and the identification of representative head kinematics and impact dynamics.
- Chapter 5 quantifies head impact mechanics encountered when falling from the back of a mounted horse, similar to Chapter 4.

- Chapter 6 details the design development of a mechanical helmet impact test rig. This includes critical review of methods for helmet impact testing and highlights key design considerations when building a guided drop impact rig.
- Chapter 7 quantifies head impact mechanics attributable to projectile thrown bricks, similar to Chapters 4 and 5.
- Chapter 8 evaluates how the head impact mechanics in drop test recreations compare to more situationally representative test conditions.
 This includes evaluation of the effects of varying biomechanical constraints and impact surfaces.
- Chapter 9 details the protective performance of current issue Public Order headgear subject to drop test impacts representing the injurious conditions identified in Chapter 3. This includes assessment of peak force reduction and the robustness of helmet designs.
- Chapter 10 evaluates the relevance of different kinematic injury metrics as a threshold for use in the test standard. This includes comparison of their relative severity predictions and reliabilities.
- Chapter 11 discusses the main findings from this programme of work, as well as its contribution to knowledge, implications, limitations, areas for improvement, and an overall conclusion.

2. Literature Review

2.1 Introduction

This chapter reviews current research for head injuries in Public Order (PO) conditions and what is needed for test standard developments. Meaney, Morrison, & Bass (2014) proposed a research cycle for reducing the societal burden of TBI, Figure 2.1 [30]. The exploration of these with application to PO can evaluate the efficacy of current PO test methodology and highlight areas for improvement.

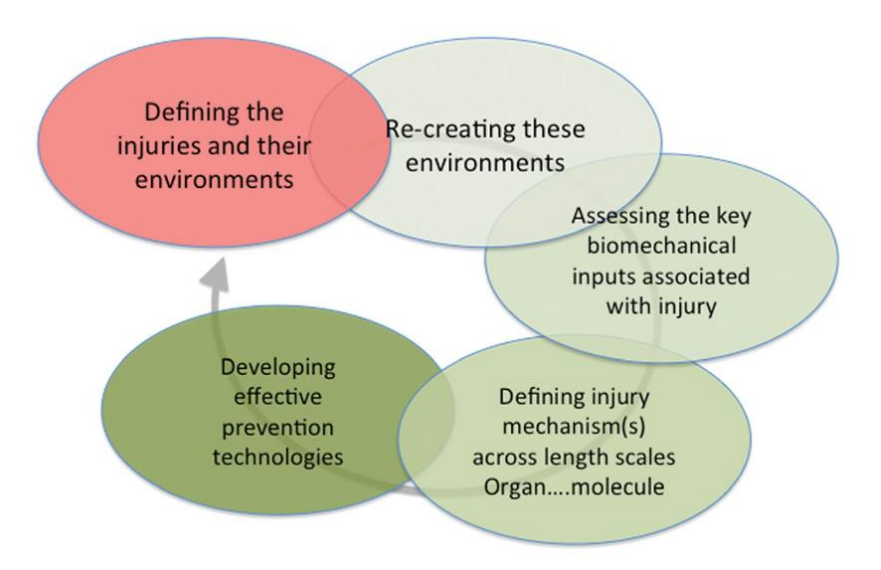


Figure 2.1, A proposed research cycle for reducing the burden of TBI in society by addressing the specific situational needs of the application [30].

Review of literature highlighted current knowledge for the definitions of injuries, their mechanism, and how other headgears have reduced the occurrence of injuries. Sources have been compiled from across medical and mechanical research to build a holistic view of the problem. The review is split into four sections that explore current knowledge to answer the following questions:

- What head injuries can be expected in PO activity?
- How can we quantify head injuries and their severity?
- How can we test the protective performance of PO headgear?
- What is the purpose of protective helmets and how do they work?

2.2 Head Trauma in Public Order Activity

2.2.1 Injury Prevalence and Causes

Police officers are at a high-risk of injury due to the propensity of assault and violence [31]. PO activity can accentuate this, as crowds tend to share a common psychology and behaviour, meaning aggressive behaviour has shown to harmonise in the situation [32], [33], [34]. In England & Wales there were 10,410 reports of 'assault with injury on a constable' between March 2019 and March 2020, although these were not published with injury details [35]. Another study highlighted that 42% of a sampled 224 United Kingdom (UK) based police officers had suffered serious injuries to the face, head, or neck [36].

The causes of head injury encountered during police activity can be found in literature, although not specifically for PO activity. A recent study with a small sample of UK police officers (54) found that 59.3 % had sustained a head or neck injury, 27.8 % met the criteria for post-concussive syndrome (PCS), and the most common cause (49.1%) was a fall or being struck by an object or person [37]. The authors highlight a prevalence of concussive brain injury in this study, the rate for police officers (38.9 %) is much greater than the general population (12.0 %), although this was taken from a small sample size [37], [38]. Another study included the injury reports of 35,406 Australian based police officers and showed that physical assault were the most common causes of injury (21.3 %), followed by slips, trips, and falls (16 %) [39]. They also differentiate officers mounted on horseback, which is common in PO, and showed a relative injury likelihood $\approx 2-3$ times that of non-mounted officers, with falls from height being the leading cause (15.9 %) [39]. It is clear the risk of head injury is high for police officers, although the specific causes of injury in PO are not well documented. As a result, there is no specific data for what loading conditions a PO helmet must protect the user from, nor what neurotraumatic injuries can be expected.

2.2.2 Head Injury Pathologies

Neurotrauma is defined as physical dysfunction of the central nervous system by result of sudden high-energy transmission to the head [3], [40], [41], [42], [43], [44]. Such injuries are categorised as 'open' or 'closed' determined by whether

penetration of the skull occurs, examples for which are summarised in Figure 2.2 [45], [46]. Open injuries are more associated with the skull and closed injuries are associated with the brain, although their occurrence is not always independent. For example, penetrative deformation of the skull can also lead to brain injury [47].

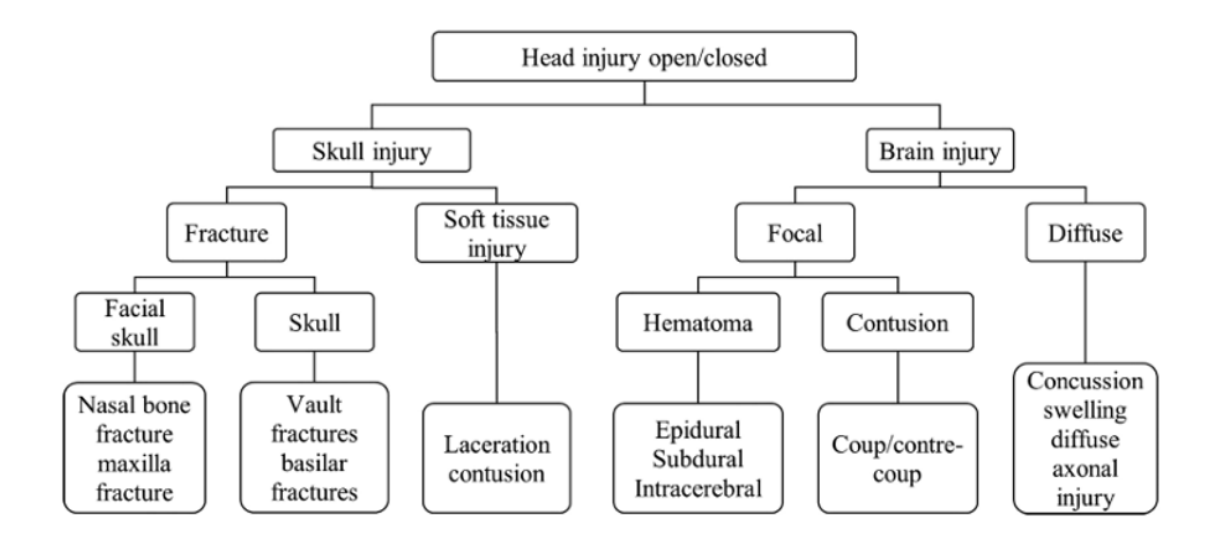


Figure 2.2, A simplified summary of blunt trauma induced head injuries and their respective categories, taken from Zheng et al., 2022 [46]. Open/closed refer to whether penetration of the skull occurs.

Skull fractures are now less prevalent in most activities where the use of headgear is common practice [9], [48], [49], [50], [51], [52], [53]. However, the prevalence of closed type head injuries, ranging from concussion to hematomas, remains a burden on society affecting an estimated 69 million people annually and the leading cause of death in middle-aged populations [5], [54], [55], [56]. The most common causes of closed type head injuries are falls, sporting injuries, road traffic incidents and assaults [57]. As a result, certain sub-populations, such as sports athletes, combat military personnel, and PO police officers, are at a higher risk of sustaining such injuries than the general population [58], [59].

Closed type head injuries can be classified into two primary groups: focal and diffuse. These are differentiated primarily on the localisation of the injury, with focal concentrated to a small area and diffuse spanning larger volumes [41], [60]. Similar to open injuries, helmet advancements within sports and automotive sectors have reduced the incidence of focal brain injuries, however the prevalence of diffuse injuries remains to be resolved [9]. Diffuse injuries can also be defined

further, as they range from temporal dysfunctions in brain metabolism to permanent structural injuries (Diffuse Axonal Injury or DAI). Though little international consensus exists, diffuse type injuries can be generally categorised as Traumatic Brain Injury with various functional levels of mild Traumatic Brain injury (mTBI), moderate Traumatic Brain Injury (modTBI), and severe Traumatic Brain Injury (sTBI). For the purpose of this work, an accepted clinical head injury grading scale, entitled the Abbreviated Injury Score (AIS), will be employed to better allow clinical meaningfulness of the testing results [53], [60], [61], [62], [63]. This grading is a tool for healthcare professionals to quickly diagnose the severity of TBI based on the persons loss of consciousness (LOC), although it does not consider any specifics for brain tissue damage or location.

Table 2.1, The Abbreviated Injury Score (AIS) range from 1-5 for non-fatal brain injuries [62].

Description	AIS Severity Score
Mild concussion, no LOC	1
LOC < 1 hour	2
Severe Concussion, LOC 1-6 Hours	3
DAI, LOC (6-24 hrs)	4
DAI, LOC > 24 hrs	5
DAI with brain stem decerebrate/ decorticate signs	5

Diffuse injuries remain a problem despite headgear advancements because they are believed to be result of different within-head mechanical phenomena, specifically the rotational motion of the brain [64], [65], [66], [67], [68]. An impact force to the head in its simplest form can be assumed as a perfectly radial load, where the force vector is directed toward the centre of mass (CoM), Figure 2.3 (A) [27], [69]. Outside of experimentation, a head impact is almost certain to be an oblique load where the head and brain experience simultaneous translational (linear) and rotational (angular) force, Figure 2.3 (B) [70], [71], [72]. DAI for example is attributed to the shearing of white matter axonal fibres, caused by the disparate relative angular motion of the skull and brain [61], [73], [74]. Conversely, skull and focal injuries are strongly associated with linear force, thus the damping properties

of headgear are typically tailored to reduce linear force transfer [9]. This is reflected in product specification standards, where until the last decade only linear thresholds were used to evaluate headgear performance [15], [75], [76], [77].

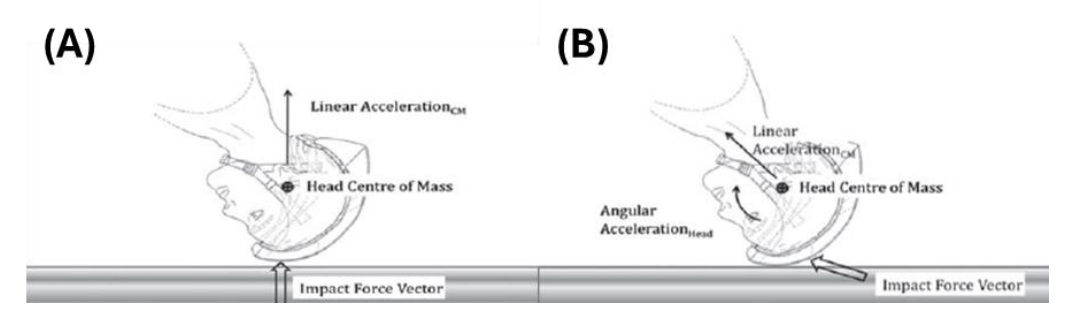


Figure 2.3, Radial (A) and oblique (B) force vectors as a result of blunt trauma head impact [70]. Radial refers to a vector in-line with the centre of mass whereas oblique incur both linear and angular motion.

2.2.3 Section Summary

Ideally, a helmet would mitigate the full breadth of head trauma present for its application, including all aspects of TBI. There are no known details for the specific neurotraumatic injuries that PO officers commonly face, only that head impacts are prevalent for Police and often caused by strikes, falls, or physical assaults. This gap makes it challenging to establish precise loading conditions or injury profiles for designing PO helmets. It is almost certain that head impacts in PO will include oblique loads, thus officers are susceptible to injuries from both linear and angular forces. The challenge for a PO helmet is therefore to:

- 1. Resist penetration.
- 2. Dissipate localised forces.
- 3. Reduce linear and angular head motion.

This should be reflected in the test standard to ensure each of these are considered by designers when developing new PO headgear.

2.3 Quantifying Head Impacts

2.3.1 Fundamentals of Head Impact Mechanics

The dynamic force relationship of an idealistic impact is a half-sinusoidal pulse shape, where force increases to a maximum and returns to zero [78], [79], [80], [81], [82], [83]. The area below the force time curve is the impulse, a direct measure for the change of momentum in a collision (Equation 2.1, F = force, t = time, m = mass of the object, Δv = change in velocity) [84]. The relationship to momentum means the magnitude of impulse is directly proportionate to the kinetic energy at impact (Equation 2.2, kE = kinetic energy).

$$Ft = m \cdot \Delta v \tag{2.1}$$

$$kE = \frac{m \cdot v^2}{2} \tag{2.2}$$

For skull fracture injuries, it is the pressure applied to the bone that mostly defines the severity, thus force is proportionate to the kinetic energy and area is dependent on the surface properties of the colliding object [85], [86], [87]. For brain injuries, the tissue of the brain is susceptible to mechanical tensile, compressive, and shear strains as the result of impulse [72], [88]. These are mostly the result of one or a combination of the following events: [64], [69], [72], [88], [89], [90].

- Contusions from the indentation/deformation of the skull.
- Intracranial pressure (ICP) differentials as the brain lags behind the moving skull.
- Concentrated tissue stresses where the motion of the brain is anatomically constrained by the skull or brainstem.

The magnitude, volume, and location of tissue strains all affect the severity and form of an occurring TBI [72], [91], [92], [93], [94]. Furthermore, they are each correlated with magnitudes of linear and angular motion, although in differing proportionalities [50], [69], [93], [95]. For example, if a hand sized object was thrown and it resulted in a mostly radial impact to the head, then skull indentation and high ICP differentials would be likely [96], [97]. This could also lead to a likelihood of open or focal injuries [72], [96], [98], [99], [100], [101], [102].

Conversely, a high-energy oblique strike to the head would cause more shearing of tissue, as the brain rotates separate to the skull yet is inhibited in its motion, thus focal and diffuse injuries are expected [65], [66], [68], [94], [102], [103], [104]. It is not possible to directly measure such responses of the brain due to physical impact, hence we use more measurable phenomena in the form of linear and angular head kinematics [61], [69], [73], [93], [95], [96], [97], [104]. These do not directly cause head injury, but they are measurable consequences of high energy transfer to the head and can be correlated to injury [69], [92].

Peak linear and angular accelerations are the most widely known predictive measures and both share a non-linear power law relationship with relative impact velocity [105], [106]. Idealistically the exponent for this is '2' to reflect a linear relation to kinetic energy although in reality energy dissipation and damping in the collision decrease this value. Peak angular velocity as a predictor gained little traction when first proposed but has recently become popular as knowledge of diffuse brain injury mechanics have advanced [69], [104], [107], [108]. Hoshizaki et al (2017) compiled head impact events across literature and grouped them based on their kinematic and durational limits, Figure 2.4 [109].

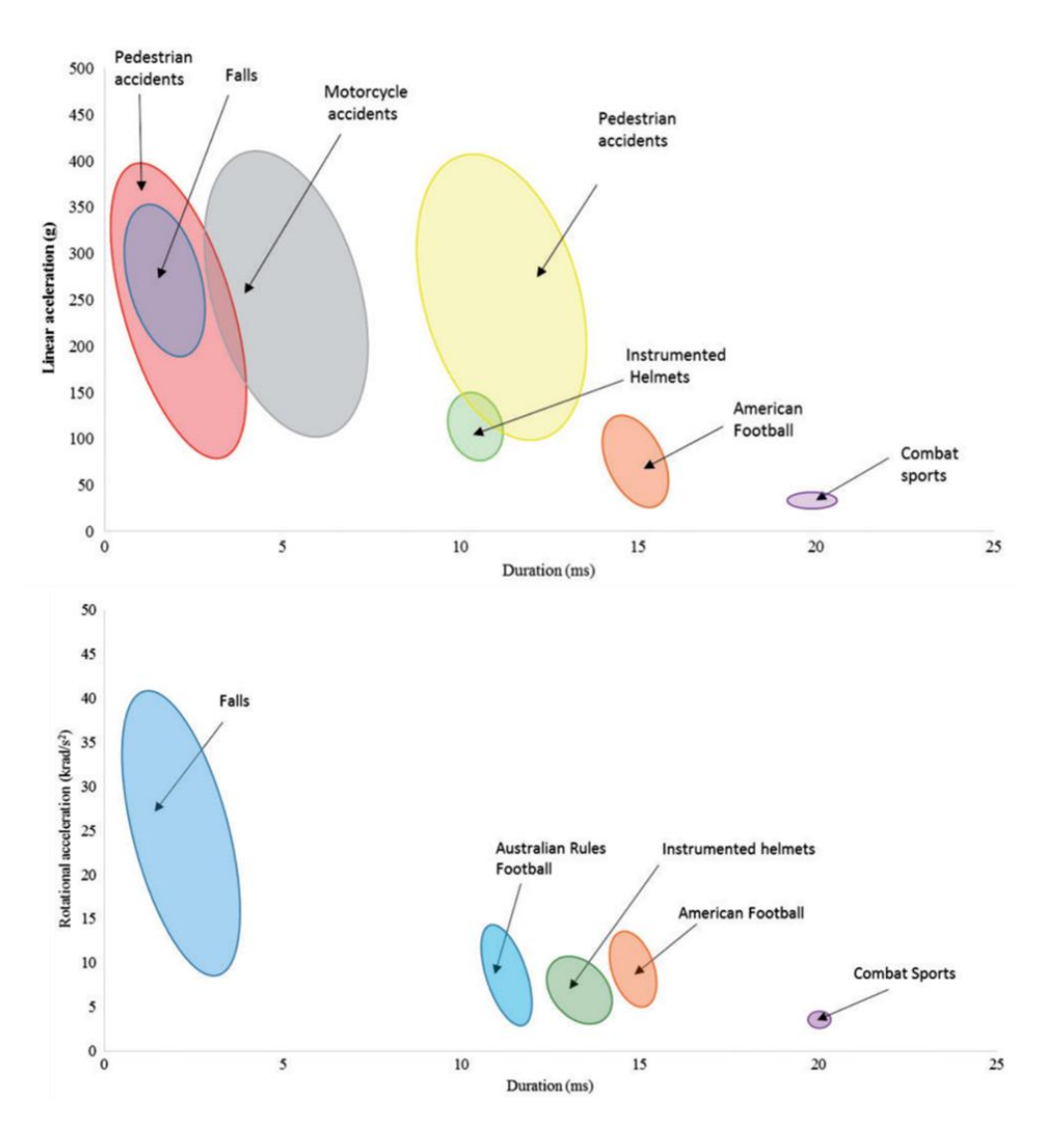


Figure 2.4, Representative groupings for head injurious events in literature, based on peak magnitudes of linear and angular acceleration as well as their duration [109].

2.3.2 Linear Kinematics

The peak linear acceleration (PLA) of the head has long been correlated with the likelihood and severities of skull fractures and focal brain injuries since early experimentations with cadaveric human and animal subjects [92], [96], [98], [99]. PLA proved to be a strong predictor for high stress concentrations at coup (close to impact) and contre-coup (distal from impact) locations, as well as close to the brain stem [90]. This has been extensively validated with broad experimental means [96], [110], [111], [112], [113], [114], [115]. As a result, linear acceleration is the most established measure of head impact severity and is incorporated within almost all recognised helmet certification standards, including for PO application [13], [18].

Zhang et al's (2004) thresholds for predicting mTBI from PLA are derived from recreations of American Football incidents and are some of the most recognised in literature [47], [50], [116], [117], [118]. These predict injury onset at PLA = 66, 82, and 106 g (g = 9.81 m/s²) for 25, 50, and 80 % risks of mTBI (AIS 2+), respectively [116]. Similarly, Newman et al (1986) determined 250 g was the equivalent for a 50 % risk of (AIS 4+) [119]. However, these are oversimplifications of the injury mechanism because the human brains tolerance of acceleration is time-dependent, decreasing with prolonged duration. The exact relationship for this is defined by the Wayne State Tolerance Curve (WSTC), where above the curve represents a life-threatening impact, Figure 2.5 [120]. The above PLA thresholds were derived from helmeted impacts with a duration greater than 5 ms, from which the WSTC shows little sensitivity to further prolonged duration. Therefore, these thresholds are only applicable to PO if tests with a helmet are greater than 5 ms.

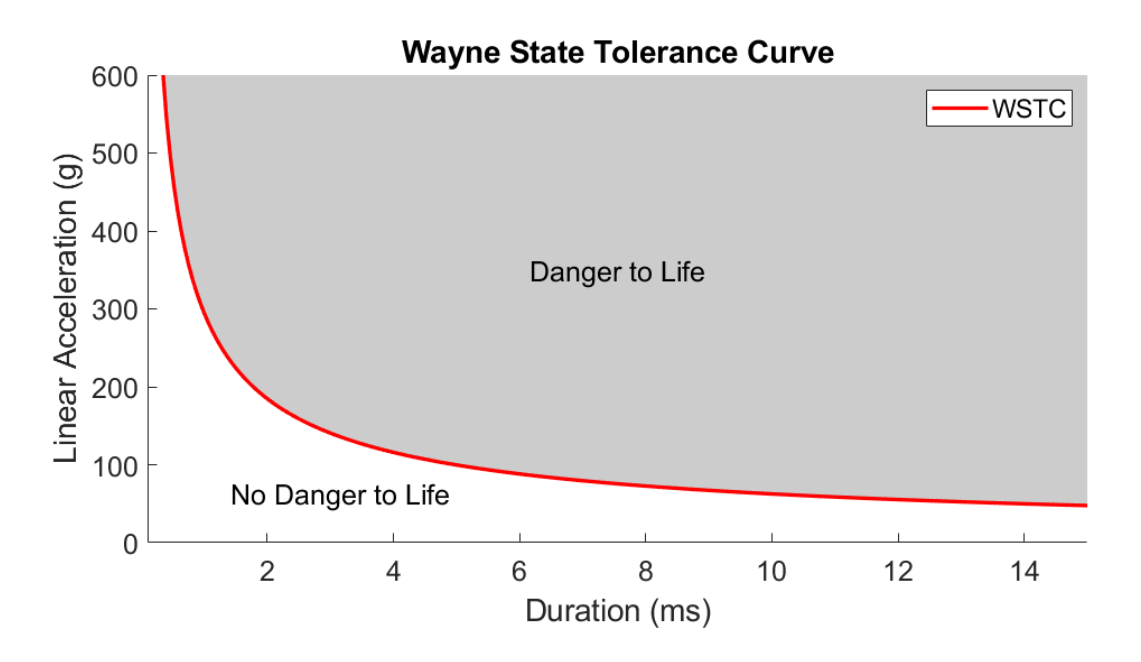


Figure 2.5, Wayne State Tolerance Curve (WSTC) depicting the brains time-dependent tolerance to linear acceleration, where a measure above the line is considered a danger to life [120].

2.3.3 Angular Kinematics

Peak angular acceleration (PAA) was first suggested as a signature of TBI in the 1940's, although widespread adoption of this theory took time and was initially believed only useful for non-impact head acceleration events, e.g. whiplash [100]. It has since been proven that high PAA is comorbid with the occurrence of focal

and diffuse injuries for head impact scenarios and that almost all closed neurotraumatic injuries can be predicted with PAA [72], [73], [74], [121], [122]. Despite this, very few helmet certification standards include rotational measures in their pass thresholds [18].

For injury to occur from angular motion there must also be a linear element to the load, as the magnitude of rotation alone would have to be extremely high [102], [123], [124]. This linear element is always present with how the brain is constrained within the skull [70], [72]. However, this makes the definition of a singular PAA threshold value more difficult. Zhang et al (2004) also proposed mTBI (AIS 2+) thresholds based on PAA at 4.6, 5.9, and 7.9 krad/s² for 25, 50, and 80 % injury likelihoods [116]. For AIS 4+, Wu et al (2021) defined an 80 % likelihood of AIS 4+ at 17 krad/s² for over 60's, although this is similar to other studies for the general population [125], [126]. However, the brain's tolerance of PAA is also time-dependent, similar to PLA [79]. The threshold curve for this relationship was developed for cycling applications by Van Lierde (2005) and then improved for more generalised sports head impacts by Hoshizaki et al (2017), Figure 2.6 [109], [127], [128].

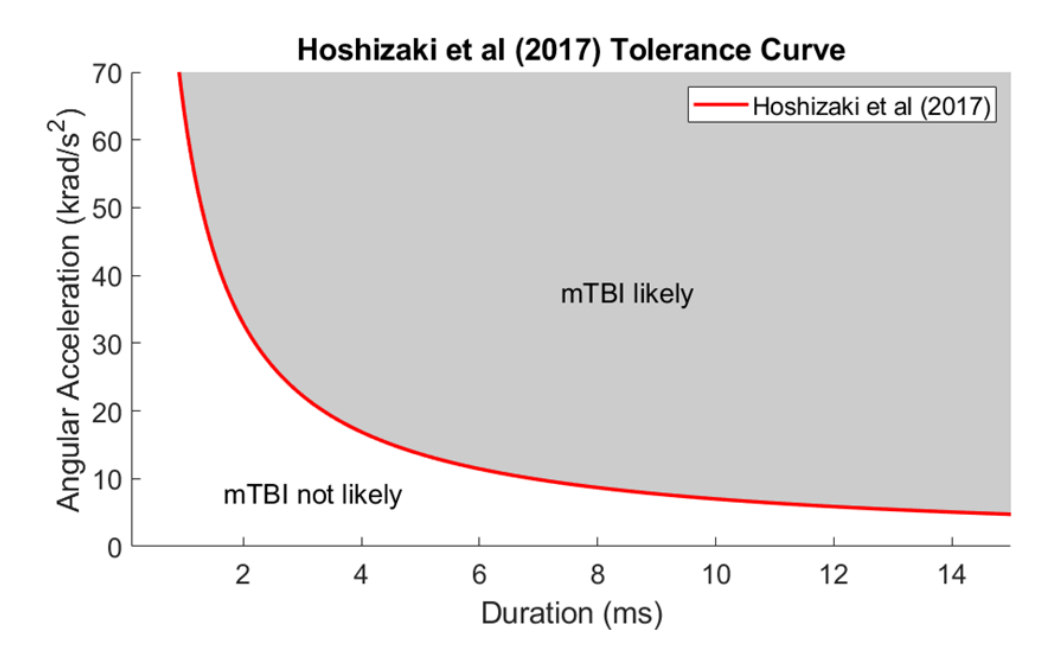


Figure 2.6, Threshold curve depicting the brains time-dependent tolerance to angular acceleration where above the line is considered the occurrence of mTBI [109].

Peak angular velocity (PAV) has shown promising correlation to angular induced neurotrauma, particularly for shorter duration events [69], [129], [130], [131]. Takhounts et al (2013) proved a slightly better brain strain correlation with PAV than PAA, although for a mostly automotive dataset [108]. Both PAV and PAA have shown to be predictors of diffuse injuries, although PAA is much more commonly reported for helmeted impacts in the sports industry. The incorporation of angular kinematic measures in a test standard better evaluates headgear performance for reducing the likelihood of angular induced neurotrauma and can lead to much improved headgear designs [50].

2.3.4 Finite Element Methods

Modern understandings of brain strain are the result of advancements in computational simulations of neurotraumatic events [132], [133], [134]. These utilise Finite Element (FE) techniques and often include standardised Human Body Models (HBMs) to recreate bio-realistic motion [132], [135], [136], [137], [138]. Popular models are validated with comparisons to radiographic imaging and cadaveric experiments, which both have limitations of time-dependent and decay effects [118], [139]. The benefit of FE methods is that the location and volume of concentrated strains can be directly evaluated and provide more detail on neurotraumatic pathologies, although at the disadvantage of being time consuming [140], [141]. Metrics derived from FE simulations include the cumulative strain density measure (CSDM) and maximum principal strain (MPS), which each correlate to injury severity [107], [108]. The success of these have resulted in many attempts to correlate with mechanical-based measurements and accelerate the injury assessment process [108], [125], [130], [142], [143], [144], [145]. Although the quality of FE methods and HBMs are improving, there are remaining inaccuracies for predicting brain deformation [107], [137], [142], [146]. This is particularly highlighted by a disparity between the models themselves for identical scenario recreations [147]. As result, and because simulated conditions are difficult to standardise, FE techniques have not yet been introduced in professional standards for headgear assessments [148].

2.3.5 Injury Criteria

Injury Criteria (IC) are formulae for predicting the more complex mechanics of neurotraumatic injuries, e.g. the effects of duration on acceleration tolerance, from more fundamental measures such as those already discussed [149], [150]. There are many IC, summarised in Table 2.2, although some of the most known are the *Gadd Severity Index* (SI), *Head Injury Criterion* (HIC), *Brain Injury Criterion* (BrIC), and *Head Impact Power* (HIP) [108], [151], [152], [153]. The formulae for each of these have different geneses although are founded on the assumption that injury is the result of linear motion, angular motion, or a combination of both. The adoption of IC within test standards was unfavoured until the recent incorporation of SI within the NOCSAE ND002-17m21 American Football helmet standard [15].

There is no consensus for which IC are the best predictors and much of the popularity is based on familiarity rather than performance [141]. Likewise, different IC have shown better predictive performance for specific types of injury, thus they likely need to be used in conjunction rather than isolation [141], [154]. For example, Levy et al (2021) conducted 672 mechanical impacts and found that UBrIC, BrIC, and DAMAGE were the strongest predictors of CSDM with R = 0.88, 0.91, and 0.92 respectively [154]. Conversely, Hernandez et al (2015) found BrIC to be the second least predictive kinematic IC for predicting on-field mTBI onset, whereas PAA was the best [150]. Zhan et al (2021) also found that PAA was the best predictor of mTBI from 2130 FE recreations of sports impacts [149].

Table 2.2, Popular kinematic Injury Criteria (IC). t = time, $t_0 = initial time$, a = linear acceleration, $\alpha = angular$ acceleration, $\omega = angular$ velocity, HIProt = the angular terms of Head Impact Power, $\beta = IC$ specific constants, $\delta = brain$ displacement calculated from viscoelastic mechanics. Subscripts: x, y, z = headform axes, i = each subsequent of x, y, z, c = critical constants. Superscripts: n, m, s = 2, s = time 1 and s = time 2 and s = time 3 and s = time 4 and s = time 3 and s = time 4 and s = time 3 and s = time 4 and s = time 3 and s = time 4 an

Kinematic Injury	Equation	Linear or
Criteria		Angular
Gadd Severity Index (SI) [151]	$GSI = \int_{t_0}^t a(t)^{2.5} dt$	Linear
Head Injury Criterion $t-t_0$ < 15 ms (HIC ₁₅) [114], [152]	$HIC = \left[(t - t_0) \left\{ \frac{1}{(t - t_0)} \int_{t_0}^{t} a(t) dt \right\}^{2.5} \right]_{max}$	Linear
Head Injury Criterion $t-t_0$ < 36 ms (HIC ₃₆) [114], [152]	$HIC = \left[(t - t_0) \left\{ \frac{1}{(t - t_0)} \int_{t_0}^t a(t) dt \right\}^{2.5} \right]_{max}$	Linear
Rotational Injury Criterion $t - t_0 < 36$ (RIC) [155]	$RIC = \left[(t - t_0) \left\{ \frac{1}{(t - t_0)} \int_{t_0}^t \alpha(t) dt \right\}^{2.5} \right]_{max}$	Angular
Brain Injury Criterion (BrIC) [108]	$BrIC = \sqrt{\left(\frac{\omega_x}{\omega_{xC}}\right)^2 + \left(\frac{\omega_y}{\omega_{yC}}\right)^2 + \left(\frac{\omega_z}{\omega_{zC}}\right)^2}$	Angular
Power Rotational Head Injury Criterion $t-t_0$ < 36 (PRHIC) [156]	$PRHIC = \left[(t - t_0) \left\{ \frac{1}{(t - t_0)} \int_{t_0}^t HIP_{rot}(t) dt \right\}^{2.5} \right]_{max}$	Angular
Rotational Velocity Change Index (RVCI) [144]	$RVCI = \max_{(t_0,t)} \sqrt{\sum_{i} \left[R_i \left(\int_{t_0}^{t} \alpha_i dt \right)^2 \right]}$	Angular
Universal Brain Injury Criterion (UBrIC) [157]	$UBrIC = \left\{ \sum_{i} \left[\omega_{i}^{*} + (\alpha_{i}^{*} - \omega_{i}^{*}) e^{-\frac{\alpha_{i}^{*}}{\omega_{i}^{*}}} \right]^{r} \right\}^{1/2}$	Angular
Diffuse Axonal, Multi- Axis, General	$DAMAGE = \beta_{max_t} \{ \vec{\delta}(t) \}$	Angular

Evaluation (DAMAGE)		
[158]		
Head Impact Power (HIP) [153] Generalized	$HIP = \sum_{i} \left[4.5 \left(\int_{t_0}^{t} a_i dt \right) \right] + 0.016 \alpha_x \int_{t_0}^{t} \alpha_x dt + 0.024 \alpha_y \int_{t_0}^{t} \alpha_y dt + 0.022 \alpha_z \int_{t_0}^{t} \alpha_z dt$ $GAMBIT = \left(\left[\left(a(t) \right)^n + \left(\alpha(t) \right)^m \right]^{1/s} \right)$	Linear and Angular Linear and
Acceleration Model for	$GAMBIT = \left\{ \left[\left(\frac{a(t)}{a_c} \right)^n + \left(\frac{\alpha(t)}{\alpha_c} \right)^m \right]^{1/s} \right\}_{max}$	Angular
Brain Injury Threshold		
(GAMBIT) [119]		
Principle Component Score (PCS) [159]	$PCS = \beta_0 + \beta_1 \cdot \overline{GSI} + \beta_2 \cdot \overline{HIC_{15}} + \beta_3 \cdot \overline{PLA} + \beta_4 \cdot \overline{PAA}$	Linear and Angular
Kleiven's Linear	$KLC = 0.004718 \cdot \overline{PAV} + 0.000224 \cdot \overline{HIC_{36}}$	Linear and
Combination (KLC)		Angular
[130]		
Probability of Concussion (CP) [160]	$CP = \beta_0 + \beta_1 \cdot \overline{PLA} + \beta_2 \cdot \overline{PAA} + \beta_3 \cdot \overline{PLA} \cdot \overline{PAA}$	Linear and Angular

Of the criteria in Table 2.2, injury risk curves (IRC) for mTBI (AIS2+) and sTBI (AIS4+) were found for HIC, BrIC, HIP, DAMAGE, RVCI, and UBRIC [108], [114], [125], [126], [145], [153], [161], [162], [163]. IRC make the selection of IC more relevant to headgear standards, as threshold values can be defined from what injury severity the headgear is expected to protect from. IC could benefit the PO standard as they improve representation of realistic injury mechanisms and can be used with mechanical test methodology. However, the selection of which IC are most appropriate for PO application is a significant challenge compared to using peak linear and angular kinematics, which have so far shown success in headgear improvements [16], [18]. A method for experimentally assessing which IRC are most appropriate for PO helmet testing is employed in Chapter 10 with a table summarising their known AIS 2+ and 4+ thresholds.

2.3.6 Section Summary

Brain strain cannot be directly measured in-situ, so it is common to predict injury with linear and angular head kinematics. Currently, the PO standard considers PLA as benchmark for helmet quality, although PAA has shown more correlation with diffuse injuries. Other helmet standards have included PAA as a threshold and studies have discovered benchmarks that correlate both of these to mild and severe TBI occurrence. However, these can be oversimplifications and only represent injury for durations exceeding ≈ 5 ms. IC offer a better representation of brain trauma from kinematic measures, although thorough study is needed for which IC are best suited for PO application. Similarly, FE techniques will provide a deeper understanding of brain injury than any kinematic measure, though these rely on high resource demand and a much-improved understanding of injurious conditions to be representative.

2.4 Head and Helmet Impact Testing

2.4.1 Test Setup and Systems

Experimental head impact assessments, i.e. non-clinical, are usually conducted one of three ways: mechanically in laboratory settings, computationally through use of FE analysis, or in-situ with direct instrumentation [12], [14], [118], [150]. Laboratory experiments are the only method used for blunt trauma energy attenuation assessment in standardised protocol, irrespective of the helmet application [18]. These commonly involve linear drops of helmet-fitted anthropometric representative headforms onto steel anvils [49], [164], [165], [166]. Though similar in their setup, the parameters amongst standards, i.e. impact velocity, location, angle, mass, surface, etc., vary to suit the application [14], [94], [167], [168].

Impact location has a large effect on injury mechanics due to the shape and mass distribution of the skull and brain [94], [122], [168]. Studies using animal cadavers and FE simulations mostly suggest impacts to the side of the head result in the greater peak accelerations and deep tissue strain than frontal impacts [61], [94], [103], [116], [168], [169]. The current PO test standard does not include an impact to the mid-coronal side of the head, only in front and behind this [13]. Impact angle

has shown to decrease PLA as the load vector shifts further from being radial [167]. This increases PAA until a maximum, \approx 30-45° relative to the headform longitudinal axis, before the lack of a radial component decreases the frictional/tangential force [106].

For a drop test, helmeted headforms are either free-fall or guided, the latter offering more control of impact location. Guidance can vary greatly between standards; common strategies to maintain head orientation include use of a cradle (common in European standards) or a rigid fixed arm (common in North American standards) [18], [170]. Rigid constraints are less popular in research, as they can over constrain headform rotation [171], [172], [173]. Likewise, cradled conditions can lack bio-realistic motion, as the head is free to rotate in any direction [173], [174]. As a result, many studies now use bio-realistic neckforms in their methods, although this has seen little uptake in test standards [18], [175], [176].

Alongside drop methods, the other most prominent head impact test methods use linear ram and pendulum systems, Figure 2.7 [12], [14], [177], [178], [179], [180], [181], [182], [183], [184]. These each use slider systems to permit translation of head and neckforms after impact, although they do not always affect head kinematics [174]. Table 2.3 summarises features for each of these methods, alongside drop tests, and includes critique of their advantages and disadvantages. Pneumatic rams are popular for testing American Football headgear and have now been incorporated in the test standard, alongside guided drops [15], [185], [186], [187], [188]. Pendulums are yet to be incorporated within test standards though are the chosen method for the Viginia Tech Summation of Tests for the Analysis of Risk 'STAR' rating system [189]. Both methods keep the headform/helmet stationary pre-impact thus impact location is suggested to be more repeatable [188].

Table 2.3, Review of systems for laboratory head impact testing with descriptions of their key features and advantages/disadvantages [190].

Method	Key Features	Advantages (+)/ Disadvantages (-)		
Guided Drop	Large structural tower.	+ High control of impact energies.		
[170], [172],	• Steel rail/cable	+ Ease of use.		
[191], [192]	guides.	+ Low relative cost.		
	• Drop cradle.	+ Small footprint area.		
	• Interchangeable	+ Can drop a helmet or an impactor.		
	impact anvils.	- Requires a large drop height.		
		- Requires one impacting body to be		
		fixed in place.		
Pneumatic	Pressurised	+ Maximum impact velocity is not		
Ram	accumulator.	dependant on ceiling height.		
[25], [177],	• Steel impactor rod.	+ Changeable impactor surface.		
[179], [193]	 Padded impact 	+ Permits inelastic kinetic energy		
	surface.	transfer with a linear slide table.		
	• Headform linear	- Large footprint area.		
	slider.	- Specialist maintenance and		
		servicing.		
		- Large relative cost.		
		- Little control of impact energies.		
		- Can produce lesser head kinematics		
		than drop methods [194].		
Pendulum	• Large pendulum arm.	+ Changeable impactor surface.		
[189], [195],	 Padded impact 	+ Low relative cost.		
[196]	surface.	+ Permits inelastic kinetic energy		
	• Headform linear	transfer with a linear slide table.		
	slider.	- Low range of impact velocities.		
	 Representative 	- Very large footprint area.		
	impact hammer	- Little control of impact energies.		
		- Non-representative impactor mass.		

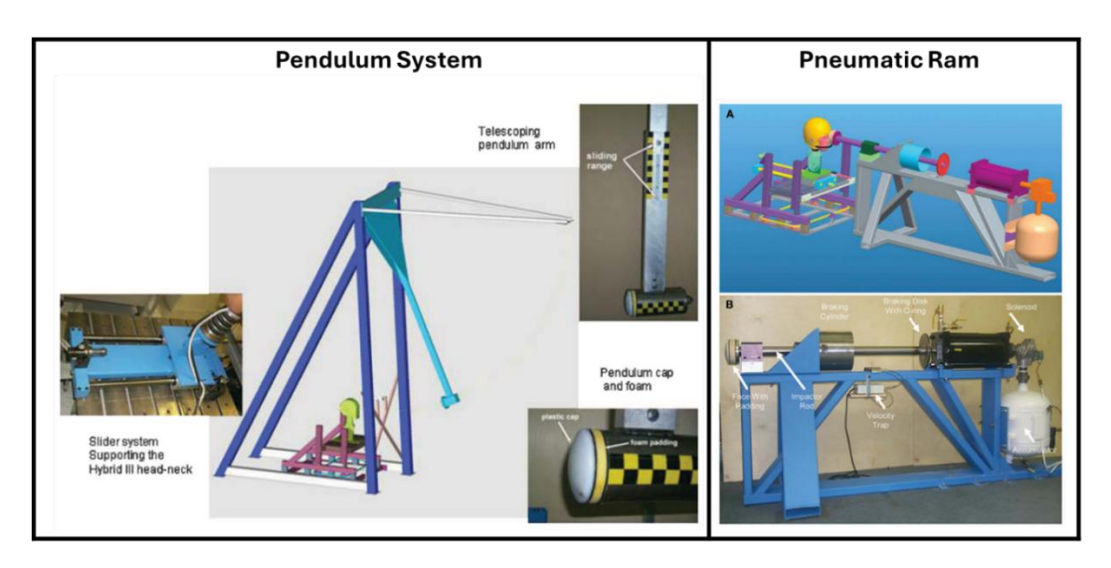


Figure 2.7, Examples of pendulum and pneumatic ram systems for laboratory head impact recreations [188].

2.4.2 Bio-realism

Test standards represent bio-realistic characteristics with use of anthropometric test device (ATD) headforms, usually representing the 50th percentile male [18], [118], [197]. The most common ATD models used in head impact research and standards are the Hybrid III (HIII) [198], NOCSAE [199], and EN 960 [185], [200], [201], [202], Figure 2.8. The HIII has shown to have realistic mass and moment of inertia (MoI) about the x-axis (roll) although slightly greater MoI about y- (pitch) and z-axes (yaw), which can affect rotational kinematic measurements [203], [204], [205]. The headform is made from cast aluminium with a removable elastomeric skin [206], [207], [208]. This skin has a frictional coefficient greater than expected for a human, which affects rotational inertia, leading to some artificially modifying the skin surface in experiments [167], [209], [210], [211], [212]. There have also been recent attempts to develop a new headform with more representative scalp properties, that looks to be introduced in standards with rotational impact criteria [213]. The HIII has bio-fidelic limitations, as do all headforms, although it remains the most popular headform in head impact research, thus making results more transferrable between head impact recreations.

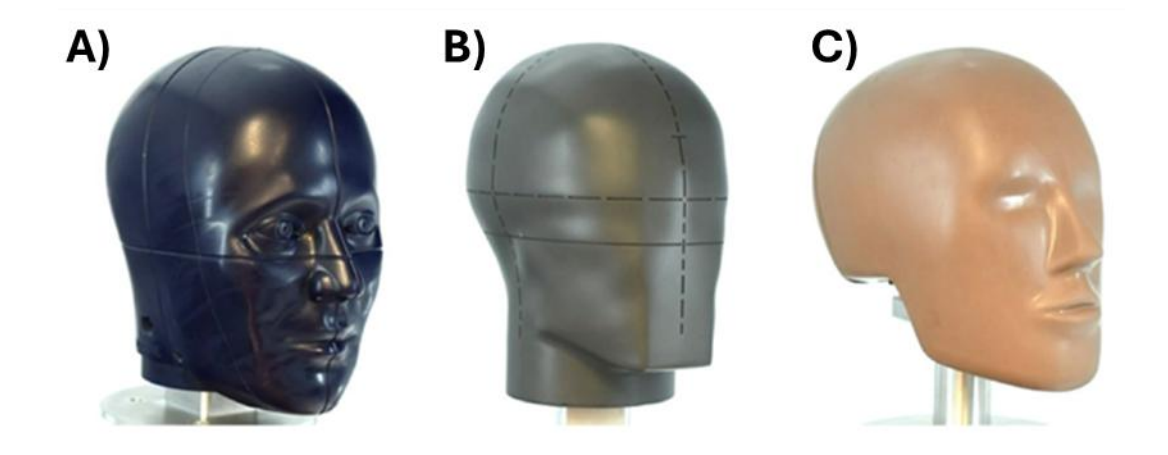


Figure 2.8, Common 50th percentile male headforms used in head impact research and helmet standards. A) NOCSAE, B) EN 960, C) Hybrid III [198], [199], [200], [201].

The HIII ATD is a full-body model with realistic joint degrees of freedom, including a bio-representative neckform [214]. The latter is composed of a series of cast aluminium disks, separated by rubber padding, and an off-central steel tension cable core. The directional stiffness properties of the neckform are inhomogeneous, similar to a human [173]. However, it is now firmly believed that only the flexion/extension stiffness is representative of human biomechanics, and a particular disparity is in the compressive stiffness [185], [188], [215], [216], [217], [218], [219], [220]. There are disagreements for whether a neckform is necessary to produce a realistic head impact response, with some arguing it only dissipates impact energy [221], [222], [223], [224], [225]. Of those that champion the use of a neckform, the effects on head impact response seem to vary [222], [223], [226], [227], [228], [229], [230]. Only two helmet impact standards are known to use neckforms with guided drop methods, despite their prevalence in head impact research [18], [118], [227], [231], [231], [232], [233], [234], [235]. However, neckforms are more commonly used with pneumatic ram and pendulum systems [21], [25], [48], [173], [174], [179], [182], [193].

2.4.3 Public Order Helmet Testing

The most recent UK standard for approval of Public Order helmets is 'PSDB 21/04', a specification set by the Home Office Police Scientific Development Branch [13]. This is also recognised as British Standard (BSI) Product Approval Specification

'PAS017'. The procedure includes a low-friction guided drop of helmeted EN 960 headform onto rigid anvils, Figure 2.9 [13]. A tri-axial accelerometer at the centre of mass is used for recording peak linear accelerations and velocity is measured 60 mm from contact. Impact sites are the front, crown, front left/right and rear left/right. These are broad areas relative to the anatomical planes of the headform and intersect a horizontal plane at the glabella height. Impact anvils are rigid steel and shaped to replicate the corner of a brick and a non-edged hand wielded cylindrical weapon, Figure 2.10. Pass criterion is peak acceleration less than 250 g for 120 and 60 J impact energies, and 150 g for another 60 and 30 J condition. Helmets must be conditioned at -20 and +50 °C for between 2 and 22 hours.

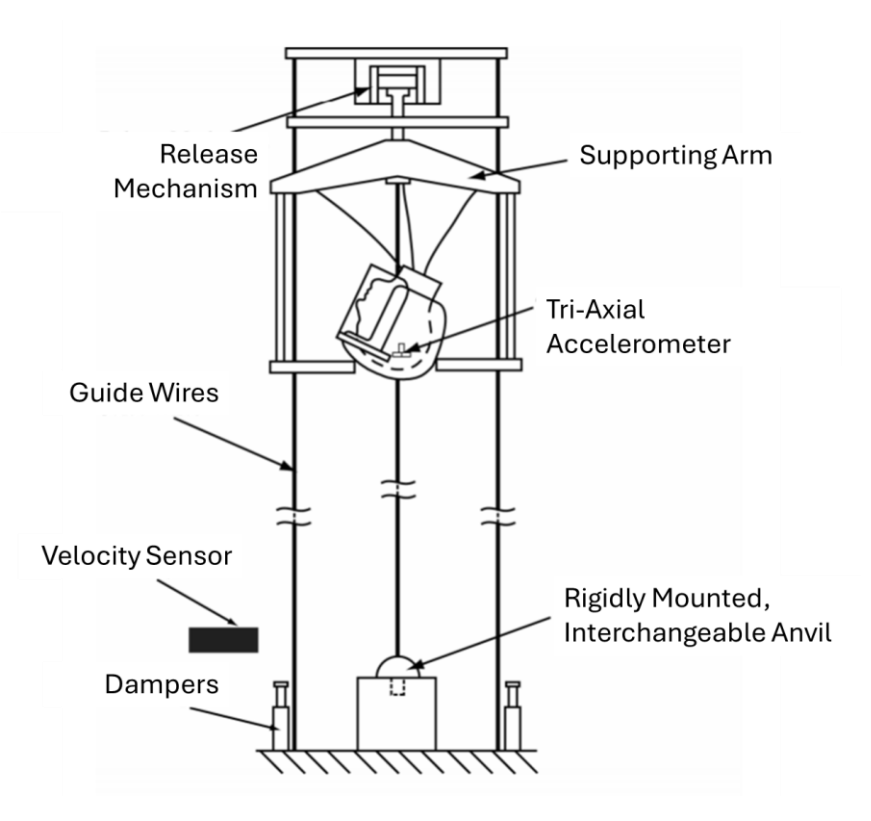


Figure 2.9, Schematic of the PSDB 21/04 standard procedure for assessing helmet energy attenuation [13].

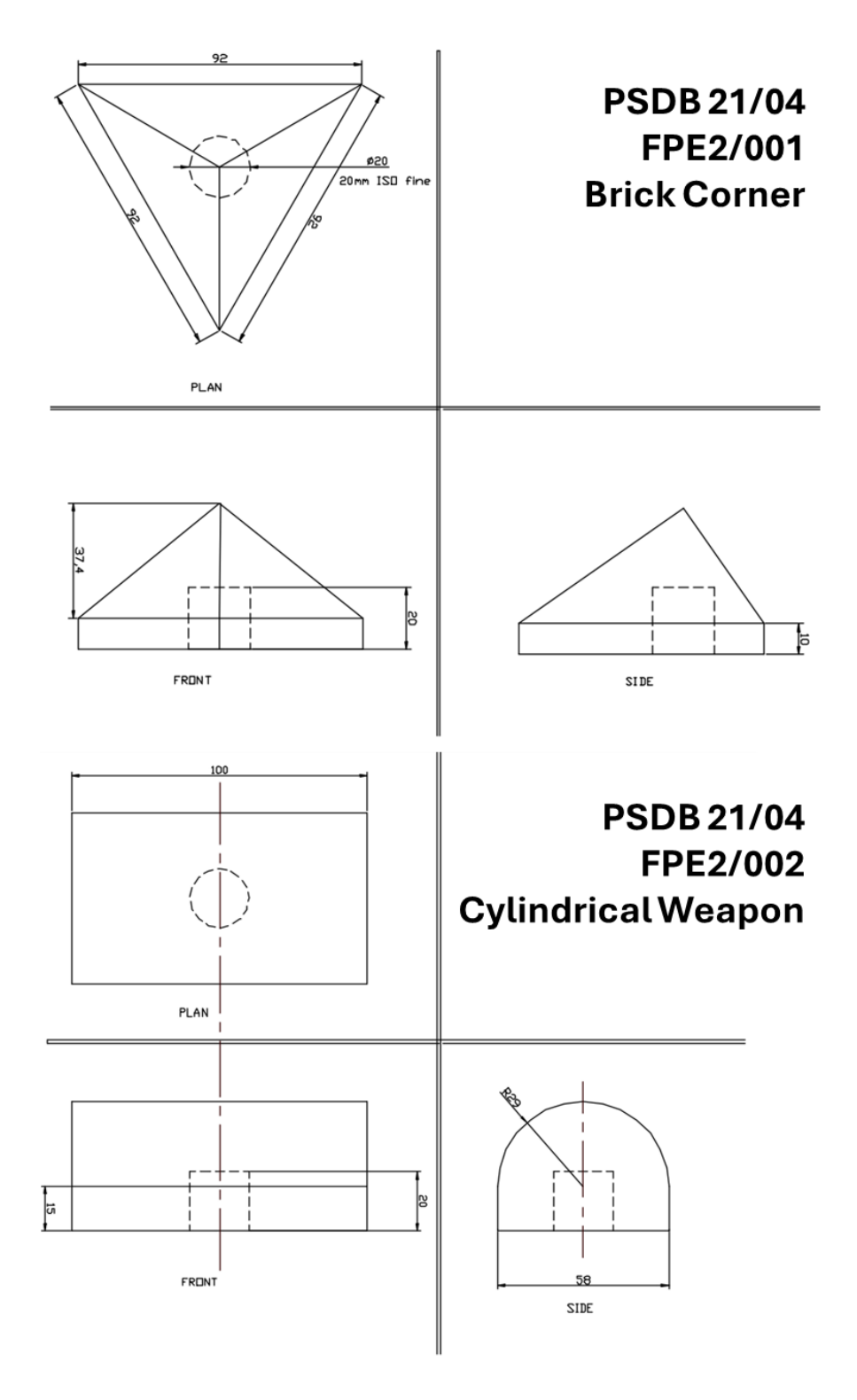


Figure 2.10, Impact anvils used in the PSDB 21/04 standard representing the corner of a brick and a curved hand wielded weapon [13].

The 120 J impact criterion is similar to motorcycle standards at the time of inception for PSDB 21/04. These also include guided drop methods, impact energies between 110 and 170 J, and slightly higher pass thresholds between 275 and 300 g [171], [236], [237], [238]. It is possible this was founded on the

assumption that motorcycle blunt trauma injury has a slightly greater severity to PO, yet it is not understood how impact characteristics translate between the two. 120 J is greater than almost all standards for non-vehicular sport applications, the only exception is Snell S-98 for skiing activity which is also 120 J [18], [239]. The estimated mass for a 50^{th} percentile male headform and PO helmet is ≈ 5.8 kg, the equivalent of 6.4, 4.6, and 3.2 m/s impact velocity to achieve 120, 60, and 30 J energies. The use of sharp-edged anvils suggests the authors were concerned with high-pressure impacts and aimed to reduce open neurotraumatic injuries with their methods. There is less consideration for closed form injuries, which could be better represented with more blunt shaped anvils. There is also a lack of concern for angular kinematics, with no non-linear headform measurement or oblique loading conditions. The threshold could also be improved further by considering a durational element alongside PLA, either in the form of IC or comparison to the WSTC.

The American equivalent PO helmet test standard 'ASTM E3343/E3343M-23' was first published in 2022 and is clearly based on PSDB 21/04, referencing it throughout [240]. Similar impact criteria are used for both standards, the only differences being use of a rigid arm monorail and the addition of flat and triangular impact anvils, which are standard ASTM equipment for headgear testing [170]. Separate to this, there is also the American National Institute of Justice (NIJ) riot helmet standard 'NIJ 0104.02', although this has not been revised since 1984 [241]. Key differences include a 300 g threshold for a 6.6 m/s impact velocity and 5.1 kg drop mass, impact locations at the front, side, back and crown of the head, and the use of a rigid test arm with hemispherical 48 mm radius anvil. PSDB 21/04 is the only PO helmet standard in Europe. The similarities between each of these test standards prevent any analogous inspiration and none elucidate injuries of concern beyond the apparent threat of sharp bricks and rounded wielded weaponry. However, all are lacking consideration of rotational induced closed form brain injuries, kinematic injury criteria, and possible neckform effects. The study of these effects could therefore have impact on both UK and American test methods.

2.4.4 Impact Monitoring and Instrumentation

Head impact exposure can be directly monitored with use of Inertial Measurement Units (IMU), usually placed at the centre of mass of headforms (CoM) [28]. The conventional polarity of these is the SAE J211 recommended instrumentation for impact tests, where x, y, and z refer to frontal, transverse, and longitudinal axes, Figure 2.11. This is relatively universal in head impact research, although some invert the +/- directions to suit their application [200], [242], [243].

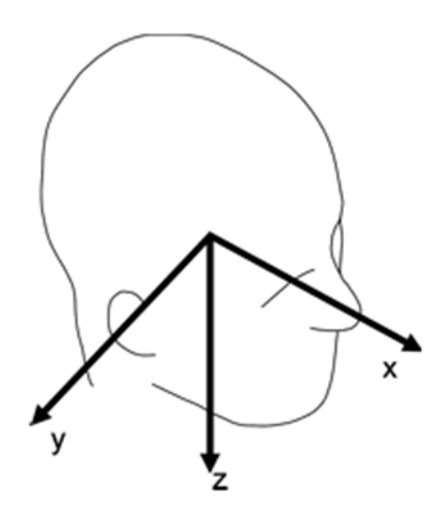


Figure 2.11, Headform polarity according to the recommended practice for instrumentation of headforms (SAE J211) [28], [244].

IMU's traditionally include an array of tri-axial linear accelerometers and angular gyroscopes for direct measures of linear acceleration and angular velocity, hence they have six degrees of freedom (6DOF) are also known as '3a3w' sensors [28], [245]. Angular acceleration can be computed by differentiating angular velocity by the sample interval, although this is known to amplify signal noise [246]. Common procedure is to apply the 5-point stencil method and average data to reduce noise, which is defined in the SAE J1727 standard for head impact data acquisition [247], [248], [249], [250]. Alternatively, one can use a nine-accelerometer array package (often called a '3-2-2-2' array or 'NAP') to directly acquire angular acceleration from tangential linear accelerometers and their known distance to the CoM [14], [251]. This was once preferred in head impact research, although they are comorbid with error from non-planar sensors [252], [253]. '6a3w' arrays permit direct measure of angular acceleration and velocity, although they are relatively more expensive, heavier, and larger than other sensor packages, thus appear less

in research [245], [251]. Data filtering is also defined in SAE J211, for a 3a3ω array they recommend a minimum 20 kHz acquisition frequency, Channel Frequency Class (CFC) 1000 filter (1650 Hz cut-off) for linear acceleration, and CFC 180 (300 Hz cut-off) for angular velocity [244], [254].

In-situ head impact monitoring is common practice within sports research [14], [150], [255], [256]. This involves direct kinematic monitoring of head acceleration events (HAE) through use of kinematic sensors and photogrammetry techniques [14]. Common in-field sensors for wirelessly quantifying HAEs include in-helmet systems such as the 'Head Impact Telemetry' (HIT) and mouthguards instrumented with IMU's (iMGs) [141], [181], [257], [258]. Other lesser-known methods have instrumented headbands, skin patches, and earpieces [197], [259], [260], [261]. The advantage of capturing in-vivo is measuring human-like motion with minimal invasion, which has led to advancements in head impact research, testing methods, and the development of standards [257]. However, in-helmet systems are expensive and require specialised product designs. iMGs have shown recent popularity and promising measurement validity, although there are concerns for user comfort, high false trigger rates, and said accuracy is largely dependent on maxillary fit [260], [263], [263], [264].

Video analysis is essential for in-situ measurements to accurately link HAEs to their causes and eliminate false triggers [141], [262], [265]. Video can also be used to measure impact conditions, i.e. inbound velocities and locations, and quantify realistic impact mechanics [266], [267]. This method uses photogrammetry to define real-world coordinates and track the positional data of bodies, although requires high-quality footage and accuracy depends on the user's skill [268], [269], [270]. This is well suited to sports applications, where there are set environments, frequent events, and quality media coverage at the professional level. For PO, the use of in-situ instrumentation and video analysis could help quantify HAEs and advise test standard impact criteria. However, the lack of set environment or irregularity of events will make the acquisition of meaningful data a challenge. Training conditions would be better suited, although the cause of injury would be less realistic and less dangerous.

2.4.5 Section Summary

Testing head impact conditions requires consideration of situational and biomechanical representation. The current PO standard uses a guided drop cradle system, similar to many European test methods. There are concerns for biorealism when dropping unconstrained headforms, as rotational motion is not constrained to the degrees of freedom of a neck. Alternative methods, such as pneumatic linear rams and pendulum systems, offer more realistic biomechanics but are rarely used in test standards and can produce lower peak kinematics. The current standard overlooks oblique loads and angular motion as a source of injury. Furthermore, the impact conditions seem advised from motorsports applications, while it is unclear how these translate to PO activity. The preference of sharp anvils over blunt surfaces highlights this standard focuses on open head injuries, which may neglect closed injury mechanisms.

2.5 Helmet Design

2.5.1 Helmet Energy Attenuation Mechanics

Generally, the role of a helmet is to dissipate impact energy so that less is transferred to the body [271]. Helmets usually consist of a retention system, comfort liner, energy attenuating layer (EAL), and hard outer shell [10], [70]. Most test standards include criteria for protecting from both blunt and penetrative forces [18], [118]. As aforementioned, current helmets have almost eradicated the occurrence of open head injuries, thus this section focuses more on blunt energy attenuation mechanics. However, in summary, penetration resistance is achieved by the stiff outer shell broadening a contact load to reduce pressure, which also has some energy attenuation benefit [10], [272].

EALs typically make up most of a helmet's volume and mitigate transfer of kinetic energy to the wearer by internal structural deformations [10], [273]. This creates a plateau in the compressive stress (σ) strain (ε) response of the material, which increases the absorbed strain energy per unit volume (W), Figure 2.12 [274]. The general purpose of an EAL is to maximise W, for which extending the plateau is always favourable. Common materials for this are cellular structures, usually foams, where deformations occur at the cell walls when compressed [271], [273],

[274]. These walls eventually contact one another, a process called 'densification' because the stiffness of the material increases and energy absorption becomes less efficient [275]. For this reason, EALs need to be tailored to their application, specifically this requires selection of relative stiffness/density [271], [276]. High stress applications require a stiffer EAL to avoid early densification, conversely too stiff and less energy will be absorbed [277], [278]. The challenge for headgear design is to maximise the effective range of the helmet for all conditions it is expected to face [20]. Viscoelastic materials are well suited to EALs for their strain rate dependent stiffness adapts to compression rate, i.e. impact velocity, thus broadening the helmets effective range [279].

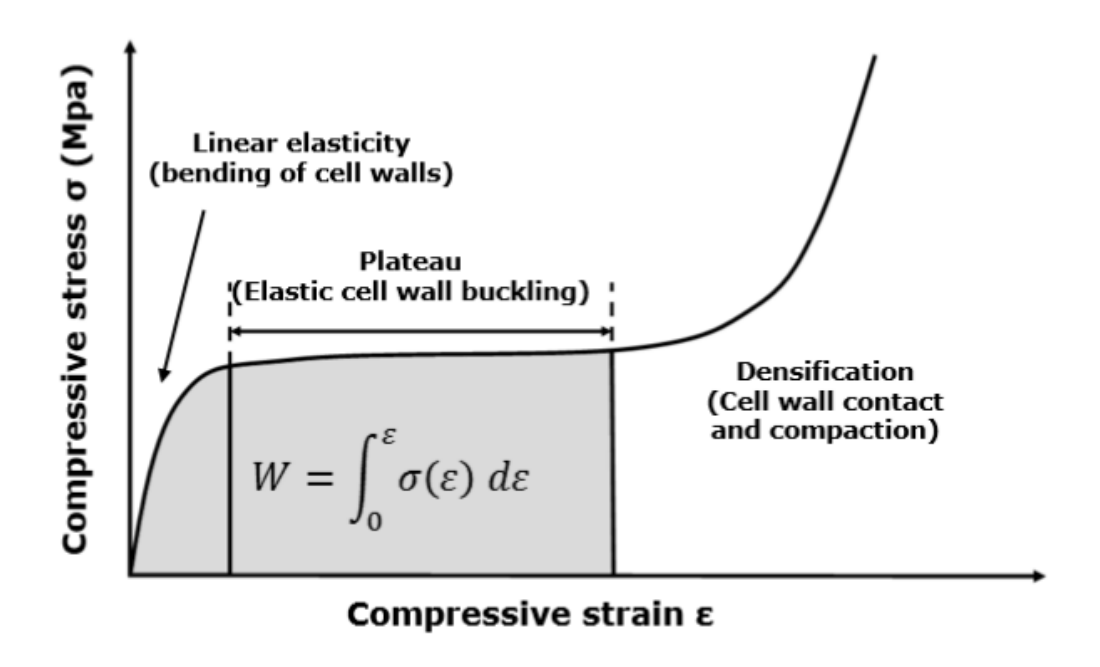


Figure 2.12, Compressive loading of cellular foams demonstrating strain energy absorption per unit volume (W) [274].

2.5.2 Helmet Features

There are two categories for helmets used in sports and automotive applications: single-impact ('crash') and multi-impact systems [9], [280]. The choice of which depends on the application, single-impact are used when activity tends to cease after a significant HAE, such as motorsports, cycling, and skiing [10]. The most common material for single-use headgear is expanded polystyrene (EPS), which is effective for reducing linear force but offers little angular protection [10]. After impact, helmets with these liners provide reduced protection and should be

replaced. Multi-impact helmets use more compliant materials that return to shape after impact [9]. These are more suited for applications such as American Football and Ice Hockey where multiple impacts can be expected in a game, although they still degrade over time [9], [281]. Common materials for these include expanded polypropylene (EPP), expanded polyethylene, vinyl-nitrile (VN), and other crosslinked foams [9]. Of these, only VN has shown some ability to reduce head rotation, although it has proven less effective for linear loads [280], [282], [283], [284]. In attempt to use linear effective materials but improve angular protection some helmets now include rotational slip planes; these permit slight rotation of the helmet (< 15 mm) relative to the head and can reduce angular acceleration [192], [215], [285], [286], [287], [288], [289], [290]. Modern attempts to reduce angular forces have included use of shear-rate dependent polymers and mechanical metamaterials [20].

The effective range for a helmet can alternatively be improved by increasing EAL thickness or including multiple layers of different stiffness [277]. However, increasing thickness requires a larger helmet; this can increase angular motion with a greater radius/torque on the head [9], [291], [292], [293]. Likewise, mass needs to be minimised because helmets must be comfortable, and distally distributed mass can increase angular momentum. EPS's popularity has mostly come from it being lightweight, as well as cheap to manufacture, easy to form, and capable of passing linear thresholds in standards [9].

2.5.3 Public Order Helmets

PO helmets require unconventional fire and chemical resistance considerations thus include features such as a fitted visor, ear coverings and a padded neck guard. As well as this, helmet features are limited in the materials they can use and the areas they must cover. The most popular PO helmet in the United Kingdom is the 'Defender' series, manufactured by MLA Ltd [2], [294]. A new 'Defender Hybrid' model was released in 2022, Figure 2.13. While the main updates were focused on the visor, the EAL and outer shell remained unchanged from the previous defender models. Notable features of this helmet are:

- The outer shell is a 28-layer glass fibre-reinforced polymer (GFRP) with flame retardant coating.
- The EAL is a singular layer of expanded polyurethane (EPU) foam.
- Thin polyurethane (PU) pads are added to the crown and along the rim of the helmet for size spacing and comfort.
- The 3 mm polycarbonate visor covers the face of the wearer and is attached with an aluminium rim.
- An adjustable and cupped chin strap is used for retention.
- The rear neck guard is made from a dual layer of 5 mm polyethylene and 13 mm medium density comfort foam (RX/200).
- Sizes range from between 510-640 mm head circumference with mass \approx 1.6 kg.



Figure 2.13, 'Defender Hybrid' PO helmet (MLA Ltd) imaged from the exterior and interior to highlight key features [2], [294].

GFRP shells are conventional in helmets, particularly for automotive headgear [9], [295]. Glass has the benefit of increased fire resistance compared with carbon and graphite fibres, although they are usually heavier [296]. Likewise, the size of these helmets are particularly large compared to traditional sports applications, the midrange size 3 for example includes > 50 mm of EAL foam in some regions. This can make the helmet uncomfortable for the wearer but means densification is unlikely.

However, this may not be the most efficient way to protect the wearer as the large radius may increase risk of rotational injuries.

Using EPU for an EAL is a less conventional choice for headgear, suggesting manufacturers use it to meet requirements beyond just energy attenuation. There are no known peer-reviewed sources that include impact assessment of EPU liners in helmets, although their application is common in packaging and cushioning [297]. EPU foam is similar to EPS in that it is a single-use crushable structure, although its stiffness has little strain rate dependence and is usually higher density (< 4.5 times that of EPS) [298], [299], [300]. This could mean the foam is effective for a very narrow range of loading conditions, specifically less-severe impacts may not be efficiently attenuated, which is a concern for high-density foams [277]. The current PO standard includes 'low energy' criteria (30 J) to evaluate this, although the threshold is the same as the 60 J condition and relatively high (150 g) [13]. Compared to Zhang et al's (2004) thresholds, this exceeds an 80 % risk for mTBI (= 106 g) [116]. Alternative PO headgear in the UK include the 'Argus' models; these are very rarely used in operation though have similar construction but with an EPS liner [301].

2.5.4 Section Summary

PO helmets, while unconventional, appear to be well-suited for mitigating high-energy linear impacts due to the thickness and relative density of an EPU liner. The exact protective performance of 'Defender Hybrid' helmets are unknown, only that they conform to PSDB 21/04 (< 250 g) [13]. However, there are no considerations for reducing rotational loads in their design, and their large size may exacerbate angular acceleration. A thinner EAL could reduce the likelihood of this, though adjustments would be needed to maintain linear protection, such as multi-layered liners. While PO helmets are restricted in terms of material choices, the use of a single-impact EAL seems unsuitable in situations where activity is unlikely to cease following an impact. These could be addressed with a revised test standard and will likely improve the protective performance of PO headgear for reducing TBI.

2.6 Chapter Summary

Despite the prevalence of head injury within PO scenarios, research for the causalities and mechanics of these is limited. Most helmet standards, including PO (PSDB 21/04), focus solely on mitigating linear impacts and use PLA as the criterion for energy attenuation. However, contemporary understandings reveal that angular motion, oblique forces, and impact durations significantly influence brain trauma severity. This suggests the focus on PLA alone neglects a broad range of head injuries, particularly diffuse TBI such as concussion and DAI. Signs for this are shown in current headgear designs, as the 'Defender Hybrid' helmet offers no rotational protective structure, and its large size may exacerbate angular forces.

It is imperative that helmets are evaluated under PO representative loading conditions. The preference of sharp and curved impact anvils is suitable for open form head injuries, although research suggests more blunt mechanics may occur in PO activity, such as falls and physical strikes. However, further research is required to address specifically what causes these injuries, and their expected loading mechanisms. In response, a four-stage research strategy was devised, advised from Meaney, Morrison, & Bass' (2014) model and common practices in the Sports Engineering sector [30].

- 1. Identify Public Order specific injury causes.
- 2. Quantify the loading conditions for these causes.
- 3. Recreate impacts for more detailed injury assessment.
- 4. Advise requirements for adaptation within the test standard.

Implementing these could lead to a more comprehensive and effective test standard, thus encouraging helmet innovation and reducing head injury occurrence in PO activity.

3. Causes of Head Injury in Public Order Conditions

3.1 Introduction

This chapter aims to elucidate the causes of head injury in PO applications by identifying weapons commonly used against PO officers and the threats they present. The lack of codified rules and controlled environment for PO result in a wide range of possible threats, more so than in most sports. For example, legislation in Rugby has been introduced to reduce the occurrences of tackle positions that were common causes of head injuries [302], [303]. A threat to head injury in PO scenarios is worthy of note if it is prevalent and/or dangerous, i.e. severe injury would be the result of an impact. The perceived danger of a threat can be estimated from the kinetic energy at the point of impact, considering the effective mass and velocity of both the person and impactor [304], [305], [306]. Sharp objects, though significant for causing bodily harm, are not a significant threat for blunt trauma injury and thus not considered in this study. The objectives of this chapter were therefore to:

- Identify the scenarios within PO activity that are a prevalent risk of head injury.
- Categorise blunt weaponry based on their prevalence, use, and characteristic properties.
- 3. Define representative head impact scenarios that would better ensure the efficacy of headgear if incorporated within in the PO helmet test standard.

3.1.1 Head Impact Monitoring

In-situ instrumentation used commonly to investigate head impact within the sports sector, such as the use of IMU's or motion tracking, is less ideal for PO applications [14], [150], [255], [256]. This is because there is no set environment or regular occurrence to PO events. This makes the setup of video capture equipment that is suitable for the quantitative analysis of head impact almost impossible. Video capture is crucial for traditional head acceleration instrumentation, such as HIT and iMGs, as it is used to timestamp loading pulses and correlate kinematic data with a description of the event [150], [262], [269]. The in-field use of iMGs is a

risk, despite their benefit of being more accurate than HIT, as they would hinder the ability of officers to communicate. Furthermore, the amount of useful data that could be gathered from PO situations is limited, due to the rare occasions of events and no guarantee of a riot or injurious occurrence emerging. With no control of the level of disorder that could occur in these events, a small sample size may belittle the dangerous situations officers face and could lead to inappropriate recommendations for a test standard.

Officers in the UK train in mock streets for situational realism, Figure 3.1. Instrumenting officers in PO training events could overcome the challenges of no set environment and irregular occurrence. Metropolitan Police training sessions do not purposefully injure personnel, although they use 0.5 kg wooden bricks and small petroleum filled glass bottles, both representative of common projectiles officers may encounter. These are considered unlikely to cause significant blunt trauma injury. Nevertheless, such reenactments would present the opportunity to set up camera equipment in these 'streets' and capture faux riot events with potential injurious occurrences. However, any data captured would be low severity with no clear understanding of how these impacts translate to a higher severity condition. It should be clear that to recreate or force any real incident in a training scenario for research purposes would severely breach ethical practice.

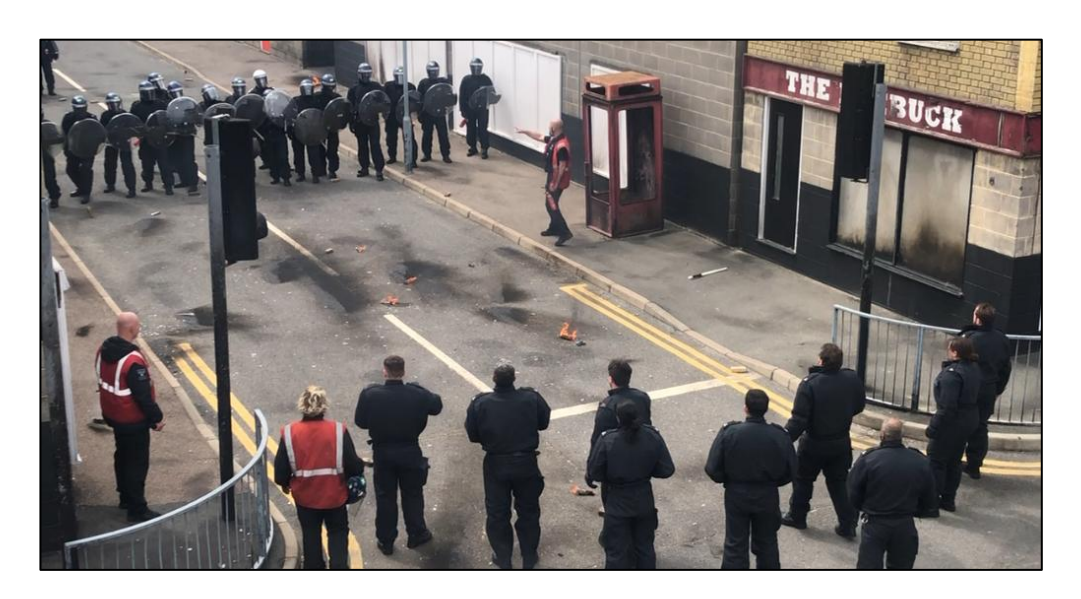


Figure 3.1, Snapshot of a Public Order training session at the Metropolitan Police Specialist Training Centre, taken May 2022. Here, officers can be seen helmeted and armed with shields and batons. Officers in the foreground are armed with projectile flammables and wooden bricks to simulate 'rioters'.

In informal conversation with protective security engineers in employment of the Metropolitan Police Physical Protection Group (MPPPG) who have supported this body of work, it was made clear that public rioters use 'whatever they can get their hands on' in order to injure officers. This in the most is anticipated to consist of bricks and stones. For this reason, when a public either becomes or has the potential to become disorderly, officers will order the closure of nearby building sites and strategically manoeuvre the public from such places where potential projectiles could be sourced. Another keynote from this conversation was the public may bring objects from home to cause bodily harm, such as knives, tools, and sports bats/clubs. Formal documentation of head injury events was requested from the MET, however these were not available at the time and no further details were disclosed.

In order to build detailed understanding of potential head injurious scenarios and the prevalence of weaponry faced by PO officers, it was necessary to use video content analysis, a technique for theming commonalities between incidents captured in media [307]. This is commonly used in the sports, automotive, and public health industries for identifying injurious events and risks [308], [309], [310]. Additionally, if footage of high enough quality can be obtained, photogrammetry can be used to track the position of weapons or threats and offer insight into typical impact velocities and energies for identified risks [141], [262]. However, this requires a set reference for calibrating image frames to real-world coordinates, which may be a challenge if footage is of low quality [268], [269], [270].

3.2 Method

3.2.1 Data Acquisition

Video content analysis was conducted using footage of PO scenarios accessible in the public domain. This was considered more optimal than capturing new footage, as it provided a larger data volume and was quicker than waiting for disorderly Public Order events to occur. Google and YouTube search engines were used to find videos using the phrases in Table 3.1. Click-throughs, pop-ups, and recommendations from websites were used to accelerate population of the database.

Table 3.1, Search engine phrases to source video data of violent riot conditions from the public domain.

Search Engine Phrases

- "Videos of riots"
- "Violent riot footage"
- "UK officer injured in riot"
- "Videos of riot violence"
- "Riot footage compilation"
- "Police officer suffers head injury in riot"
- "Violent riots UK"

The selection criterion favoured videos of incidents in the UK, though permitted those from other countries. This was because choice of blunt weaponry did not seem dependent on geographical location, political policy, or economic status. The use of other weaponry, such as flammables, explosives, and firearms, were apparently dependent on video location though were not the focus of blunt trauma injury and were therefore omitted from this study. Likewise, video of incidents with militaristic intent or backing were excluded so to not saturate footage with non-publicly available weaponry. Videos also had to be of events in the last 15 years to ensure data is contemporary. Efforts were made to not include more than 15 minutes of footage from the same event, so not to bias data with what was available in that condition.

3.2.2 Data Analysis

In total 81 videos were sourced, accumulating to 5 hours and 12 minutes of footage (Appendix A.3.1). The average clip time was 3 minutes and 51 seconds. Most videos were uploaded by commercial news organisations, though typically included clips recorded by the general public. The occurrence of visible head impacts, situations likely to result in head impacts, and blunt objects/weapons being used were individually counted and accompanied with a concise description (Appendix A.3.2).



Figure 3.2, Screenshots from videos in the content analysis of riot scenarios. Highlighted are example weapons that were identified as likely to cause severe blunt trauma head injury [311], [312].

Dangerous objects were recorded as a singular event, not by count of what was visible in that instance. This avoids biasing data with a moment where an object may have been prevalent. For instance, a clip showing multiple glass bottles would be counted as a single occurrence, rather than counting each bottle separately. The inter-rater repeatability for identifying instances with dangerous objects was assessed between two independent observers using Cohen's Kappa statistics (k) [310], [313], [314]. This method was deemed appropriate considering the subjectivity of decisions by the raters and that k compensates for the probability of any agreements made coincidently. The analysis was structured with a binary coding for each rater so that 1 = observation made and 0 = observation not made (Appendix A.3.3). Lastly, dangerous objects were categorised to reduce the substantial number of recorded threats into more comparable groups. Objects were clustered for their similarities in material, shape, and how the public was using them. Disagreements in assigned categories between the two raters were discarded from the dataset so to not falsely skew results.

3.3 Results

Analysis of Public Order footage produced 23 accounts of visible head impacts, 35 dangerous situations, and 49 instances of blunt objects being used in attempt to harm police officers, Table 3.2. Head impacts were predominantly caused by thrown projectiles (n = 8), followed by wielded implements (n = 7), then physical attacks such as a punch or kick (n = 3). Head impacts with the surrounding environment, such as the ground or a nearby wall, also occurred as a result of a physical attack (n=2). Officers equipped with shields experienced head impacts transmitted through or from the shield, as rioters would hit their shields into them with physical strength or blunt objects (n=3).

Table 3.2, Occurrences of events that can be linked to head injury likelihood from footage of riot conditions.

Content	Description	Occurrence
Head impact	A clearly visible impact to an officer's head.	23
Dangerous	An instant where a head impact is likely and not	35
Situation	visible.	
Dangerous	A visible blunt object used by the public to attempt	49
Object/Weapon	harm.	

Dangerous situations were predominantly crowded instances with close-quarters violence or groups of officers covering from thrown projectiles. Videos also showed dangerous situations with officers mounted on horseback and facing abuse from the public (n = 10). In cases, this caused a visible loss of control of the horse. One of these situations resulted in a head impact that hospitalised the officer [315].

A wide variety of blunt objects were used in attempt to harm officers. Documented examples include bricks and stones, fence posts and poles, sports equipment such as skateboards and bats, and streetside objects such as traffic signs. There were also situations where the public would take police batons and shields from officers to use against them (n = 4). Inter-rater reliability for the identification of dangerous objects was considered "almost perfect agreement" (κ = 0.85) with a 93 % agreement and 51 % chance of agreement.

Dangerous blunt objects were first categorised as either wielded or projectile, based on how the public used them. Wielded objects were sub-categorised by the perceived material, i.e. wooden or metallic, and shape of the object. 'Wooden

beams' encompassed 12 of the 23 documented wielded weapons, and mostly included objects such as fence posts, picket signs, and sports bats. 8 implements were categorised as 'metallic poles' and mostly contained pipes and bars. Police batons are commonly made from hardwood, high-strength metals, or hard polymers. In this analysis, batons used against officers (n = 2) were considered metallic because impact force is suggested to be similar between materials, though steel batons are typically narrower and impart greater pressure [316], [317], [318]. The remaining 3 wielded weapons categorised as 'other' were a traffic barrier and 2 cases of stolen police shields swung at officers. Wielded wooden and metallic weapons were also thrown at times; these were logged as wielded because it was believed they would cause a more severe injury if impact should occur this way. Of the 26 visible projectile weapons 18 were 'bricks and stones'. The remaining 8 'other' included equal counts of glass bottles and common streetside objects, such as bins and traffic cones.

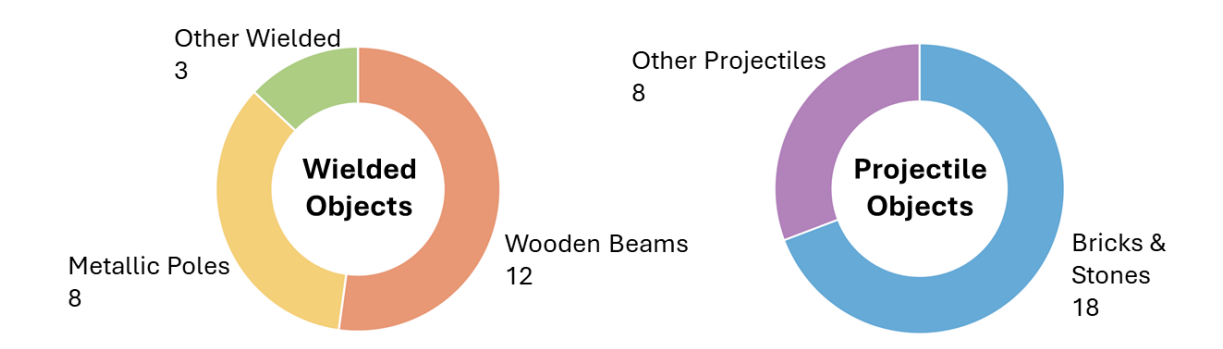


Figure 3.3, Categorised occurrences of prevalent blunt objects used in PO that are a danger of causing head injuries. Numbers are the accumulative occurrences taken from five hours of riot footage.

Table 3.3, Prevalent objects used as weaponry in public order conditions with description of their common characteristics.

Object	Common Material	Presumed mass (kg)	Typical morphology	Surface	Use in riots
Construction brick	Clay. Concrete.	2 to 4	Rectangular cross section. UK bricks are usually 215 x 102.5 x 65 mm.	Hard and rough surface. Flat faces with sharp edges.	Thrown. Dropped from elevated height.
Fence beam	Treated softwood.	0.5 to 2	Square or rectangular cross section. Edges 25 < 100 mm. Lengths 500 < 2000 mm.	Treated hard surface. Flat faces with sharp edges.	Wielded by the public and swung to cause injury. Sometimes thrown.
Construction pipe/tubing	Steel alloy. Aluminium. Copper. Lead.	0.5 to 5	Circular cross section. Diameter 20 < 60 mm. Lengths 300 < 3000 mm.	Hard and smooth surface. Curved faces.	Wielded by the public and swung to cause injury.
Sports Equipment	Hardwood (skateboards), Softwood (cricket bats). Fibre- reinforced composites (Ice hockey sticks). Aluminium (baseball bat).	0.5 to 2.5	Broad range of cross sections including flat and curved faces. Few sharp edges. Lengths 700 < 1500 mm.	Hard and smooth surfaces. Curved edges.	Wielded by the public and swung to cause injury.
Police baton	Steel alloy. Aluminium. Hardwood. PVC plastic. Vulcanised rubber.	0.5 to 1	Circular cross section. Diameter 10 < 60 mm. Lengths 300 < 1000 mm.	Hard and smooth surface. Curved faces.	Wielded by the public and swung to cause injury.
Drink bottle	Glass.	0.1 to 1	Circular cross section. Diameter 10 < 60 mm. Lengths 150 < 500 mm	Brittle surface. Curved faces. Sharp edges.	Thrown projectile.

3.4 Discussion

Video analysis comprehensively shows situations and objects that are likely to result in head injury for PO officers. The method offered a means to collect contemporary data without interfering in PO operations or with in-situ personnel. Inter-rater reliability (k) suggests "almost perfect agreement" between raters for the coding of dangerous objects in PO situations [310], [313], [314]. The differences in coding were due to raters missing the occurrence of a visible object and it was seemingly irrespective of which category that object would be grouped into. There was one disagreement between raters for the categorisation of threats; one observer recorded a projectile as a stone while the other coded a glass bottle. In this scenario, the incident was discarded so as not to misalign data.

The most prevalent threat that could result in head injury was from projectiles identified as bricks/stones, thrown by members of the public. The supports statements from the MPPPG and validates why the MET replicate thrown brick conditions in PO training operations. A brick impact is likely to be severe, as they typically weigh over 2 kg and can be thrown at a considerable velocity.

Documented throws were usually from ground level, the same elevation as the responding officers, although occurrences happened where the public would throw objects from a higher elevated position. In these situations, injury severity could be more severe due to greater potential energy.

Wielded objects were a common feature in footage, though varied greatly in specificity of use. As suggested by the MPPPG, these seemed to be mostly "findable" objects from the local built environment, such as fence posts, scaffolding poles, and pipes. If wielded objects were not common in the local environment, they were usually household sports equipment or police equipment taken from officers. Wielded objects were usually swung along the vertical plane in a downward motion onto officers, though incidents were also observed where they were jabbed and thrown. This is because situations were usually crowded and prevented individuals from swinging in any other plane. There was an apparent geometry difference between the wooden and metallic objects. Wooden implements were commonly a square cross-section whereas the metallic were circular. In addition, there is likely a large difference in the masses and

compliance/hardness of these two categories due to the respective densities of material. It is therefore expected that the two most prevalent categories of wielded weapons would have different impact characteristics. The demand for a helmet design that would effectively protect from both could be challenging. Wielded objects were estimated to be mostly between 0.5 and 1.5 m in length, long enough to cause harm but easy enough for someone to swing and carry. However, the nature of video analysis is that larger objects would have been more recognisable to observers, thus it is likely that smaller objects could have been missed by both raters. Larger objects will also typically have more mass and are therefore likely to result in more severe impacts than smaller objects. They can therefore be considered a greater threat and more appropriate for representation in the test standard. Objects in the 'other' categories, such as glass bottles and roadside equipment, were not prevalent enough for their own distinctive category. They were also considered to be of similar or less severity to the more prevalent threats and thus less important for consideration in the test standard.

The footage included 10 instances of officers mounted high on horseback with only one visible head impact. However, many of these instances were considered dangerous situations as the public would throw objects or harass the horse while the officer was saddled. The recorded head impact incident was a collision with a traffic light as the officer lost control of a startled horse and was the knocked to the ground. It is likely the head-ground impact when falling from a horse would be within the upper range of head injury severity, due to fall height and the body mass increasing impact energy [231]. Helmets for equestrian activity are a current focus in research, with a new standard released in 2023 [19], [319], [320]. Falls from horseback may be a condition worth representing in the standard to better provide protection for horseback mounted officers.

Officers were often equipped with shields in attempt to mitigate threats, though it was clear that shields did not completely prevent the chance of head impact occurring. For example, projectile and wielded objects that officers did not see would pass over the protective shield. In cases, officers received repeated head impacts as their own shield was hit against them, either by a blunt object or the physical strength of the rioters. Visibly, these did not cause a significant enough

injury to immediately deter officers from their duties. However, it is known that repeated low-severity head impacts can affect long term brain health, including the development of Chronic Traumatic Encephalopathy (CTE) [321], [322]. Further work could explore this effect to advise what requirements there are for PO headgear to attenuate repetitive low-risk impact energies.

The identified threats from this work can contribute towards the development of a standard test procedure that better represents the in-field conditions. For example, in lab based mechanical impact assessment, impacted anvil forms should be representative of threats to ensure effective helmet attenuation is met. The PDSB standard currently includes anvils with a sharp edge and the curved face of a cylinder [13]. These would suitably represent the geometry of a metallic pole or the corner of a projectile brick. However, the current PO helmet standard does not address blunt trauma from the flat surfaces of bricks or beams, nor a fall to the ground. Flat impacts would have different loading characteristics to curved and edged surfaces because the load is applied over a broader area and the helmet would indent less. It has been shown with motorcycle helmets that impacts from flat anvils consistently resulted in greater injury risk across six different injury metrics when compared with hemispherical curved and kerbstone edged anvils [46].

The video analysis method, while valuable for identifying threats, did not allow for the capture of kinematic data using photogrammetry. This was primarily due to poor video quality, low lighting, and the lack of fixed camera reference points meaning measures would not be accurate or repeatable between videos.

Therefore, in this qualitative study no descriptive kinematics for dangerous objects could be obtained. This data could be useful for advising appropriate parameters and conditions for helmet test standards, i.e. impact velocities, locations of impact, and angles. Matching impact velocity could be important to ensuring that helmet material components are appropriate for use, particularly as the mechanical properties of viscoelastic materials depend on the rate of strain [20], [271], [277], [278]. The loading characteristics and resultant injury likelihood of prevalent injury conditions identified in this chapter, i.e. projectile bricks, wielded

wooden and metallic implements, and falling from horseback, are explored in Chapters 4, 5, and 7.

3.5 Chapter Conclusion

Video analysis has elucidated scenarios and associated weaponry that are likely to result in head injury for PO conditions. 78.3 % of visible head impacts (n = 23) were due to weapons used by the public. Of all accounts of weapons being used (n = 49) bricks and stones were the most prevalent (36.7 %), followed by wooden (24.5 %), and metallic (16.3 %) implements. 35 dangerous situations were recorded where head injury was likely but not visible, 10 of these involved officers on horseback with one account of seemingly severe head injury occurring to a mounted officer who fell from their horse. It is apparent that the current PO standard test method does not fully address the identified variety of threats officers are subject to, for example it does not simulate impacts from flat surfaced objects like bricks and wooden beams, which are the most common choice of weaponry. The impact characteristics, velocities, and energies of prevalent threats could not be quantified from the video as direct kinematic measurements were not possible due to poor video quality. To obtain such metrics, mechanical or computational experimental means are required for quantified data. Tested conditions should include projectile bricks, swung wooden, and metallic implements. In addition, testing head-first falls from horseback provides comparison for weapon threats with a severe impact scenario known to happen in PO conditions. This would ensure that prevalent and dangerous scenarios for head injury are better represented in the test standard and can advise the development of more scenario appropriate headgear.

4. Injury due to Wielded Blunt Implements

4.1 Introduction

Head injury risk in PO conditions is attributable to the prevalence of projectile bricks/stones and wielded beam-like implements used by the public, as discussed in chapter 3. Horseback mounted officers are also at substantial risk of injury, should events cause a head-first fall to the ground. To appropriately advise PO specific standard procedures, each of these require a quantified account of their respective loading characteristics and associated injury severity. This cannot be accurately assessed from existing source video material using photogrammetric techniques, as described in Chapter 3, thus the decision was made to determine values through experiment. The differences in loading conditions for each scenario requires a different setup procedure to remain representative of the in-field conditions, i.e. thrown, swung, and falling. Experiment investigating injury attributable to falls from height, and thrown projectiles, are presented in Chapters 5 and 7. This chapter outlines data collection for injury characteristics due to wielded blunt weaponry, such as seen in Figure 4.1. To achieve this, the following objectives were set:

- Simulate wielded weapon impacts with representative loading and biomechanical constraints.
- 2. Quantify key metrics for defining impact mechanics and injury risk due to wielded weapons.
- 3. Advise which metrics can be used to better represent wielded weapon conditions with more repeatable test methodology in a test standard.



Figure 4.1, Example of rioters wielding blunt weaponry, taken from video footage of riots on Youtube.com [311].

4.1.1 Methods for Recreating PO Conditions

Loading conditions in PO situations can be quantified with human-like biomechanical representation in place of live participants. Live data capture is unlikely to produce appropriate results within the time restrictions of PhD study and has potential to belittle the dangers officers face. Lab-based mechanical recreations and computational simulations are both appropriate experimental means for maintaining realism with the use of anthropometric test devices (ATDs) and human body models (HBMs), respectively [133], [234], [323].

Use of computational methodology, such as FEA, allows for high control over loading conditions, i.e. impactor characteristics, impact locations, speeds, and angles [141], [295]. It also permits in depth analysis of brain injury response, such as identifying diffuse and haematoma injuries [107], [147], [324]. Although the use of FEA can provide valuable insight and is a powerful tool, issues exist regarding the consistency of modelling approaches and the validation of results. Although HBM's are validated with realistic means, i.e. cadaveric and volunteer datasets [139], [253], [324], [325], different models can produce disagreeing results for identical HAEs [30], [136], [326]. Validation of FEA with PO can currently only be made through visual comparison of the external body impact response, using exemplary video footage of an incident or scenario. As previously discussed, it is not possible to obtain kinematic data that could be used in validation, nor is it

possible to understand the internal damage mechanisms to the brain in these scenarios that researchers often attempt to predict.

In this investigation it was therefore decided to conduct experiment mechanically with ATD's. This guarantees realistic physical phenomena and obtained results for headform kinematics could be used to aid validation of any future FEA validation for future work undertaken. It is also less assumptive to identify the limitations of an experiment using an ATD, such as concerns for representativity of neck stiffness, than it is to assume the sources of error in a simulation [136], [327].

Mechanical recreations should remain as true to in-field loading conditions as possible. Common experimental means for recreating head impacts in a lab, such as those using a drop rig, excessively control impacts to make them more repeatable and improve data quality. For example, few sports helmet test standards include use of anthropometric neckforms [18]. Such assumptions remove biomechanical phenomena which can affect the heads response to mechanical force [221], [227], [229]. Therefore, testing with repeatable methodology at this stage raises too many questions for the representativity of impact recreations. The aim of this study was to produce methodology that closely represented each of the following in-field characteristics, while further steps to recreate impacts with more repeatability are discussed in Chapter 8.

- 1. Morphology and material properties for the cause of injury.
- 2. Biomechanical constraints of the head and human body.
- Representative impact conditions: velocities, angles, and locations on the head.

Video review of PO conditions showed 87 % of wielded weapons could be categorised as either wooden or metallic implements. The typical morphology and material characteristics of these have been previously obtained and are summarised in Chapter 3, Table 3.3.

The exact biomechanical constraints of the human head and body are not fully recreated by ATD's but they are designed to be representative. ATD headform inertial and mass properties are built to replicate a generalised anthropometry of a

specific population, i.e. 50th percentile male. Likewise, the neckform motion is constrained to similar degrees of freedom as the human neck [328]. Currently, there are no validated procedures for mathematically translating kinematic measures between headform sizes, though there is evidence that size effects the form of sustained injury and its likelihood [329], [330]. Multiple ATDs are required to represent more than one population in mechanical testing, making thorough investigation expensive. However, different anthropometric conditions could be tested with FEA simulation, using standardised ATD models of different populations [331], [332].

In this instance, it is intended to impart impacts in a manner representative to those seen in the field, rather than through the use of an impact rig [234], [323], [333]. Chapter 3 explained how the public would almost always swing implements downwards along a vertical plane. Although officers would typically be facing the public during operations, vertical swings could still impact any location on the head. Impact locations in PSDB 21/04 are defined as the front, crown, and front/rear left/right, i.e. impacts anterior and posterior to the mid-coronal plane of the headform [13]. Impacts to bare headforms at 5.5 m/s have shown that side impacts nearer to the front/rear produce significantly lower PLA than impacts normal to the mid-coronal plane (front side = -23 %, rear side = -30 %) and that PAA is only larger for more rear side impacts (front side = -1%, rear side = +22 %) [334]. The current standard defines PLA as the pass threshold metric, therefore mid-coronal plane side impacts may be better suited for PO threat recreations.

4.1.2 Injury Risk for Wielded Blunt Weapons

It is difficult to predict which of wooden and metallic implements are more of a threat to head injury from solely information provided by video review, although some predictions can be made. The flat surface profile of a wooden beam can induce greater headform acceleration than the curved profile of a metallic pole, if they were swung under identical conditions [46]. Conversely, a metallic implement can have a less compliant surface than wood, which has shown to significantly increase peak headform kinematics [193], [335], [336], [337], [338], [339]. Both of these assume identical kinetic energy at impact, whereas maximum swing velocity

is restricted by the moment of inertia (MoI) about a centreline at the butt end of rod and beam like objects (I_o) [340], [341], [342]. This relationship is determinable with a power law, though it has not been applied outside sports applications, nor with I_o in a range expected for swung implements in this study [340], [341], [342], [343], [344], [345] (Equation 4.1, V = tip velocity, C is a participant specific constant, and r is a best fit gradient). I_o can be calculated for uniformly distributed objects, such as wooden beams and metallic poles, by first calculating the MoI about the centre of mass (I_{COM}, Equation 4.2, m = mass, L = object length) and applying the parallel axis theorem to shift the pivot point to where someone would be holding the object, i.e. the maximum distance from butt to grip \approx 20 cm for an adult male [346] (Equation 4.3, I_{GRIP} = moment of inertia about the persons grip pivot, m = mass of the object, d = distance from centre of mass to the grip pivot).

$$V = \frac{C}{I_o{}^r} \tag{4.1}$$

$$I_{COM} = \frac{1}{12} mL^2 \tag{4.2}$$

$$I_o = I_{GRIP} = I_{COM} + md^2 (4.3)$$

In summary, mechanical experimentation can be used to quantify loading mechanics in the absence of valid in-situ methods. Wooden flat-faced beams and metallic curved poles were identified as prevalent threats in Chapter 3 worthy of further analysis, though which are more of a threat is dependent on the 'swing weight' trade-off, as increasing I_0 will limit the maximum velocity a person can swing the implement. Therefore, this work looks to recreate conditions in a manner similar to what would occur in-field, to capture realistic impact dynamics for later assessment with methodology more suited for test standard.

4.2 Method

4.2.1 Experimental Arrangement

This experiment used a full-bodied 50th percentile male HIII ATD (mass = 77.7 kg, JASTI Co. Ltd.) in place of an officer, during recreation of threats from swung weaponry. This eliminated ethical concerns for exposing individuals to dangerous

conditions. The bare headform (mass = 4.54 kg, circumference = 57.2 cm) was equipped with a 6DOF $3a3\omega$ sensor package (Slice 6DX PRO, DTS) at the CoM and was affixed to the torso by a neckform (mass = 2.11 kg, length = 18 cm, axial tension = 1.10 Nm) [154], [173], [320], [347]. The ATD was fitted with a safety harness around the waist and shoulders and held upright with a hydraulic jack powered crane, Figure 4.2. The feet were planted onto a rigid surface and the crane was lowered so the weight of the ATD kept the feet in place, with a slight bend in the knee. Use of the full ATD body was favoured over securing the base of the neckform to a rigid point, with intention of improving biomechanical realism.

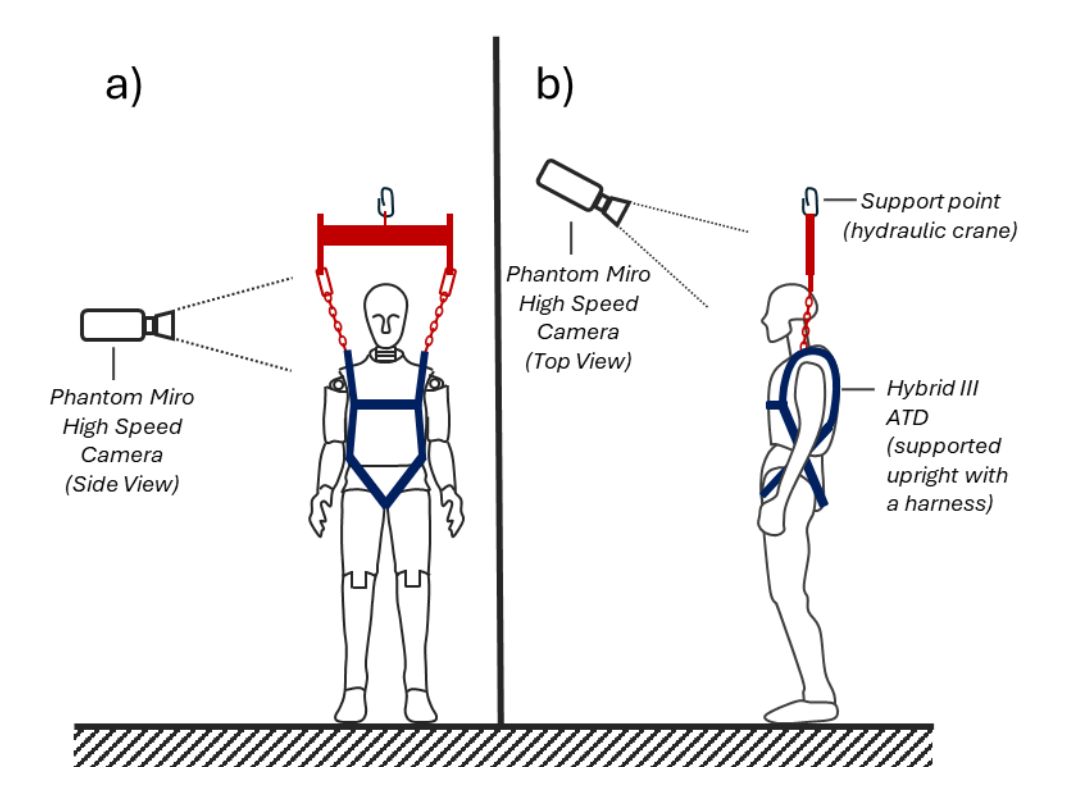


Figure 4.2, Hybrid III ATD setup for measuring head impacts due to swung weaponry. In this scenario, implements were swung along a vertical plane by a participant, the ATD was rotated around the longitudinal axis to vary head impact location.

4.2.2 Swung Implements

Wooden and metallic implements were swung by a healthy and able-bodied male wearing protective gloves, helmet, and eye protection (age = 25, height = 182 cm, mass = 83 kg). Swung implements were chosen to represent those identified in Chapter 3, characteristic properties of these are described in Table 4.1. I_0 was calculated with Equations 4.2 and 4.3 assuming a 20 cm grip. Each weapon was swung downwards along a vertical plane to replicate common practice in PO

conditions. The participant was instructed to grip implements at the butt end, start with it behind their head with arms raised, and swing with as much effort as possible. A minimum of 5 minutes rest was given between repeated trials for recovery. Impacts were directed to the headforms back (upper posterior border between parietal bones), crown (vertex where parietal bones meet frontal), front (medial frontal), and side (lateral parietal), Figure 4.3 [348]. A minimum sample size of 3 repeats per condition was determined from pilot data of impacts to the back of the headform for both swung implements (Power analysis, Cohen's d = 2.09, α = 0.05, power = 0.8). In total, 12 repeats were conducted per condition to account for high variation and maintain statistical power after removing outliers/invalid trials. No more than 24 repeats were done in a day to further reduce fatigue effects. When changing impact location, the ATD was rotated along a vertical axis. The neckform adjustment was maintained for back, front, and side conditions, though angled down 20 degrees for impacts to the crown to simulate a forward lean. This is because the height of the ATD made it not possible to impact the crown when upright. For side impacts, attachments holding the ATD upright were moved from the shoulders to the chest and back, so to not obstruct the swing plane. ATD head height was kept constant throughout all trials so to not change the swing arc length.

Table 4.1, Characteristic properties of implements for the study of wielded blunt weapon head impact conditions [349].

Parameter	Wooden Implement	Metallic Implement	
Material	Treated softwood.	Galvanised steel (< 0.2%	
		carbon).	
Common use	Outdoor light construction.	Scaffolding (BS EN 39:2001).	
Length (m)	1.2	1.15	
Mass (kg)	1.88	4.94	
I_0 (kg.m ²)	1.43	2.97	
Cross-section	Square 51 mm.	Circular 50 mm diameter,	
		5 mm wall thickness.	

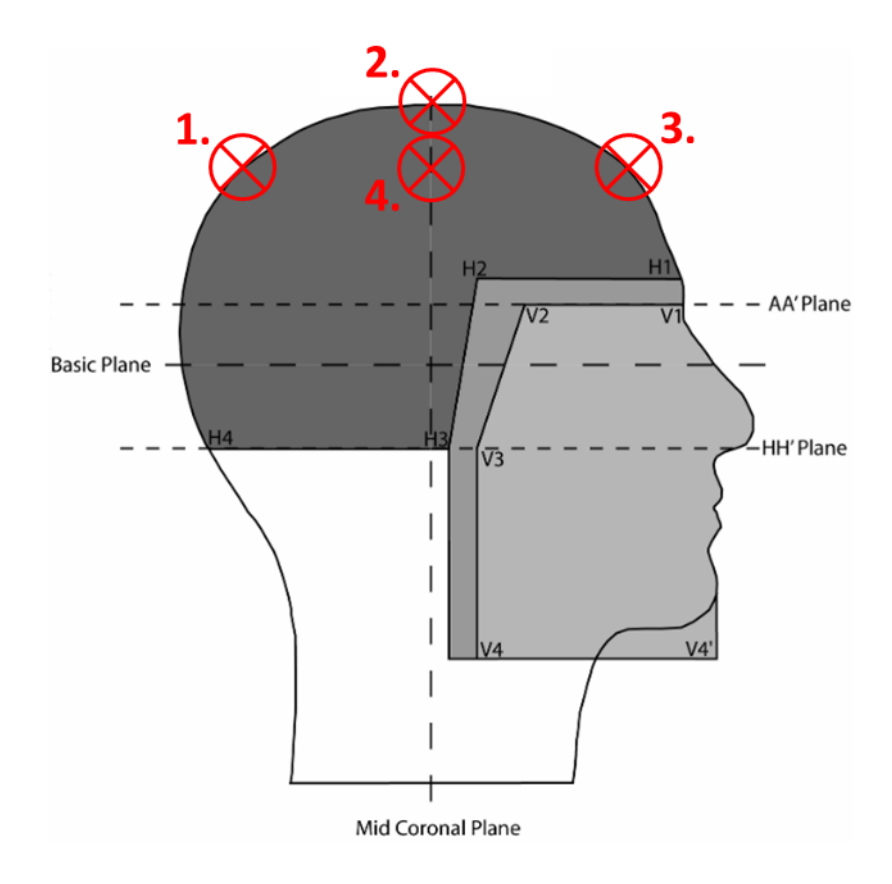


Figure 4.3, An adaptation of the PSDB 21/04 reference image to show all headform target locations in this study of threat recreations using swung implements. 1. 'Back', 2. 'Crown', 3. 'Front', and 4. 'Side' [13].

4.2.3 Tracking of Swung Implements

Implements were fitted along their lengths with 5 adhesive circular 20 mm diameter markers for tracking impact velocity with high-speed video (HSV). Markers were separated at 50 mm between centres, starting 50 mm from the marker centre to the tip of implements. To improve contrast, markers were adhered to matte black tape on the face of each implement and a dark screen was placed for the background. A single side-view HSV camera (Phantom Miro R311) captured the position of markers at 4000 Hz from a distance of 1.2 m, perpendicular to the swing plane. Field of view was adjusted to capture minimum 0.5 m of swing path above the headform and ensure head translation post-impact was visible. A secondary top-view 4000 Hz camera was positioned looking down on the ATD for qualitative assessment of impact locations, Figure 4.2.

The method for automatically tracking velocity using HSV was validated with a 1 m free-fall drop steel ball (n = 4, Δ V = -0.76 %, std dev = 1.5 %, Appendix A.4.1). Camera calibration was performed using a 30 mm checkerboard pattern and the MATLAB 'Camera Calibrator App' (Matlab 2023b [350]) to correct fish-eye lens distortion and compute intrinsic camera parameters [351], [352], [353], [354]. A minimum of 20 checker frames were uploaded at random angles and distortion corrected reprojections had to produce error less than 0.2 pixels before proceeding [354]. HSV frames from each trial were binarized to maximise contrast and only the marker closest to the impact point for each trial was selected for tracking. Marker centroid cartesian coordinates were recorded in metric units using the extrinsic properties (translation and rotation vector) for a checkerboard frame in-line with the swing plane. Horizontal and vertical position changes over 40 frames (10 ms) prior to contact were differentiated into velocities, considering the camera frame rate as a time interval ($\Delta t = 1/fps$). Impact velocities are the resultant magnitude of component velocities, calculated with Pythagorean theorem. Marker tracking for each trial was qualitatively checked by a plot of the marker path imposed over the image at contact, Figure 4.4.

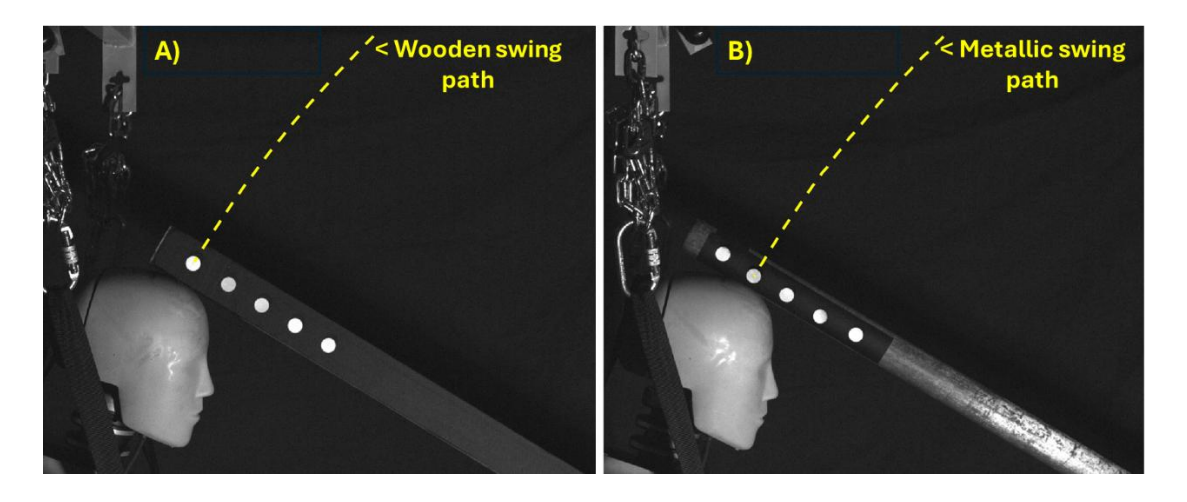


Figure 4.4, Swing paths of wooden (A) and metallic (B) implements for frontal impact recreations. Frames are taken from a side-view high-speed camera. Dashed plots are the positional coordinates of marker centroids, only the marker closest to impact was tracked for each trial.

4.2.4 Kinematic Measurement & Analysis

The measured kinematics from the headform included linear acceleration and angular velocity. Headform IMU data was recorded at 100 kHz with the $3a3\omega$

sensor array [251], [355]. Axis coordinates were to match SAE J211 notation, meaning positive orthogonal directions from the headform CoM are described as 'x' for acceleration travelling posterior to anterior, 'y' for lateral out the right side, and 'z' for superior to inferior [28], [244]. The standardised minimum sample rate for HAEs is 20 kHz [244], this was increased because there were no limiting factors for increased data storage and it was expected that bare-head impacts would have a steep and narrow acceleration response. The IMU array was set to trigger with a 5 g threshold in any of three accelerometers, capturing 0.02 s prior and 0.1 s post impact using SliceWare software. Data was filtered using a Channel Frequency Class (CFC) 1000 filter (1650 Hz cut-off) for linear acceleration and CFC 180 (300 Hz cut-off) for angular velocity, in accordance with SAE J211 [244], [254]. Angular acceleration was calculated by differentiating angular velocity using the 5-point stencil method to reduce noise effects, as recommended in SAE J1727 [247], [248], [249], [250]. Angular velocity was not considered as an injury metric at this stage because angular acceleration is more common in sports head impact research, although it is included in Chapter 10 with assessment for helmeted headforms.

Data was processed and analysed using MATLAB script (MATLAB 2023b). A two-tailed equal variance t-test was employed to assess the differences between impact velocity based on weapon type with a 95% confidence interval (P = 0.05). Data achieving P < 0.01 is highlighted to show 99 % confidence. Datapoints for impact velocity outside of 99.3 % of normal distribution coverage were considered outliers. The variance of a data group was assessed using standard deviation statistics and coefficient of variation (CV%). A two-way 'Analysis of Variance' (ANOVA) was used to assess if impact location or weapon type significantly affected peak headform kinematics (PLA and PAA), and to identify interactions between them [21], [356]. A post-hoc Tukey's test identified the differences and similarities between these groups, based on the ANOVA findings. Relationships between peak headform kinematics and independent variables, i.e. impact velocity, were plotted as both linear and exponential relationships with R² statistics to assess quality of model fit. The same was done for the relationship between PLA and PAA to assess interrelation in the two headform measures. Impact data was

grouped based on impact condition and mean PLA and PAA were calculated as the average of all peaks within each group. Mean kinematic time plots were calculated by first synchronising the trigger points of all trials in that group and then averaging the orthogonal component data. Resultant kinematics were calculated as the 3-dimensional Pythagorean result of these components. A 'pulse' was considered the primary loading curve contributing to injury from the headform sensor array. Pulse duration was calculated as the difference between the start and end time of a pulse. Injury criteria (IC) were not calculated for this specific study because it was unclear at this stage which IC would be best suited to PO application. IC are explored in Chapter 10, when a more holistic view of PO head injury is discussed.

4.3 Results

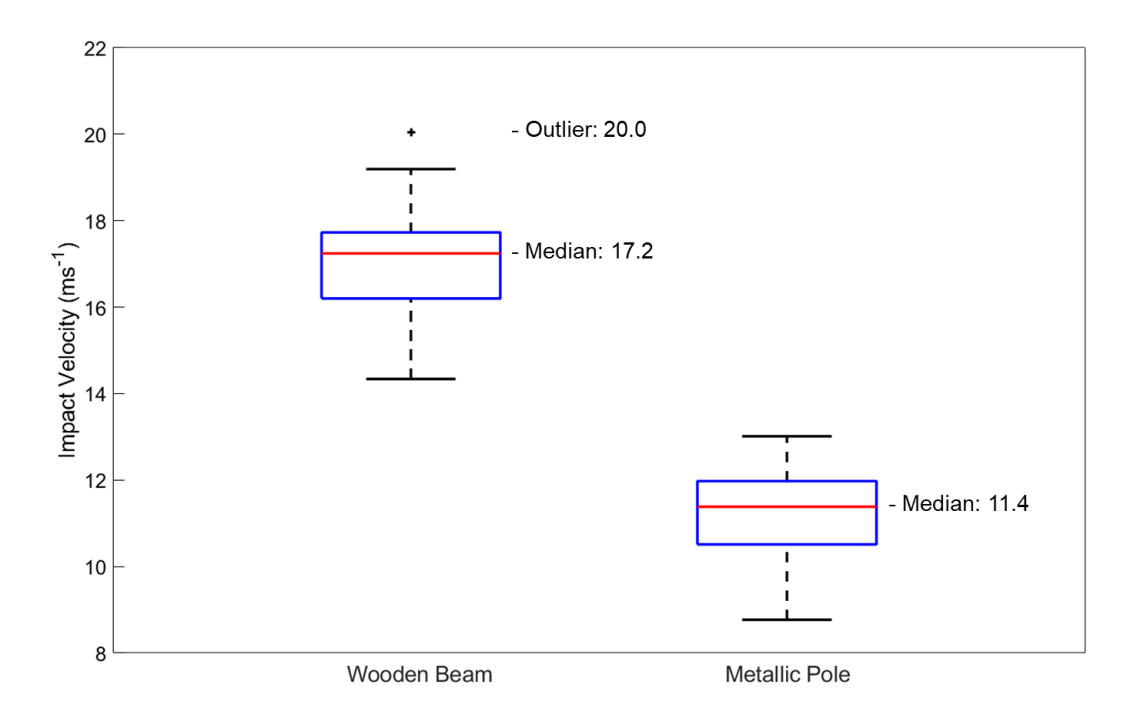


Figure 4.5, Impact velocity comparisons of all wooden and metallic swung implement trials (n = 96). Median values for each group are labelled, as well as the only outlier of the dataset (Wooden, Side Impact, Trial 5).

Significant difference in the impact velocity between wooden (mean = 17.1 ± 1.2 m/s) and metallic (mean = 11.2 ± 1.0 m/s) swung implements (P < 0.01) was observed in experiment. This can be seen in Figure 4.5 by a difference in median values = 5.8 m/s and no overlap between the data groups. The kinetic energy of

metallic implements (310 J) was 13 % greater than wooden (275 J), when calculated with the mass of each object (metallic = 4.94 kg, wooden = 1.88 kg) and means of the measured impact velocities. Within-group velocity variations were small considering it was a low-control setup condition (CV wooden = 7.2 %, CV metallic = 9.0 %). One datapoint (20.0 m/s) was considered an outlier, this corresponded to a wooden trial impacting the side of the head. Review of HSV for this trial showed that nothing unusual occurred in the swing, impact location was similar to other trials, and impact velocity did not change when measured again with manual digitisation, thus the datapoint was not removed.

Table 4.2 summarises the relative angles of each implement at contact with the headform and shows that angle between implement and headform, Figure 4.6, changes based on the position of the ATD. Back impacts have the lowest angle as the ATD was slightly leaning away from the participant, crown angles were the greatest as the neck angle adjustment simulated a more forward lean, front impacts were second largest with the standard neck angle but facing the participant, and side was in-between back and front angles as the ATD was leaning perpendicular to the swing plane. Mean absolute angles between implements and the camera horizon show that absolute impact angles were similar across all locations (max Δ = 10.2° between wooden crown and metallic side, Appendix A.4.2).

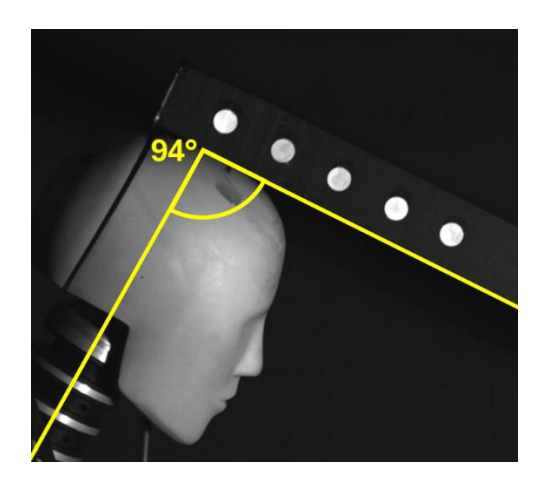


Figure 4.6, Example of relative angle between headform and swung implement at contact (Trial 1, Wood Crown).

Table 4.2, Mean (± one standard deviation) angles for wooden and metallic implements at the point of impact, taken relative to the longitudinal axis of the headform.

Implement	Mean relative impact angle (degrees)				
	Back	Crown	Front	Side	
Wooden	44.8 (± 2.3)	94.1 (± 1.7)	71.8 (± 3.6)	59.1 (± 1.5)	
Metallic	36.2 (± 3.1)	89.4 (± 2.9)	73.4 (± 3.2)	51.7 (± 3.8)	

Top-view HSV footage showed variation in impact locations between repeated trials, though all impacts were considered close to their descriptive positions, i.e. 'back'. There was also variation in where impact occurred down the lengths of each implement. No impact occurred outside of the regions where markers were fitted so this error did not influence impact velocity measurements. Impact location variations for both headform and implement are presented in Figure 4.7.

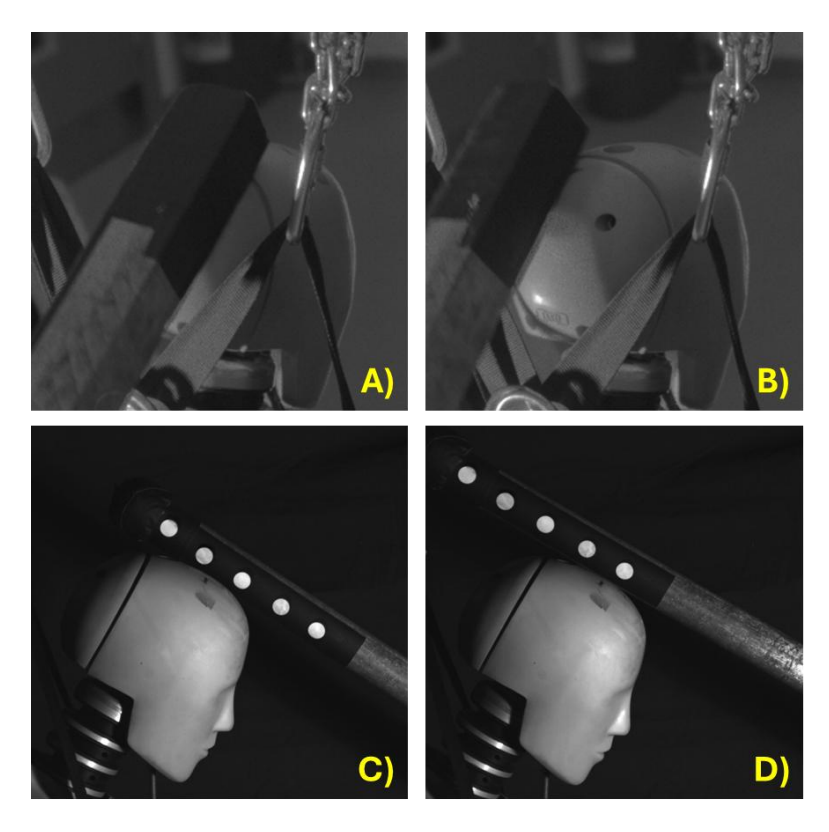


Figure 4.7, HSV frames indicating variations in impact location on the headform (A and B: Wooden, Back, trials 1 and 2) and swung implement (C and D: Metallic, Crown, trials 11 and 3).

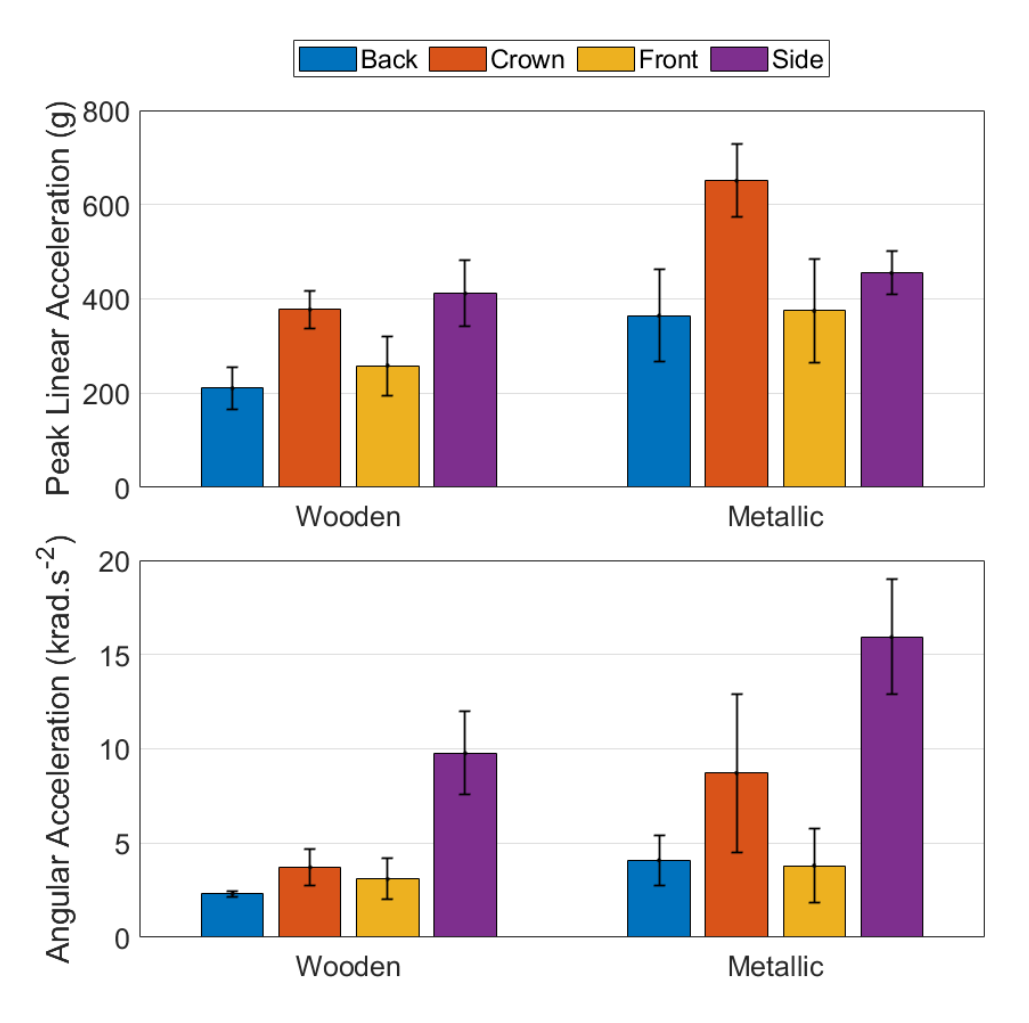


Figure 4.8, Peak resultant headform kinematics (PLA and PAA) for swung weapon impacts to the back, crown, front, and side locations (coloured). Error bars indicate one standard deviation.

Figure 4.8 shows PLA and PAA for both weapon types across all impact locations. For both PLA and PAA, two-way ANOVA results showed significant effects (P < 0.01) for weapon type, impact location, and the interaction between them (Appendix A.4.3 and A.4.4). For PLA, post-hoc Tukey's test show metallic impacts (mean = 458 g) were significantly greater than wooden (mean = 314 g, P < 0.01). Crown impacts were the greatest PLA of any location (mean = 509 g), followed by side (mean = 433 g), while front (mean = 317 g) and back (mean = 287 g) impacts were similar to each other (P = 0.55). The interactive effects for PLA suggest metallic crown impacts were uniquely greater than any other condition (mean = 640 g, P < 0.01), while wooden front (mean = 259 g) and back (mean = 210 g) were the lowest mean PLA of all conditions and similar again (P = 0.78). All other interactions between weapon type and location were statistically similar (P > 0.05).

For PAA, metallic impacts (mean = 8.61 krad/s²) were again significantly greater than wooden (mean = 4.72 krad/s^2 , P < 0.01). Like PLA, back (mean = 3.20 krad/s^2) and front (mean = 3.45 krad/s^2) impacts were the lowest peak and similar to one another (P = 0.986). Unlike PLA, side impacts (mean = 12.6 krad/s^2) were significantly greater than crown (mean = 7.16 krad/s^2 , P < 0.01). Interaction effects showed metallic side impacts were the greatest PAA (mean = 15.92 krad/s^2 , P < $0.01 \text{ for conditions other that metallic crown where P = <math>0.02$), metallic crown (mean = 10.61 krad/s^2) and wooden side (mean = 9.77 krad/s^2) were similar and the second largest, while all other conditions were statistically similar and less than these (P > 0.05).

For all comparisons between peak kinematics and impact conditions, a non-linear relationship was as insignificant or worse than a linear relationship. Overall variation for both PLA and PAA showed weak correlation with impact velocity, max R^2 = 0.61 between PLA and metallic impacts to the crown, whereas all others were less than 0.33, Appendix A.4.5. The same was the case for contact point on the implements for almost all conditions, there was one exception again although this time for wooden front impacts (R^2 = 0.66, Appendix A.4.6). These findings suggest within-group (weapon type and impact location) peak kinematic variations are more a result of deviation from the desired impact location on the headform than anything else, as this is the only remaining independent variable, although was not quantified. There was also little correlation between PLA and PAA within data, though wooden trials (R^2 = 0.43) showed a more predictive relationship than metallic (R^2 = 0.17).

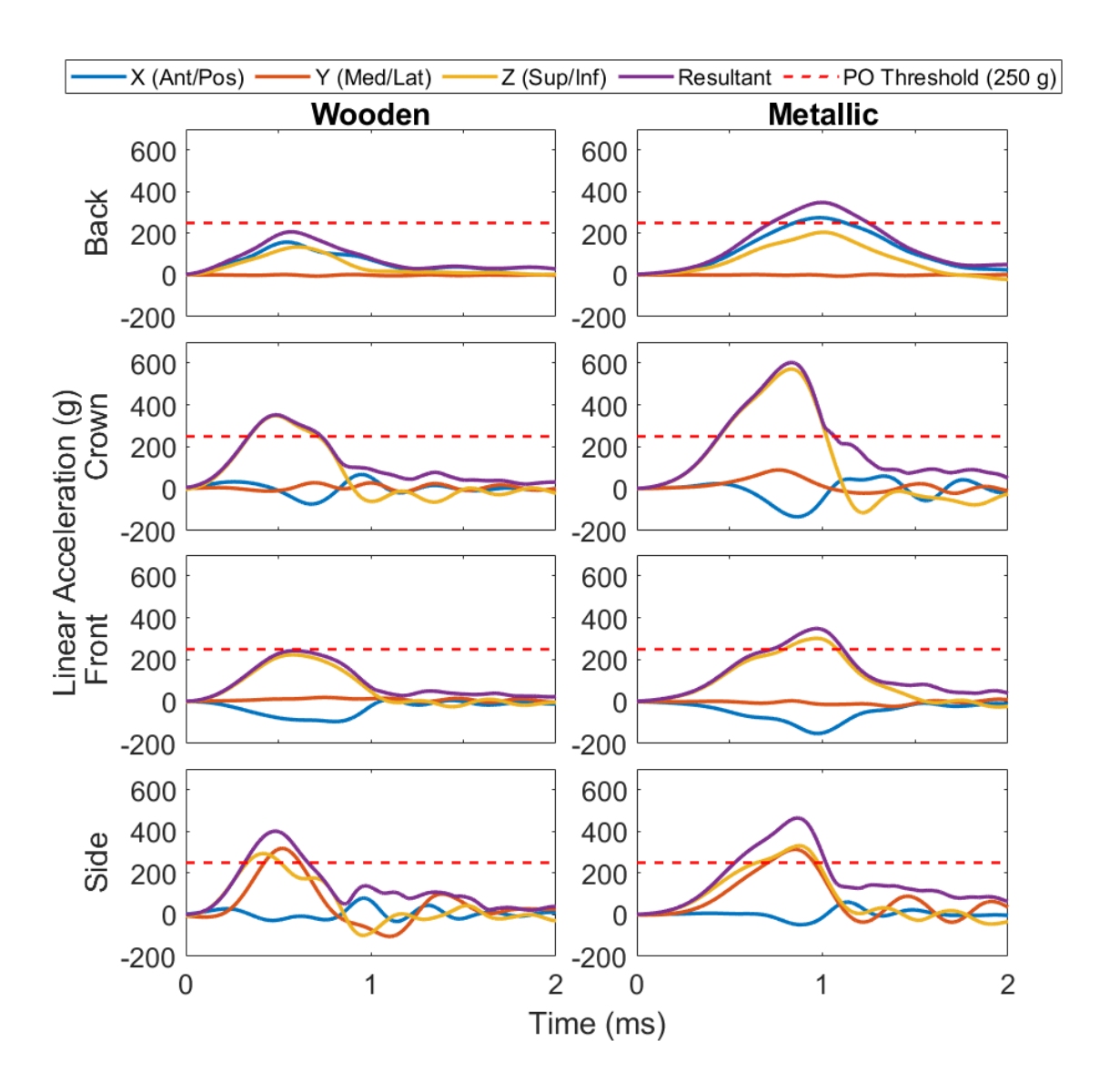


Figure 4.9, Mean headform linear acceleration (x, y, z, and resultant) vs time for wooden and metallic swung weaponry trials impacting the back, crown, front, and side of the headform. Red dashed line shows the 120 J impact pass threshold outlined in PSDB 21/04 [13].

Mean transient linear acceleration curves show a dominant loading pulse with short duration for swung implement head impacts, Figure 4.9 [109]. Plotted lines for the 120 J impact pass threshold (250 g) give example of the resultant accelerations a helmet would have to mitigate to pass these conditions. Mean resultant PLA exceeded this threshold for 6 of the 8 conditions, was similar to the threshold for wooden to front impacts and below it for wooden to back.

Plots from orthogonal accelerometers show the share of acceleration measured across x, y, and z directions was dependent on impact location, yet irrespective of weapon type. Side impacts were a factor of both y and z acceleration in almost

equal measure. Back impacts were dominated by x acceleration, with considerable influence from z as well. Front impacts were different to back in they were more a factor of z acceleration than x, which can be explained by the difference in impact angles, Table 4.2. Crown impacts were almost entirely factored by acceleration in the z direction. These crown impacts show a significant x pulse starting ≈ 0.5 ms, this occurs after peak resultant for wooden trials and simultaneously with peak for metallic. This amplifies the peak for metallic only, making it the condition with the greatest magnitude and explains why crown is greater for metallic and whereas side is greatest for wooden. This pulse in x shifts the mean acceleration vector for metallic crown impacts at the moment of PLA more anterior on the headform, as visualised in Figure 4.10, though is not indication of a more frontal impact, as x acceleration would show an earlier pulse if this was true.

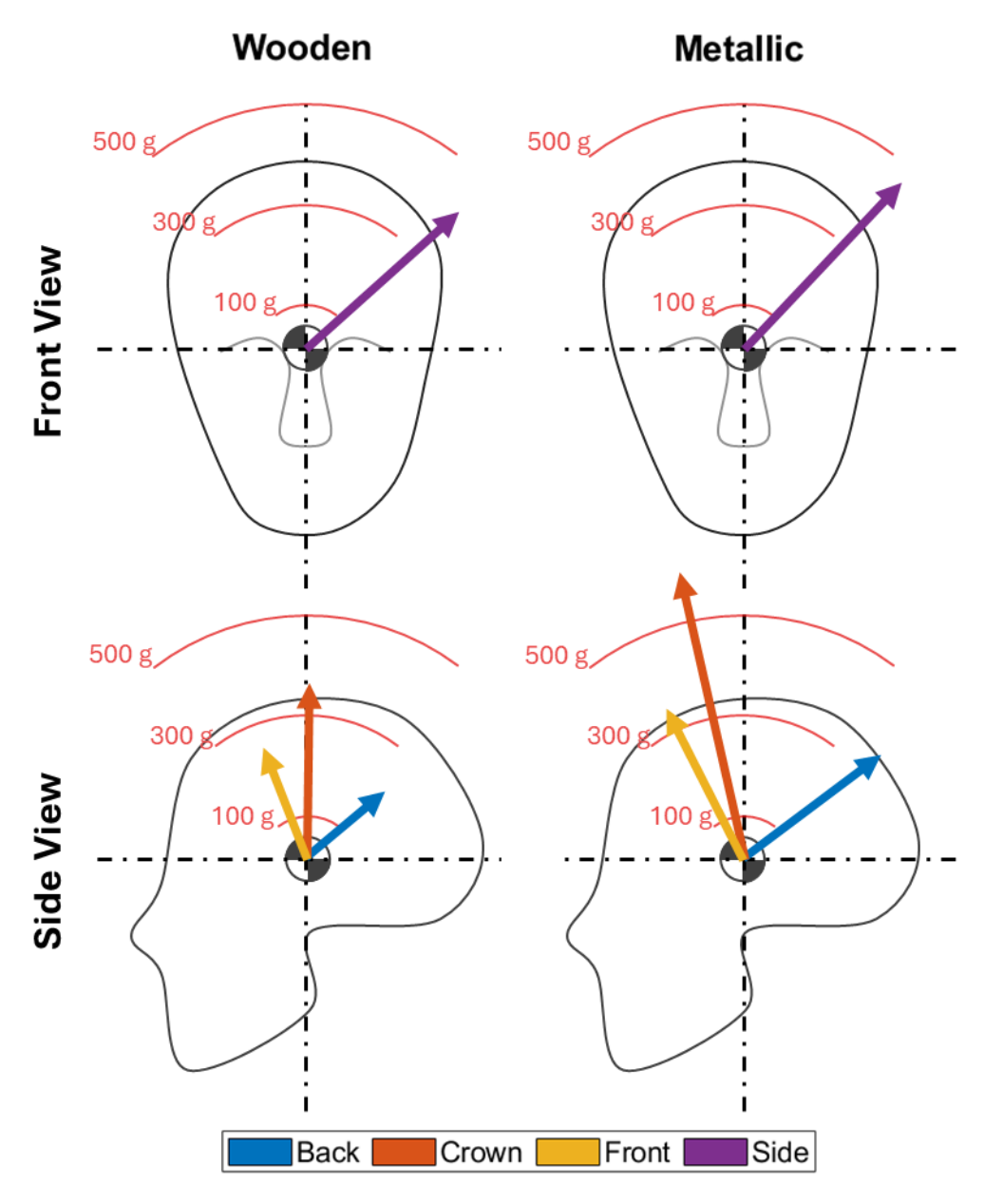


Figure 4.10, Visualisation of mean reaction linear acceleration vectors at each instance of peak resultant for impacts to the back, crown, front, and side of the headform. Vector lengths are normalised by the greatest PLA (metallic crown) with length demonstrating magnitude and the directions calculated using the pythagorean resultant of orthogonal data. Red concentric rings represent scale of 100, 300, and 500 g magnitude.

Metallic linear acceleration pulses averaged a longer duration than wooden (metallic = 1.93 ms, wooden = 1.49 ms). Average TTP linear acceleration is also larger for metallic impacts (metallic = 0.86 ms, wooden = 0.52 ms). The participants description of the perceptive differences between wooden and metallic impacts was that wooden impacts would often rebound from the headform, whereas metallic would come to a stop or brush-off. This was confirmed with HSV, as shown in Figure 4.11, where the wooden implement

bounces back along the direction of swing and the metallic remains in contact with the headform. This is a demonstration of kinetic energy returning to the wooden implement whereas for metallic more is transferred to the headform and dissipated in other forms, i.e. as sound.

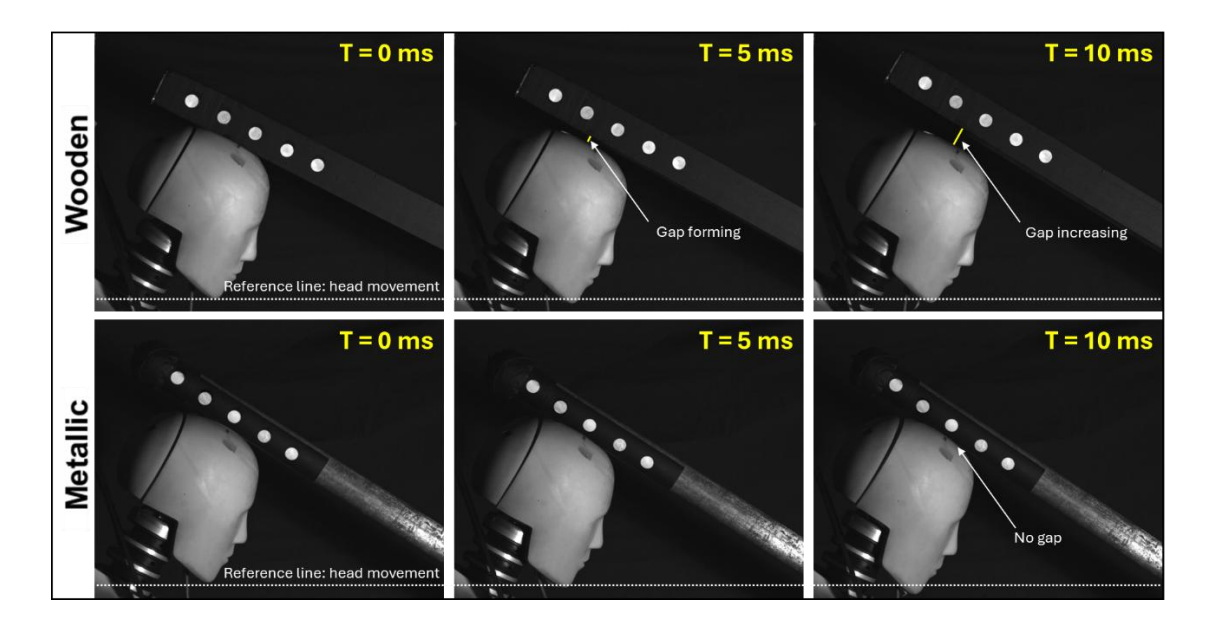


Figure 4.11, Common post-impact dynamics of wooden and metallic implements. Images show wooden implement rebound with an increasing gap between headform and wooden implement over 10 ms after impact (Time (T) = 0 ms) and little headform movement (see reference line in contact with the apex of the chin at contact). The rebound effect did not happen for metallic implements where contact with the headform was maintained and more headform motion was visible (more chin visible under reference line).

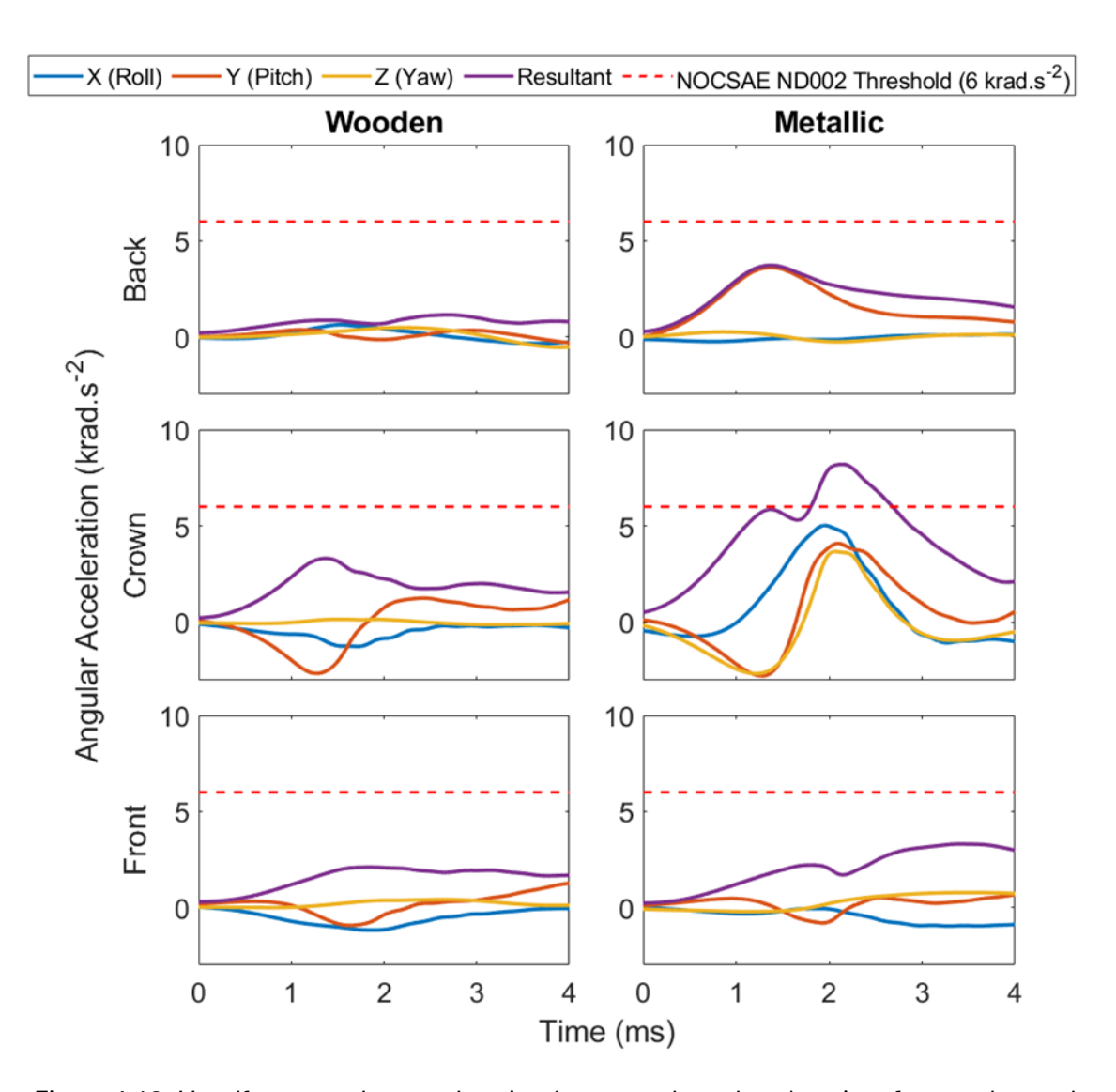


Figure 4.12, Headform angular acceleration (x, y, z, and resultant) vs time for wooden and metallic swung weaponry trials impacting the back, crown, and front of the headform. Red dashed line shows an example angular acceleration pass threshold (6 krad/s²) for American Football helmets [15].

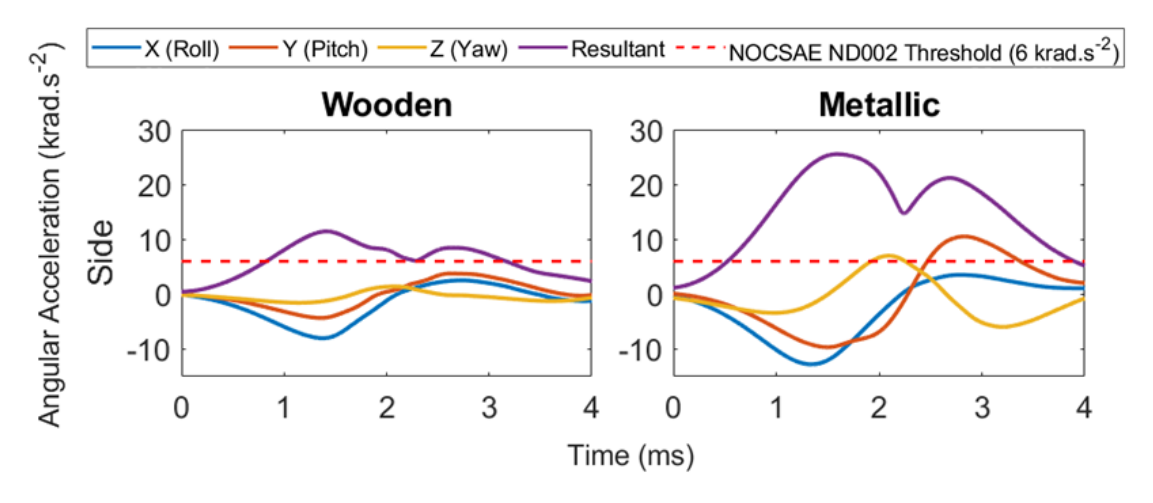


Figure 4.13, Headform angular acceleration (x, y, z, and resultant) vs time for wooden and metallic swung weaponry trials impacting the Side of the headform. Red dashed line shows an example angular acceleration pass threshold (6 krad/s²) for American Football helmets [15].

Mean angular acceleration pulses, Figures 4.12 and 4.13, show a more complex shape than linear acceleration with asynchronous peaks and ends, a common characteristic for head impacts with a neck-like degrees of freedom [150], [357]. Wooden back and front impacts showed wave-like pulses though were much lower magnitude than other conditions and in a range that is low probability of injury [116], [358]. Conversely, impacts to the side of the headform were significantly larger than other locations, thus plotted on different axes, Figure 4.13. Resultant angular acceleration for metallic crown, metallic side, and wooden side exceeded the 6 krad/s² threshold of the American Football helmet standard, NOCSAE ND002-17m21. For metallic crown and side conditions, the neckform shows significantly large counteracting torques on the headform post-impact, which change the direction of angular acceleration, and in some directions exceed the peak from initial impact. This occurs at different rates and magnitudes for each orthogonal direction, further diverging their motion and making resultant shapes more complex. This shift in direction is amplified for metallic conditions despite initial loads being similar to wooden, for example, both crown conditions show the same y acceleration curve for the initial ≈ 1.7 ms until the change in torque shifts the direction of metallic impacts only. This is possibly a result of the rebound effect shown in Figure 4.11.

Similar to linear acceleration, the share of resultant angular acceleration factored about x, y, and z axes is dependent on impact location. Both front conditions and

wooden back show little rotation, whereas metallic back have a dominant pitch response (rotation about y). Pitch is also a dominant factor for all crown impacts, though metallic crown is heavily influenced from all directions, as is metallic side. The greatest factor for wooden side impact is headform roll (x) as expected. Angular accelerations showed similar mean pulse durations between wooden and metallic implements (metallic = 3.65 ms, wooden = 3.46 ms) and longer durations than wooden and metallic linear accelerations (Δ mean metal = 88.8 %, Δ mean wood = 132.3 %).

4.4 Discussion

This study quantifies loading conditions and head injury risk due to wielded blunt implements in PO scenarios. Findings suggest there are significant effects on injury biomechanics due to swung implement properties, impact velocity, head impact locations, and the interactions between impact velocity and location. The metallic weapon had a greater I $_0$ than wooden, thus the participant was unable to swing them at the same speed (Δ mean = -35 %). Despite this, the metallic weapon had the greater kinetic energy at impact (Δ mean = +13 %). Consequently, metallic impacts resulted in a significantly higher PLA (Δ mean = +46 %) and PAA (Δ mean = +82 %) than wooden implements. Impact angles were consistent between implements and there was little intra-group correlation between velocity and peak kinematics, this further suggests variance in PLA and PAA is predictable by weapon type.

Impact location also significantly affected peak kinematics. PLA was greatest for crown impacts (509 g), followed by side (Δ = -76 g), while PAA was greatest for side impacts (12.6 krad/s²), followed by crown (Δ = -5.44 krad/s²). Front and back impacts were similar to each other and the lowest magnitudes for both PLA and PAA. There is little consensus for predicting brain injury severity with only peak kinematics, Zhang et al (2004) suggested 106 g and 7.9 krad/s² as 80 % likelihood thresholds for mild brain injury (AIS 2+) [116]. All impact conditions exceeded this threshold for PLA, whereas only three did for PAA (metallic side, crown, and wooden side). It can therefore be ascertained that swung weapon conditions pose more a threat to linear induced neurotrauma, such as open skull injuries, than they

do angular [9]. There was also little correlation between PLA and PAA, suggesting there is no significant trade-off between the two in this impact scenario.

The brains tolerance for injury is also dependent on the duration of applied kinematics for both linear and angular motion [109], [120]. Pulse durations in this study were short for the spectrum of studied head impacts in literature, i.e. less than 5 ms, due to the fact a bare headform was used and both impactors were lowcompliance materials [109]. This suggests there is scope for a helmet to effectively dissipate swung weapon impact energies by extending the duration and effectively 'cushioning' the impact. Metallic impacts had a significantly larger average duration than wooden for linear acceleration (Δmean = 29.8 %), and slightly larger for angular acceleration (Δ mean = 5.47 %). This, in combination with the greater linear and angular magnitudes, suggests metallic implement in this study was more of a threat to brain injury. When applying mean PLA, PAA, and respective pulse durations to the tolerance curves for linear (WSTC) [120] and angular acceleration (Hoshizaki et al (2017) [109], both metallic and wooden impacts sit above the linear threshold for 'danger to life' yet below the angular mTBI threshold. This further supports that linear associated injuries are more likely to be severe than angular for swung weapon impact conditions.

The experimental setup successfully represented real world PO conditions by including the same swung implements that are used in situ, wielding implements in the same manner as the public, and simulating the human-like biomechanical constrains of an officer. The use of HSV and headform instrumentation permitted quantification of both impacting scenario and resultant head motion as intended. This resulted in comparative analysis for weapon threat, as well as elucidating the injury risk that can be expected in this injurious scenario. The consideration for testing multiple head locations also showed certain areas of the head, i.e. crown and side, may be at greater risk of injury than others. This finding can aid the development of test standard procedure and PO headgear design, where efforts may be needed to account for this. The inclusion of side impacts, despite the location not being in the PO test standard, seems validated and worthy of further consideration within this project, for side impacts were some of greatest PLA and PAA. The use of a neckform was noticeable in the results of angular acceleration,

as a counteractive torque was applied to the headform after impact. This was due to the stiffness of the neck, suggesting a phenomenon that may be desired to include in standard impact methodology. However, it should be acknowledged that the stiffness properties of the HIII neckform are known to be different from those of a typical human [185], [188], [215], [216], [220].

This study is limited by the lack of inter- and intra- repeatability for impact conditions, considering they were conducted by a human participant. For example, it is likely others will achieve different swing velocities that those in this study, as well as different grip mechanics, swing arcs, and impact angles. One example where variation could be reduced is by maintaining a consistent contact point on the swung implements, as wooden front impacts showed mild correlation between PLA and contact distance from the tip. A mechanical impact system, i.e. a drop rig, pendulum, or pneumatic ram, could be used to improve consistency of impact conditions. This could be arranged to closely replicate this study's acceleration curves and validate that protocol is representative of the in-field and biomechanical conditions.

This work had valid reason for using mechanical experimentation over FEA simulation because sources for model validation were of low quality. This study can now act as a source of validation for future FEA work, which is beyond the scope of this project. This could benefit understandings of wielded weapon conditions by including implements of broader impact characteristics such as I_0 , while also considering other head sizes, genders, ages, and with more defined impact locations.

4.5 Chapter Conclusion

This chapter quantifies the injury risks posed by swung blunt implements in PO scenarios while upholding biomechanical and situational representation using a full-bodied Anthropometric Test Device (ATD) and realistic cause of impact. In doing so, this work meets the objectives outlined in section 4.1 and provides baseline metrics to advise how the PSDB 21/04 standard can better represent wielded weapon conditions. Metallic swung implements resulted in significantly higher peak linear (Δ mean = +46%) and angular accelerations (Δ mean = +82%) compared to wooden implements, despite metallic weapons being swung at lower speeds (Δ mean = -35%). This is attributed to metallic implements having a greater mean kinetic energy at impact (Δ mean = +13%). Both metallic and wooden impacts were considered in the injurious range of the WSTC (metallic = 458 g, 1.93 ms & wooden = 314 g, 1.49 ms), whereas they were below the mTBI tolerance curve for angular acceleration (metallic = 8.61 krad/s², 3.65 ms & wooden = 4.72 krad/s², 3.46 ms). Impact location showed to have significant effect of headform kinematics with crown (mean = $509 \, \text{g}$, $7.16 \, \text{krad/s}^2$) and side (mean = $433 \, \text{g}$, $12.6 \, \text{m}$ krad/s²) impacts having significantly greater angular and linear acceleration peaks than impacts to the front (mean = 317 g, 4.72 krad/s^2) or back (mean = 287 g, 3.20krad/s²). Linear and angular acceleration vs time curves can be recreated with repeatable test methodology, such as a drop rig, to comprehend how wielded weapon conditions could be simulated in a method representing a test standard.

5. Injury due to Falling from Horseback

5.1 Introduction

An officer falling from horseback during PO conditions, has been identified as a further threat to head injury, alongside impacts from projectiles and swung blunt weaponry, as discussed in Chapter 3. In analysed video data, falls were less prevalent than the two weapon groups although considered likely to result in severe injury due to fall height [359]. For example, video review of PO conditions included one incident where a mounted officer was hospitalised following a fall from the horse [315]. The objective for this study was to quantify the loading and injurious mechanics when falling from horseback. As in the swung blunt weapon studies detailed in Chapter 4, this study was undertaken to advise if and how fall from height conditions could be represented in a test standard.



Figure 5.1, Screenshot of UK officers mounted on horseback during PO conditions [360].

A recent review of police injury data between 2014 and 2020 found that injury incidence rates were 2-3 times greater per 1000 personnel for mounted officers compared to non-mounted [39]. Of these mounted incidents (n = 150), falls from height were the most prevalent specified cause of injury (24 cases, 15.9 %), 3 cases resulted in a head impact, of which 2 resulted in considerable concussive/cranial injuries. Though PO specific horse fall conditions have not been quantified to date, analogous inspiration could be taken from studies of equestrian sports. Firstly, head and brain injuries are some of the most common outcomes of

falls from horseback [361], [362], [363], [364], [365], [366], [367]. A ten-year review of equine-related activity showed falls were the predominant injury cause and the head/brain was the second most frequent injured location (21.5 % of all incidents) [366]. For such incidents, soft tissue and concussive brain injuries commonly occur, as well as skull fractures [364], [368]. As a result, riders falling from horseback have shown to suffer neurological disorders [369], loss of motor function [368], and sometimes death [364], [366], [368]. Helmets have not eradicated head/brain injuries from the sport, and their efficacy for appropriately attenuating impact energies is continuously debated within literature [368], [369], [370], [371], [372], [373].

Video review in combination with FEA has also been used for predicting fall mechanics with equestrian sports [319], [320], [374]. Bourdet & Willinger (2015) simulated 1000+ falls from a horse and found frontal (front), parieto-occipital (back), and temporo-facial (front/side) regions of the head were the most common impact locations and impact velocities ranged between 6.6 – 7.5 m/s [374]. Most studies of horseback falls have been for running and jumping horses, whereas horseback officers in video review in this investigation (Chapter 3) were commonly stationary, moving slowly, or performing short galloping manoeuvres. Impact velocities will be greater for running and jumping conditions because the rider and horse have greater initial velocity at the start of fall, and jumping would increase the fall height. The direction of fall will also be different, i.e. a horse that trips in a race will eject the rider in a different manner than an officer falling from one that is stationary [319], [374]. Traditional means for simulating equestrian head impacts, including test standards, use a freefall unsupported headform drop test similar to PSDB 21/04 [19], [375]. Clark et al (2020) used an angled rail impact system to better replicate the fall mechanics of a running horse, after simulating common fall conditions in equestrian sports [320]. They also suggest equestrian activity should adopt thresholds of 89 g and 4 krad/s for 80 % probability of mTBI onset.

To date, there are no known equestrian related studies that use a neckform to constrain head motion. However, studies of more generic human fall mechanics, unrelated to equine activity, have included FE simulation and ATDs with necks and bodies as means for quantifying impact mechanics in a representative manner

[135], [323], [333], [376], [377], [378], [379]. Hajiaghamemar et al (2015) reported that both linear and angular accelerations showed severe injury levels when simulating standing falls with full-bodied ATDs (146 – 502 g, 8.8 – 43.3 krad/s², impact durations < 4.1 ms) [323]. Hamel et al (2011) simulated standing falls with head impact velocities in the range 3.5 – 6.5 m/s and found skull fracture occurrence is dependent on impact velocity, surface properties, cortical thickness, and cortical density [87]. Yu et al (2023) simulated unbraced trips and 0.5 m falls and found median head impact velocities were in a similar range (= 4.3 and 3.5 m/s, respectively) [377]. Multiple studies of falls from height onto hard surfaces, such as concrete, found that the large magnitude for impact energies in these scenarios result in linear acceleration being the best metric for predicting head/brain injury [127], [376].

While prior research appropriately quantifies loading conditions from equestrian activity and standing falls, there is little focus on the common conditions faced by officers, i.e. when the horse is stationary, moving slowly, or galloping. It can be expected that horseback falls in PO conditions would have impact velocities and head kinematics between those of a standing fall and equestrian sport, as there is a greater fall height than when standing, though a lesser velocity than when running/jumping. Simulating these with appropriate headform degrees of freedom and quantifying the loading/injury conditions can advise a more holistic view of falling from horseback to advise future development of PO headgear. It can also advise how best to take inspiration from research of non-police specific fall scenarios when advising PO headgear testing. Given the significant risk for head injury due to falling from horseback, and that riding hat effectiveness is debated, it may be the case that helmets are currently incapable of attenuating an impact of such magnitude. Alternatively, if horse fall impacts are vastly different from other PO conditions, it may mean horseback officers would require different headgear for this scenario. It is therefore imperative that horseback fall conditions are not just compared to research into fall mechanics but also the conditions of other PO scenarios, such as wielded blunt weapons. This is discussed in Chapter 8, when projectile brick impacts can also be discussed.

This chapter looks to characterise the impact mechanics of falling from horseback so to obtain representative metrics for advising repeatable test methodology. To do this, the following objectives were set:

- Simulate PO horseback fall conditions with similar biomechanical and situational constraints to the in-field condition.
- Quantify key loading conditions and head impact mechanics when falling from a horse.
- Advise what metrics can be used to support better representation of horseback fall conditions in more repeatable head impact test methodology.

5.2 Method

5.2.1 Experimental Arrangement

The same full-bodied HIII ATD and headform sensor package as Chapter 4 was used for quantifying the loading conditions of falls from the back of a stationary horse: 50th percentile male, 77.7 kg full mass, 4.54 kg headform mass, neck tensioned to 1.1 Nm (JASTI Co. Ltd.), with a 6DOF 3a3ω IMU (Diversified Technical Systems 'DTS'). A 1.73 m tall platform, similar to the withers height of a horse (i.e. the shoulder blades, often used to describe the seated height of a rider), was used with the ATD positioned on top in a seated posture, Figure 5.2. The ATD torso/waist was fitted with a safety harness to assist with lifting onto the platform. A short right-angled support was positioned behind the ATD's lumbar spine to keep it sat upright and the arms were rested on the lap, as if holding reigns. Load was manually applied in a lateral direction to the shoulder joint of the ATD using a push rod. The ATD was left to roll over the side of the platform and freely fall to the concrete floor, which represents common surface in PO operations, such as a road or pavement.

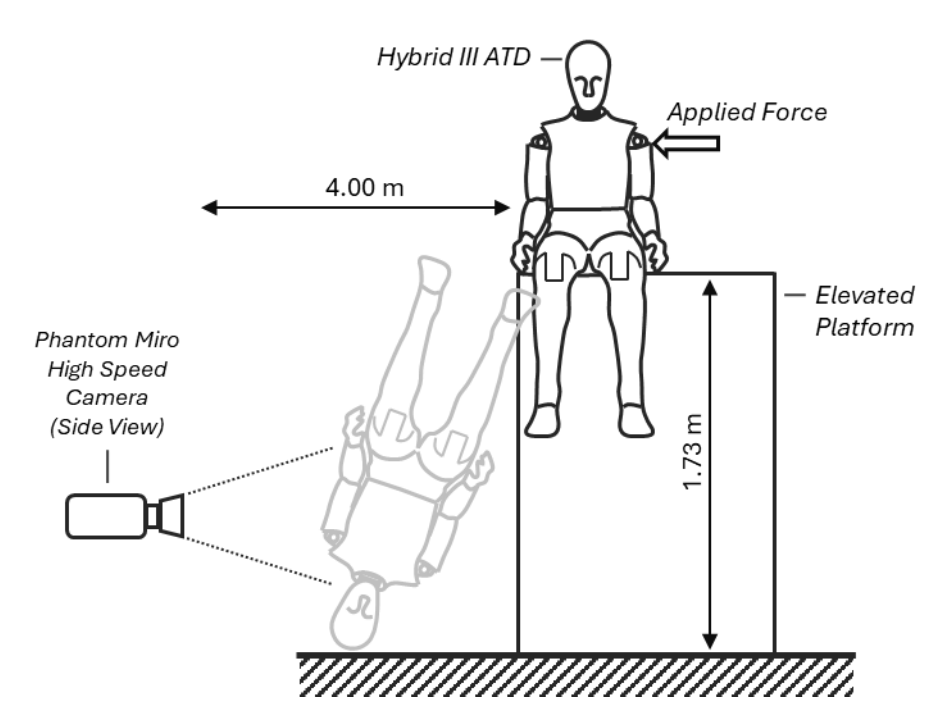


Figure 5.2, Setup for recreating falls from a stationary horse using a Hybrid III ATD [380].

A HSV camera of 4000 Hz frame rate was positioned 4 m from the lateral of the ATD with a field of view = 1.3×1.0 m to capture the direction of fall and contact with the ground. A secondary camera was positioned perpendicular to the first, at 4 m from the anterior of the ATD, in case of need for an additional view. Calibration was the same procedure as Chapter 4, using a 30 mm checkerboard to build real-world coordinates and correct lens distortion [351], [352], [353], [354]. A white circular marker of 20 mm diameter was placed on the side of the headform, in line with the CoM, with contrasting tape behind. The marker centroid was recorded over 40 frames (10 ms) pre-impact using the script discussed in Chapter 4 and differentiated into velocity by the time between camera frames (Matlab 2023b [350]).

5.2.2 Kinematic Measurement & Data Capture

Headform kinematics were collected at 100 kHz with CFC 1000 and 180 filters for linear and angular measures respectively, in accordance with SAE JS211 [244]. The IMU was set to trigger with a 5 g threshold in any of three accelerometers, capturing 0.02 s prior and 0.1 s post impact. Linear and angular accelerations were the considered metrics for quantifying impact magnitude, so to permit comparative analysis with Chapter 4 and equestrian head impact literature.

Angular acceleration was calculated by differentiating angular velocity with the 5-point stencil method, as previously discussed [247], [248], [249], [250].

Trials were repeated 25 times to exceed the minimum sample size calculation in Chapter 4 (3 repeats), and because other studies using ATD's for fall assessments involved circa 20-25 repeats [319], [320], [323], [333]. 3 trials were removed from the dataset post-testing because the arm contacted the floor before the headform, a further 2 trials were removed because headform sensors triggered before impact. Headform data, including calculation of peaks, mean curves, and pulse durations was analysed in the same manner as in Chapter 4. Likewise, IC are not yet considered for horseback fall conditions, though are discussed alongside swung weapon and projectile bricks in Chapter 10. Angles between the headform and ATD torso were calculated as relative angles, considering the joint at the back of the ATD headform was in-plane with its vertical axis and the torso segment was in-plane with a straight line between the centres of joints at the hip and shoulder [214].

5.3 Results

Loading the shoulder joint in seated position rolled the ATD over the side of the hip, creating an inversion of the body and resulting in a head-first fall to the ground. Head impact location was the crown of the headform for all trials, despite no control of fall direction. The greatest variation in fall dynamics was the relative rotation of the ATD about a vertical axis, which extended the length of fall path, as shown in Figure 5.3. Despite this, impact velocities were consistent with a mean of 4.45 (±0.27) m/s, as was headform data.

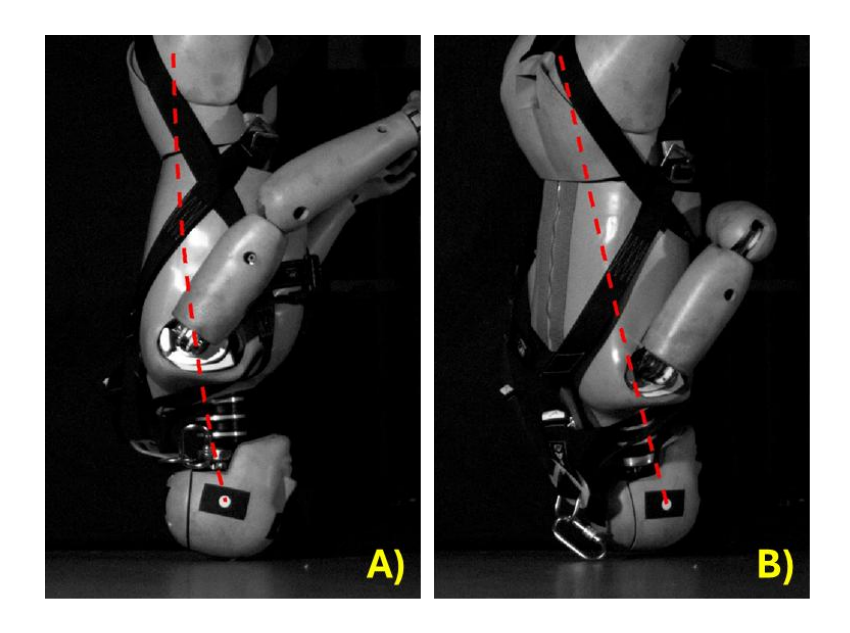


Figure 5.3, HSV frames at the point of impact between the ATD and floor for trials 10 (A) and 12 (B) when simulating falls from horseback. Red dashed lines show the headform marker trajectory from entering frame until impact.

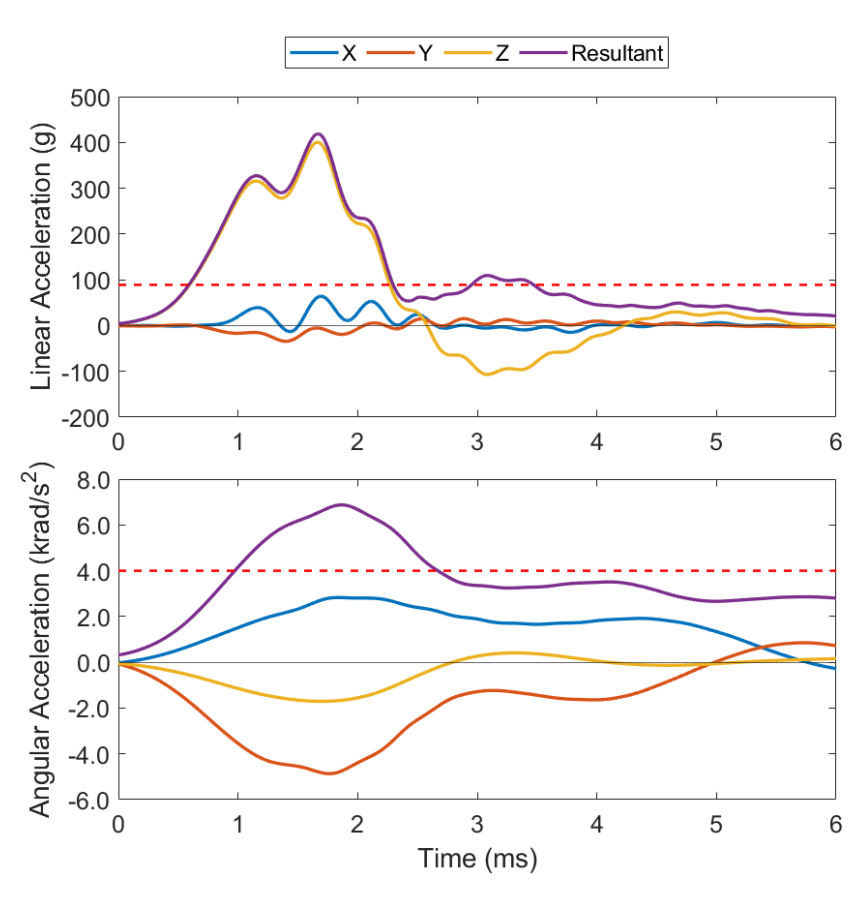


Figure 5.4, Mean headform linear and angular acceleration (x, y, z, and resultant) vs time curves for horseback fall scenarios. Red dashed lines indicate proposed 80 % likelihood of mTBI thresholds for equestrian falls by Clark et al (2020) [320].

Figure 5.4 shows that linear and angular acceleration curves for horseback fall conditions had relatively short pulse durations (mean linear = 2.64 ± 0.12) ms, mean angular = 3.76 ± 0.82) ms) [109]. Mean PLA and PAA across all trials was 460 (\pm 46) g and 8.39 (\pm 2.29) krad/s², respectively. Every trial exceeded the thresholds for mTBI outlined by Clarke et al (2020) (89 g and 4 krad/s²), while PLA relatively suggests much greater risk (\pm 417 %) than PAA (\pm 110 %). Overall, there was no significant predictive relationship between PLA and PAA across trials (R² = 0.06), Appendix A.5.1.

The magnitude of resultant linear acceleration was almost entirely a factor of acceleration in the superior/inferior (z) direction, as expected with an impact to the top of head, with little influence from anterior/posterior (x) and medial/lateral (y) acceleration. After the initial impact, and acceleration in the z axis returning to 0, a secondary and considerably injurious loading pulse in the opposite direction was observed (peak = -107 g, duration = 1.63 ms). This coincided with compression of the neckform as the mass of the ATD body, lagging behind the headform, applied a compressive downward force. Figure 5.5 includes an example trial with evidence for synchronous neck compression from HSV. The mean loading pulse for angular acceleration concludes around 3 ms, though y and x maintain < 2 krad/s² until 5 and 5.8 ms, respectively. Resultant angular acceleration was dominated by rotation about the y axis (pitch), with some influence of x (roll) and little z (yaw). Pitch occurs when a region anterior/posterior from the mid-coronal plane of the head contacts the ground first, creating an oblique force and torque on the headform. The presence of x in the mean impact curves is a result of trials where impact was off the sagittal plane of the headform thus roll torque was introduced, for 8 trials x peak was greater than y. The presence of both components contributed to there being more variation in PAA (CV% = 27 %) measures than PLA (CV% = 10%), which were almost solely influenced by z.

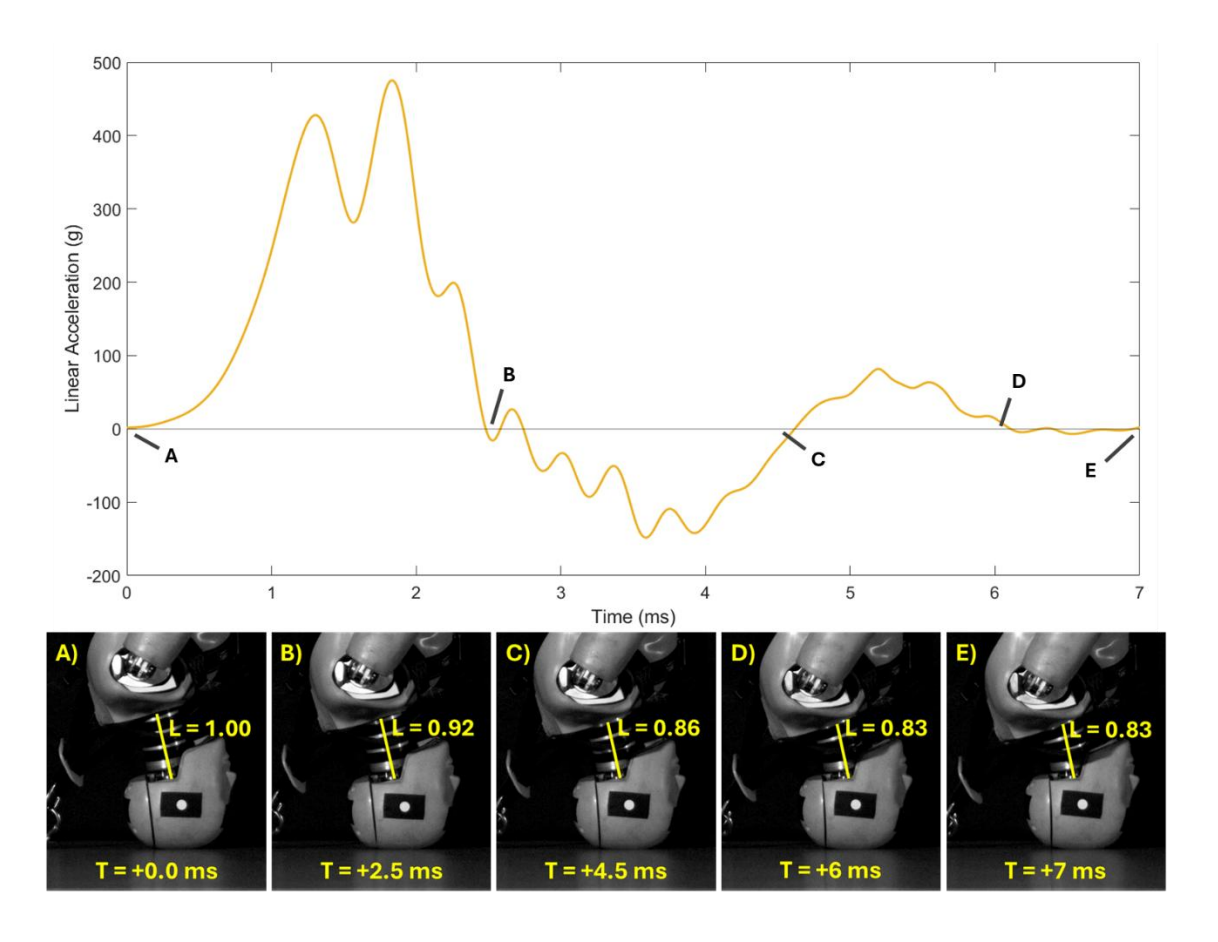


Figure 5.5, Z (superior/inferior) acceleration for trial 5 of horseback fall recreations. The impact is synchronised with HSV frames to show simultaneous neck compression across 3 cyclic loading peaks. L is the distance between neckform pin joint and torso, normalised by the distance at contact T=0 ms. Note that both neck compression and head kinematics stay ≈ 0 between 6 and 7 ms (D and E).

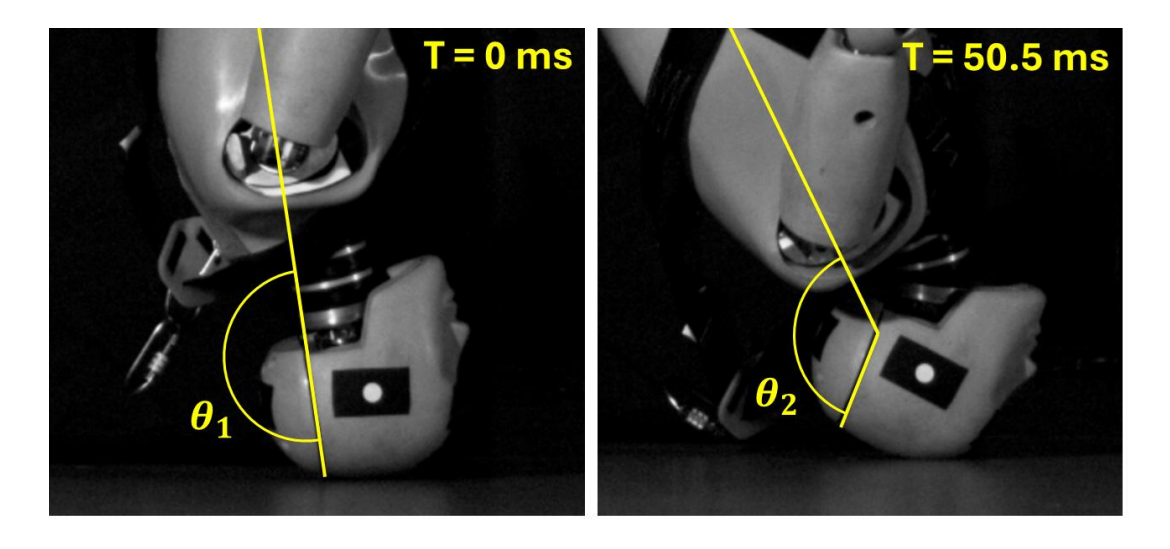


Figure 5.6, Relative angle change between the headform and torso at contact (T = 0 ms) and 50.5 ms. Change in angle ($\theta_2 - \theta_1$) = -45.4°.

The position of torso relative to the headform defined which direction the body pivoted after impact before hitting the ground. This motion further induced torque on the headform, though occurred after the primary loading pulse (> 10 ms) and was relatively small, never exceeded 2 krad/s². Though this may be less significant for head/brain injury, the motion created a substantial neck deflexion that could be the cause other injuries. Figure 5.6 shows an example of this, with a maximum relative angle between headform and torso = -45.4° at 50.5 ms after impact.

5.4 Discussion

This study quantifies the head injury conditions for PO officers falling from the back of a stationary horse. Mean impact velocity (4.45 m/s) was the equivalent of a 1 m freefall drop (assuming g = 9.81 m/s^2), despite a platform height of 1.73 m. This is because the ATD rolling over the side caused an inversion, where the head-floor displacement was less than platform-floor once falling began. Mean PLA (460 g), PAA (8.39 krad/s²), and their respective durations (2.64 ms, 3.76 ms) are similar to the FE recreations of 9 fall and trip scenarios onto hard surfaces by Post et al (208 – 521 g, 7.8 – 21 krad/s², 3 - 4 ms) [127]. However, PLA was in the upper range of these, whereas PAA was near bottom. Similar to this study, the full-body biomechanics simulated by Post et al also produced a secondary loading pulse in linear acceleration [127]. Additional body components, i.e. neckforms, in experimentation has commonly shown secondary pulses in linear acceleration data, attributed to the headform compressing between impact surface and the delayed mass of a still-falling body/test rig [219], [347], [357], [381]. It is common practice to remove second pulses and only consider the first for injury prediction, even if they are significant enough for injury on their own [357]. This could be an overlooked and potentially injurious mechanism, particularly if there are accumulative damage effects from successive loading pulses [321], [322]. The use of a full-body ATD also induced angular acceleration, beyond 10 ms after impact, as the torso rolled over the headform [382]. Although PAA during this period was not a significant range for causing brain injury, the resultant bending of the neck could potentially cause cranio-vertebral injury that could be limited with PO

headgear design or additional PPE. One example for this is the 'Head and Neck Support Device' (HANS) used in auto racing [383].

The ATD inversion resulted in impacts to the top of head for every trial, which produced a resultant linear acceleration dominated by force in the z direction, with little influence from x and y. Angular acceleration was factored primarily by pitch (y) and roll (x) torque, when impacts occurred slightly in front/behind the midcoronal plane of the headform or to the side of the mid sagittal plane. These directional measures portray potential protective requirements, i.e. extra protection to the top of head, though cannot be confidently advised until a more holistic view of falling from horseback is considered.

The results of this study are closer to those of standing and at-height fall recreations in literature, than they are for equestrian related activity [87], [323], [376], [377]. For example, equestrian sport research includes greater head impact velocities, more oblique angles, and lower head kinematics due to use of compliant surfaces [319], [374]. Police horses are unlikely to remain stationary during operations, nor will officers always fall sideways from a lateral load. The following explains how research for trips, slips, and falls from height can appropriately advise PO representative impact characteristics for variations in head impact location due to fall direction, as well as impact velocity.

5.4.1 Head impact location

4 m/s drops of a HIII head/neckform produced similar PLA (335 – 445 g) yet significantly greater PAA (23.7–51.2 krad/s²) than this study for impacts to the front, back, and sides of the head [376]. Other studies using FE techniques agree with this, also showing in-range PLA (237-638 g) and much greater PAA (26.2 – 44.8 krad/s²) to this study [135], [379]. Firstly, it should be acknowledged from these studies that head kinematics representative of falls can be accurately recreated with a head/neckform using a drop tower. Secondly, Increased PAA for variations in fall dynamics and head impact locations can be attributed to the cumulative effect of the following phenomena:

- 1) Mass and the torso position coming down on the head creates a moment arm to induce torque on the headform [135], [370], [382], [384].
- 2) The change in head impact location that occurs when the body is not above the head can produce a more oblique impact vector [192], [217], [228], [385].
- 3) An abrupt stop of the body when landing torso-first transfers momentum to the head that creates large angular accelerations as it pivots about the neck, particularly if landing on ones back, this can also then result in head impact with the ground [386].

Collectively, these explain how PAA can drastically increase for variations in fall dynamics compared to the findings of this study and therefore, horseback fall conditions are a threat for both linear and rotational induced brain injuries.

5.4.2 Head impact velocity

Variation in head impact velocity is correlated with a change in skull fracture risk, though has shown to have less effect on peak kinematics than impact location does [87], [135]. It is fair to assume equestrian sport studies with a running/jumping horse would be the maximum impact velocities of any horseback fall condition. These are greater than the mean velocity in this study (+48 - +69 %) [374]. As mentioned in Chapter 2, Peak linear acceleration has a non-linear positive correlation with increasing impact velocities normal to the head, though has little to no correlation with increasing tangential components [105], [106]. Therefore, because falling from a moving horse is known to eject the rider at more of an angle, thus producing a more oblique impact, PLA is not likely to increase much with impact velocity [192], [217], [228], [385]. Further increase in PAA should be expected, though up to a maximum before decreasing as the impact becomes too oblique to grip the head and cause significant tangential load. This has shown to occur at angles $\approx 30^{\circ}$ - 45° from the ground when simulated at 8.49 m/s ejections with helmeted PAA = 11 krad/s² [106].

The intention of using an ATD was to uphold biomechanical and in-field representation in experimentation without need for live participants. The ATD

falling in a similar manner to what is expected when falling from a stationary horse shows realistic impact conditions and resultant head kinematics that can aid the development of representative PO helmet test protocol. In particular, it is clear the mass of the ATD body coming down on the headform did not influence PLA as expected. For example, PLA was similar (-2.4 %) to that of a same speed impact with monorail drop rig, rigid neck (total mass of both = 5.1 kg), and flat steel impact anvil [387], as well as to a 3.5 m/s unsupported freefall drop of a bare headform impacting the top of the head (+3.9 %) [211]. Ghajari et al (2013) also found the mass of an ATD body does not always influence peak kinematics, though it does affect the bottoming out of helmet liners [228]. They propose adding mass to the headform/drop system as suitable means for overcoming this. The magnitude of PLA in the z direction in this programme of work is likely greater than a live human, due to the superior compressive stiffness of the HIII neckform [173], [215], [216], [217], [218], [357], though the general motion and physical phenomenon remain as true as can be understood with current head injury biomechanics knowledge.

The findings of this work improve understanding of PO horseback fall conditions, particularly when used in conjunction with other research for falls from height, though there are several limitations to address. The experimental setup represents stationary horse conditions with a top-down fall characteristic, though including oblique impacts such as use of a moving platform or floor, would improve relevance to the in-field scenario [217]. This also allows for parametric study of injurious effects due to broader impact velocities and angles. Alternatively, this work can act as validation for studying head injury mechanics with computational simulation.

The human-like biomechanics represent a 50th percentile male, whereas size, mass, gender, and age variations contribute to impact mechanics and the resultant injury [126], [235], [269], [329], [330]. Therefore, efforts should be taken to broaden representation in the data. The use of an ATD also assumes the rider would have no influence in effecting the impact conditions, i.e. by tensing their body, ducking their head away, or using their arms to brace the impact. The concrete surface is representative of most PO activity and has produced PLA in the upper range expected for these conditions, however it does not simulate more

compliant surfaces where injury occurs with prolonged acceleration exposure [336]. These compliant surfaces are more relevant to the previously discussed equestrian injury thresholds by Clark et al (2020) [320].

The headform data, particularly for linear acceleration, showed extreme vibration as the ATD landed on the top of its head, normal to the stiffest axis of the 'skeleton' (noticeable in Figure 5.5). The filtering procedure of the SAE JS211 standard may need a higher cut-off frequency for ATD drop conditions onto hard surfaces similar to this to reduce vibration, i.e. top of head, high stiffness, and high mass impacts. Other filters were not applied as it was necessary horseback fall conditions remained comparable to other PO injuries for further study.

5.5 Chapter Conclusion

This chapter has demonstrated that head-first falls from horseback in PO conditions are likely to result in head and brain injuries. A 50th percentile male Hybrid III ATD rolling from the side of a 1.73 m platform produced a mean impact velocity the equivalent of a 1 m freefall drop (4.45 m/s). As result, peak linear (460 g) and angular (8.39 krad/s²) accelerations significantly surpassed mTBI thresholds recommended for equestrian activity (PLA = +417% and PAA = +110%), with PLA seeming more injurious than PAA. Setup simulated a stationary horse fall condition; for this, findings of impact characteristics and resultant head kinematics are more similar to literature on slips, falls, and trips than they are for equestrian activity. Considering alternative fall characteristics will occur in field, i.e. impact location, angle and velocity, literature advises that PAA could substantially increase (falls have shown PAA up to 510 % greater) whereas any PLA increase would be less drastic (up to +39 % is shown in literature).

The use of full-body biomechanics with the inverted fall was portrayed, as the stiff vertical axis of the body produced a dominant z linear acceleration pulse. A secondary loading pulse from the mass of the body lagging behind the head could be significant enough for injury (-107 g peak and 1.63 ms duration), despite common practice being to discard this. Comparisons with drop rig impacts suggest representative head accelerations can be appropriately achieved with just a head and neckform, removing need for further testing with the rest of the body and better controlling the experiment.

This work contributes to the development of test methodology for PO helmets by identifying realistic head acceleration ranges for another dangerous situation in PO conditions. In particular, the requirements of a PO helmet to reduce angular forces to the head is highlighted, despite there being no angular protective requirements in the PSDB 21/04 standard. The next step is to recreate these loading conditions with repeatable methodology and compare headform kinematic responses. For these, recreating the linear response of the head should be prioritised, as linear acceleration has proven to be the best predictor for head/brain injury in fall conditions.

6. Development of a Helmet Impact Test System

6.1 Introduction

6.1.1 Rationale

This chapter highlights the design process for a bespoke head impact rig to simulate injurious PO conditions with a high degree of control and repeatability. The need for this became apparent after difficulties when pilot testing projectile brick conditions. The brick impact method used a free-fall 1.5 m drop (5.4 m/s), though produced large variability in brick orientation at impact, despite the use of a vacuum powered frictionless release system. This was attributed to inconsistent release mechanics caused by surface undulations at the seal between bricks and the vacuum nozzle, as well as the inhomogeneous mass distribution of the bricks causing rotation at the start of fall. The resultant head kinematics were extremely affected by these changes in brick orientation, as they caused variation in head impact location, impactor shape (flat face or sharp edge of brick, Figure 6.1), and collision characteristics (brick bounce, roll, slip, etc.).



Figure 6.1, Different brick orientations at the point of contact with the helmeted headform. This demonstrates variation in brick impact conditions for free fall drop simulations, leading to inconsistent head impact measurements [190].

It was decided that brick impacts could not be appropriately simulated with this setup, thus a different system was required. Looking forward, a new system would also benefit the recreations of injurious conditions by offering more repeatability for impact conditions. This can then be used to advise test standard setup, which builds on the findings of Chapters 4 and 5 and contributes to the overall aim of this PhD study.

Impact rigs are available to purchase, such as the Cadex Monorail Tower and Pneumatic Linear Impactor (Cadex Inc.). However, such systems are costly and come as standard, i.e., dimensions, components, operating procedure, etc., which can limit compatibility with head/neckforms as well as impact surface size and shape. The decision was made to develop a system in-house to have more control over the design, meaning guarantee that it meets the requirements for achieving the long-term aims of this project.

6.1.2 Objectives

The design of a bespoke helmet impact rig permits further study to elucidate injurious conditions in PO and advise how test standard protocol could better replicate them. To do so, the design should improve upon common systems used in literature by offering more versatility for what can be recreated. To achieve the goals of this PhD project, the system must include:

- 1. Compatibility with head and neckforms for biomechanical representation and measurement of both linear and angular kinematics [191].
- The choice of impacting headforms with representative objects, as well as using the headform to impact surfaces and anvils, as per standard procedures [13], [19].

The system could be used for further headgear testing beyond this project, i.e. other than PO helmets. Being able to meet the equipment requirements for helmet test standards allows for a versatile system with broad potential applications. The system developed in this chapter is not intended to be an exemplary design, for its purpose is to meet the needs of this project. Despite this, the design processes such as specification, safety considerations, design refinement, and qualities/limitations of the final product could aid the development of future head impact systems.

6.2 Background

6.2.1 Impact Methods

As discussed, freefall drops are not suitable to achieve the goals of this project, thus a decision was required for whether a guided drop, pneumatic ram, or pendulum-based system would be most appropriate. Comparison for each of these is in Chapter 2, Table 2.3. The decision was made to develop a guided drop system, as there were few drawbacks relevant to this project. For example, this method is the most common setup used in headgear test standards, including PO headgear in PSDB 21/04, Figure 6.2 [13], [18]. Guided drops have also shown to be capable of accurately recreating head impacts due to falls from a height, which will support horseback fall recreations [376], and they offer simplicity and accessibility for others to replicate this work in future. In addition, using a similar set up to PSDB 21/04 makes the translation of results more relevant to current testing procedures, and a guided drop can be more easily modified to suit the needs of headgear testing beyond PO application.

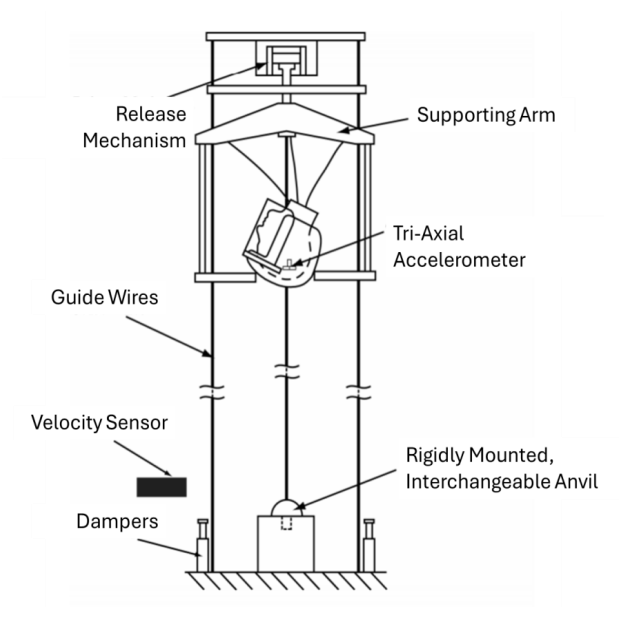


Figure 6.2, PSDB 21/04 standard schematic for assessing helmet energy attenuation using a guided drop system [13].

6.2.2 Head Impact Constraints

Whyte et al's (2019) review of standard headgear impact methods highlights drop guidance systems with rigid affixations for headforms can overly constrain motion, thus inhibiting realistic angular inertia [18], [170]. Conversely, guided cradles, such

as those used in PSDB 21/04 as well as ISO and CEN standards, allow for unrestricted motion of the headform following impact, though can lack biomechanical representation [18], [171], [172], [388], [389]. Very few standards that use drop methods also use neckforms, despite their representation of head injury biomechanics [18], [118], [227], [231], [231], [232], [233], [234], [235]. This is likely due to increased test inconsistency, disagreements on the bio-realism of current neckforms, less control of the impact location as the neckform is a non-rigid component, and the added mechanical strain experienced by the drop system [105], [118], [192], [193]. Figure 6.3 includes examples of guided drops, with drop systems that include linear rails (A, mass = 14 kg [192]) and steel cables (B, mass = 6.8 kg [105]) for guiding the descent.

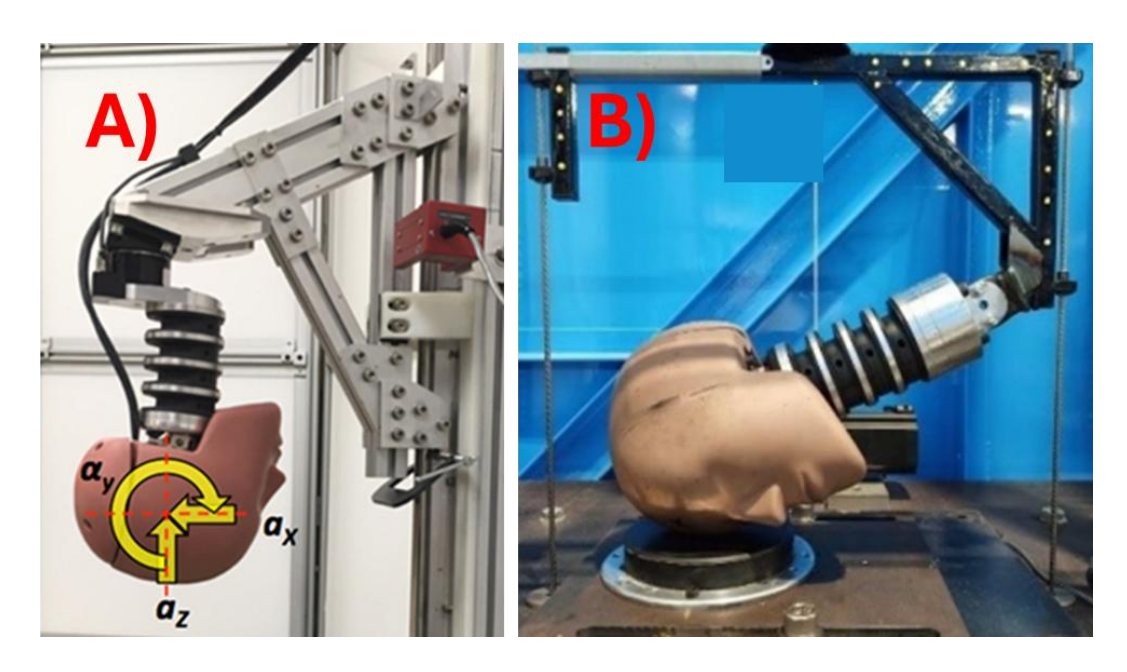


Figure 6.3, Examples of guided drop rigs using Hybrid III head and neckforms in research.

A) Head Impact Testing Facility, Portland Biomechanics Lab, USA [192]. B) University of Canterbury, New Zealand [105].

Guide rails are more rigid and frictional than cables, they keep force transfer in the head/neck region yet withstand significant loads at impact. Cables are lower friction yet can deform with impact and reduce representative neck effects, Figure 6.4. The decision for which would best suit PO application depends on the expected loading conditions, i.e. magnitude and direction, as typically cables are more susceptible to terminal damage when experiencing large forces/torques, thus they are rarely used for oblique impacts.

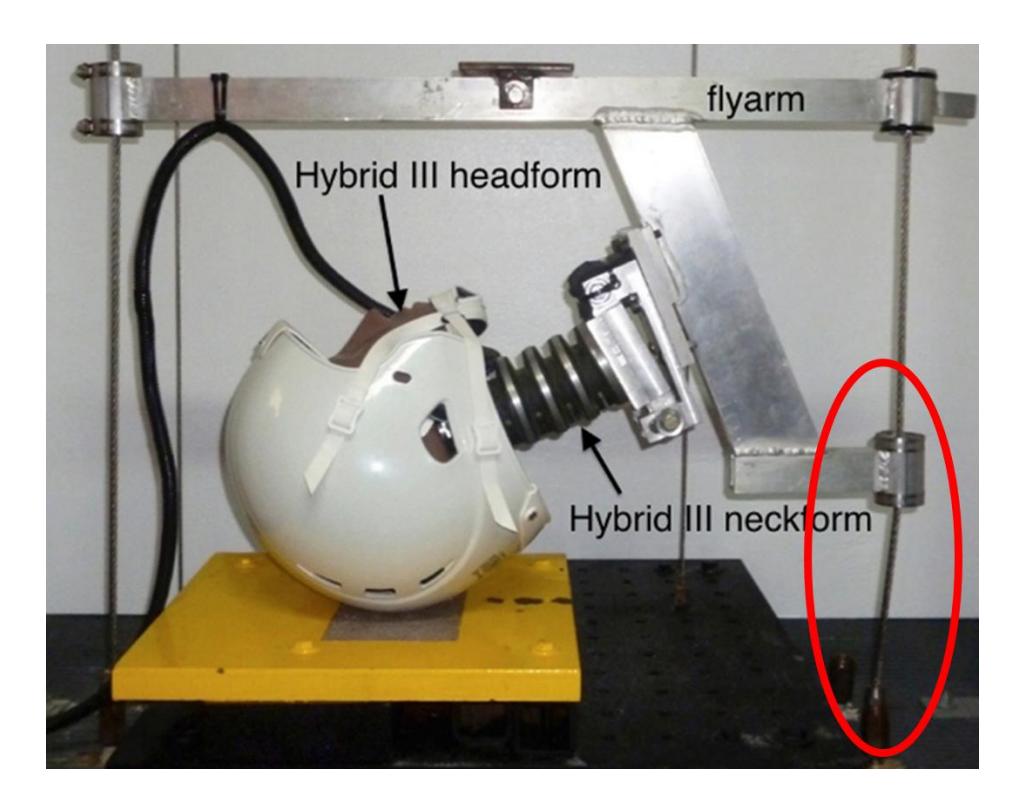


Figure 6.4, An example of steel guide cables deforming at impact (highlighted in red), thus reducing motion in the head/neckform [390].

Limiting the mass of a drop system is optimal for improving user control over the impact mechanics, as it is easier to add mass when required than to remove it. Impact velocities for non-vehicular headgear test standards using guided drop methods range between 3.46 – 6.9 m/s (30 – 120 J when considering headform and helmet drop mass) [15], [18], [75], [77], [391]. PSDB 21/04 also defines a maximum 120 J impact energy for PO headgear [13].

6.3 Design Definition and Methodology

6.3.1 System Requirements

The requirements for a guided drop rig design were compiled in a product design specification (PDS) to identify what was essential ('demands', D), and desirable ('wants', W) from the system, Appendix A.6.1. These included guidance for the systems function, operation, materials, construction, size, and integration within the lab. The primary objective of the PDS was to ensure the system is capable of producing representative head impact recreations, while ensuring rigidity, safety, and quality throughout. Many requirements are defined to meet those of standard

protocol, i.e. permitting adjustable impact velocities and various impact surfaces [13]. Key examples that define the function of the system from the PDS include:

- Adjustable impact velocities in the range 3.4 6.9 m/s to meet the requirements of all non-vehicular helmet standard drop test procedures [13], [392].
- A maximum drop mass of 15 kg to remain in line with other guided drop systems using head and neckforms, and to provide a benchmark 'worstcase' load for safety calculations.
- Compatibility with standard head and neckforms, such as Hybrid III (HIII).
- Unrestricted impact capability to non-facial headform locations.
- Interchangeable impact surfaces and the ability to choose if the headform is being dropped or a representative object will be dropped onto the headform, i.e. to simulate a projectile brick.

Alongside the PDS, there were environmental restrictions limiting the design, such as a maximum floor to ceiling height and limited footprint available. These define the maximum dimensions for the system to 2 x 2 x 4 m. There was also no backup power supply in the laboratory, meaning components for operating the drop rig could not be electronically controlled, i.e. an electromagnetic release system, as loss of power could cause an accidental drop that leads to damage of equipment or physical harm. Further safety requirements were included for the design, such as a safety factor of 3, the ability to be operated by one person, a mechanical safety catch mechanism, minimum working load ratings of 25 kN for all weight bearing equipment, and a remote arming/lifting procedure, Appendix A.6.1.

6.3.2 Key Design Features

Table 6.1 includes example decisions that constituted key components of the system. These were made with intention of meeting the requirements of the PDS and to provide a baseline for design ideation.

Table 6.1, Decisions and rationale for key components of the guided drop system, made to advise design ideations.

Design Decision	Rationale	
Floor-to-ceiling	4 m ceiling height provides impact velocities up to the	
construction.	maximum for guided drop sport and PO impact	
	standards (6.9 m/s), providing friction does not reduce	
	acceleration below 60 % that of gravity.	
Multi-railed drop	Rails strengthen the system against a wider range of	
guidance.	loading conditions, particularly for impacts off the	
	longitudinal plane of the drop tower which induce high	
	lateral torque.	
Lightweight drop	Broadens range of permissible impact energies while	
assembly.	reducing system wear and offering more operational	
	control.	
Option to cradle or affix	Permits recreation of PSDB 21/04 standard methods	
headforms/helmets.	as well as those from broader helmet applications.	
Remote arming	Ensures operators are away from the impact zone	
procedure with	when armed to improve safety and useability of the	
mechanical release.	system.	

A floor-to-ceiling drop height maximised the achievable impact velocity. The system at 4 m height afforded frictional force up to 40 % of gravity (drop acceleration = min 0.6 g) to achieve the maximum impact velocity requirements of non-vehicular drop standards (6.9 m/s). However, drop height was expected to be less than this once an impact surface and release mechanism were included above and below the drop assembly. Efforts were made to limit the combined height of these components as much as possible throughout the design process.

Linear guide rails were chosen over steel cables because the system was expected to be subject to high impact forces. This force was assumed = 21 kN considering the affixation of headform to the rig was a rigid component and a 15 kg drop mass with short 5 ms impact duration, i.e. a worst-case scenario. Rails offer more rigidity than cables, with less deformation under impact load (Figure 6.4 was an example of this). It was believed that cable deformation would be more likely to cause terminal damage to the system. Alongside this, deformation would reduce the resultant kinetic energy of the head and neck, thus portray a less severe impact result. Linear guide rails are notched profiles with bespoke roller bearings capable of self-aligning to improve smooth motion, Figure 6.5 [393]. Many systems utilise monorails, such as the Cadex drop rig, though these are primarily designed for rigid affixations of headforms with non-oblique impact surfaces [170]. They utilise bearings above and below the drop mass to distribute any torque imparted by the impact. Under oblique conditions, or when loads are applied off the longitudinal plane of the drop assembly, large torques can be expected in the lateral direction as the system tries to roll. Two vertical rails were used for the design to reduce the individual share of this torque across bearings and in doing so, reduce likelihood of rail damage with prolonged use.

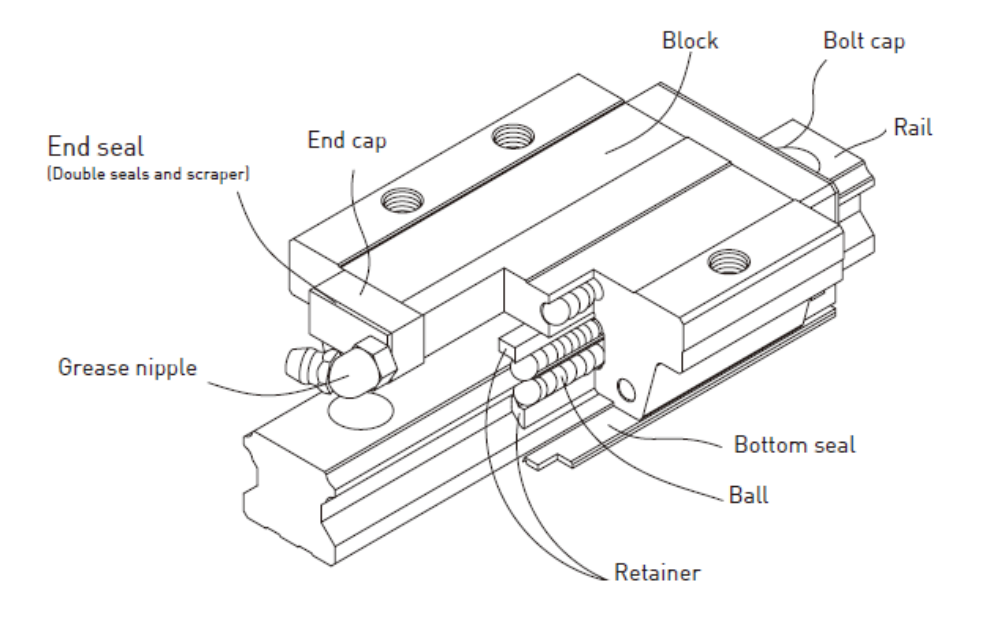


Figure 6.5, Diagram of HIWIN linear guideway HG series rails and bearings used for guiding the decent of drop assembly [393].

A rigid component was required between the neckform fixture and bearings to ensure load was equally distributed between them, and that deformation remained in the anthropometric test device (ATD) components, rather than rig. The rigid component was designed to be stiff, withstanding 21 kN impact loads (F) with negligible deflexion. A 16 mm thick (d) square plate (termed 'drop plate') of anodised aluminium 6082 alloy (assumed modulus of elasticity E \approx 68 GPa) was considered suitable for this load, with deflection (δ_{max}) < 0.1 mm, Equation 6.2 [394]. This considered a 0.5 m square plate (w), simply supported between 0.5 m separated bearings (L), Equation 6.1, I_{depth} = 1.7 x10⁻⁴ m⁴. This formula assumes the plate as a long slender beam for simplification; plate deflection was further assessed with FE analysis, as discussed in section 6.4.3. The drop plate also acted as a foundation for affixing a drop cradle, with possible attachment points at the four corners, Figure 6.6. This cradle permits the controlled decent of an unconstrained headform as per PSDB 21/04 [13].

$$I_{depth} = \frac{dw^3}{12} = \frac{0.016 \times 0.5^3}{12} = 1.7 \times 10^{-4} m^4$$
 (6.1)

$$\delta_{max} = \frac{FL^3}{48EI_{denth}} = \frac{21000 \times 0.5^3}{48 \times 68 \times 10^9 \times 1.7 \times 10^{-4}} = 4.8 \times 10^{-6} m$$
 (6.2)

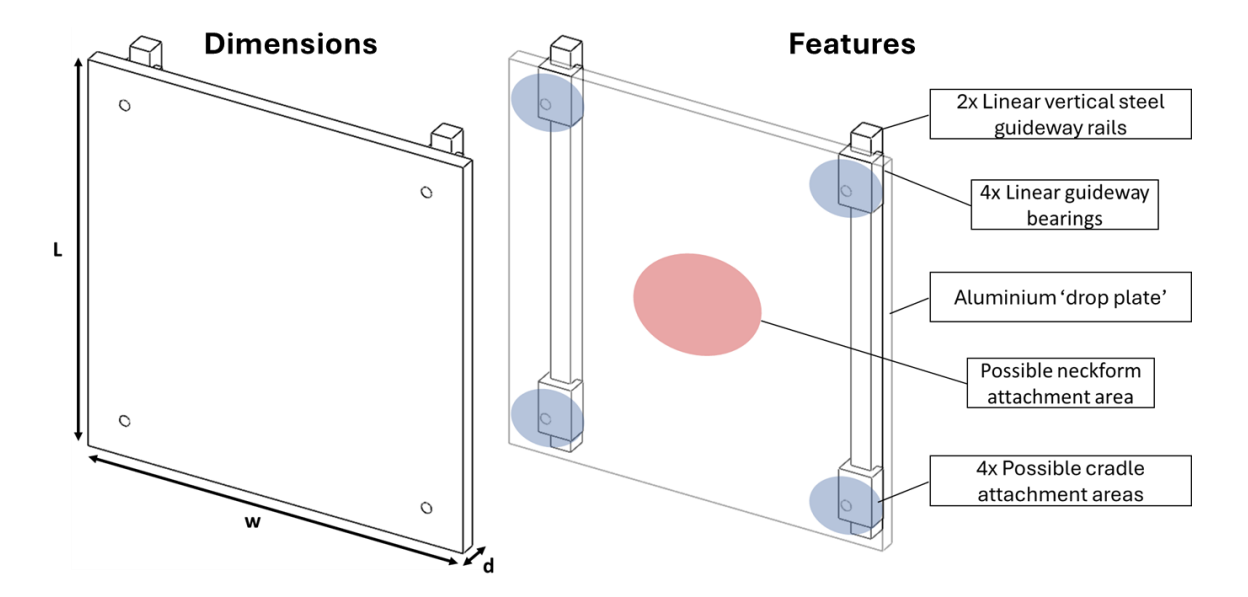


Figure 6.6, Initial concept for an aluminium 'drop plate' to act as a rigid component between the affixation of neckform or cradle and guide rails.

For safety reasons, the lifting and release mechanism had to be operable from a distance while not being electronically controlled. This prevented the use of a remote winch and cable system for lifting the drop assembly. Instead, a manual mechanism was devised using a rope and pulley that offers 2:1 mechanical advantage to reduce effort when lifting, Figure 6.7. The operator pulling down on the rope raises the plate and a ratchet system was added to prevent the rope slipping backwards should the operator let go, preventing accidental drop while arming. An adjustable stopper bracket on the drop tower defines the height of release as it compresses the button of a ball locking pin placed above the drop plate. This pin release descends the drop plate and any affixed or cradled ATD components.

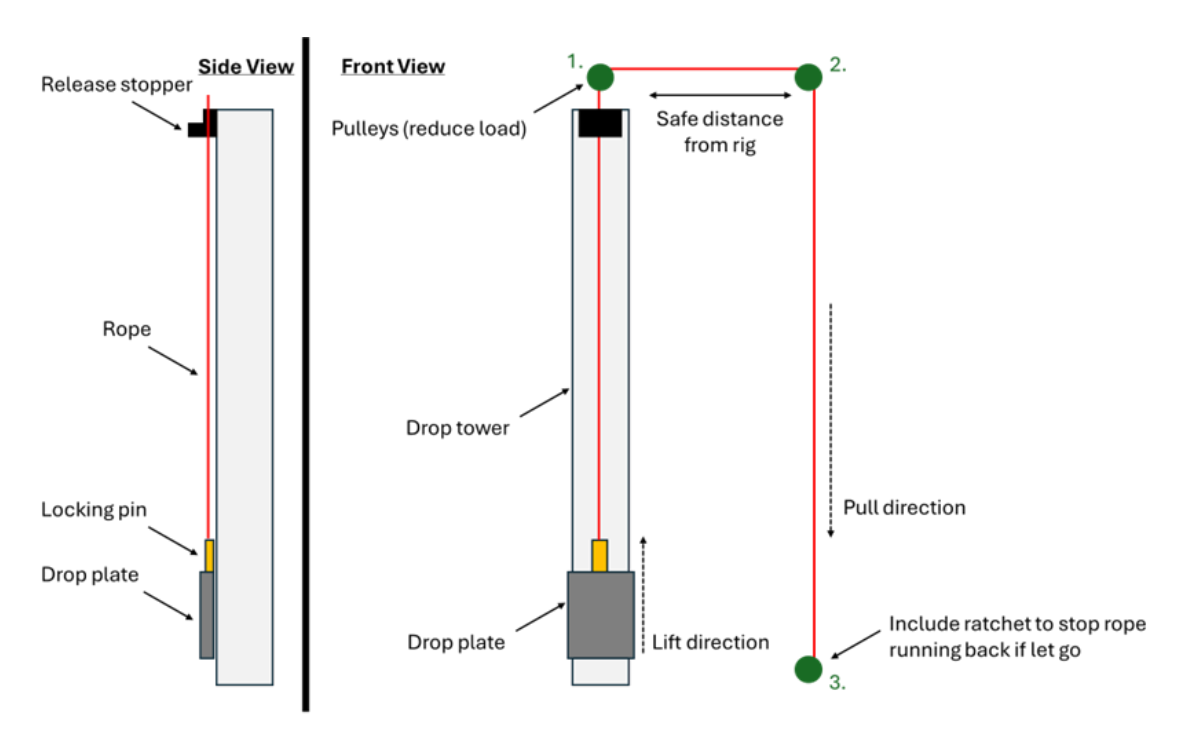


Figure 6.7, Initial sketch of the drop plate lifting and release mechanism. The operator pulls down on the rope above pulley to lift the drop assembly with mechanical advantage.

6.4 Final Design

6.4.1 Summary

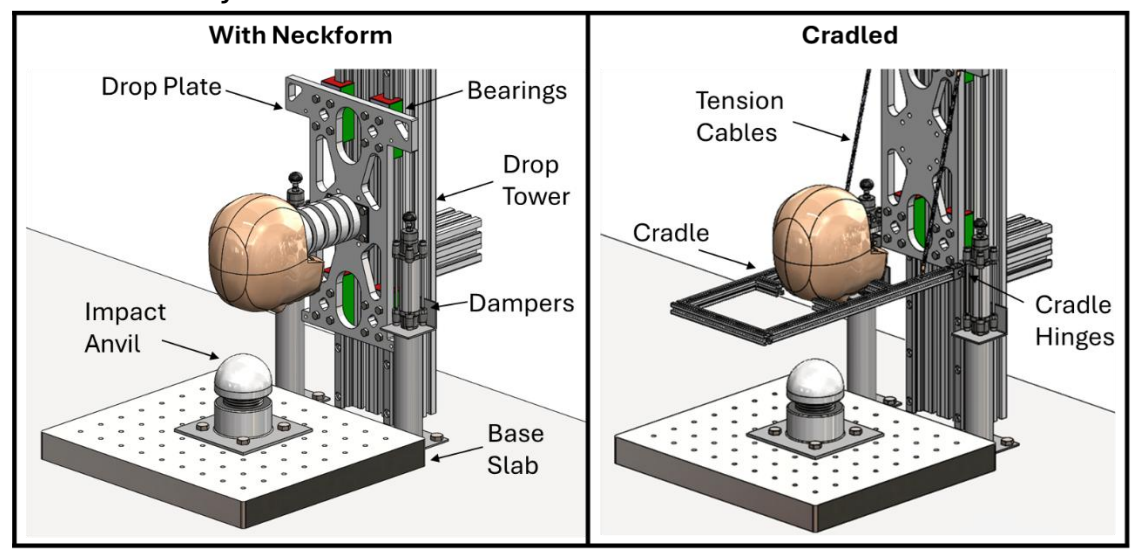


Figure 6.8, 3D CAD model of the designed guided drop system in configurations for affixing headforms with a representative neck or cradling without further support.

A single aluminium floor-to-ceiling strut 'tower' was used to support the drop system, measuring 160 x 80 mm in profile with the rails spaced 120 mm apart at the centres. The drop plate permits compatibility with headforms as either cradled, rigidly mounted, or affixed with a surrogate neckform. Configurations for these are shown in Figure 6.8. The drop assembly has a combined mass of 6.82 kg, or 13.47 kg when equipped with head and neckform. Impact anvils are interchangeable and can be fixed to a rigid steel base slab measuring 0.5 x 0.5 x 0.05 m. This slab features a grid of M12 tapped holes, spaced 0.05 m apart, to accommodate various fixings. Two pneumatic dampers with a 32 mm rod diameter and 60 mm stroke length are incorporated to control deceleration after impact [395].

As discussed in section 6.2.2, limiting the mass of a drop system offers more user control when defining impact energies. This does not apply to the cradled configuration because the headform is an independent body resting on the drop assembly, thus mass is that of the HIII headform only (4.54 kg). The target for the affixed configuration was to match guided drops using neckforms found from literature (\approx 14 kg) [192], [396]. This includes the combined mass of 50th percentile male ATD components (6.65 kg). The final design achieved this, with a combined

total mass of 13.5 kg for the drop assembly. Target areas for limiting mass were the bearings and drop plate, with intention to remove unnecessary weight and not compromise strength. An example result of this is visible in Figure 6.8, where the drop plate has visible subtracted material. The following sections discuss how this was achieved by optimising the separation of bearings and identifying regions of low structural benefit to be removed from the drop plate.

6.4.2 Optimising Bearing Separation

As previously discussed, four bearings were required to sufficiently withstand impact loads and reduce likelihood of damaging the guidance system. Guideway bearings range between 0.18 and 9.82 kg, while heavier models have a significantly greater load rating [393]. The challenge was to use bearings with as low of a mass as possible, yet still meet strength requirements and conforming to a safety factor of 3 as per the PDS.

The effective load on each bearing is inversely proportional to their vertical (V) and horizontal (D) separations. However, increased separations require a larger, thus heavier, drop plate. Static equilibrium torque calculations were therefore used to optimise separations and advise bearing selection, Figure 6.9.

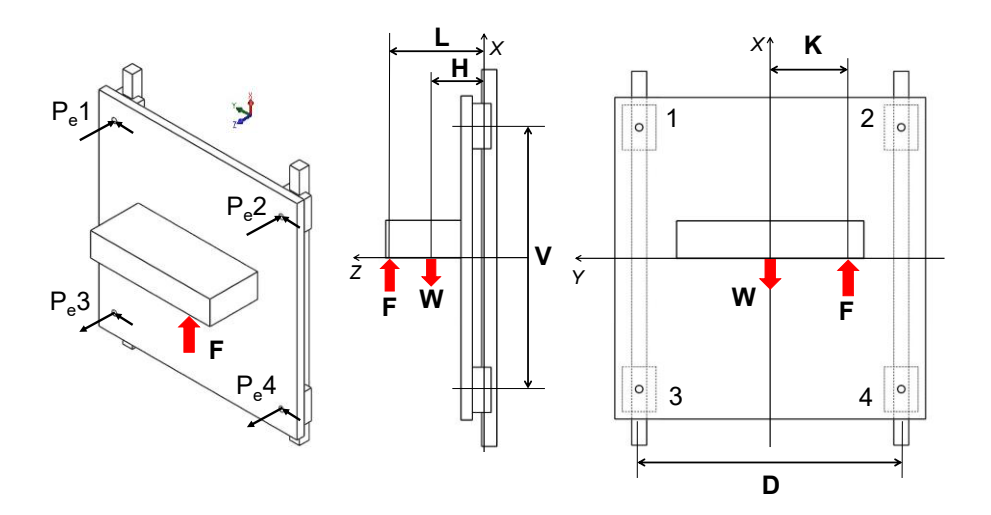


Figure 6.9, Forces and moments considered in calculating the effective bearing reaction forces (P_e) across varying vertical (V) and horizontal (D) separations between 0.1 and 0.7 m.

The effective reaction force on each bearing (P_e) was determined by summing its axial (P_a , Equation 6.3) and radial (P_r , Equations 6.4 and 6.5) components, as recommended by the manufacturer [393]. Therefore, an impact that is off plane from the longitudinal axis of the drop plate would induce the greatest P_e on bearings. P_e was evaluated at 0.01 m intervals of V and D within a range of 0.1 to 0.7 m. A 'worst-case' 21 kN impact force (F) was used, as calculated from an impulse equation assuming 6.9 m/s velocity, 15 kg drop mass (W = 147.15 N), and a short 5 ms contact time [13], [109]. This was applied to the tip of a rigid cantilever, protruding perpendicular from the face of the plate, with length (E) 0.4 m to represent ATD components. The load was offset (E) 0.075 m from the longitudinal plane to simulate an extreme oblique contact point. The centre of mass for the cantilever was considered to be 70 % along the length (E) 0.28 m) to represent how the headform is heavier than neckform.

$$P_{a1}: P_{a4} = \frac{F \cdot L}{2V} - \frac{W \cdot H}{2V}$$
 6.3

$$P_{r1} = P_{r3} = \frac{F}{4} - \frac{W}{4} - \frac{F \cdot K}{2D}$$
 6.4

$$P_{r2} = P_{r4} = \frac{F}{4} - \frac{W}{4} + \frac{F \cdot K}{2D}$$
 6.5

Variations in D mainly affected the distribution of load between left and right bearings, without impacting the total. In contrast, V had a more significant effect on bearing strength requirements, showing an inverse exponential relationship to P_a . The optimal range for V was between 0.35 and 0.45 m, beyond which increasing separation added mass for minor strength gains. P_e per bearing was equal to 22.9 kN for V = 0.35 m and D = 0.12 (width between T-slots on the tower). This equates to 68.7 kN with a safety factor of 3. The selected bearings were 'Heavy Load Type HGH25HA' models with an individual load rating of 69 kN and mass of 0.69 kg. The total mass for four bearings was 2.76 kg. Increasing V to 0.45 m still required the same bearings, thus it would have added volume to the drop plate for no benefit with bearing selection.

6.4.3 Refining Drop Plate Mass

The dimensions of the drop plate were set to accommodate 0.35×0.12 m bearing separations. This was initially designed as an 'I' shape to provide space for attaching a cradle at the corners. Figure 6.10 shows this design and how that equated to an estimated plate mass of 4.7 kg, efforts to remove unnecessary material reduced this by 43 % (mass = 2.7 kg). The upper protruding part of the 'I' was widened to provide area for pneumatic dampers. This was favoured to dampers catching the bottom of the plate as it resulting in less drop height loss. The lower protrusion of the I was made much smaller, though still large enough for affixing a cradle. A detailed engineering drawing of this plate is in the Appendix A.6.2.

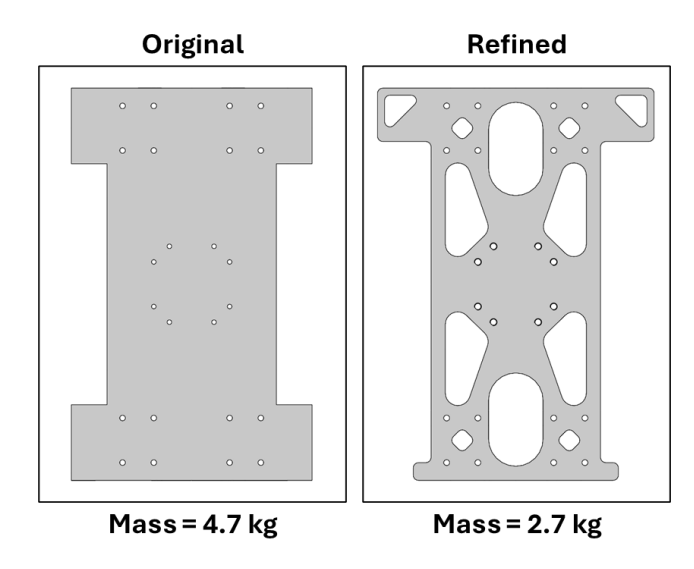


Figure 6.10, Original and refined drop plate designs following the removal of unnecessary mass using Finite Element Analysis. The final design was a 43 % mass reduction.

Finite element analysis (FEA) was used to locate regions of high stress on the plate using Ansys Explicit Dynamics [397]. The setup simulated an 8.5 m/s drop of the plate with affixed head and neckform onto a flat rigid anvil of infinite density, this was an assumed freefall of drop height = 3.7 m (4 m ceiling height – 0.3 m for release and anvil). The geometry was halved along the longitudinal plane to reduce computational effort. Figure 6.11 shows the geometry for initial (A) and final (B) plate designs, as well as an annotated side view of the full setup (C). Bearing holes were constrained to only permit vertical motion, so to represent coupling to the rails. The material properties for each component in the setup are summarised in Table 6.2. An iterative process was adopted, where material was gradually

removed from regions experiencing low stress. A design iteration was rejected if any region of the plate exceeded the yield stress of aluminium (280 MPa) [398]. The mesh was hexahedral-preferred, refined to 0.2 mm at curvature, with minimum 3 divisions along edges and 8 along the plate depth. Mesh independence was achieved with a minimum of 7560 cells for the drop plate; the final mesh had 10,720 cells in the plate and a total of 85,811 cells when including the ATD head and neck model. Peak deflection for the initial and final designs were well within the elastic range for aluminium at 0.14 mm (44 MPa) and 0.17 (91 MPa), respectively. The calculation estimating maximum deflection of a solid beam from section 6.3.2 was 0.0048 mm.

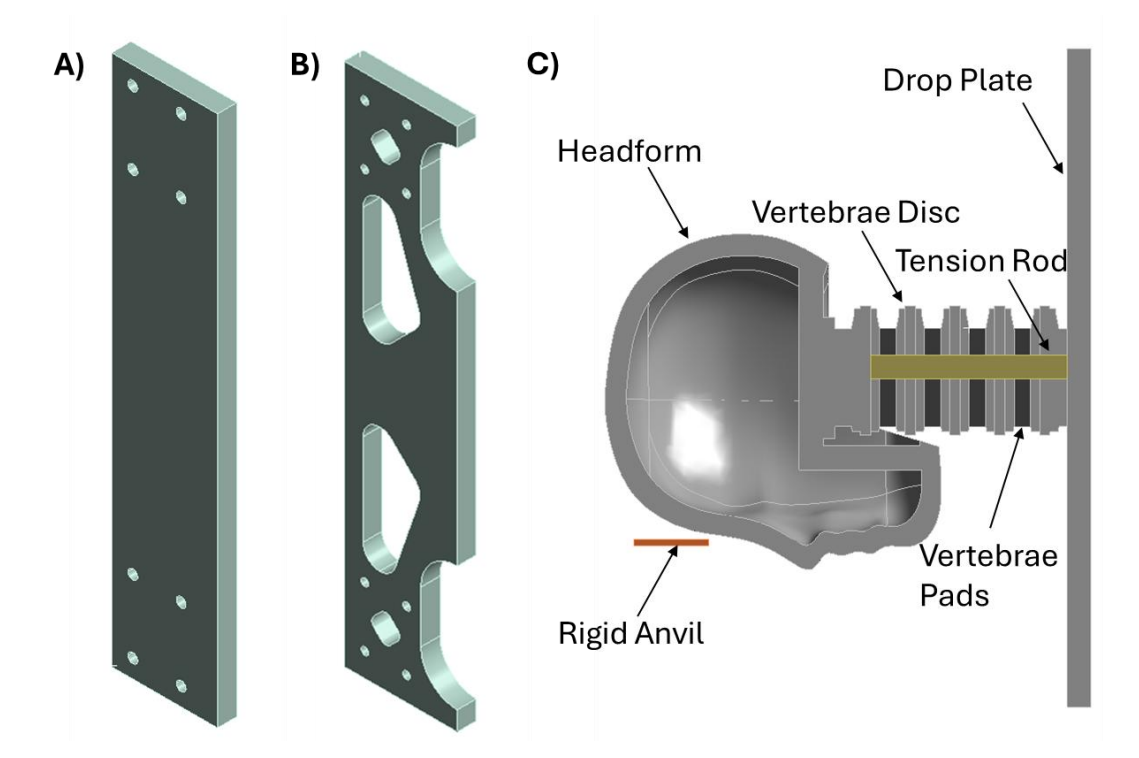


Figure 6.11, Modelled geometry for identifying and removing regions of low structural support on the drop plate. A) initial plate half geometry, B) final plate half geometry, C) Side cross-sectional view of plate, ATD components, and impact anvil [190].

Table 6.2, Density and elastic moduli of materials used in the simulation and the components they were applied to [190].

Assigned Material	Component	Density (kg·m⁻³)	Elastic Modulus
			(MPa)
'Aluminium Alloy'	Plate	2770	7.1 x10 ⁴
	Headform		
	Vertebrae Discs		
'Neoprene	Vertebrae Pads	1150	2.75
Elastomer'			
'Steel Rope' [399]	Tension Rod	7850	1.9 x10⁵

6.4 Implementation

6.4.1 Installation Compromises

Further details for each component of the system, including key safety requirements and additional strength calculations, are in Appendix A.6.3. The design was finalised in Summer 2022 though installation of the system required 23 months (completion June 2024) because of complications with facility legislations and staffing availability. The constructed rig required temporary design compromises to ensure it was useable for this project:

- Replacement of pneumatic dampers with a rubber stack to decelerate the drop assembly after impact.
- A stainless-steel bracket for inverting the neckform affixed head, Figure 6.12
 (C).
- A cradle structure with smaller profile struts and temporary tension cable fixings, Figure 6.12 (D).

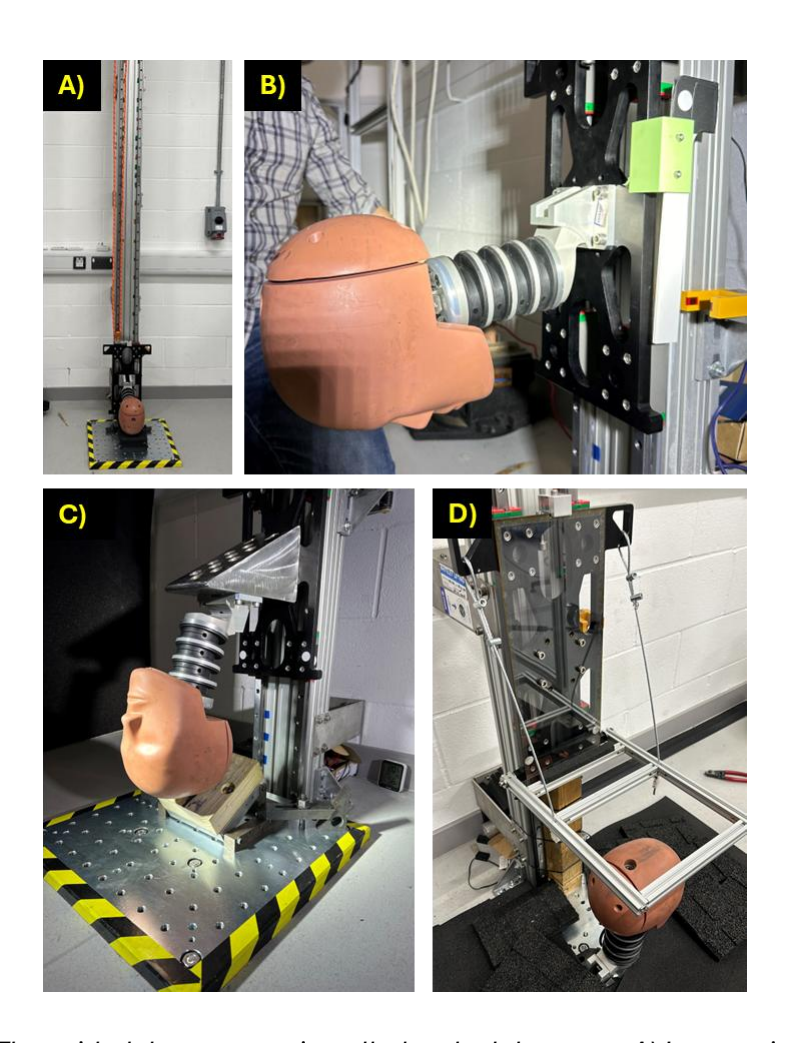


Figure 6.12, The guided drop system installed at the laboratory. A) Impact rig showing the lower portion of drop tower height, B) HIII ATD head and neck components affixed to the drop plate, C) Inverted HIII ATD components with temporary steel bracket between neckform and drop plate, D) Temporary cradle for dropping an unconstrained headform or simulating projectile bricks.

6.4.2 Added Features

The tower required six stainless steel brackets between it and the wall to guarantee rigidity while staying upright. These were placed equidistant, starting 0.3 m from the top to avoid mounting to a non-solid obtrusion. The wall itself was not completely upright, so these included an adjustment fixing to keep the system vertical. Each bracket protruded 0.29 m from the wall and had a thickness of 5 mm. These were bolted to the wall with an M6 x 70 mm anchor bolt torqued to 8 Nm and used eight M5 x 10 mm bolts to fix with the T-slots of the tower.

Protective shielding was added to surround the base slab and prevent any access or egress during testing. It was made mandatory that this was in place whenever the system was lifted. It comprised a 20×20 mm Bosch Rexroth frame with polycarbonate panels on the front and sides of the impact zone. The top and back

were left unshielded to allow for easy positioning around the tower, without interfering with impacting components.

6.4.3 Operating Procedure

The following procedure is a step-by-step process for how the system is operated, which explains how each feature of the design contributes to achieving repeatable head impact conditions. This process assumes the headform is being dropped with the neckform affixed, though it is still applicable for when the headform is not constrained or when a brick is dropped.

Pre-Test:

- Bolt the base of the neckform to the central threaded holes on the drop
 plate and ensure orientation is correct for the desired impact, i.e. impact
 location is facing down.
- Ensure impact surface/anvil is directly below the head impact location and firmly bolted to the base slab.
- Adjust the release stopper to the desired drop height.

Arming:

- Fit the locking pin inside the socket at the top of the drop plate and ensure it
 is securely fitted before lifting.
- At the other end, thread the rope through the ratchet and firmly secure to the fitted eye bolt with a locking carabiner. Pull through, so there is tension on the rope.
- Secure the test area with the polycarbonate shielding before raising the drop assembly.

Testing:

 Stood away from the test area, pull down on the rope while making sure it threads through the ratchet. The drop assembly will lift up equal to half the distance pulled.

- Continue pulling, the button of the release pin will compress against the stopper as they meet, causing the drop assembly to fall.
- Acquire impact data and inspect the test system for damage before rearming the system.

6.4.4 Cost

The cost of the system, with materials being purchased between July 2022 and June 2024, was £2930. A detailed breakdown for this is in Appendix A.6.4. This was cheaper than the predicted cost of a pendulum or pneumatic ram system, £5900 - £6700 (estimated from a part breakdown list), Appendix A.6.5.

6.4.5 Implementation Challenges

The system is now operational and capable of impact velocities up to 7 m/s. However, despite thorough design considerations, there were early challenges that had to be resolved for achieving repeatable impact velocities. Firstly, initial trials produced varied impact velocities for no change in release height. The issue was the guidance system required a 'settling in' period to produce consistent fall mechanics, this consisted of 300 preliminary drops. Following this, the system produced repeatable impact velocities, Coefficient of Variation (CV%) = 0.67%, when trialled at 3, 4, 5, and 7 m/s over a total of 120 trials. However, it was noticed that impact velocity would substantially decrease after every 7-10 drops, thus policy was set to lubricate the rails following every five trials to maintain repeatability.

The friction between bearings and rails was greater than expected, as the supplier recommended a 'heavy' preload setting to reduce damage affects from impact [393]. This creates a negative clearance between the bearing balls and grooves of the rail, causing a compressive force that increases friction. This preload could not be reduced for concerns of damaging the system with prolonged use. However, impact velocity was still above the desired maximum of 6.9 m/s, so preload was not considered a further issue, though this would not have been the case if the system was limited by a lower ceiling height.

The greatest challenge when operating the system was finding the correct drop height for the desired impact velocity. Freefall systems use standard equations of motion to estimate drop height, considering an unresisted acceleration due to gravity (g = 9.81 m/s²). The intention was to estimate the effective friction in the rails and do the same for this system. However, the frictional effect between the bearing and rails was subject to the mass of the drop assembly. This was an inverse relationship, where increasing mass decreased the effective frictional force and resulted in greater impact velocities. The plan was to formulate a model for predicting impact velocity while considering mass, though this was complex because how mass was positioned would also influence velocity. For example, mass was concentrated further from the tower when the headform was affixed with a neck, which caused more binding between bearings and rails than when mass was added directly to the drop plate. A separate research project has now been established to produce a model for predicting drop height for this system, though drop height was determined with repeated trial and error means for the remainder of this project.

Overall, these challenges have not affected the capability of the system, though difficulty with predicting drop height greatly affects useability. 7 m/s is achievable without adding further mass to the neckform affixed test configuration, thus it can meet the requirements of all non-vehicular drop test standards [18]. However, the reduced mass of the drop plate means additional weight (2.5 kg) was required to achieve this with cradled conditions. This does not affect the headform impact mechanics, as the weight is coupled to the drop plate and the headform remains an unconstrained entity. The addition of 2.5 kg is therefore compensating for the absence of neckform weight only.

6.5 Discussion

6.5.1 Design Review

The designed test system provides means for repeatable head impact testing that can be used for this project as well applications beyond PO. The design meets the objectives outlined at the start of this chapter, which have resulted in compatibility with headforms under various constraints and a broad variety in head impact recreation setups. As a result, it meets the requirements of all non-vehicular guided drop methods in headgear test standards, including PSDB 21/04 [13], [18]. The methods shared for each stage of the design process, including definition, ideation, refinement, and implementation, can also help advise future head impact test system developments. This has potential to contribute towards homogenising the methods and equipment for simulating realistic head impacts under controlled conditions, so to make research more comparable and repeatable.

A highlight of the design is the ability to achieve repeatable impact locations and velocities (CV% = 0.67) while using a dual-railed guidance. This reduces the likelihood of damage to the rails, bearings, and other components without compromising impact control. Steps were taken to minimise the weight of the drop assembly, including the optimisation of bearing selection, separations, and drop plate volume, to achieve a maximum drop mass in-line (Δ = -0.53 kg) with monorail systems found in literature [192], [396]. The system was produced cheaper than the expected costs of pneumatic ram and pendulum-based equipment (£2930, compared to \approx £5900 – £6700). The use of a guided drop is also a more universally recognised method for impact testing that is easier to translate to the majority of head impact research [191]. It is also commonly used in test standards, has a lower footprint area requiring less lab space, and is simple to operate, train personnel on, and maintain.

Despite thorough planning, there were challenges faced with the implementation of the system. These were primarily due to the delayed installation period and the unanticipated affect drop mass would have on fall friction. Though the desired impact velocities were achieved with this design, selecting the correct drop height for a desired velocity remains a challenge. This is because the distribution and

quantity of mass on the drop assembly influenced the magnitude of friction between the bearings and rails. A plan was set to create a predictive model for this, though it was not completed in time for this project as the delayed installation postponed all testing to later in the timeline. The delay also forced compromises with certain features of the system so that it was ready in time for testing: the replacement of pneumatic dampers with a rubber stack, a basic stainless-steel bracket for inverting the neckform, and a reduced strength cradle. These changes did not affect the ability to produce representative impact conditions, as discussed in upcoming chapters, though will eventually need replacing to ensure the prolonged rigidity of the test system.

6.5.2 Further Improvements

The primary area for improvement of this system is the sensitivity between fall velocity and the mass of the drop assembly. This is unlikely to be fixed without replacing the bearing and rail system, thus efforts should be made to instead make the velocity more predictable from the drop assembly conditions. A model could be used to advise anticipated impact velocity based on the set drop height, the amount of mass on the drop assembly, and how this is distributed. The inclusion of instrumentation for direct velocity measurements would accelerate the development of this model and provide instantaneous feedback to operators.

The cradle is currently built with narrower profile struts and temporarily fixed tension cables with no shielding. These are expected to experience large amounts of wear, as they are components of the drop assembly and subject to a large force following impact. Should this wearing affect the properties of the cradle, i.e. shape or angle from the drop plate, then the impact conditions would be adjusted midtesting, and data could be affected. In addition, if the cradle experiences damage to the point of failure, unplanned drops could occur, and safety would be of concern. Replacing these with stronger components is a simple and easy solution, such as larger profile struts, shielded tension cables, and the strengthening of fixed points between the cradle and drop plate. However, efforts should be made to keep cradle components low cost, so they can be regularly replaced. This is a more efficient policy compared to producing a singular expensive piece with a long

expectancy of use, as damage is still likely, yet it may not be easy for an operator to recognise.

Lastly, the nature of guided drop methods is to have one of the impacting bodies fixed in place. Traditionally, this is the impact surface at the base of the system [170], [171]. Both pneumatic rams and pendulum systems tend to include linear slide tables to permit up to 0.5 m translation of the ATD components after impact [25], [177], [188]. This was designed to replicate more realistic post impact kinematics, i.e. the motion of a torso. Slide tables are now a part of the testing requirements for newly manufactured American Football helmets (NOCSAE ND002-17m21) and have been adopted in the Virginia Tech 'STAR' rating [15], [184], [189]. Should widespread adoption of slide table lead to mandatory inclusion in test systems, this would be a challenge for any guided drop method to easily adopt. However, slide tables have not seen much adoption within standards across the ≈ 20 years since they were proposed, thus it is unlikely to see such implementation in the near future without more firm evidence for their benefit.

6.7 Chapter Conclusion

This chapter details the development of a bespoke system for repeatably testing head impact conditions. The completion of objectives laid out in section 6.1.2 means the guided drop system can meet the criteria of PSDB 21/04 PO impact standards, while also being compatible with ATD components for representative head impact measurements. In addition, the versatility of the system to allow for dropping headforms under different constraints as well as situationally representative objects, such as bricks, means it meets the needs for the remainder of this PhD project. This versatility also lets it meet the needs for all non-vehicular headgear standards that require guided drop methods. Though this system is not intended as an exemplary design, the detailed discussion of design process and implementation can help advise future head impact test system developments. The next steps are to use this rig when simulating projectile brick impacts, to further build towards a holistic view of head injury conditions in PO. The system can then be used again to advise how a guided drop test method could be setup to best replicate PO injurious conditions.

7. Injury due to Projectile Bricks

7.1 Introduction

Projectile bricks and stones were identified as the most prevalent threat to head injury in PO operations. This was supported by protective security engineers in employment of the Metropolitan Police Physical Protection Group (MPPPG), who stated thrown bricks were the weapon they most anticipate the public using. As such, in their PO training procedure they include thrown low-mass (0.25 kg) wooden bricks, consolidating that they view bricks as a threat officers should be prepared for. Despite this, there are no known studies quantifying the injury mechanics of thrown bricks to the head. This chapter aims to elucidate the head impact mechanics of thrown bricks, in a similar manner to Chapters 4 and 5 that studied wielded blunt weaponry and falling from horseback. This can advise how PO standard test methodology could best represent projectile brick conditions when assessing the protective efficacy of headgear.



Figure 7.1, Bricks remaining on the floor in the aftermath of a PO event, after the public used them as projectile weaponry [400].

Research on falling objects in construction sites highlights the severity of head and brain injuries in these scenarios, although these lack specificity for the details of brick-like objects that the public could throw [210], [401], [402], [403], [404]. These include typical kinetic energies, i.e. masses and throw velocities, that are required

for studying head impact predictions. Therefore, the objectives of this chapter are to:

- 1. Quantify the expected mechanics of a person throwing a brick.
- 2. Study the kinematic effects of head impacts due to projectile thrown bricks.
- Advise loading conditions that should be replicated when testing PO headgear.

7.2 Quantifying Thrown Brick Mechanics

7.2.1 Brick Characteristics

In the United Kingdom (UK), bricks are traditionally made to the dimensions of the withdrawn standard BS 3921:1985 (withdrawn 2007), as the current guidance only defines how manufacturers should report brick properties (BS EN 771-5:2011) [405], [406], [407]. The size, $215 \times 102.5 \times 65$ mm, makes them easy to throw as they are designed for picking up with one hand to be laid on mortar [405].

The example for gross density of an unspecified brick within 'Annex A1:2015' of BS EN 771-5:2011 is given as 2000 kg/m³, which equates to 2.9 kg with traditional dimensions [406], [407]. Though this could be an overestimate, as many bricks come with voids to make them lighter, easier to handle, and more insulated [405]. Therefore, in this study, six traditional engineering bricks were collected and measured for their mass (mean = 1.92 kg). These had the same external dimensions as the withdrawn standard (BS 3921:1985), though included ten, 30 mm perforated holes, which reduced the volume by 32 %. The gross density of these bricks (mean = 1974 kg/m³) is similar (Δ = -1.3 %) to the example of BS EN 771-5:2011+A1:2015, thus confirming the example is representative. Therefore, for simplicity in this study, the masses for traditional clay bricks can be constrained to an upper limit of ≈ 3.0 kg with no voids, and a lower limit ≈ 1.2 kg, as regulation defines no more than 55 % of volume can be voids [407], [408].

7.2.2 Throw Mechanics

Throw analyses assumed the release height of a thrown brick was equal height to the impact for simplicity, thus the velocity at release is the maximum velocity of the bricks trajectory [409]. In reality, bricks could be dropped from an elevated position and velocity at impact would be greater than release, although the variation in this is vast and would be overly complex to predict for this stage of research. Cross (2004) describes the physics of overarm throwing with a study of five male participants throwing objects of various shape and mass [410]. These included lead 'blocks' and 'bricks' of 1.4 and 3.4 kg, respectively. The mean throw velocities for each these were roughly 11 and 8 m/s. The author states a power law relationship between object mass and throw velocity, where n = 0.4 for masses between 0.72 and 3.4 kg, Equation 7.1 (v = throw velocity, k = a person-specific constant, m = object mass). Mean k, which describes the innate capability of the thrower, was therefore 12.8 kg·m/s. Using this, throw velocities for bricks of mass between 1.2 and 3 kg would be within 8 and 12 m/s.

$$v = \frac{k}{m^n} \tag{7.1}$$

A brief study was conducted to verify these throw velocities for a household brick. The method included use of two clay bricks, with properties as in Table 7.1. To represent an extreme example of someone in the public throwing a brick, a singular able-bodied male participant was selected (age: 28 years, height: 188 cm, mass: 110.2 kg) with a history of playing rugby (+15 years). They were instructed to throw each brick as far as possible under two conditions: from a stationary starting point and with a 3-metre run up. The instruction was given to throw the brick in a manner natural to them, in which they opted for an overarm right-handed throw. Three trials were conducted for each brick and condition, totalling 12 throws. The participant was provided a dynamic warm up and three minutes rest between each throw, to reduce fatigue effects. A single video camera (60 Hz) positioned 4 m perpendicular from the plane of motion captured brick trajectory up to at least the apex of flight. 'Tracker' digitisation software (Tracker: Video Analysis and Modelling Tool, [411], [412], [413]) was used to measure the two-dimensional centroid of

bricks over 20 frames following release. The throw velocity over this period was calculated as the ratio of the resultant displacement and change in time.

Table 7.1, Dimensional and mass properties of clay bricks used in the preliminary study to quantify achievable throw velocities.

Property	Brick A	Brick B
Size (mm)	215 x 102.5 x 65	227.5 x 107.5 x 75
Mass (kg)	2.48	3.46

Mean release velocities across each condition are shown in Table 7.2, the maximum was 9.82 m/s for a 2.5 kg brick and run up throw. For both bricks, the run up permitted a faster throw, though this was more influential on the 3.5 kg brick (Δ = +13 %) than the 2.5 kg (Δ = +5.4 %). The velocity difference between the two masses thrown from stationary equates to k = 13.1 kg·m/s when subbed into Equation 7.1, which shows these throws are above the average ability of participants from Cross (2004) [410]. With a run up, k increases to 14.3 kg·m/s. From this, the range of anticipated velocities for a mass between 1.2 and 3 kg and a run up throw are calculated at 9.2 – 13.3 m/s.

Table 7.2, Mean throw velocities (± one standard deviation) at the moment of release for 2.5 and 3.5 kg clay bricks.

Release condition	Mean release velocity (m/s)		
	Brick A	Brick B	
Stationary	9.32 ±0.12	7.75 ±0.18	
3-metre run up	9.82 ±0.11	8.75 ±0.20	

Figure 7.2 shows achievable throw velocities (Equation 7.1) and the resulting kinetic energies for bricks between 1.2 and 3 kg, for assumed average stationary (k = 12.8 kg·m/s) and more extreme run up (k = 14.3 kg·m/s) throw capabilities. From this, the range of kinetic energy to be expected for projectile bricks is within 85 J (lowest k, lowest mass, greatest velocity) and 127 J (greatest k, greatest mass, lowest velocity).

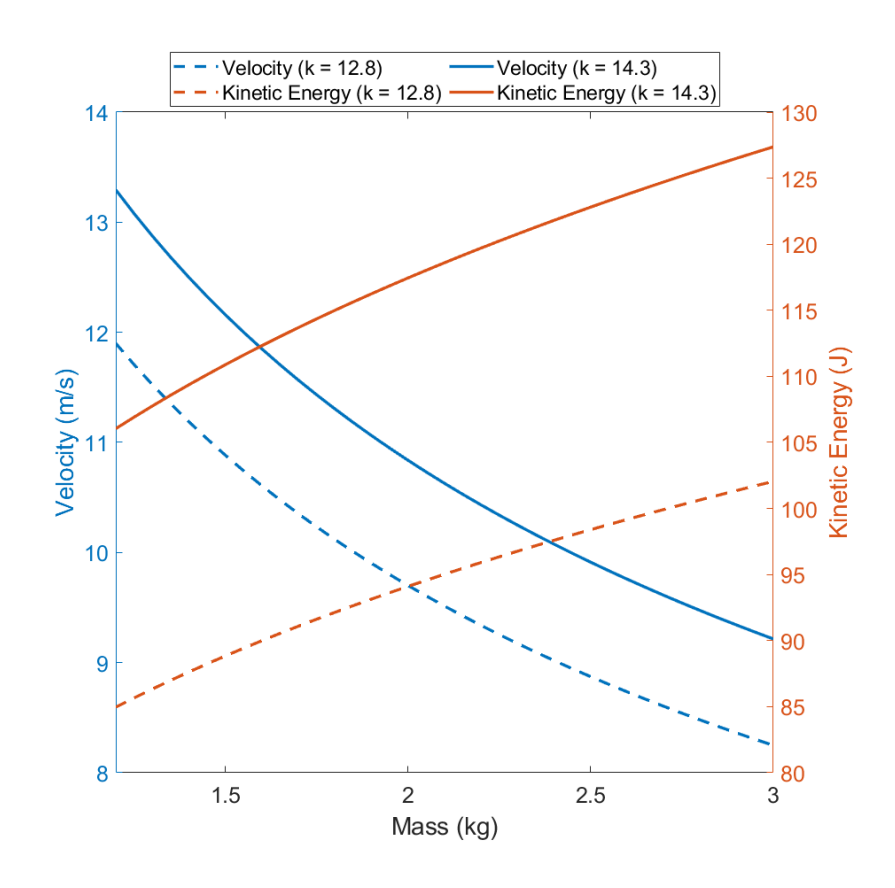


Figure 7.2, The relationship between achievable throw velocity and resultant kinetic energy for mass in the range expected of traditional clay bricks (1.2 – 3 kg). k = 12.8 and 14.3 are constants representing realistic average and extreme throw capabilities.

These impact energies (85 – 127 J) provide representation of projectile brick loading mechanics that can advise study of head impact effects, therefore meeting objective 1 of this chapter. The following steps applied these conditions in a manner similar to the work of Chapters 4 and 5 to quantify the representative head kinematics. This contributes towards advising how standard methodology can be setup to represent realistic projectile brick conditions in PO headgear assessments.

7.3 Head Impact Recreation Methodology

7.3.1 Experimental Arrangement

As discussed in Chapter 6, freefall drop methods were inadequate for producing repeatable brick impact conditions, thus a guided drop system was developed. This utilised a Hybrid III (HIII) 50th percentile male headform (mass = 4.54 kg, circumference = 57.2 cm) and neckform (mass = 2.11 kg, length = 18 cm, axial tension = 1.10 Nm) for biomechanical representation [173]. Impact locations were

the back, crown, front, and side of the headform, so as to replicate experimental testing in Chapter 4. The neckform was affixed directly to a steel slab at the base of the drop tower when impacting the headform crown, whereas a rigid bracket was used to angle the ATD and permit testing on the headform back, front, and side, Figure 7.3. Back and side impacts were set at an angle 90° to the base, whereas front impacts were angled up 45° so the brick hit square with the forehead. This meant impacts avoided the face, which would be guarded by a face shield if this was a helmeted officer, and there was less chance of bricks hitting the nose before the skull.

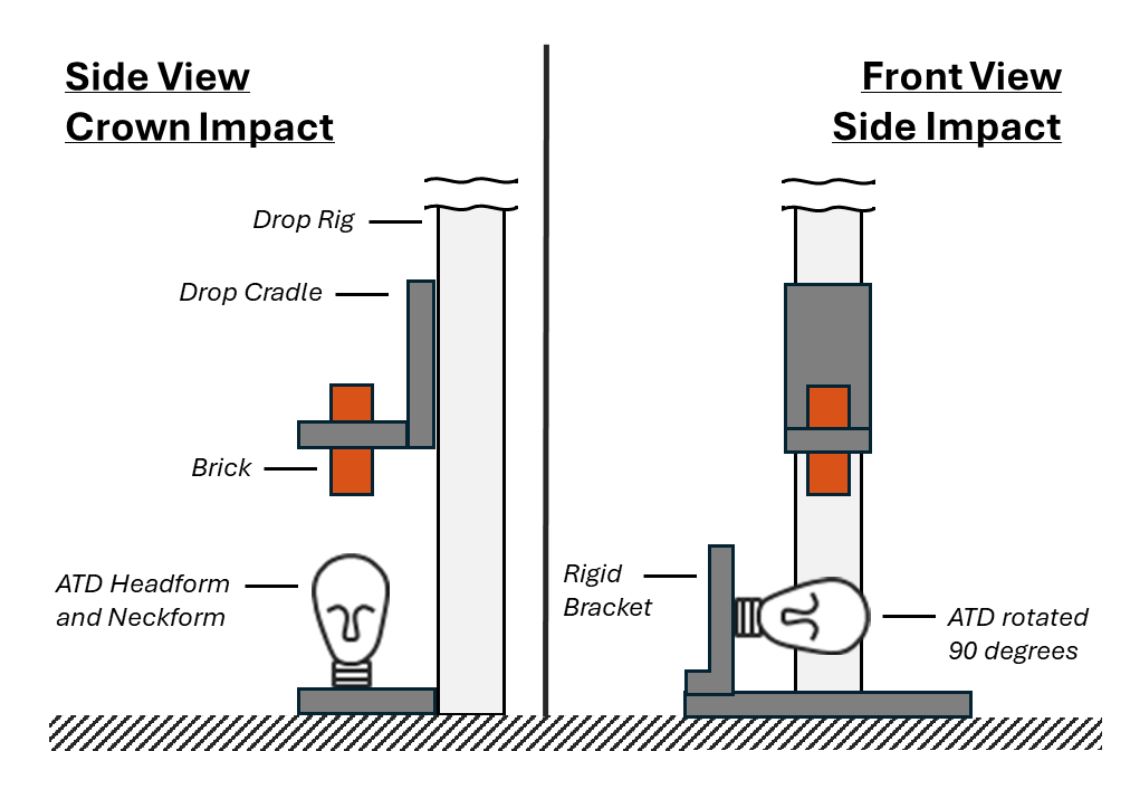


Figure 7.3, Experimental arrangement for simulating cradled brick impacts to the head using a drop rig. Bricks were cradled and dropped from a known height. The neckform constraint was rotated to permit different impact locations on the headform.

A clay brick of mass 1.91 kg and dimensions 215 x102.5 x 65 mm was dropped to simulate a projectile; this was cradled on the drop rig with a low-mass (0.33 kg) armature for support. The angle of the brick was set so the long edge was parallel with the height of the drop tower, a flat face would contact the headform, and the full weight of the brick is directly behind it. Cradling the brick was considered more representative than fixing it to the drop tower so the combined mass of brick and armature (2.24 kg) were all that contributed to impact energy, not any mass effects

from the rig. This also permitted rebound of the brick off the headform as expected in-field. Brick mass was measured again after testing, showing little change (Δ < 0.5 %).

Impact velocities of 8.7 and 10.6 m/s are required to produce kinetic energy of 85 and 127 J with a drop mass of 2.24 kg. These were not permissible with the height of the drop rig; 6.5 m/s was the maximum due to the low drop mass and friction of the guide system. Instead, incremental measures at 3, 5, and 6.5 m/s (10, 28, and 47 J) were taken, and the relationship between them (section 7.3.2) used to advise higher speeds. Each of these were repeated 5 times at each location, totalling 60 trials.

A high-speed video (HSV) camera (4000 Hz) was positioned 1.5 m laterally from the drop rig, with a field of view = 0.62 x 0.98 m to capture impact and the subsequent motion of head and neckform. A secondary camera was positioned perpendicular to this, 1.5 m from the front of the rig, for an additional view if required. Calibration procedure was as Chapter 4, using a 30 mm checkerboard to build real-world coordinates and correct lens distortion [351], [352], [353], [354]. To capture impact velocity with HSV, a white circular marker of 20 mm diameter was placed on a rail bearing on the drop assembly. The marker centroid was recorded over 40 frames (10 ms) pre-impact using the script discussed in Chapter 4 and was differentiated into velocity by the time between camera frames (Matlab 2023b [350]).

7.3.2 Head Impact Assessment

Headform kinematics were recorded with a 6DOF 3a3ω sensor package (Slice 6DX PRO, DTS) located at the headform CoM [251], [355]. Sample rate was set to 100 kHz and CFC 1000 and 180 filters were used for linear and angular measures respectively, in accordance with SAE JS211 [28], [244]. The IMU trigger was set to 5 g in any of three accelerometers, capturing 0.02 s prior and 0.1 s post contact. As in Chapters 4 and 5, linear and angular accelerations were the considered metrics for quantifying head impact magnitude, so to permit comparative analysis. Angular acceleration was again calculated by differentiating angular velocity with the 5-point stencil method [247], [248], [249], [250].

Headform data was processed and analysed using MATLAB script (Matlab 2023b [350]). Resultant kinematics were calculated as the 3-dimensional Pythagorean result of x, y, and z components. Pulse durations were recorded as the time difference between the start and end time of each initial loading curve. Mean values were calculated for impact velocities, resultant peak linear acceleration (PLA), and resultant peak angular acceleration (PAA). Standard deviation and coefficient of variation (CV%) were used describe within group variance. Two-way 'Analysis of Variance' (ANOVA) with a 95 % confidence interval was used to assess if impact location or velocity had significant effects on peak headform kinematics [21], [356]. Post-hoc Tukey's tests provided detailed comparisons for each condition, including their interactive effects. F statistics were used to quantify the amount that varying impact velocity or location influenced headform kinematics. Interrelation between PLA and PAA across all loading conditions was compared for both linear and non-linear relationships, using R² to assess model fit.

Mean kinematic time relationships were calculated by synchronising the trigger points of every trial within each group and averaging the resultant data. These were calculated for 3, 5, and 6.5 m/s, while 8.7 and 10.6 m/s were calculated using nonlinear regression as peak kinematics have a power law relationship with impact velocity [105]. This can be derived as Equation 7.2 where y = any kinematic variable, v = impact velocity, and A and B are the linear and exponent coefficients for the model. Instead, A and B were calculated for each impact location using the means of 3, 5, and 6.5 m/s impacts to fit the model [414]. The mean of residuals and RMSE were reported alongside each regression to assess goodness of fit.

$$y = A \cdot v^B \tag{7.2}$$

Predicted values for peak kinematics and pulse durations were used to plot example curves (y = linear or angular acceleration, x = time) for 8.7 and 10.6 m/s impacts. These assumed a symmetrical half-sinusoidal shape that starts and ends at y = 0, using Equation 7.3 [80], [81], [82], [83].

$$y_{Linear/Angular} = Peak_{Linear/Angular} \cdot \sin\left(\frac{\pi \cdot x}{Duration_{Linear/Angular}}\right)$$
(7.3)

7.4 Results

7.4.1 Peak Headform Kinematics

Mean impact velocities for each drop height were 3.2 (\pm 0.04), 4.9 (\pm 0.08), and 6.5 (\pm 0.26) m/s. CV% for impact velocities across all trials was 2.4 %, due to necessary height adjustments between impact location setups. The within group variation was considerably more repeatable, with a mean CV% across all conditions = 0.73 %.

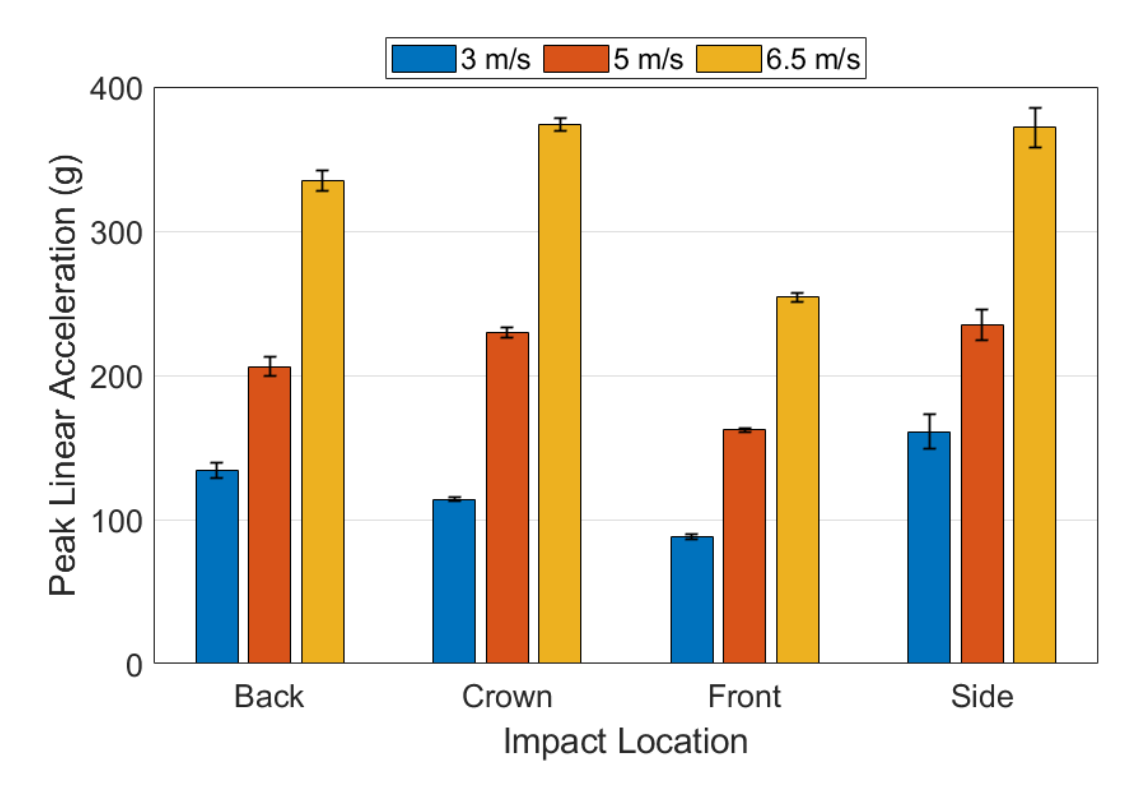


Figure 7.4, PLA for all headform locations with brick impact velocities of 3, 5, and 6.5 m/s. Error bars indicate one standard deviation colours represent impact velocity.

Two-way ANOVA statistics for PLA showed significant effects (P < 0.01) of impact location, velocity, and the interaction between these test variables, Appendix A.7.1. Of these, velocity had the greatest influence on PLA variation (F = 3098), followed by location (F = 331), and then their combined effect (F = 29.1). Each location was significantly different (P < 0.01), the greatest PLA was for side impacts (mean = 256 g), closely followed by crown (239 g), then back (225 g). Frontal PLA values were much lower on average than the other locations (168 g). Mean PLA was statistically different between impact velocities (P < 0.01) and exponentially increased between 3, 5 m/s, and 6.5 m/s (Δ PLA = +83.6 g between 3 and 5 m/s, ΔPLA = +126 g between 5 and 6.5 m/s). The interaction effects showed 6.5 m/s crown (374 g) and side (372 g) PLA were indistinguishable (P = 1), and greater than any other condition. Other similar interactions included 5 m/s crown (230 g) and side (235 g), as well as between 5 m/s front (162 g) and 3 m/s side (161 g) impacts. Mean linear pulse durations were 1.54 ms, with low standard deviation across all groups (≤ 0.1 ms). Front impacts had the longest duration (mean = 2.04 ms) followed by crown (1.53 ms), back (1.32 ms), and side (1.26 ms).

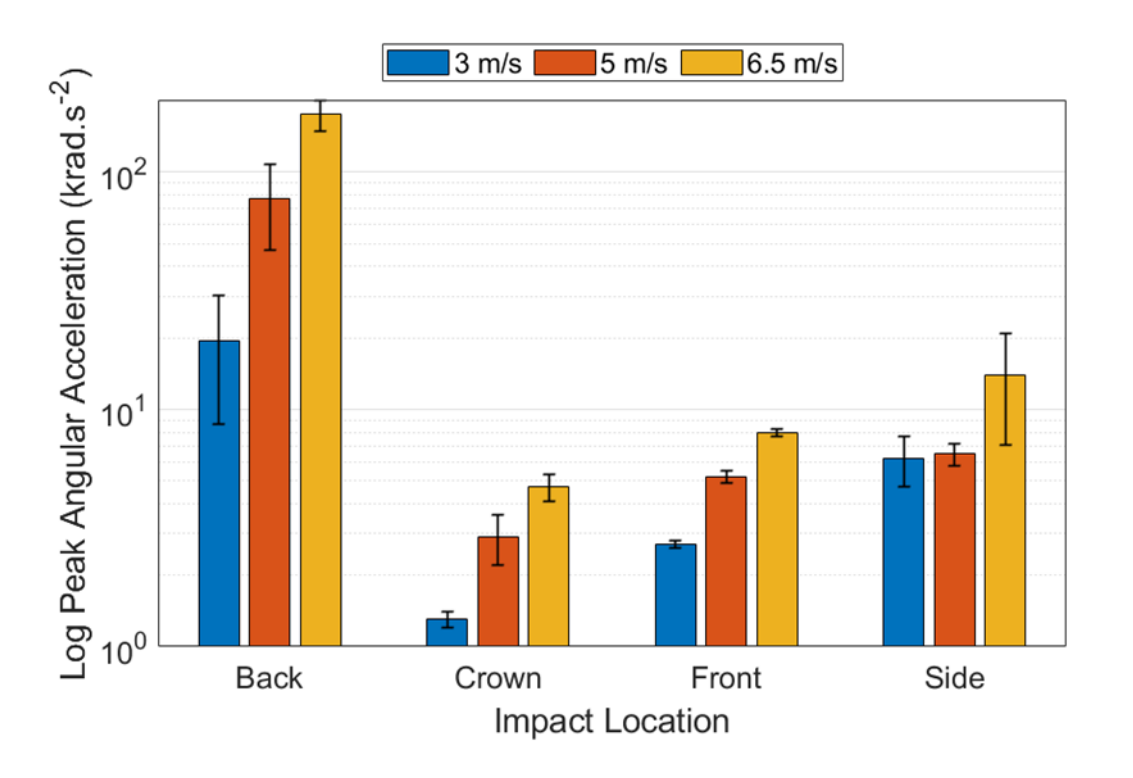


Figure 7.5, PAA for all headform locations with brick impact velocities of 3, 5, and 6.5 m/s. Error bars indicate one standard deviation. Y axis is shown as logarithmic to accommodate the difference in magnitude between back impacts and other locations.

PAA was also affected by impact location, velocity, and the interaction between them (P < 0.01), Appendix A.7.2. Unlike PLA, PAA variation was more influenced by location (F = 132), followed by velocity (F = 42.4), and combined effect remained the least influential (F = 34.7). Back impacts were significantly larger than all other groups (Mean = 90.9 krad/s^2 , P < 0.01), though the size of this difference suggests a drastic change in the impact characteristics. Figure 7.6 shows high-speed frames over 12 ms for back and front impacts which highlight how the brick bounces off the headform for back impacts, though remains in contact for frontal impacts. This was also reflected in the angular pulse duration, where the mean of front impacts was 50 % greater than back (back = 1.8 ms, front = 2.7 ms). Crown and side impacts had mean durations of 1.5 and 2.2 ms, respectively. The change in headform orientation ($\Delta\theta$), measured from the relative angle of the rear cap seal at the back of HIII headforms, shows back impacts rotated significantly more than front (Δ = 40 %) within a short time period (4 ms). A greater PAA for back conditions was therefore likely, though perhaps the magnitude is more reflective of the experimental arrangement than the realistic condition. Further analysis for this is apparent in section 7.4.2.

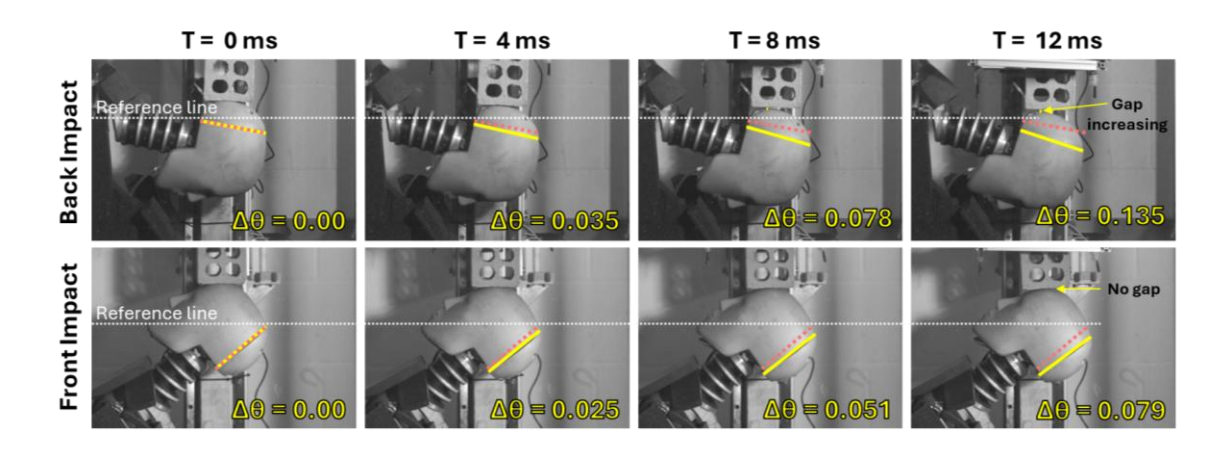


Figure 7.6, High-speed video frames at 0, 4, 8, and 12 ms after impact for trials to the back and front at 6.5 m/s. Frames show how the brick bounces from the headform for back conditions though not for front, and how rotation of the headform is greater for back impacts.

Due to the magnitude of back measures, there was no significant difference between PAA for other locations (P > 0.7), though the mean for side impacts (8.89 krad/s²) was greater than front (5.33 krad/s²) and crown (2.96 krad/s²). Mean PAA was statistically different (p < 0.01) between all velocity groups: 3 m/s = 7.44

krad/s², 5 m/s = 23.1 krad/s², and 6.5 m/s = 50.5 krad/s². However, the only indifferent interaction effects were back impacts at 5 and 6.5 m/s (P < 0.01); all other conditions were P > 0.67. The ANOVA when conducted without back impact data still shows that location has the largest effect on PAA (P < 0.01, F = 15.0), though it is closer to the effect of velocity (P < 0.01, F = 13.4), and the interaction effect is no longer significant (P = 0.24). Side impacts were statistically greater to the others (P < 0.01), though front and crown were still statistically similar (P = 0.09). 6.5 m/s conditions (8.90 krad/s²) were the greatest (P < 0.01), whereas 5 (4.87 krad/s²) and 3 m/s (3.40 krad/s²) were similar (P = 0.35). Of the interaction effects, all conditions shared overlapping similarity (P > 0.05), except that 6.5 m/s side impacts were larger than any other condition (P= 0.04).

The relationship between PLA and PAA showed to be more linear, as non-linear had no significant R^2 values. There was predictive significance for crown impacts across all velocities (R^2 = 0.74, 0.79, and 0.72 for 3, 5, and 6.5 m/s respectively). The strongest relationship overall was for 3 m/s side (R^2 = 0.93), though this was not the case for side at 5 (R^2 = 0.30) or 6.5 m/s (R^2 = 0.07). Front impacts showed no correlation between the two at any velocity (max R^2 = 0.08). The relationship between PLA and PAA for back impacts was assessed, despite doubts for the accuracy of back PAA; there was a strong relationship for 3 m/s (R^2 = 0.84) though nothing significant for 5 (R^2 < 0.01) or 6.5 m/s (R^2 = 0.41).

7.4.2 Predicting Larger Impact Velocities

Table 7.3, Regression parameters between headform data and impact velocity at each head impact location. A and B denote coefficients for a power law relationship, Equation 7.2. Predicted values for 8.7 and 10.6 m/s represent expected measures at human throw-like impact energies.

Impact	Α	В	Mean	RMSE	Predicted	Predicted	
Location			residual		v = 8.7 m/s	v = 10.6	
						m/s	
PLA (g)							
Back	28.26	1.30	1.04	17.9	473	612	
Crown	17.83	1.62	0.80	8.89	591	814	
Front	16.75	1.44	0.49	6.88	380	505	
Side	39.16	1.18	0.98	20.6	506	639	
Linear F	Pulse Dura	tion (ms)					
Back	3.41	-0.63	-1.6 x10 ⁻⁴	0.01	0.87	0.76	
Crown	2.83	-0.41	1.6 x10 ⁻⁵	0.003	1.17	1.08	
Front	3.39	-0.34	6.7 x10 ⁻⁵	0.02	1.63	1.53	
Side	2.07	-0.33	-3.7 x10 ⁻⁴	0.12	1.02	0.95	
PAA (kra	ad/s²)						
Back	0.63	3.01	0.46	1.71	420	761	
Crown	0.18	1.75	0.008	0.07	7.78	11.0	
Front	0.54	1.43	0.01	0.14	12.0	15.9	
Side	1.00	1.37	0.12	1.85	19.1	25.1	
Angular Pulse Duration (ms)							
Back	1.88	-0.02	6.0 x10 ⁻⁷	0.06	1.81	1.80	
Crown	1.93	-0.16	1.3 x10 ⁻⁶	0.002	1.37	1.32	
Front	5.33	-0.44	5.1 x10 ⁻⁵	0.009	2.06	1.89	
Side	2.94	-0.18	-9.2 x10 ⁻⁵	0.09	1.99	1.92	
							

Table 7.3 summarises A and B power law coefficients for each headform variable and impact location, alongside predictions for 8.7 and 10.6 m/s impact velocity (85 – 127 J). Model fits across all variables have low RMSE and show no tendency to over/under predict with residual means close to zero. Predicted PLA values for higher impact velocities suggest crown impacts will surpass side to become the

largest condition. Back and side PLA will be relatively similar to one another, and front impacts will remain the lowest of all locations. The location hierarchy for PAA does not change for predicted values, keeping the hierarchy of back, side, front, then crown. Figure 7.7 provides visual representation of the relationships formed from coefficients in Table 7.3 across 2 to 12 m/s impact velocities. Peak kinematics show to exponentially increase with B coefficients greater than 1, whereas pulse durations decrease at a slowing rate with negative B, the rate of which was larger for linear than angular. B coefficients for PLA and PAA also show the presence of damping in the collision, i.e. B = 2 reflects all of the squared relationship between velocity and energy is being experienced by the headform, thus no energy loss. Back PAA in Table 7.3 show an unusual relationship with B > 2, suggesting additional rotational momentum is being applied to the headform other than just the change in velocity. Details for this occurrence are discussed in section 7.5 though in summary, this suggests angular back findings are the result of experimental artifact and therefore not representative, thus they were not considered for further analyses.

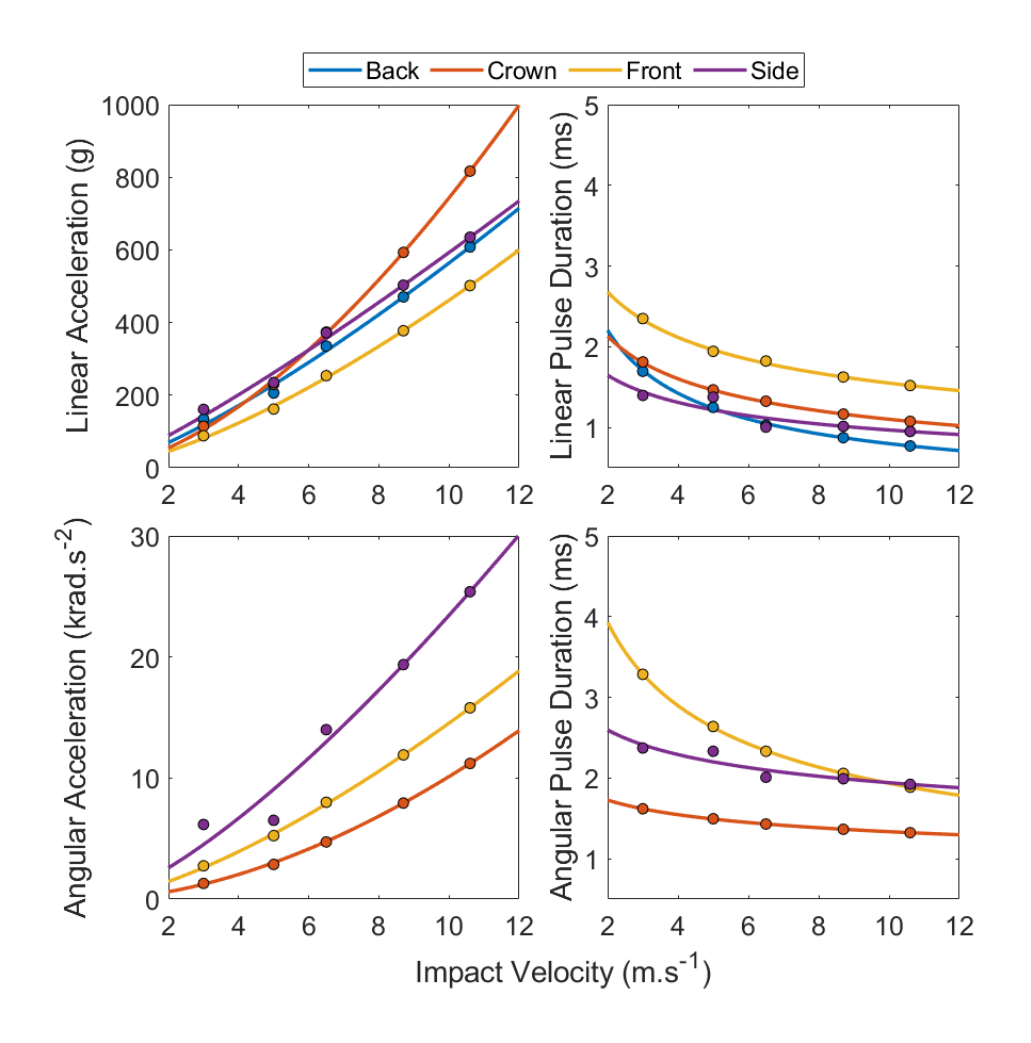


Figure 7.7, Visualisation of power law regression plots for headform data over impact velocities 2 - 12 m/s. Markers show measured kineamtics at 3, 5, and 6.5 m/s with predicted values at 8.7 and 10.6 m/s.

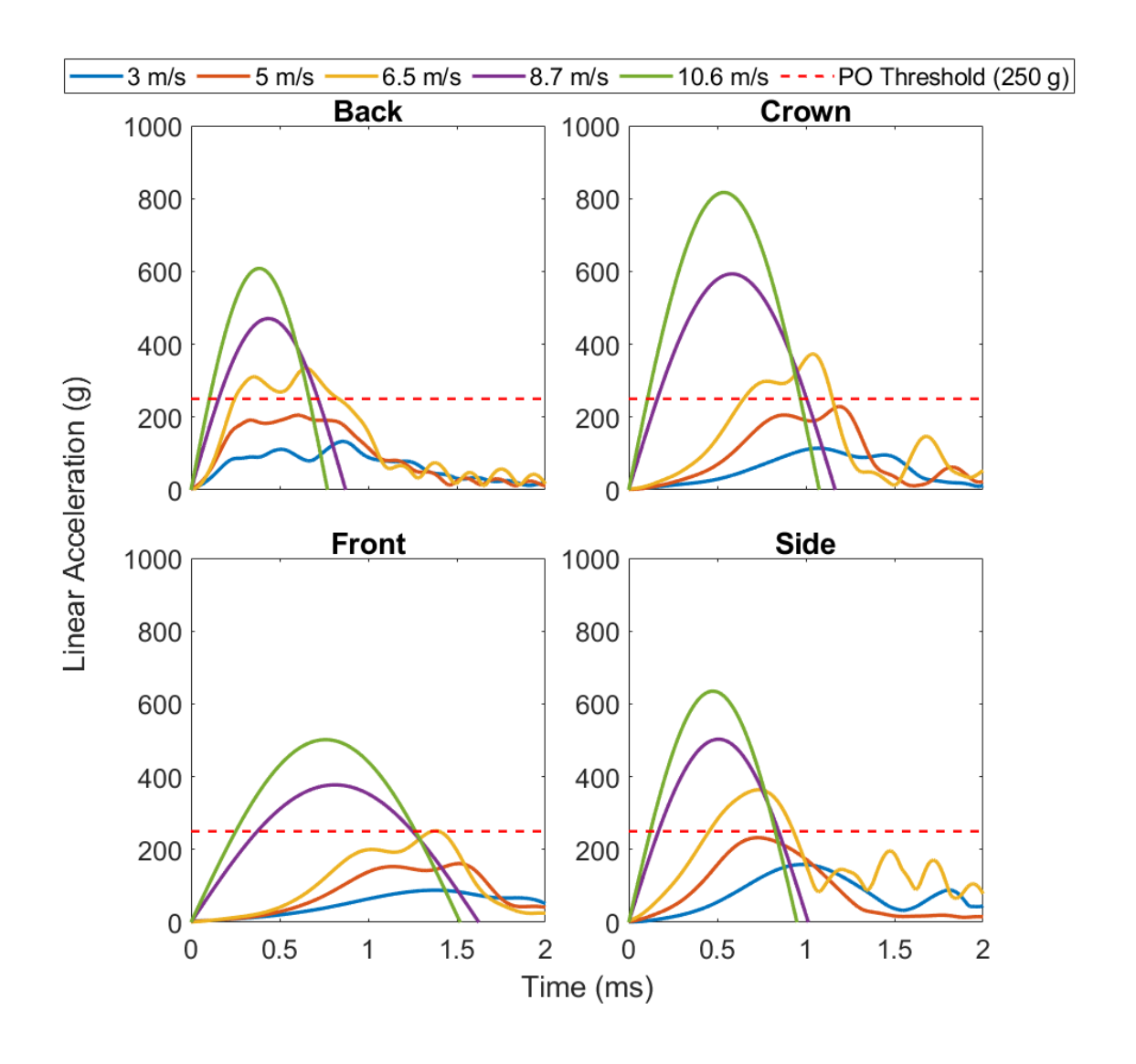


Figure 7.8, Mean headform resultant linear acceleration vs time curves for tested (3, 5, and 6.5 m/s) and predicted (8.7 and 10.6 m/s) impact velocities. Predicted curves are formed as a half sine wave from Equation 7.3 and Table 7.3. Red dashed lines indicate the high energy impact pass threshold in PSDB 21/04 [13].

Linear resultant acceleration curves in Figure 7.8 show a single dominant loading pulse within a relatively short time period (< 2 ms) for all conditions. 3 m/s impacts are the shortest and widest curves at every location, and this is maintained for each increase in velocity. Plotted lines for the PO standard pass threshold (high energy threshold: 6.8 m/s drop with 4.5 kg) show no impacts at 5 m/s or below exceeded 250 g. All locations exceeded 250 g for 6.5 m/s, though only just for front impacts. Predicted curves for 8.7 and 10.6 m/s impacts represent impact-like sinusoidal characteristics due to the regression coefficients in Table 7.3. Curves follow the same trend to the experimental data, exponentially increasing in amplitude and narrowing in duration. The initial loading phase of half-sinusoidal

pulses is steeper than experimental data because the method assumes no energy dissipation in the system.

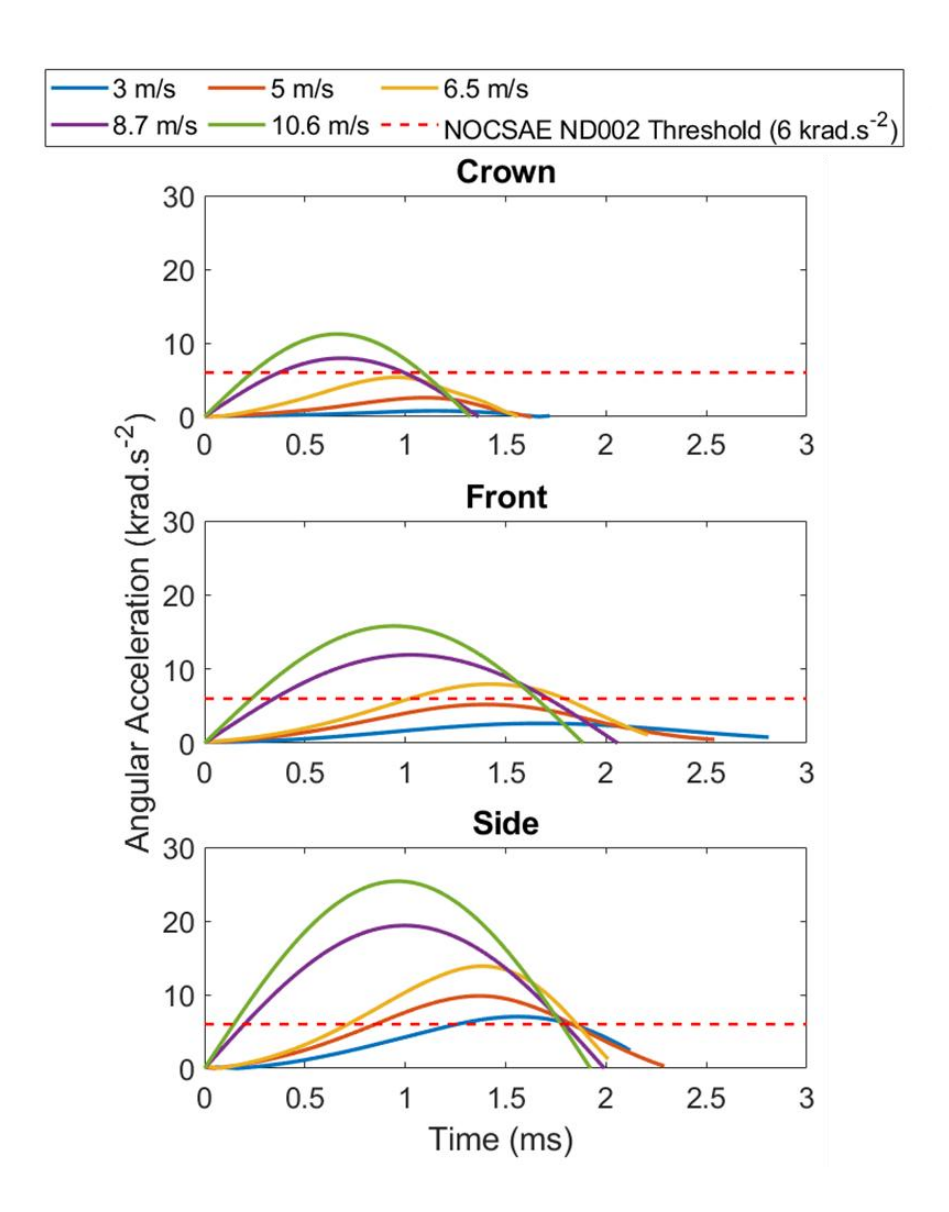


Figure 7.9, Mean headform resultant angular acceleration vs time curves for tested (3, 5, and 6.5 m/s) and predicted (8.7 and 10.6 m/s) impact velocities. Predicted curves are formed as a half sine wave from Equation 7.3 and Table 7.3. Red dashed lines show the angular acceleration pass threshold (6 krad/s²) for American Football helmets [15].

Experimental resultant angular acceleration pulses at 3, 5, and 6.5 m/s in Figure 7.9 are cropped after the first loading pulse to make the plots clearer, as after this they were always smaller and less significant for characterising injury. Mean pulses show a similar relationship to the linear acceleration curves, with increasing peaks and decreasing durations for greater impact velocities. Pulse durations are longer on average than linear (Δ mean of all locations = +48 %). Crown pulses are much

shorter and narrower than the other locations, side are the tallest, and front are the widest. However, the rate of duration decrease for front is greater than that of side, shown by a narrower 10.6 m/s curve. All side impact curves exceed the 6 krad/s² threshold of the American Football helmet standard [15], suggesting a potentially high threat loading condition. The opposite is the case for crown impacts, where only the predicted curves at 8.7 and 10.6 m/s exceed 6 krad/s². Like linear, the angular predicted curves follow a realistic looking trend with the experimental data by narrowing and increasing exponentially in height, although initial loading phases are again steeper than the experimental curves.

7.5 Discussion

7.5.1 Impact Location Effects

Impact location had a significant effect on PLA variance (P < 0.01, F = 331). Side impacts produced the greatest PLA at 3 m/s, while PLA for crown impacts increased to be similar to side for 5 and 6.5 m/s. This greater rate of increase influenced PLA predictions for higher impact velocities, as crown superseded side at 8.7 (Δ = +17 %) and 10.6 m/s (Δ = +27 %). This was because the compressive stiffness of the neckform is known to be greatest in the longitudinal compressive direction, far exceeding that of the actual human neck [185], [188], [216], [217], [218]. This causes less dissipated energy for higher impact velocities, as there is less compressive compliance, though the crown impacts may overestimate from realistic PLA as a result. PLA was lowest for front impacts (P < 0.01) because the greater compliance and range of motion of the neckform in this direction permitted greater energy dissipation. This is supported by a much longer linear pulse duration for front impacts (Δ = +49%) compared to others.

Location was the greatest influence on PAA variance (P < 0.01, F = 15), although PAA was still less influenced by impact location than PLA was (ΔF = -60 %). Side impacts were significantly larger PAA than front (Δ = +67 %, P < 0.01) and crown (Δ = +200 %, P < 0.01), which were statistically indifferent (Δ = 2.37 krad/s², P = 0.09). Back impacts showed an unrealistic PAA compared to other locations, with no plausible explanation (Δ mean = 85.2 krad/s²). Review of HSV (Figure 7.6) suggested back impacts would have a greater mean angular velocity than front, by

showing greater rotation over 4 ms, though this did not explain the scale of the difference. Raw headform data did not show any unusual loading characteristics, other than the vertical scale of the measures. The B coefficient for back being greater than 2 suggested more rotational momentum was applied to the headform in this condition. Review of HSV showed this was not due to a change in impact location, but instead it was noticed the rear cap of the headform was moving throughout impact. This sliding motion is believed to have increased tangential force on the headform, thus increasing PAA. Fixings for the cap were tightly bolted, thus this effect was unavoidable when impacting the back of the head, and consistently occurred over all 15 repeated trials. Further validation for this comes in Chapter 9, where back PAA, tested on the same day with identical loading conditions, does not show this effect with a helmeted headform.

Overall, crown impacts were the only location with a consistent predictive relationship between PLA and PAA (mean R^2 = 0.75). In this scenario, the head was effectively more constrained because the force vector was in line with the longitudinal axis of the neckform. As discussed, this is the least compliant neckform direction, thus very little angular motion could occur and there was less opportunity for energy loss due to the motion of ATD components throughout impact.

7.5.2 Impact Velocity Effects

Impact velocity was by far the dominant cause of variation in headform PLA (P < 0.01, F = 3098), suggesting the ability to throw a brick at high speed is the greatest threat to linear induced head and brain injuries. Though a significant effect was also seen for PAA, the influence of this was much less than linear (P < 0.01, F = 13.4). Non-linear power law regression between impact velocity and peak kinematics showed to also be appropriate for this dataset, with low RMSE and mean residuals close to zero for each model [105].

Stitt et al (2022) produced power law coefficients for PLA and PAA with increasing impact velocity, though theirs were not directly applied in this for it was unclear if their setup was relevant for brick impacts. For example, they used a guidewire

system to drop a headform at energies mostly lower than this study (starting at 4.2 J), though there was some overlap between their higher conditions (13 and 17 J) and the lower brick velocities in this programme of work [105]. A condition similar to this, where the headform affixed with a neck impacted a modular elastomer pad (MEP), produced similar mean B coefficients to this study for both PLA (% of brick mean, Δ = - 7 %) and PAA (Δ = -4 %) [105]. The B coefficient is most representative of the biomechanical phenomena during the impact, specifically how much velocity influences peak kinematics. It can therefore be concluded that experimentation in this study represents realistic head impact biomechanics for increasing impact velocities, thus so should the predictions at greater velocities. 'A' coefficients are more specific to the constants of the impact conditions, i.e. compliance, impacting geometry, biomechanical degrees of freedom, masses, etc. Stitt et al's work were marginally greater for PLA (Δ = +14 %), and much greater for PAA (Δ = +244 %). This will likely be because they included an oblique impact location at the rear boss of the headform. Although this does not discredit the relationship with increasing velocity for brick impacts, it does highlight the importance of situational representation in the experimental arrangement.

The predicted curves for linear and angular accelerations at higher impact velocities (8.7 and 10.6 m/s), a symmetrical half sinusoidal wave, look idealised yet not unrealistic when compared with the experimental data, Figures 7.8 and 7.9. For example, the changes in peaks and durations follow a logical trend, yet in all cases, the initial loading phase shows a steeper curve as the method does not consider energy dissipation. This would be less apparent if the headform was unconstrained, i.e. not fitted with a neckform [227], [357]. However, this only effects the time to peak, a metric not considered in this work, thus the peak kinematics and impact durations remain relevant.

7.5.3 Indicators for Injury Predicting

Predicted kinematics at 10.6 m/s suggest crown impacts were the most severe for linear acceleration (814 g), though they were the least for angular (11 krad/s²). Side impacts could be considered more severe as they were the second greatest for linear (639 g) and the greatest for angular (25.1 krad/s²). All head impact locations

exceed the WSTC threshold for linear kinematics, though none exceed the Hoshizaki et al (2016) angular equivalent [109], [120]. This suggests projectile brick impacts are more of a potential threat to linear induced head injuries than angular. This was also found for wielded blunt weapons; further comparisons between injurious conditions are discussed in Chapter 8.

7.5.4 Method and Limitations

The validity of this work is dependent on the situational representativity of chosen throw velocities, section 7.2. These were chosen from mathematically estimating average and upper throw capabilities of males [410]. This assumes an exponent = 4, Equation 7.1, for masses in the range expected of bricks, though in reality this is continuously decreasing as mass increases. However, n = 4 is relevant for most traditional sized bricks (1.2 – 3.0 kg), as it was derived from four masses between 0.73 and 3.4 kg [410]. Constraints had to be made for experimental setup to limit the scale of work, though in reality, bricks of larger sizes could also be used in PO situations, particularly if other stone-like objects were considered. Despite this, findings from this chapter could be used to estimate head injury for a broader range of projectile weapons, by considering regression with impact velocity. Stitt et al (2022) validated that the exponent (B) between kinetic energy and peak kinematics is always half that of impact velocity, thus a much broader range of impacts could be considered, though it can be expected that A coefficients would be less accurate [105]. Alternatively, more broad impact conditions, including head locations and more person-specific characteristics such as gender, could be looked at with computer simulation, using this work for experimental validation as discussed in Chapters 4 and 5.

The experimental setup permitted repeatable impact velocities (CV% = 0.73 %) with motion for brick to head impacts that represented an actual projectile brick. However, there was limitation in that typical throw velocities were not achievable with the available drop height, thus they had to be predicted. Before testing, an alternative method to achieve higher energies was trialled, where the head and neckform were dropped onto brick shaped anvils. There was a problem with this in that the weight of the drop assembly dragged the headform across sharp edges of

the anvil, causing a small non-penetrative tear in the skin. As a result, this method was abandoned before meaningful damage was done to the headform. Although higher velocities had to be predicted, the results of this chapter are believed representative of the upper and average in-field conditions, while the experimental work at 3, 5, and 6.5 m/s still highlights the lower bounds of what could be expected. Therefore, this work meets the objectives outlined in section 7.1, while the next steps are to advise standard test setup methodology by first comparing the loading mechanics between bricks, wielded weapons, and falling from horseback and recreating them under more controlled conditions.

7.6 Chapter Conclusion

This work meets the objectives laid out in section 7.1 and contributes to the overall aim of the project by quantifying head impact biomechanics for another dangerous PO condition. The mechanics for throwing a brick were specified as kinetic energy equal to 85 J for the average male and an upper limit of 127 J. This was calculated from the typical mass properties of a brick (1.2 – 3.0 kg) and a power law relationship between object mass and achievable throw velocity [410]. In practice, broader masses and throw velocities will occur in riots, though these boundary conditions are representative of high severity brick impacts and the findings of this study can advise broader conditions in future work.

Experimental recreations of projectile bricks using a guided drop tower and Hybrid III ATD permitted study of injurious metrics while representative of in-field conditions. The method permitted impacts of a similar motion to bricks when inair, though with more repeatable control over impact velocity and location. Headform PLA was greatest for impacts to the crown (374 g) and side (372 g) when tested at 6.5 m/s. Front impacts consistently showed the lowest PLA across all conditions (168 g), attributed to the greater neckform compliance in this direction. PAA was the greatest for back impacts, though these were discarded after experimental artifact was found to artificially increase results. Excluding these, side impacts produced the greatest angular accelerations (8.9 krad/s²) when tested at 6.5 m/s and impact location was shown to marginally be the greatest cause of variance in peak angular acceleration data.

Impact velocity was the greatest influence on PLA findings and almost equal to location for PAA. Experimental constraints limited testing to maximum 6.5 m/s (47 J), thus regression was used to predict greater velocities. A non-linear power law relationship, where peak kinematics exponentially increased with velocity and pulse duration decreased, was found across all locations. From this, predicted impacts at 8.7 and 10.6 m/s (equivalent to 85 and 127 J) highlight more risk for linear-induced injuries, as all tested conditions exceeded linear injury thresholds, though not the angular equivalent [13], [15], [109], [120]. The results of this work can be used alongside those of wielded blunt weapons and falling from horseback to advise more situationally representative test setup when testing PO helmets.

8. Recreating Public Order Impacts with a Drop Rig

8.1 Introduction

Previous chapters have identified key head impact kinematics for thrown bricks, wielded blunt implements, and falling from horseback. Collectively, these highlight injury risk across most of the prevalent and dangerous injurious situations faced by PO officers. The experimental method for these aimed to stay as true to representing in-field conditions as possible, adopting full-body biomechanics in the form of ATDs and imparting impacts in a manner similar to those the public would cause. However, to make recommendations for a test standard it must be understood how to recreate conditions with more repeatability and control. This chapter aims to highlight specifically how a guided drop rig, such as that required in the current PO standard [13], can be best setup represent PO specific loading mechanics. To do this, the following objectives were set:

- Compare the head impact biomechanics of injurious conditions tested in previous chapters and define targets to be recreated with a drop rig.
- Test a multitude of setup conditions and assess the capabilities of a drop rig for producing PO specific loading dynamics.
- 3. Suggest how drop rig protocol can be set to recreate specific injurious conditions in PO.

8.2 Comparison of Head Injury Mechanics Across Dangerous PO Conditions

8.2.1 Quantification of Typical Head Impact Mechanics

Head impact mechanics across experimented PO conditions were quantified with peak linear (PLA) and angular (PAA) accelerations as proxies for neurotraumatic injury. Figure 8.1 compares the mean PLA, PAA, and respective pulse durations across all tested PO dangerous situations. Each mean value includes all tested impact locations and velocities for that experiment; thus error bars (one standard deviation) are relatively large. This figure indicates how impact mechanics range across the entire simulated spectrum of PO head injury. From these, we can define boundaries for the maximum and minimum head kinematics expected in PO, Table

8.1. These are defined from the most distal standard deviation limits, i.e. 771 g refers to the mean of 10.6 m/s brick impacts plus one standard deviation.

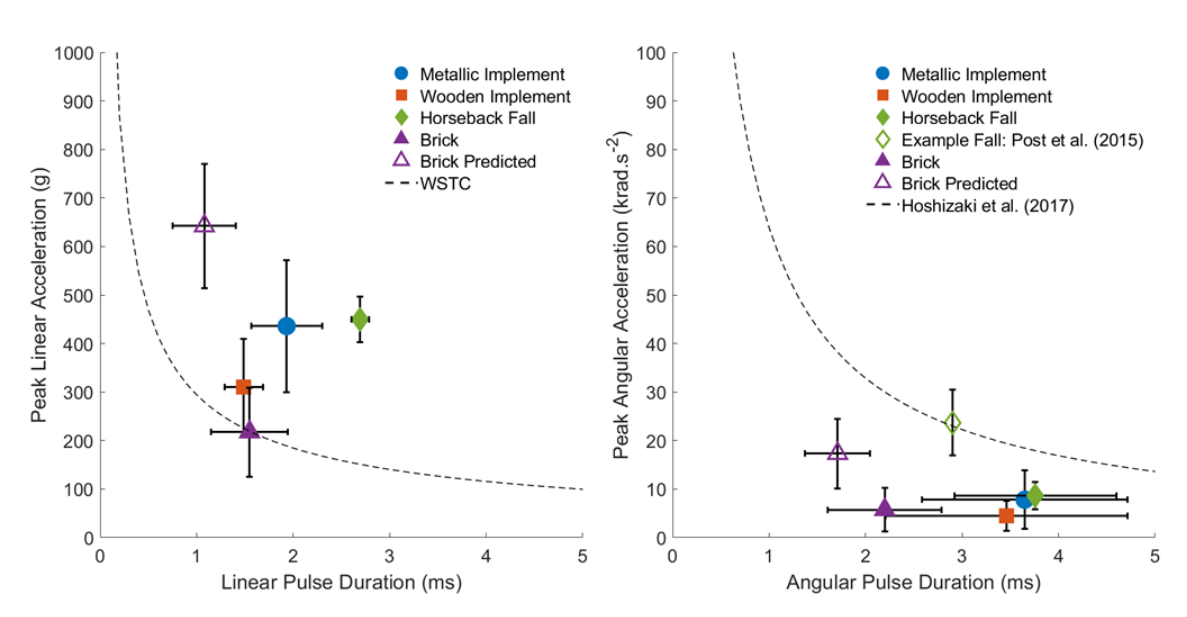


Figure 8.1, Mean PLA, PAA, and respective durations for experimented PO scenarios. Predicted brick data refers to 10.6 m/s conditions from non-linear regression (Chapter 7). The Post et al (2015) example shows the potential increase in PAA for moving horse conditions. WSTC and Hoshizaki et al (2017) curves demonstrate thresholds for life-threatening and mTBI injury, respectively [109], [120].

Table 8.1, Range of expected magnitudes for PLA, PAA, and pulse durations in PO conditions. These are equal to the greatest/lowest mean ±one standard deviation, shown in Figure 8.1.

		Linear	Angular		
	PLA (g)	Duration (ms)	PAA (krad/s²)	Duration (ms)	
Maximum	771	2.79	24.5	4.71	
Minimum	126	0.75	1.30	1.37	

Hoshizaki et al (2017) summarised impact durations and magnitudes for brain injury reconstructions across many applications [109]. The range for linear pulse durations in PO (0.75 – 2.79 ms) is on the lower end of some pedestrian accidents, falls, and motorcycle accidents [109], [135], [166], [379], [415] and the minimum PLA (126 g) is similar to the upper limits of American Football concussive incidents [14], [109], [116], [160], [255]. The upper PLA limit (771 g) far exceeds other

conditions, the closest being falls and motorcycle accidents (Δ = +371 g), which highlights the necessity for effective headgear in PO. Hoshizaki et al did not distinguish linear and angular pulse durations, so the same comparisons for linear limits can be applied to angular. The maximum limit for PAA (24.5 krad/s²) was greater than all sporting conditions [14], [109], [116], [160], [255], [416], [417], [418] though less than falls (defined as '30 krad/s² or more') [135], [379], [415]. This reinforces that angular induced injuries are substantial, if not as relatively severe as linear, thus headgear should consider means for attenuating angular forces. The boundary limits do not include the predicted angular accelerations for greater horseback fall conditions in Chapter 5, although an example is shown in Figure 8.1. This was because they were predicted from drop rig data in Post et al (2015), thus could bias the boundary limits with drop rig specific mechanics.

Threshold curves for the brains tolerance to linear and angular accelerations are shown in Figure 8.1 with the Wayne State Tolerance Curve (WSTC) and Hoshizaki et al's angular equivalent [109], [120]. Distance from the curve indicates the relative severity of each situation, where above the line is a potential threat for severe injury. From this, it can be seen that all PO conditions are a high risk of linear induced injury, with each marker above the WSTC. Horseback fall conditions are the furthest from the curve, with the second greatest mean PLA (449 g) and longest mean duration (2.70 ms). Predicted 10.6 m/s brick impacts show the greatest PLA (643 g), although shorter duration (1.08 ms). Likewise, the error bars for metallic impacts show how the dataset exceeds the peak of horseback falls despite a lower mean. This is an effect of impact location as crown metallic impacts were much greater than other locations.

Unlike PLA, all tested situations are below the tolerance curve for angular acceleration, suggesting PO situations universally have a relatively lower risk for angular induced injuries. However, this does not suggest they are mild in severity, as all situations exceed thresholds found in helmets standards (e.g. 6 krad/s², NOCSAE ND002-17m21) within one standard deviation [15]. The predicted PAA from Post et al (2015) is an example fall recreation, for which authors shared the peak (with standard deviation) and pulse duration [376]. The real maximum from this study, as discussed in Chapter 5, was 51.2 krad/s². This was not plotted

because pulse duration was unknown, the authors only state that it was below 5 ms. Should this condition exceed \approx 1.2 ms then this would also surpass the Hoshizaki (2017) threshold [109].

The full severity hierarchy for PO situations, with respect to both linear and angular tolerance curves, is listed in Table 8.2. The detailed data for this is in Appendix A.8.1. This includes head impact location and was calculated as the vertical distance between each mean and respective tolerance curve. The intention was to also consider x distance and compute Euclidian distances, though the difference in scale between x and y would nonetheless heavily bias results to vertical distance. An alternative was to normalise or weight each component, although this was deemed inappropriate, as they are unequal factors for injury onset nor is the exact ratio of their contribution constant. From the hierarchy, we can see there is a clear trade-off between linear and rotational acceleration for 10.6 m/s bricks to the crown, which top the linear ranking yet are bottom of the angular. Metallic implements to the crown are seemingly the most severe, shown as second for linear and first for angular. Other notable conditions near the top of both rankings are 10.6 m/s bricks to the side and horseback falls to the crown. All wooden and 6.5 m/s bricks are near the bottom half of each hierarchy, suggesting a much lower relative severity.

Table 8.2, Injury severity hierarchy (most to least) of each PO condition relative to linear and angular tolerance curves [109], [120]. Difference refers to the vertical distance from that groups mean to its respective tolerance curve.

		lines:			A marula ::	
		Linear			Angular	
	Impact Cond	ition	Difference	Impact Cond	ition	Difference
			(g)			(krad/s²)
1	Brick, 10.6	Crown	535	Metallic	Crown	-8.91
	m/s					
2	Metallic	Crown	436	Brick, 10.6	Side	-9.06
				m/s		
3	Brick, 10.6	Side	334	Horseback	Crown	-9.53
	m/s			Fall		
4	Horseback	Crown	307	Metallic	Side	-9.71
	Fall					
5	Brick, 10.6	Front	284	Metallic	Back	-12.0
	m/s					
6	Brick, 10.6	Back	258	Metallic	Front	-13.0
	m/s					
7	Metallic	Side	247	Wooden	Front	-13.2
8	Metallic	Back	194	Brick, 6.5	Side	-13.6
				m/s		
9	Metallic	Front	185	Wooden	Back	-13.8
10	Wooden	Side	166	Brick, 6.5	Front	-15.0
				m/s		
11	Wooden	Crown	138	Wooden	Side	-16.5
12	Brick, 6.5	Crown	127	Brick, 10.6	Front	-18.8
	m/s			m/s		
13	Brick, 6.5	Side	77.7	Wooden	Crown	-20.0
	m/s					
14	Brick, 6.5	Front	55.8	Brick, 6.5	Crown	-21.8
	m/s			m/s		
15	Brick, 6.5	Back	40.7	Brick, 10.6	Crown	-37.9
	m/s			m/s		

16	Wooden	Front	36.9
17	Wooden	Back	7.25

8.2.2 Assessing the Representativity of Drop Rig Setups

When testing with a drop rig, it is reasonable to setup impacts within the identified boundary range (Table 8.1) and state the method is representative of PO loading conditions. More detail can be added by studying the transient loading dynamics for each condition. For example, recreating the impact curves themselves would mean the setup is a complete mimic of the actual condition. However, this would be almost impossible to achieve in practice, as it requires simultaneously replicating four variables (PLA, PAA, and each duration). Instead of being the target, recreating impact curves can be a better indication of how to refine the setup for improved situational representation. For example, an impact within the boundaries for PO could then be compared to the transient curve of the actual injurious scenario. Should the durations be similar, yet peak is lower, it can be ascertained that increasing impact energy is a better option than reducing the compliance of impact surface. From this, much more can be said for how to set up a drop rig to recreate injurious conditions in PO.

Figures 8.2 and 8.3 show resultant headform acceleration time histories from chapters 4, 5, and 7. As previously discussed, all pulses are within a relatively short pulse duration (<5 ms) for head injury [109]. Horseback falls have a longer linear pulse duration than all other conditions, though the peak remains relatively mid-to-high range. Likewise, head impact location has a clear effect, for example metallic implements are much greater PLA than 6.5 m/s bricks at the crown, although the two are closer for all other conditions. Looking at angular acceleration, it is clear that PAA was universally greater for side impacts than any other locations, and this is the only occurrence of an experimented impact (metallic implement) matching the peak of the predicted 10.6 m/s brick condition. The secondary peak at this location is the result of an asynchronous pulse between orthogonal directions.

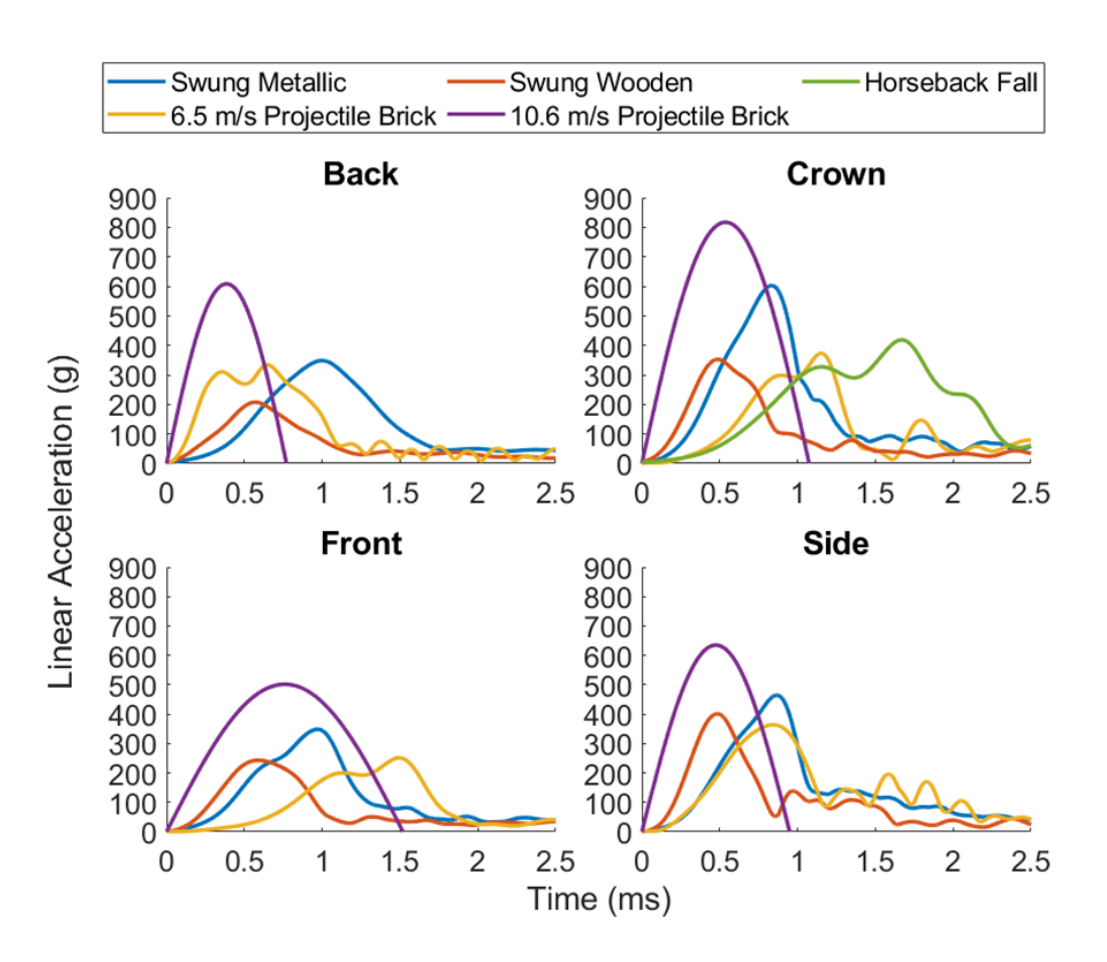


Figure 8.2, Transient resultant linear headform acceleration curves for all experimented PO conditions at each head impact location (Back, Crown, Front, and Side).

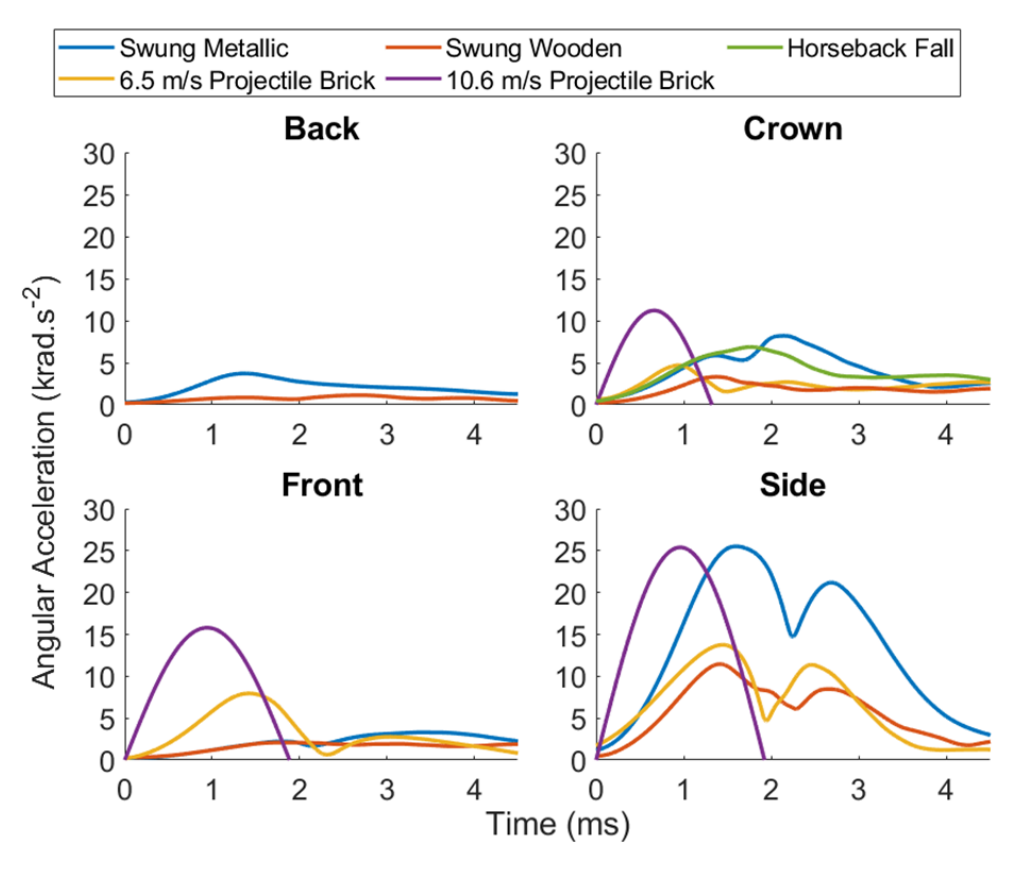


Figure 8.3, Transient resultant angular headform acceleration curves for all experimented PO conditions at each head impact location (Back, Crown, Front, and Side).

8.2.3 Determining Drop Rig Setup Parameters for Recreating PO Conditions All PO conditions are relatively similar when compared to the broad scale of head impact mechanics [109], thus recreating them with a drop rig should be possible with few setup changes. As there is a large range for both linear and angular accelerations (Table 8.1), multiple impacts should be simulated across a broad range of velocities. A minimum of three permits the development of regression between velocity and peak accelerations, similar to that in Chapter 7.

Means for PO conditions in Figure 8.1 are all close to the steep gradient region of the WSTC and Hoshizaki curves, thus impact duration has a large influence on injury severity [109], [120]. The contrast for this would be greater than ≈ 5 ms, where threshold acceleration is mostly unaffected by further prolonged duration. This narrow pulse is important to replicate with a drop rig, as alongside anatomical tolerance it also affects the performance of viscoelastic liners in headgear. Narrow pulses require low-compliance impact anvils [336], [376], which is similar to the properties of simulated conditions in PO, i.e. steel, treated wood, concrete, etc.

Therefore, drop rig setup can trial anvils with representative materials to compare if their properties are important for recreating conditions and ascertain which anvils produce the most realistic durations. Anvils should also be set to produce both radial and oblique loading conditions, so that both linear and angular measures will show significant pulses. Oblique angles should replicate the realistic conditions, which were only applicable for wielded weapons and equal to $56 \pm 14^{\circ}$ relative to the headform.

Few test standards incorporate neckforms in their setups, despite the relevance for maintaining biomechanical realism [18], [118], [227], [357]. This is contrasted with a large uptake of neckforms in research over recent decades [231], [231], [232], [233], [234], [235], [376]. Studies with a guide wire system reported that representative angular accelerations were not achieved with a neckform [181], whereas the opposite was found in a separate study with a monorail [376]. As such, assessing impact dynamics with the headform constrained to the degrees of freedom of a neckform and unconstrained in a cradle, as per the current PO standard [13], elucidates if the neck is necessary for accurate biomechanical representation.

8.3 Method

8.3.1 Experimental Arrangement

The guided drop system for this experiment was discussed in Chapter 6 and trials used the same Hybrid III (HIII) head and neckform arrangement of Chapters 4, 5 and 7 (50th percentile male, 4.54 kg headform mass, neck tensioned to 1.1 Nm) (JASTI Co. Ltd.). In all cases, ATD components were dropped onto rigid anvils at the base of the drop tower. These were setup to replicate wielded metallic implements, wooden implements, and horseback falls. Brick impacts were not recreated, as these were simulated with a drop rig in Chapter 7. Descriptive details for each setup are in Table 8.3.

Table 8.3, Setup conditions for recreating experimented PO conditions with a guided drop rig. Impact angles are relative to the longitudinal axis of the headform. Each condition was repeated five times.

Anvil description Steel pipe. 50 mm diameter circular cross section.

Head Impact Location Back Crown Front Side

Impact Angle

(Degrees) 60 90

Impact Velocity (m/s) 3 5

Wooden Implement

Treated softwood. Flat face, greater than 300 x 300

Anvil description mm.

Head Impact Location Back Crown Front Side

Impact Angle

(Degrees) 60 90

Impact Velocity (m/s) 3 5 7

Horseback Fall

Anvil description Flat steel plate, greater than 500 x 500 mm

Head Impact Location Crown

Impact Angle

(Degrees) 90

Impact Velocity (m/s) 4.5

Head impact locations were the same as those experimented in previous chapters. Impact angles (relative to the headform longitudinal axis) were set to 90° for crown (radial) and 60° for other locations (oblique). These represent the means for radial and oblique wielded implements: 92° and 56°, respectively. The angle bracket could be set to 30, 45, or 60 and was clamped rigid to the base plate. The bracket was removed and anvils were clamped to the base slab for 90° trials.

Wooden impacts were tested at 3, 5, and 7 m/s velocities, as it covered full range of the rig's capability and regression for headform kinematics could be calculated. Metallic implements were not tested at 7 m/s, as pilot tests suggested a high risk

of damaging the skull of the headform. Likewise, horseback falls were tested at the same impact velocity to the experimented work to compare between rig and full body ATD drops.

The base of the neckform was affixed to a steel member, protruding perpendicular from the drop plate. This inverted the headform, allowing all locations to be impacted with the same drop setup, Figure 8.4. The total drop mass was 12.4 kg, the equivalent of 56, 155, and 304 J impact energies when tested at 3, 5, and 7 m/s. Drops were also conducted by cradling the headform, similar to PSDB 21/04, so that comparative analyses could be made for neckform effects [13]. The impact criteria for these were kept the same, although only 5 m/s trials were conducted, the equivalent of 57 J with headform mass. Only wooden conditions were simulated, as the temporary cradle (discussed in Chapter 6) was too narrow to pass over other anvils.

Each test condition, i.e. anvil type, location, velocity, and headform constraint was repeated 5 times, totalling 125 impacts. This was considered sufficient for analyses, as the within group variance on a drop rig would be less than that with swung implements, for which minimum sample size was 3 repeats (Power analysis, Cohen's d = 2.09, $\alpha = 0.05$, power = 0.8).

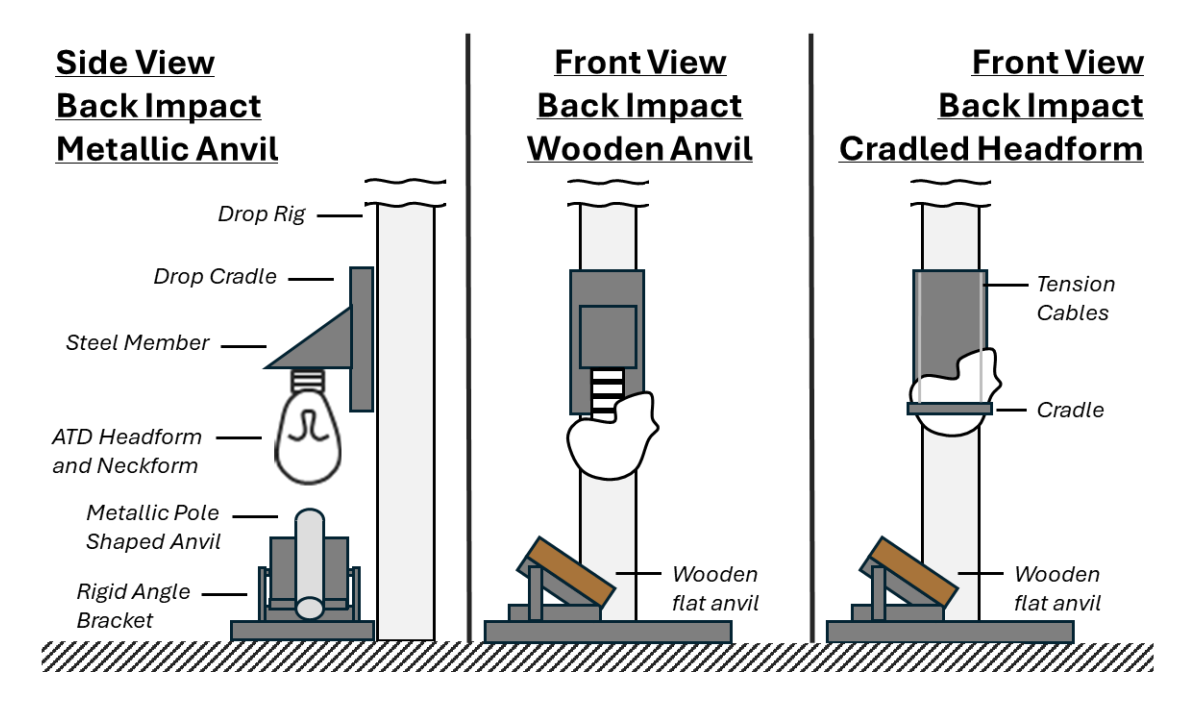


Figure 8.4, Experimental setup for dropping a neck affixed and cradled headform onto representative anvils. The headform was rotated in its constraint to achieve different impact locations. Impact velocity was defined by varying drop height. Impact surfaces were set to replicate weapons identified in PO activity (Chapter 2).

8.3.2 Data Capture

Two high-speed video (HSV) cameras were used to capture impact events from anterior and lateral views of the headform. Cameras were placed 1.5 m from the impact, perpendicular to one another. Video was recorded at 4000 Hz, with a field of view = 0.62 x 0.98 m. Calibration was the same procedure as Chapter 4, using a 30 mm checkerboard to build real-world coordinates and correct lens distortion [351], [352], [353], [354]. Likewise, impact velocity measures were the same as Chapter 7, using a 20 mm marker on the drop assembly and recording velocity over 40 frames (10 ms) prior to impact (Matlab 2023b [350]).

As before, headform kinematics were captured with a 6DOF 3a3ω sensor package (Slice 6DX PRO, DTS) at the CoM [251], [355]. Sample rate was 100 kHz, and CFC 1000 and 180 filters were used for linear and angular measures, respectively [28], [244]. The IMU trigger was set to 5 g, capturing 0.02 s prior and 0.1 s post contact and angular acceleration was calculated from angular velocity with the 5-point stencil method [247], [248], [249], [250].

8.3.3 Data Analysis

Resultant (Pythagorean) kinematics were computed for PLA, PAA, and their respective pulse durations (MATLAB 2023b). Of the 125 trials, 16 were removed due to anomalous loading curves and no less than three datapoints were left within a group. 'Analysis of Variance' (ANOVA) was used to assess the effects of anvil type, impact velocity, and impact location on PLA and PAA [21], [356]. These were conducted one-way instead of a multi-factor analysis because the degrees of freedom between groups were inconsistent. Anvil type effects were calculated from all 5 m/s crown trials, assuming 4.5 m/s fall trials were 5 m/s, as this was the only comparable condition. Impact location effects were calculated from all wooden and metallic trials at 5 m/s. Velocity effects were calculated from only wooden trials, as these were the only condition tested at 3, 5, and 7 m/s. Post-hoc Tukey's tests were used to collate mean values for comparisons between groups.

Within group repeatability was assessed with coefficient of variation (CV%). Headform data was compared to the boundary of kinematics expected within PO conditions from Table 8.1. Regression between peak kinematics was calculated as a power law with A and B coefficients like in Chapter 7 [105], [418]. These were derived separately for radial and oblique loads, following recognition that they produced contrasting peak kinematics. Mean transient loading curves were calculated by synchronising the trigger points of every trial within each group and averaging the resultant data. This was done for all drop rig conditions; comparisons were made between anvil types and the target condition they aim to recreate. Mean transient curves were also compared between neckform affixed (constrained) and cradled (unconstrained) headforms, and percentage differences were computed for their peak kinematics and pulse durations (unconstrained – constrained).

8.4 Results

8.4.1 Drop Rig Setup Repeatability

Mean impact velocity for trials at 3, 4.5, 5, and 7 m/s setups were 2.93, 4.50, 4.93, and 6.85 m/s, respectively. The corresponding mean CV%'s within each group were 2.17, 2.18, 2.12, and 3.66 %. This resulted in low within group CV% for linear kinematics: mean for PLA = 2.48 % and duration = 2.49 %. Angular kinematics showed slightly more within group variation than linear as PAA CV % = 7.91 and duration = 5.88 %. This was expected as angular acceleration was calculated and not a direct measurement, the CV% of measured angular velocity peaks was 1.74 %.

8.4.2 Drop Rig Peaks Compared to Representative PO Limits

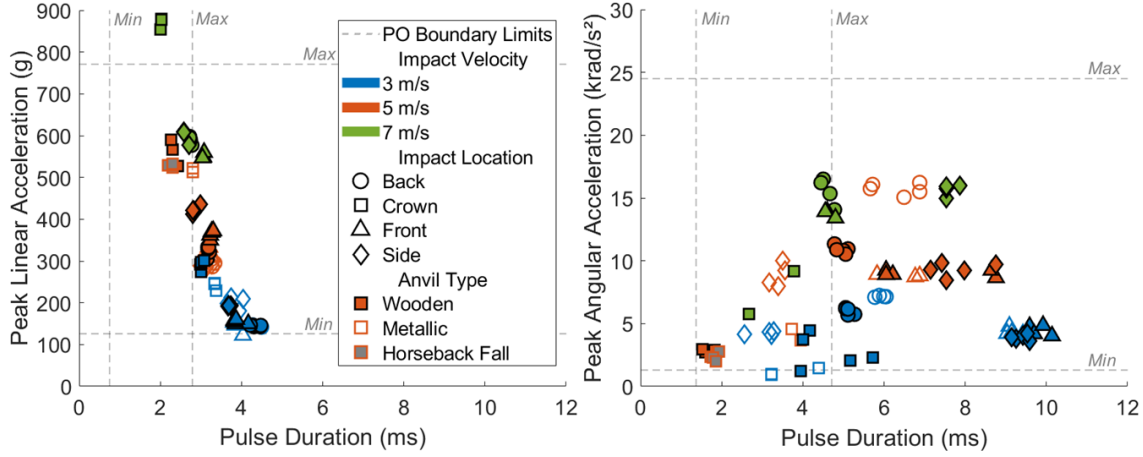


Figure 8.5, Scatter plots for PLA, PAA, and respective pulse durations across all drop rig tested conditions with a neckform. Grey limits represent the maximum and minimum region expected for PO conditions, Table 8.1.

Few drop rig impacts sit directly within the PO boundaries for linear (17.4 %) and angular (31.4 %) kinematics, Figure 8.5. However, when considering only peak accelerations, 95.4 % are within the boundary for PLA and 96.5 % for PAA. For pulse duration, 19.8 % are within the linear range and 34.9 % is for angular, thus the duration is what mostly causes the dissimilarity. Durations outside of PO limits were always greater, the maximum difference being +1.70 ms for PLA and +5.42 ms for PAA.

Peak accelerations span the lower 72.6 and 64.9 % of the boundary ranges for PLA and PAA, respectively. Wooden crown impacts at 7 m/s were the only condition to exceed the PLA boundary. ANOVA showed head impact location had a significant effect on both PLA (P < 0.01, F = 35.6) and PAA (P < 0.01, F = 49.3). Crown impacts were the greatest for PLA (mean = 544 g), while all other locations were similar to one another (e.g. side = 362 g, P > 0.05). Most locations had statistically different PAA (P < 0.01), except front (8.9 krad/s²) and side (9.1 krad/s²), which were almost identical (P = 0.99). Back impacts were the greatest mean (13.3 krad/s²) whereas crown impacts were significantly lower than all other locations (mean = 3.4 krad/s², P < 0.01).

Impact velocities of 3, 5, and 7 m/s produced significantly different peak kinematics and had greater influence than location or anvil type did (P < 0.01, PLA F = 108, PAA F = 62.8). Power law coefficients for the relationship between peak accelerations and impact velocity are summarised in Table 8.4. Model fits across all variables have low RMSE and show no tendency to over/under predict with residual means close to zero. Plots for these equations are in Appendix A.8.2.

Table 8.4, Power law coefficients for change in peak headform kinematics with respect to impact velocity for oblique (back, front, and side) and radial (crown) experimented conditions. PLA has a lower error relationship with the radial load, although both are low, whereas PAA has high error with radial conditions.

Impact Condition	Α	A B Mean		RMSE
PLA (g)				
Oblique	35.06	1.45	-0.65	7.52
Radial	70.94	1.29	0.01	0.18
PAA (krad/s²)				
Oblique	1.11	1.34	5.9 x10 ⁻³	0.08
Radial	0.26	1.69	0.11	0.93

8.4.3 Comparing Between Drop Rig and Situationally Representative Conditions

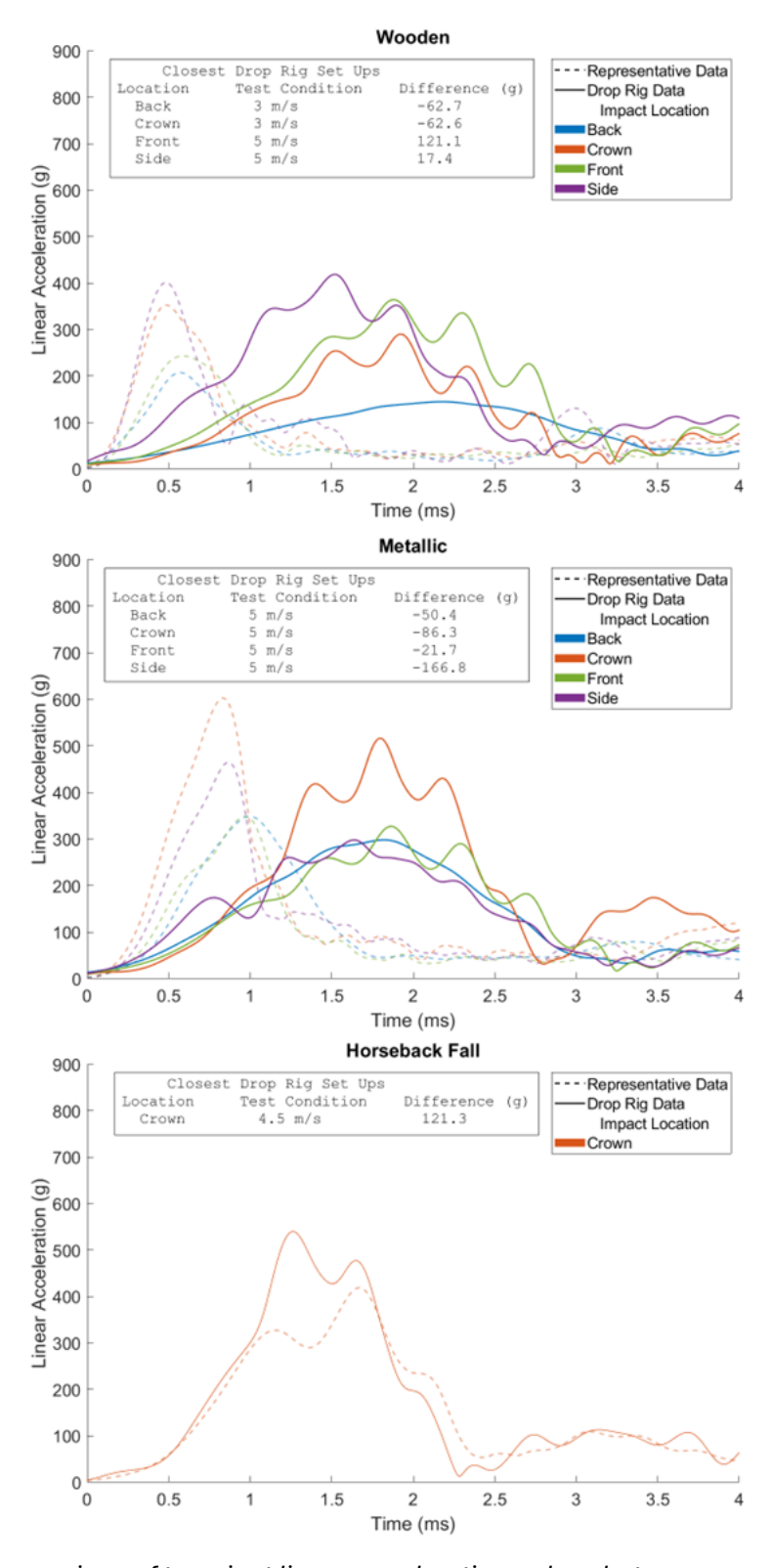


Figure 8.6, Comparison of transient linear acceleration pulses between representative PO injury recreations (chapters 4 and 5) and drop rig tests with replica impact anvils (wooden, metallic and rigid floor surface). Graphs show tested impact location and a summary table for which setup had the closest peak acceleration.

Drop rig impacts mostly produced similar pulse durations across all anvil types (Δ max \approx 0.2 ms), Figure 8.6. Pulse durations for wooden and metallic recreations were larger (\approx +2.0 ms) than the target duration, whereas horseback fall trials were very similar. However, this was because the target pulse was a longer duration than wielded implements (Δ \approx +1.5 ms). There was no significant difference between pulse durations for angular conditions. Within-plot tables highlight setups with the closest PLA to the representative conditions for each location, along with their difference. Despite similarity in duration, horseback falls produced a greater PLA (Δ = +121 g) on the drop rig. When tested without a drop rig, wooden impacts were much lower PLA than metallic, thus the closest setups were one of 3 or 5 m/s depending on impact location. 5 m/s was the closest setup for all metallic conditions, although peaks were always lower with an especially large difference for side (Δ = -167 g).

Angular pulses were also compared, Appendix A.8.4, although there was little similarity between the experimental methods. This was due to target accelerations being relatively low to begin with, as six of the nine conditions were less than 5 krad/s². Therefore, the closest drop rig setups were those that produced the least angular force. For those above 5 krad/s², no drop rig setup was similar. Wooden side were the closest difference = -2.4 krad/s² (-21 %), followed by metallic crown = -4.5 krad/s^2 (-55 %), and then metallic side = -16.9 krad/s^2 (-66 %).

ANOVA for anvil type showed significant effects for both PLA (P < 0.01, F = 11.0) and PAA (P < 0.01, F = 16.7) though there was less influence than velocity or location. Despite that the steel was a stiffer material than wooden, mean PLA for wooden anvils was greater than metallic (Δ = + 71 g, P = 0.03). This suggests an effect with the shape of anvils; wooden was a flat surface and the metallic was curved. PAA was the opposite, in that wooden anvils produced lower PAA (Δ = -1.25 krad/s², P = 0.02).

8.4.4 Differences Between Cradling the Headform and Affixing a Neckform

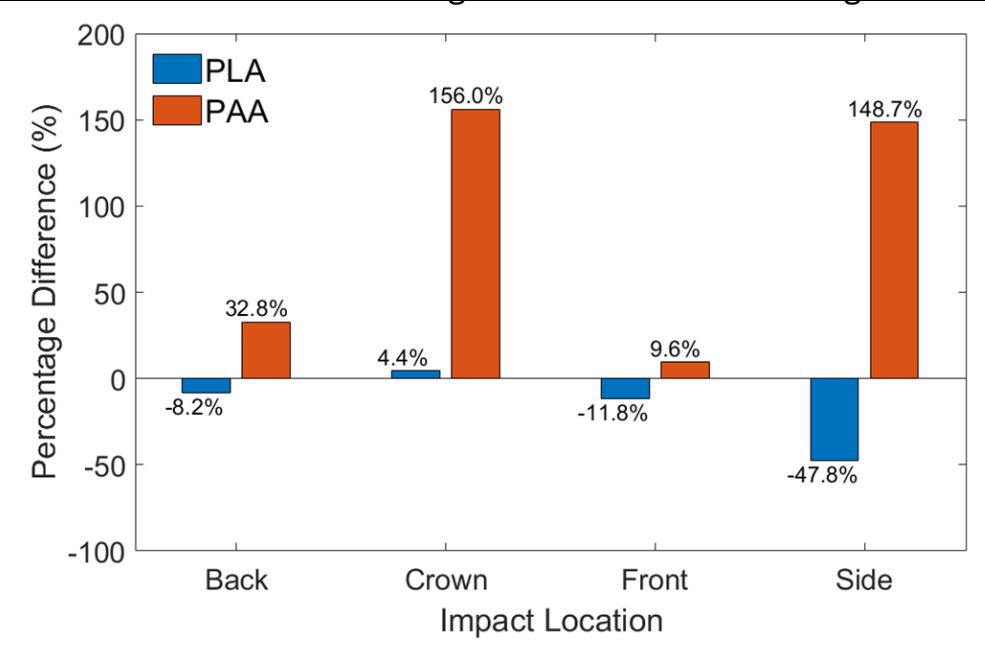


Figure 8.7, Percentage difference between constrained and unconstrained headforms when dropped at 5 m/s onto wooden anvils. The constrained (neckform affixed) condition is considered the baseline, thus positive percentages show an increase in peak for cradled conditions and a negative shows a decrease in peak.

PLA decreased on average when cradled (unconstrained) compared to affixed with a neckform (constrained) (Δ mean = -15.9 %) and location had a clear effect on the magnitude of this, Figure 8.7. This was greatest at the side (Δ = -47.8 %), while back (Δ = -8.2 %) and front (Δ = -11.8 %) were similar decreases. Crown was the only location to increase, though only slightly (Δ = +4.4 %). Overall, mean PLA ranged from 587 g (crown) to 220 g (side) when cradled, while back and front impacts had means of 298 and 322 g, respectively. On average, linear pulse durations increased when cradled (Δ = +34.6 %), Appendix A.8.3. Back, crown, front, and side locations increased by 38.4, 34.4, 44.3, and 21.1 % respectively.

PAA universally increased for the cradled setup, and by a substantial factor (Δ mean = 86.8 %). However, the significance of this is exaggerated by PAA being relatively smaller than PLA to start with. For example, the 156 % increase for crown PAA equates to a difference of 4.49 krad/s². The most significant increase was for side impacts (Δ = +13.9 krad/s²). The range of PAA was the reverse of PLA, in that side was the greatest (23.2 krad/s²) and crown the lowest (7.36 krad/s²). Back and front had means of 14.5 and 9.86 krad/s² respectively. Overall, angular pulse

duration decreased on average (Δ = -11.9 %), each of back, front, and side decreased by -27.6, -11.0 and -58.6 % respectively. Crown was the only location to increase (Δ = +49.7 %).

Comparative to the PO boundary limits, cradling the headform shifted linear kinematics slightly further from the range because of increased pulse duration. Conversely, angular kinematics were mostly brought to within range, as only front impacts (mean = $9.86 \, \text{krad/s}^2$, $6.36 \, \text{ms}$) exceeded the duration limit. The increase in PAA for cradled side impacts was just below the upper boundary of PO conditions (mean = $23.1 \, \text{krad/s}^2$, $3.22 \, \text{ms}$), whereas PAA spanned up to $65 \, \%$ of the range when constrained.

Transient resultant accelerations with the headform cradled and affixed with a neckform show the cradled headform produced smoother linear acceleration curves, Figure 8.8. This was attributed to less vibration with absence of coupled components, i.e. the neckform and drop assembly. Both linear and angular impacts were also more defined to a singular pulse, with no secondary loading phase as commonly found with neckforms [357]. A second peak is shown for front angular data when cradled, caused by a smaller and delayed roll pulse to the primary pitch response. A similar response occurs for side constrained, where a delayed yaw pulse followed the primary roll acceleration. These are not representative of the constraint, rather an effect of variation in impact location.

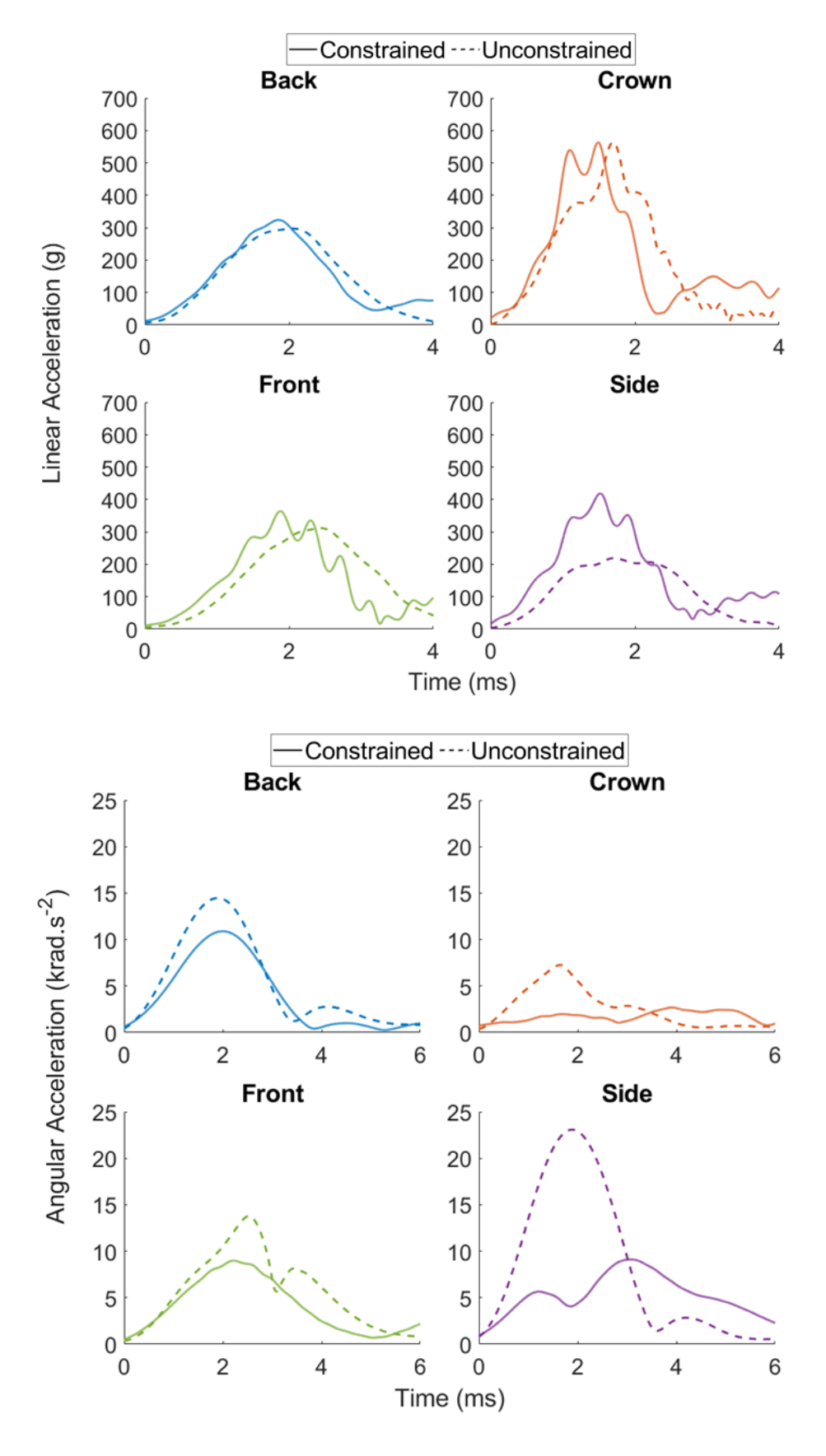


Figure 8.8, Transient linear and angular acceleration curves for drop rig head impact recreations when setup for 5 m/s wooden anvil trials. Curves show the difference between a headform constrained to the degrees of freedom of a hybrid III neckform and unconstrained in a cradle, similar to PSDB 21/04 protocol [13].

8.5 Discussion

Guided drops were used to produce more repeatable and controllable conditions than the representative experimentation of previous chapters, similar to what would be used in test standards. Repeatability was achieved with low CV% for headform measures across all setup conditions. Angular PAA had the greatest CV% (7.91%), as it was derived from angular velocity and duration, thus inherently amplified any noise/variation [250], [254], [269]. An alternative method for direct acceleration measurements is a nine-accelerometer package, though they are known to be similar in performance to 6DOF arrays and include error due to non-perpendicular planarity between sensors [245], [251], [252], [253]. Control of the impacts was also shown to be high, as low CV% suggests impact locations were repeatable, while the maximum relative deviation for velocity was -0.07 at 3 m/s (-2.3%).

8.5.1 Comparison to Representative Kinematics

Peak kinematics from drop tests showed to be within the boundary representative of PO; 95.4 and 96.5 % were within for PLA and PAA, respectively. However, the drop rig produced larger pulse durations than the target conditions. The difference in pulse durations from the PO boundary were much closer for linear measures (Δ max = +1.7 ms) than angular (Δ max = +5.4 ms), suggesting the drop rig was better at creating representative linear forces.

Including radial and oblique conditions is important when considering both linear and angular forces cause neurotraumatic injuries [50], [69], [73], [99]. This is shown with this study, as the only radial location (crown impact) was significantly greater for PLA (P < 0.01) yet lower PAA than the oblique (P < 0.01). Moreover, all oblique impacts were similar for PLA (P > 0.05), front and back were similar for PAA (P = 0.99), and side were significantly greater for PAA (P < 0.01). The latter was attributed to a greater contact area between headform and anvil for the side compared to front and back, and the different directional moments of inertia [150], [153], [213].

8.5.2 Comparison of Acceleration-Time Histories

Anvils of similar material properties to those in PO injurious conditions were included to assess how impact curves directly compared to the experiments in previous chapters. This is similar to how non-rigid anvils, such as the modular elastomeric pad (MEP), are used in sports standards to produce more realistic impact mechanics [15], [75], [391]. Representative materials were shown to not be required for PO conditions, as despite a significant difference with peak kinematics (P < 0.01), all conditions produced relatively similar pulse durations (Δ max \approx 0.2 ms). As discussed, peak kinematics can be achieved with impact velocity control whereas pulse duration is dependent on compliance [336]. The flat wooden anvil produced greater PLA on average than the curved metallic, despite that the steel was less compliant than wood (Δ = + 71 g, P = 0.03). In line with other studies, this suggests a flat surface imparts more blunt force to the headform [46]. As such, the test standard should include flat surfaced anvils to ensure headgear can successfully protect from them. This is important as each of swung implements, falling from horseback, and projectile bricks have flat surfaces.

Pulse durations for wielded implements were too narrow for recreation with the trialled drop rig setups (wooden < 1.25 ms and metallic < 1.75 ms), brick impacts from Chapter 7 were also similar to these (< 1.53 ms). Durations can be reduced with less compliant anvils or decreasing impact energy [336], neither of which are possible in this case. Anvils are already low compliance, for example steel, and peak kinematics would not be possible at lower impact energies unless excessive mass was added. However, the disparity for pulse durations between the test rig and wielded weapons is still relatively small for head impact mechanics in general (Δ max \approx 2 ms).

Horseback fall recreations on the drop rig produced very similar duration to the representative condition. This was set up with a steel flat anvil to replicate the rigid floor in Chapter 5. However, there was a dissimilarity in PLA (Δ = 121 g), suggesting the drop rig was a stiffer system than a full-body ATD. For wooden implements, target peaks were relatively low. The closest drop rig conditions were either 3 or 5 m/s depending on impact location, although 3 m/s was always lower (Δ = -62.7 g) and 5 m/s always greater (Δ = +69.3 g). Metallic target curves were much taller than

wooden, thus the closest setup for PLA was always 5 m/s. However, this was consistently lower than the representative peaks (Δ mean = -81.3 g), the greatest disparity being for side impacts (-167 g). From these, we know that impact velocities \approx 4 m/s can be used to represent wooden, and horseback fall conditions, whereas > 5 m/s is required for metallic.

Impact velocity had more influence on peak kinematics than location or anvil type (P < 0.01, PLA F = 108, PAA F = 62.8). This is because velocity and kinetic energy have a squared relationship [105], [418]. This emphasises the importance of repeatability with the test method, as minor velocity changes will have great influence on peak kinematics. Ranges of test velocities to represent PLA across all PO target conditions, Table 8.1, are summarised in Table 8.5; these are guidance values calculated from the identified power law relationships, Table 8.4. The upper velocity limit for oblique loads is greater than the capability of most drop rigs, as well as larger than any other non-automotive test standard [18]. This gives further reason for the test standard to include both radial and oblique conditions to assess linear and rotational measures separately.

Table 8.5, Impact velocity ranges to represent PLA of injurious PO conditions with radial and oblique loading setups. Values are specific to the neckform affixed system in this study.

Cause of Injury	Target PLA	Impact Velocity	Impact Velocity	
	(g)	Radial Load (m/s)	Oblique Load	
			(m/s)	
Wooden Implement	210 – 410	2.32 - 3.90	3.44 - 5.45	
Metallic Implement	300 - 572	3.06 - 5.04	4.40 - 6.86	
Horseback Fall	402 - 497	3.84 - 4.52	5.38 - 6.23	
Projectile Brick (10.6 m/s)	514 - 771	4.64 - 6.36	6.37 - 8.43	
Maximum Range	210 - 771	2.32 - 6.36	3.44 – 8.43	

Of the target injurious conditions, three showed significant angular pulses (> 5 krad/s²). The drop rig was incapable of producing similar PAA to these with the neckform affixed (Δ = -21, -55, and -66 %). This was overcome with the absence of a neckform, although regressions could not be calculated, as they were only trialled at 5 m/s. However, as discussed in the following section, greater impact velocity is needed for meeting the upper PLA limit than for PAA, thus the recommendation for the standard is advised from PLA regression.

8.5.3 The Influence of a Neckform on Head Impact Biomechanics Drop rig trials with a neckform produced peaks within the range representative of PO although most pulse durations were larger. This was improved for angular measures by removing the neckform and cradling the headform similar to the current PO standard [13]. PAA increased (Δ = +86.8 %) while angular duration decreased (Δ = -11.9 %), shifting almost all conditions to within the PO boundary range. For linear measures, the absence of a neckform worsened the likeliness to PO conditions, with a minor decrease in PLA (Δ = -15.9 %) and increase in pulse duration (Δ = +34.6 %). However, the duration increase equates to little change relative to head impact dynamics in general (\approx 0.5 ms) and the slight decrease in PLA can be overcome with an increase in velocity. The guidance velocities in Table 8.5 suggest there is scope for increasing velocity with radial loading setups, as non-automotive headgear standards test up to 7 m/s with drop tests [18], [239].

Transient loading curves for cradled conditions also showed less vibration throughout the impact. This was present with the neckform affixed because of the coupling to the drop rig, as each components experienced a share of the load. Vibrational effects are unfavourable for a test standard as they create maxima and minima in the data series, thus have influence on peak measures. This could be mitigated with a lower cut off frequency although it means deviating from the SAE J211 standard and risks attenuating the signal peak [244]. Also, vibrations will be system and situationally specific, thus defining a single frequency for all PO headgear testing would not be universally translatable. Vibrational effects could be identified with a Fast Fourier Transform (FFT) and then appropriately attenuated. However, this will not be the same frequency for all investigators, thus may lead to

unwanted variation between test facilities if used in a standard. Cradled conditions make the impact more universally translatable, with less system specific effects, thus increases inter-rater reliability.

In summary, the use of a neckform is not necessary for recreating impact dynamics in a drop rig test standard for PO headgear, and the absence of one improves the in-field representation of angular measures. However, neckforms still have place in PO head impact research, as they represent more bio-fidelic properties such degrees of freedom and and stiffness [185], [188], [245], [357].

8.5.3 Drop Rig Setup Recommendations from Current Understandings The following summarise what recommendations can be made for the PO helmet test standard, based on current understandings:

- The head impact accelerations due to projectile bricks, wielded wooden and metallic implements, and falling from horseback can all be achieved with a drop rig, with similar setup to traditional head impact standards [18].
- Pulse durations equal to those in found in PO injurious conditions can be recreated for angular motion, although linear are expected to be up to 2 ms greater.
- Representative anvil materials are not required to produce realistic impact dynamics, although anvils must be minimal compliance to achieve representative pulse durations.
- Flat surfaced anvils should be included in the standard to better represent injurious conditions and impart greater blunt forces. Chapter 9 includes an assessment of current headgear subject to flat and cylindrical impact anvils.
- Both radial and oblique loading conditions should be used in the test standard. PAA measures are not appropriate for radial loads, thus should be assessed with oblique impacts only. Similarly, oblique loads require too high of an impact velocity for representative PLA, so this should be measured using radial impacts.

- An impact angle of 60° relative to the headform is representative of head impacts from wielded blunt implements and also recreates PAA in the upper range for what can be expected in PO activity.
- A neckform is not recommended for achieving representative head impact mechanics, the absence of one improves repeatability and angular measures.
- The lower bound of PO representative PLA (210 g) can be simulated with a radial load at velocity close to 2.3 m/s.
- The upper bound of PO representative PLA (771 g) can be simulated with a radial load at velocity close to 6.4 m/s.
- The upper bound of PO representative PAA (24.5 krad/s²) can be simulated with oblique load at velocity close to 5.0 m/s.

Further work is required before these recommendations can become more defined amendments to the test standard. For example, cradled conditions were tested at 5 m/s, and it is unknown what linear and angular regressions will be for radial and oblique loads. Moreover, regression for PLA with radial loads was determined solely from crown impacts, whereas there may be locational variation such as those shown with oblique loads at the back, front, and side. Recommendation for producing the upper bound of PAA is based on the limit of projectile bricks at 10.6 m/s, though it is likely a moving horseback fall will be greater PAA. Literature suggests this could be up to 51.2 krad/s² [106]. However, greater impact velocity is required to achieve the upper limit of PLA than it is for PAA (summarised above), thus testing oblique impacts as high as 6.4 m/s velocity would better capture the potential for greater PAA in-field. In addition, the frictional coefficient of the anvil surface should be controlled and high to maximise the tangential force component [211], [243], [419].

There are no defined head impact locations in the above recommendations; these should be parametrically assessed with a drop rig following the finalisation of impact velocities. For this, the back, crown, front and side locations should be compared alongside the front and rear boss impacts from the current standard

[13]. The choice of headform will also affect findings, all work in this project is subject to the fidelity of the Hybrid III [173], [216], [357].

Alongside being representative of PO loading conditions, the standard must also successfully scrutinise helmet performance and ensure that thresholds accurately represent the correct head injury pathologies. For example, it is unknown how current PO helmets will perform against flat anvil conditions, for it is not currently required in the test standard, nor are there angular considerations. Future work should look to assess how headgear performs under PO representative loads, as well as offer insight to appropriate threshold metrics.

8.6 Chapter Conclusion

Guided drop rig methods can produce repeatable impacts (coefficient of variation < 2.5 %) similar to the in-field loading conditions for Public Order (PO) activity. Peak linear (PLA) and angular accelerations (PAA) spanned the lower 73 and 65 % of the respective PO boundary limits when tested at 3, 5, and 7 m/s impact velocities. Regression statistics suggest the upper limit of PLA can be achieved with radial impact conditions at 6.4 m/s. The difference between drop rig and representative impact dynamics was that linear durations for wooden, metallic, and brick impacts were too narrow to recreate when dropping the headform (Δ max = -1.75 ms). These could not be improved without sacrificing peak kinematics.

Testing without a neckform increased the representativity of angular measures, which reached the upper PO limit at 5 m/s, and also improved the signal quality of all data. Cradling the headform is therefore recommended for recreating PO conditions. Both radial and oblique loading conditions should be used to separately assess how helmets protect linear and angular components of force. Oblique angles of 60° relative to the headform represent the mean angle of wielded blunt weaponry, although smaller angles would produce more rotation if necessary. Material representation is not necessary; impact anvils should be rigid steel and incorporate flat surfaces, which produced greater PLA than curved (Δ = + 71 g) despite a less compliant material (treated wood compared to steel).

These recommendations are a step towards finalising how the PO standard can improve situational representativity in its energy absorption assessment protocol. Further work is required to finalise impact velocities for radial and oblique measures, identify the most appropriate metrics for pass thresholds, and ensure conditions successfully scrutinise headgear design.

9. PO Helmet Impact Attenuation Performance

9.1 Introduction

Chapter 8 compared the bare head biomechanics between situationally representative and more controllable impact methodologies. This advised how Public Order (PO) specific injurious conditions can be represented with a more repeatable drop rig setup, similar to the current test standard [13]. While drop rig setups intend to replicate in-field conditions, it is crucial to ensure they are effective in assessing the design quality of PO headgear. For example, one methodology may produce lower peak headform kinematics than another, thus it will be more likely to approve poorer helmet designs.

This work aims to experiment headgear under the same loading conditions of previous chapters and evaluate their protective performance. This ensures that recommended setups meet the needs for appropriately assessing helmet energy attenuation, alongside replicating real-world loading mechanics. To achieve this, the following objectives were set:

- Simulate PO representative impact conditions with current issue headgear using the drop set ups from previous chapters.
- 2. Quantify the protective energy attenuation performance of PO headgear subject to representative conditions.
- 3. Highlight the implications for headgear assessments within a test standard.

9.1.1 PO Helmet Design Features

A detailed description of the helmet most commonly used by PO officers in the UK, the 'Defender Hybrid' Figure 9.1, is in Chapter 2 [294]. In summary, the outer shell is a 28-layer glass fibre reinforced polymer with flame retardant coating. The energy absorbing liner (EAL) is a singular component of expanded polyurethane (EPU) foam. Thin polyurethane (PU) pads are included at the crown and along the rim of the helmet for size spacing and comfort, and a cupped retention strap is used for retention.



Figure 9.1, 'Defender Hybrid' PO helmet (MLA Ltd) imaged from the exterior and interior with annotated key features [2], [294].

The external dimensions of the size 3 (mid-range male, $58-59\,\mathrm{cm}$ head circumference) Defender Hybrid are $\approx 285\,\mathrm{x}\,250\,\mathrm{x}\,240\,\mathrm{mm}$ and mass $\approx 1.6\,\mathrm{kg}$, without the visor or its rim mass $\approx 1.25\,\mathrm{kg}$. These are greater than many sports helmets, for example cycling, ice hockey, and equestrian riding hats though are more comparable to those in extreme sports and motorcycling. The large size offers a greater permissible EPU thickness, thus broadening the effective compression range of the design [10], [280]. The thickness of EAL for a size 3 Defender Hybrid is $\approx 55\,\mathrm{mm}$ at the crown and $\approx 35\,\mathrm{mm}$ at the brim. However, large helmets can reduce impact pressure and thus compress less under load [420]. They can also induce more angular torque as the radius from the head centre of mass increases [421]. Currently, the only understanding for the protective performance of Defender Hybrid helmets is that they pass the minimum attenuation requirements of PSDB 21/04 [13].

9.1.2 Helmet Impact Attenuation Mechanics

The failure thresholds for lower (30 J) and upper (120 J) impact energies in PSDB 21/04 are 150 and 250 g, respectively [13]. Expanded foams, such as EPU in the Defender Hybrid, are effective at attenuating a singular significant impact, following which the helmet will need replacing [10], [186]. This is due to permanent compression of the foam increasing the effective density, thus stiffening the material and requiring a lesser compressive strain to cause densification if

impacted again [10]. Therefore, the testing of PO specific loading conditions is essential when assessing headgear performance, as it is necessary to understand when excessive EAL compression occurs.

This study evaluates helmeted headform PLA and PAA under the same conditions as Chapter 8, permitting direct comparison to bare head mechanics. Similar to Chapter 8, varying drop rig impact surfaces, angles, and locations permits study for how they affect helmet performance, enabling more justified recommendations for the PO helmet test standard. Lastly, while not the primary focus of this chapter, testing PO headgear under situationally representative conditions provides an opportunity to investigate realistic helmet wear and damage that can inform design recommendations for future headgear developments.

9.2 Method

9.2.1 Experimental Arrangement

Impacts were conducted with a floor to ceiling guided drop rig and Hybrid III (HIII) head and neckform arrangement (50th percentile male, 4.54 kg headform mass, neck tensioned to 1.1 Nm) (JASTI Co. Ltd.). The headform was fitted with a size 3 Defender Hybrid Public Order helmet [2], [294]. A limited number of helmets were available due to high local demand for PO headgear at the time of testing (July 2024). These were manufactured in January 2023 and tested within their seven-year shelf life [294]. The visor was removed from all helmets to prevent unwanted collision with anything but the shell. As per PSDB 21/04, helmets were fit so that the eye line was visible, with the lip of the helmet on the glabella [13], [422], [423], [424]. The retention strap was fit so the cap cupped the chin and was tightened as much as possible by hand, as per BS EN 13087:2000, which is referenced within PSDB 21/04 [13], [425], [426].

Helmet performance was assessed at 5 m/s impact velocity to permit direct comparison with the bare head drop rig impacts in previous chapters. For the same reason, impact locations were the back, crown, front, and sides of the headform. Four setups were derived to simulate different impacting objects, referred to as 'impactors', Figure 9.2. Three of these were the wooden, metallic,

and cradled wooden conditions in Chapter 8 where the headform was dropped with the neckform affixed for the former two (impact energy = $170 \, \text{J}$) and was unconstrained in a cradle for the latter (72 J). Impact angles were kept as 90° and 60° relative to the headform longitudinal axis for radial (crown) and oblique (back, front, and side) loads, respectively. The metallic anvil was a 50 mm diameter cross section steel pipe and the wooden was a flat surface of treated softwood greater than $300 \times 300 \, \text{mm}$. The fourth impactor was a dropped brick, replicating the exact method from Chapter 7. The $215 \times 102.5 \times 65 \, \text{mm}$ brick was cradled on the drop rig with the long edge parallel to the height of the drop tower. The total drop mass was $2.24 \, \text{kg}$, the equivalent of $28 \, \text{J}$ impact energy.

Two high-speed video (HSV) cameras (4000 Hz) were positioned 1.5 m from the lateral and frontal views of the impact. Field of view = 0.62 x 0.98 m was set to capture collision and the subsequent motion of head and neckform. Calibration followed the method outlined in Chapter 4, employing a 30 mm checkerboard to build real-world coordinates and correct lens distortion [351], [352], [353], [354]. A 20 mm white marker on the rail bearing was tracked over 40 frames (10 ms) prior to impact to measure impact velocity. The marker position was processed using the script described in Chapter 4 and differentiated into velocity (Matlab 2023b [350]).

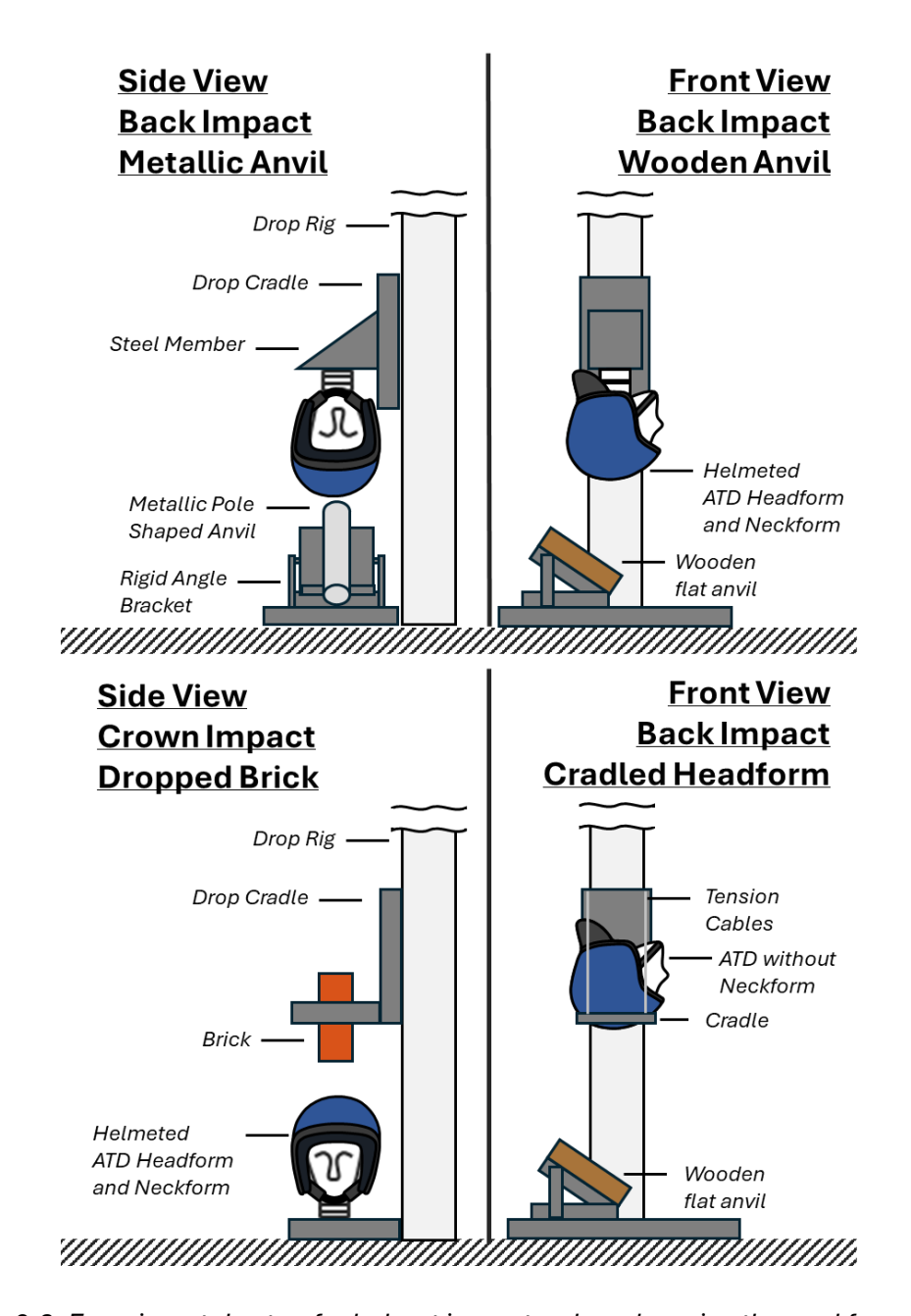


Figure 9.2, Experimental setup for helmet impacts when dropping the neckform affixed headform onto representative metallic and wooden anvils (top row), dropping a clay brick (bottom left), and dropping an unconstrained cradled headform (bottom right).

9.2.2 Head Impact Analysis

Headform kinematics were measured using a 6DOF 3a3ω sensor package (Slice 6DX PRO, DTS) positioned at the headform CoM [251], [355]. Data were sampled at 100 kHz, with linear and angular signals respectively filtered at CFC 1000 and CFC 180, in accordance with SAE JS211 [28], [244]. The IMU triggered at 5 g on any of the three accelerometers, capturing data from 0.02 s before to 0.1 s after impact. As before, linear and angular accelerations were used to quantify head impact

magnitude. Angular acceleration was derived from angular velocity by differentiating with the 5-point stencil method [247], [248], [249], [250]. Headform data was processed and analysed using MATLAB script (Matlab 2023b [350]).

Resultant kinematics were calculated as the 3-dimensional Pythagorean result of x, y, and z headform components. Mean values were calculated for impact velocities, resultant PLA, and resultant PAA. Impact repeatability was assessed with coefficient of variation statistics (CV%). Peak headform kinematics and standard deviations were highlighted for each impactor, irrespective of headform location. These were compared to the upper and lower thresholds of PSDB 21/04 and the angular equivalent from the American Football standard for evaluating protective performance [13], [15]. This was further quantified with the percentage change in PLA and PAA between helmeted and bare headform impacts for each impactor condition. Crown impacts were removed from angular assessments for they were not oblique loading conditions, thus they biased results to make headgear seem less effective.

Two-way 'Analysis of Variance' (ANOVA) was used to quantify the effects of impact location, impactor type, and their interaction on peak kinematics and their change when helmeted [21], [356]. Post-hoc Tukey's tests provided detailed comparisons for each condition, including their interactive effects. F statistics were used to quantify the magnitude of effect. There were complications with the two-way method for angular analyses because of the erroneous bare headform data for brick impacts to the back (Chapter 7). These biased the reduction in PAA to make helmets seem more effective, thus were omitted from the analysis. Degrees of freedom were no longer consistent between variables, thus change in PAA for impact location and impactor type had to be assessed independently with one-way ANOVAs and interactive effects could not be quantified.

The effects of wear on a helmet were quantitatively assessed with mean PLA and PAA at each impact location. 'New' helmets were considered any that had not been impacted in that location, whereas 'Used' were anything from one impact onwards. These were directly compared for metallic and dropped brick impacts, as they were the most and least severe of identified in-field conditions. Helmet wear effects could have been made for wooden and cradled impacts, although there

was little statistical significance with only a single new helmet per condition. For each condition, two tailed t-test statistics were used to assess similarity between new and used helmets with α = 0.95.

Wear on the helmets was further assessed by qualitative means after three impacts per site of each headgear (Back, Crown, Front, and Side). Images were taken of the helmet exterior, with view of the front and crown impact locations, and sections were made down the mid-sagittal and coronal planes of the helmet [13]. Cuts were made with the bandsaw in that order, Figure 9.3, thus half of the helmet is shown for the sagittal cuts and a quarter for the coronal images. Sagittal views showed the internal damage of front, crown and back impact sites (marked with an arrow) and side impacts were shown with the coronal view.

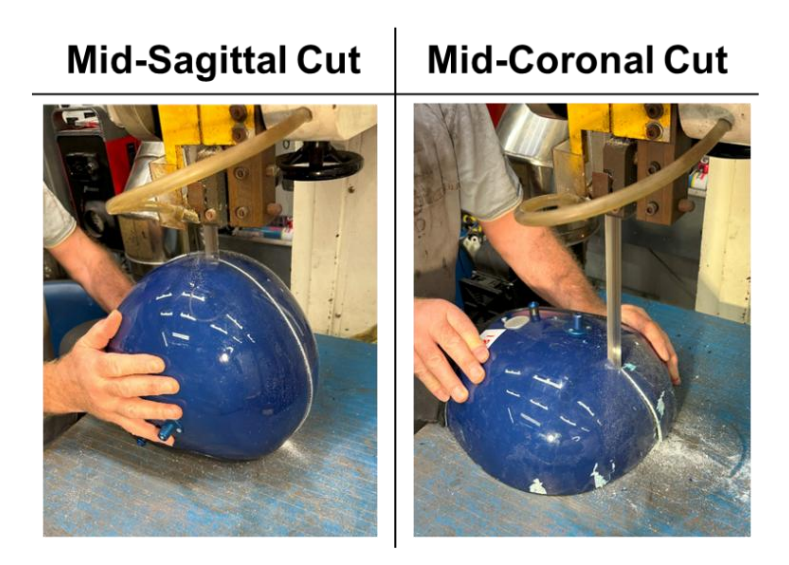


Figure 9.3, Helmet sections, in-line with the anatomical mid-sagittal and coronal planes, for assessing internal wear and damage.

9.3 Results

9.3.1 Peak Headform Kinematic when Helmeted

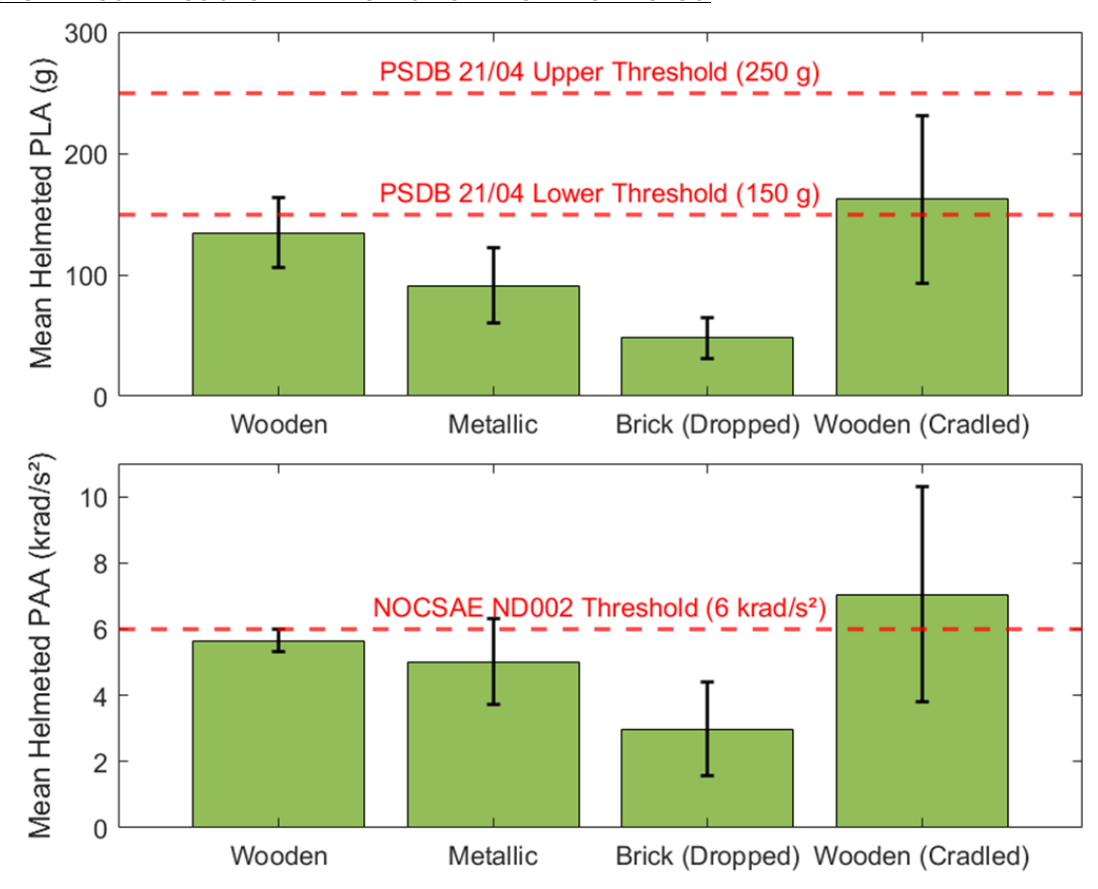


Figure 9.4, Mean peak linear (PLA) and angular acceleration (PAA) for helmeted headforms at each drop rig setup condition. Standard deviations are large because means include all head impact locations.

Mean impact velocity across all conditions was 4.94 (\pm 0.10) m/s. There was significant standard deviation of peak kinematics for each impactor (mean CV% = 32.5 %) due to variation between impact locations and changes in helmet performance when new and used. The hierarchy of mean peak kinematics based on impactor, Figure 9.4, was the same for both PLA and PAA; wooden cradled produced the greatest (162 g and 7.05 krad/s²), followed by wooden with a neckform (135 g, 5.65 krad/s²), metallic (91.2 g and 5.00 krad/s²), and brick (47.9 g and 2.98 krad/s²).

Of all conditions, only cradled impacts to the crown had a mean greater than the upper threshold of the PO standard, 258 (\pm 84) g, although the standard deviation suggests a large portion of distribution would be below. Of the other conditions, only crown impacts with the wooden impactor exceeded the lower PO threshold

(175 (\pm 7.9) g). For PAA, cradled wooden impacts to the side surpassed the NOCSAE ND002-17m21 threshold (9.54 (\pm 0.61) krad/s²), as did metallic front (6.18 (\pm 0.97) krad/s²). Wooden impacts to the back showed much of the distribution would exceed the threshold, although mean was just below (5.95 (\pm 0.24) krad/s²).

9.3.2 Energy Attenuation Performance

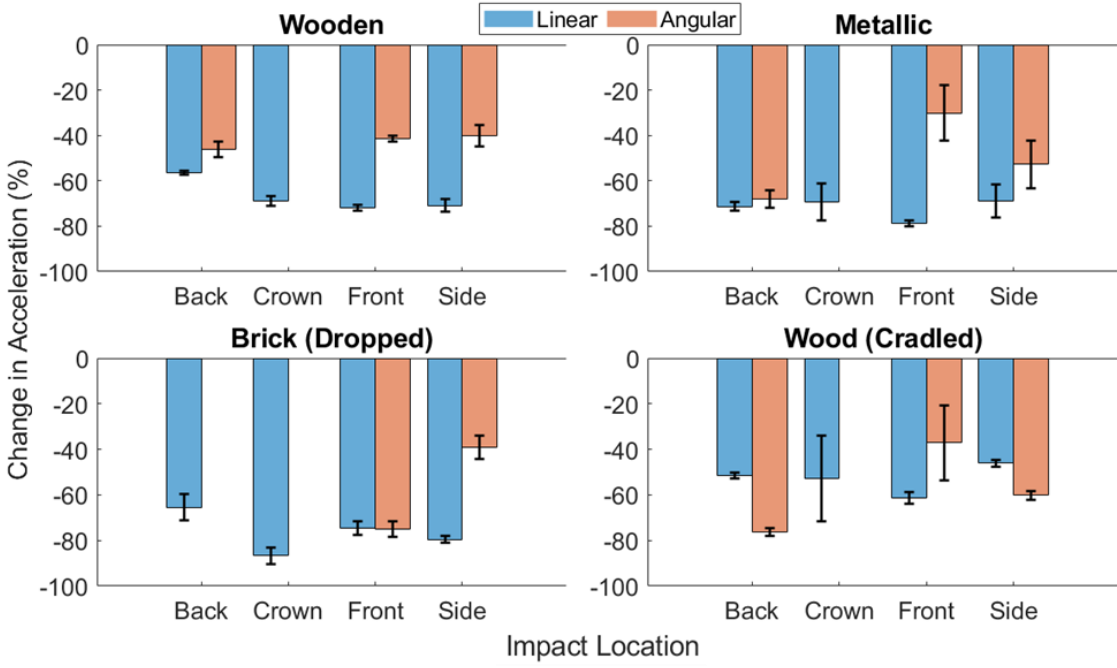


Figure 9.5, Change in linear and angular acceleration between helmeted and bare headforms to assess the protective performance of PO headgear. Figure tiles represent the setup condition, and each setup is separated by impact location. There was no bare brick data to compare angular measurements to and crown impacts were radial, thus irrelevant for angular comparisons in this analysis.

ANOVA showed there was significant effects due to impactor type, head impact location, and their interaction on helmeted reductions of PLA (P < 0.01). Impactor type had the greatest influence on PLA reduction (F = 52.9), followed by location (F = 12.3), and then their interaction (F = 5.65). Helmets reduced a greater percentage of PLA for brick impacts (-76.6 %), followed by metallic (-72.1 %), wooden (-67.0 %), and cradled wooden (-53.0 %). Of these, each group was statistically different, other than metallic and brick impacts (P = 0.06). The disparity between impact locations was less than impactor type (Δ = 10.5 %); front impacts were the greatest reduction (-71.7 %) and were similar to crown (-69.4 %, P = 0.68), which were

similar to side (-66.4 %, P = 0.42). Back impacts were less than all others (-61.2 %, P < 0.04). Of the interactive effects, all shared similarity with at least two other conditions (P > 0.08). Brick impacts to the crown were the greatest reduction (-86.6 %) although they were similar to brick side (-79.5 %) and metal front (-78.8 %). Cradled impacts at all locations showed the least reduction and were statistically similar (P > 0.14); side were the lowest (-46.1 %) and front were the greatest of these (-61.3 %). Wooden back impacts were also within similar range to this group (-56.5 %). For PAA, impact location had a significant effect (P = 0.03, F = 3.84) although this was not the case for impactor type (P = 0.14, F = 1.93). Back impacts were the greatest reduction (-63.9 %) and were similar to front (-49.6 %, P = 0.09), while front impacts were similar to side (-46.2 %, P = 0.84). Although no group was statistically independent, cradled reduced the most PAA (-60.5 %), followed by brick (-57.0 %), metallic (-50.3 %), and wooden (-42.6 %).

9.3.3 Helmet Wear and Damage

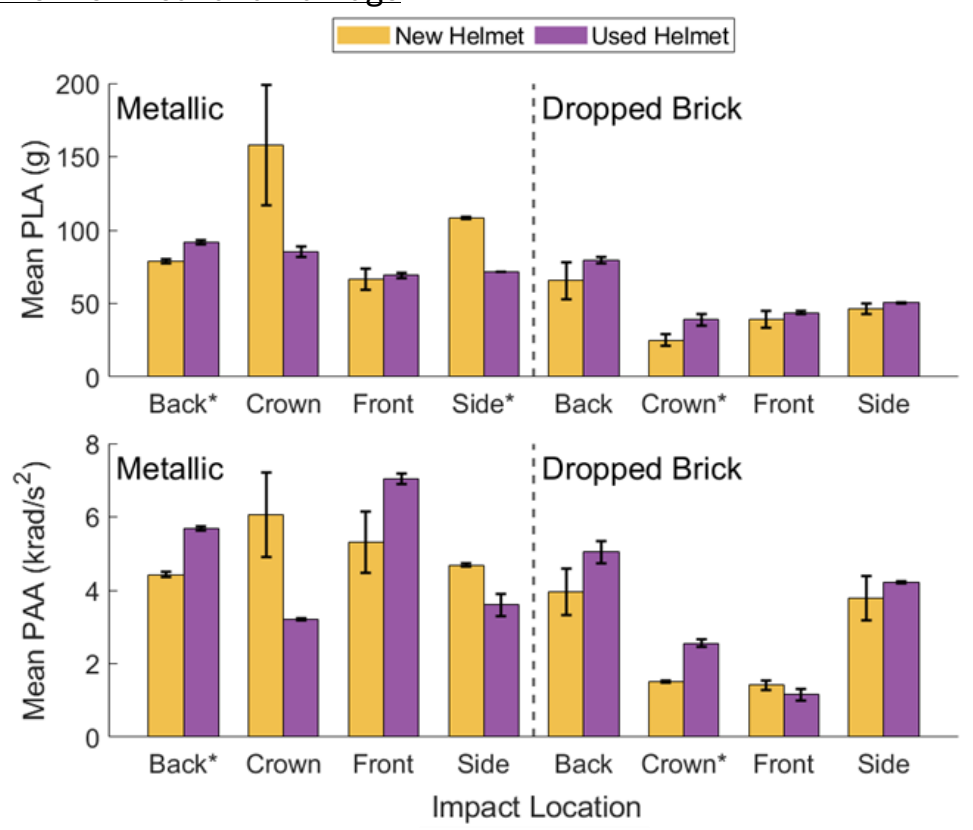


Figure 9.6, Differences in mean PLA and PAA between new and used (anything greater than one impact) PO helmets. * Indicates significant P < 0.05 difference between new and used headgear.

Eleven of the sixteen impact conditions showed no significant difference between new and used helmets, Figure 9.6. Of those that did, back impacts for metallic anvils showed significant increase for both PLA (Δ = 20.3 g, P = 0.015) and PAA (Δ = 1.25 krad/s², P = 0.003). Brick impacts to the crown also showed this for PLA (Δ = 13.9 g, P = 0.049) and PAA (Δ = 1.41 krad/s², P = 0.035). Five of the sixteen conditions decreased with used headgear, suggesting better protective performance after being used, although only one of these was significant (metallic side PLA, Δ = -36.6 g, P = 0.010).

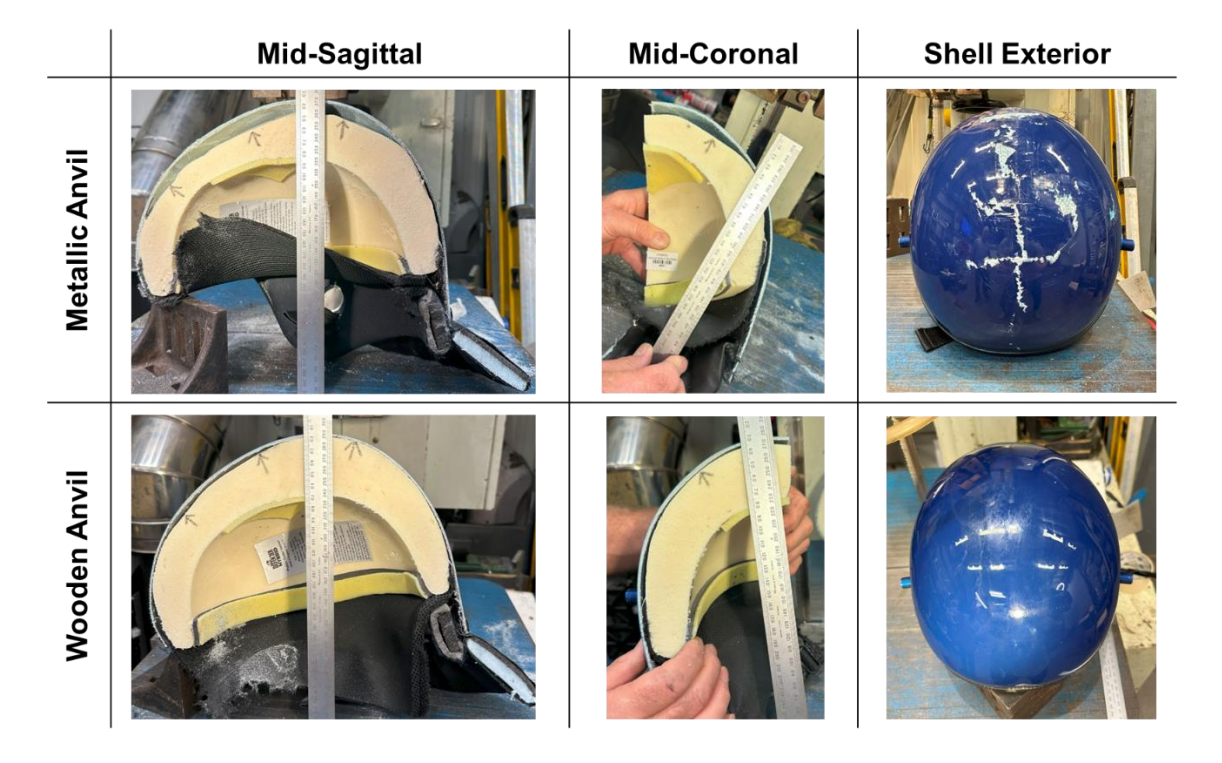


Figure 9.7, Internal and external damage of PO helmets following three repeated impacts to each of the back, crown, front, and side impact locations. Rows represent damage after repeated trials with a metallic cylindrical anvil, such as the current requirement of PSDB 21/04, and a flat surfaced wooden anvil.

The helmet wear comparisons in Figure 9.7 are made because metallic and wooden impacts were identical impact energy (170 J), with the only difference being anvil type. There is clear visual difference between these for both the helmet exterior and interior. On the exterior, the wooden impact showed insignificant visual wear with minor scuffs on the shell. The opposite was the case for the metallic, where the rounded surface of the anvil indented the shell to cause permanent penetrative fracture, shattering the plastic coating and splitting the fibreglass laminate irrespective of location. On the interior, the EPU liner of

helmets shows the extent this indentation; the foam is much more compressed at the impact zones (shown with an arrow) for metallic conditions. Wooden show slight deformation in the foam at front and crown zones but it is less drastic, as shown by a gap between the EAL and shell. Cradled and projectile brick impacts showed almost identical wear to wooden conditions, the only difference being more scratches than scuffs on the exterior for brick conditions.

9.4 Discussion

9.4.1 Effects of Drop Rig Setup on Helmet Performance

Impactor type had the greatest effect on PLA reduction (P < 0.01, F = 52.9), although this was insignificant for PAA (P = 0.14, F = 1.93). Therefore, choice of drop rig set up affects the protective performance of headgear with regards to the magnitude of linear force. Cradled impacts showed to be the most challenging for a helmet to attenuate impact energy as they reduced the least PLA (Δ = -53 %) when comparing between helmeted and bare head conditions. They also produced the greatest mean PLA (162 g) and PAA (7.05 krad/s²) of all setups and were the only condition to exceed the upper PLA threshold (Δ = +8.03 g) of PSDB 21/04 [13]. For PAA, they also exceeded the 6 krad/s² threshold of NOCSAE ND002-17m21 (Δ = +58.9 %) [15], although this was also achieved by metallic front impacts with much less of a margin (Δ = +3.0 %). Cradled impacts were also the preferred setup from the bare head drop rig experiment, thus it can be confidently recommended as the test setup for PO helmet test standards.

The flat wooden anvil produced a greater mean PLA (Δ = +43.5 g) and PAA (Δ = +0.64 krad/s²) than the curved metallic anvil under identical loading conditions, despite that wood is a more compliant material. This same finding occurred for PLA with the bare head condition in Chapter 8 (Δ = +71 g). The cradled wooden setup, which uses a flat anvil, also exceeded the PSDB 21/04 threshold (mean = 258±84 g) despite that impacts were less severe (Δ = -1.44 m/s, -48 J) [13]. For reference, much of this distribution is below the threshold because standard deviation is relatively large. Nevertheless, the findings suggest flat anvils produce greater PLA than the curved and edged anvils in the current standard, otherwise the design would not have passed current certification. This reinforces the findings

of chapter 8 in that incorporation of flat surfaces in the test standard can benefit helmet assessment and lead to future design innovation.

Head impact location had a significant effect on the reduction of both PLA (P < 0.01, F = 12.3) and PAA (P = 0.03, F = 3.84) with a helmeted headform. Back impacts reduced slightly less PLA than other locations, although the difference was statistically significant (-61.2 %, P < 0.04). PSDB 21/04 currently does not include the back as an impact location, thus there is potential for current helmets to have less protection in this area [13]. For PAA, the effect of location was relatively low (F = 3.84) meaning the directional effect of these helmets damping impact energy is less influential for angular than it is linear (F = 12.3).

9.4.2 Helmet Wear and Damage

Mean PLA and PAA was different between new and used helmet trials for all conditions, although only five of sixteen comparisons were statistically significant (P < 0.05). Metallic conditions had a significant increase in both PLA (P = 0.015) and PAA (P = 0.003) for used helmets with back impacts, whereas brick showed the same finding for crown (PLA P = 0.049, PAA = 0.035). This suggests the damage on helmets is setup specific, as can be expected with differing loading mechanisms and impactor masses. One impact condition significantly improved PLA reduction after having received an impact (metallic side, Δ = -36.6 g, P = 0.010) suggesting it benefitted from the shell being damaged and the EAL being a greater effective density.

There were visible differences in damage between metallic and wooden conditions, Figure 9.7. The metallic showed large indentation and permanent fracture of the shell, due to the greater pressure from a smaller surface area impact anvil. It is unknown how much of the foam compression in metallic trials was due to the first impact or if it was the accumulative compression of all 3. However, the shell visibly fractured after the first impact, suggesting significant compression. Despite the drastic difference in damage, the metallic anvil only dampened impacts slightly more than the wooden setup (Δ = -5.1%, P = 0.048) and there was no significant difference between the two for PAA. The limited

availability of new helmets constrained statistical comparisons to only metallic and brick conditions. Further work should look to assess the damage effects for cradled impacts if they are to be used in the test standard. Nevertheless, the study showed that damage effects are possible with PO representative impactors at energies less than the most severe conditions expected in-field.

Expanded foam EALs are effective at reducing the severity of a singular impact, thus are appropriate for applications such as road traffic accidents and fall protection [224], [238], [387]. However, the nature of PO events suggest multiple impacts are likely, as the source of impact comes from a crowd of aggressors. In addition, officers are unlikely to immediately exit the situation if they do not recognise the severity of a sustained head impact, which is made more likely with high adrenaline levels. The crowded nature may also make it difficult for them to leave, even if this is what they are attempting. From an informal conversation with the Metropolitan Police Physical Protection Group (MPPPG), a senior PO officer mentioned "wearing the scratches on their helmet like battle scars", suggesting that replacing the helmet is not an interest for some officers. In summary, there are many potential limitations for the use of single-use headgear in PO application, thus it could be beneficial for the PO helmet standard to encourage multi-impact protective systems in future designs [9], [280].

9.4.3 Limitations and Further Work

The aim to evaluate PO helmet performance with representative impact loads was achieved by the completion of objectives set in section 9.1. The use of Defender Hybrid helmets represents the most popular and modern headgear used by the UK Police; results therefore apply to most PO operations and national constabularies. However, alternative headgear, such as 'Argus' models, may be used by constabularies, though their construction is similar to the Defender and would likely have similar performance [301]. The results of this study are also transferrable to older Defender models, as the 2022 issue did not change the EAL or shell design [294]. However, this work was limited by the availability of helmets at the time of testing (July 2024), therefore constraining experimented conditions to only 5 m/s so comparisons to bare head impacts could be made. If more

helmets were available, testing a range of impact velocities for the preferred cradled setup would have provided insight for headgear performance, ideally these would span the recommended test velocities of 2.3 to 6.4 m/s from Chapter 8.

This work validated the guided drop setup in the current standard procedure is fit for purpose as cradled conditions were the best setup for impact representation and helmet performance assessment. Further work is required before exact setups can be advised for the PO helmet standard, this should address the effects of varying impact velocity, helmet damage at higher energies, environmental conditioning, anvil surface friction, head impact location, and headform/helmet sizing. These were not explored in this work for the test rig was designed to compare neck affixed and cradled conditions; instead, using the setup in PSDB 21/04 negates any potential system specific effects.

9.5 Chapter Conclusion

This study highlighted the performance of Public Order (PO) helmets under situationally representative impact conditions using a guided drop rig setup. Cradled impacts were identified as the best performing test configuration for use in a standard, producing the greatest peak linear (PLA, Δ min = +20.0 %) and angular accelerations (PAA Δ min = +24.8 %) of all tested setups. Peak kinematics exceeded the PSDB 21/04 PO linear threshold (250 g) for crown impacts and the NOCSAE ND002-17m21 American Football angular threshold (6 krad/s²) for side impacts [13], [15]. This was despite that impact velocity was below the current maximum impact energy in PSDB 21/04 (Δ = -1.44 m/s, -48 J), suggesting a flat impact surface produces greater blunt impact than the current curved and edged anvils in PSDB 21/04 [13].

Wear and damage were noticeable on the helmet from as early as a single impact in some conditions. This significantly (P < 0.05) increased headform PLA and PAA for two of eight impact scenarios respectively, whereas a further five and four conditions increased with less significance (P > 0.05). However, metallic side impacts improved PLA reduction after repeated impacts (Δ PLA = -36.6 g), likely benefitting from the fractured shell removing a stiff layer so the foam could indent

more. Although not a primary focus of this work, concerns for the practical limitations of single-use helmets in PO situations are highlighted, suggesting it may be desirable to encourage multi-impact protective systems in future standard revisions.

The findings of this study reaffirm much of the work from bare head impact recreations, namely that cradled impact setups, the use of flat anvils, and inclusion of radial and oblique loads are of benefit to headgear testing. This can encourage development of innovative headgear designs with lower injury risk. Further work should expand on the effects impact velocity has on PO headgear performance, as well as ascertain if passing the standard is possible with recommended setup conditions. Further studies should also look to quantify the effects of environmental conditioning, surface friction, head impact location, helmet and head size, and head impact location using the impact system in PSDB 21/04 before finalising experimental protocol in a revised test standard.

10. Injury Metrics for PO Helmet Testing

10.1 Introduction

Impact severity throughout this programme of work has been quantified with peak linear (PLA) and angular accelerations (PAA) although, as discussed in Chapter 2, there are limitations to these metrics. Firstly, injury tolerances to linear and angular force, which acceleration is a proxy for, are time-dependent [109], [120]. Thresholds which correlate these to mild (mTBI) and severe (sTBI) traumatic brain injuries rely on pulse durations exceeding the steep region of tolerance curves, ≈ 5 ms. Mean pulse durations for 5 m/s cradled impacts with a helmeted headform in Chapter 9 were 8.13 (\pm 3.11) ms for linear and 6.35 (\pm 2.36) ms for angular. Therefore, there is no guarantee that helmeted impact recreations will always be of sufficient duration to validate the use of peak kinematics alone.

This chapter summarises the severity predictions of alternative injury metrics, using data for 5 m/s cradled helmet drops in Chapter 9. This can inform which thresholds may be most appropriate in the test standard, for example one that predicts a high severity would better scrutinise headgear design quality. However, this dataset alone is insufficient for determining suitable metrics for the test standard, which will require more repeats, the full range of test conditions, and a finalised test system for the standard. This work only aims to demonstrate a method for comparing injury predictions of common metrics, including kinematic injury criteria (IC), and benchmark their performance for future studies to build on. To achieve this, the following objectives were set:

- Compile injury risk thresholds that correlate metrics to mTBI and sTBI likelihood.
- 2. Compare the relative injury severity predictions, using a PO representative dataset with helmeted headform.
- 3. Discuss which metrics seem best suited for use in the PO test standard, and the implications this would have on future helmet design.

10.1.1 Injury Thresholds

Healthcare professionals use the Abbreviated Injury Score (AIS) to quickly assess the severity of TBI based on a patient's loss of consciousness (LOC). AIS scores for TBI range from 1-6 depending on expected mortality, level of required care, and quality of life following an incident [62]. AIS 2 and AIS 4 refer to the boundaries of mild to moderate and moderate to severe TBI respectively. This is not an accurate assessment of injury, i.e. haematoma, contusion, etc., although is the focus of injury risk curves (IRC) for many kinematic metrics [114]. IRC simply display the relationship between a variable and the probability of sustained injury (0-1 scale), thus making them more comparable and universally accessible. However, not all IC have IRC to advise AIS boundary thresholds, thus this study only considers popular IC for which AIS 2 and 4 IRC could be found in literature. Table 10.1 includes kinematics and IC that were used in this analysis, along with their corresponding thresholds for 80 % likelihood of injury. Findings from Wu et al (2021) are included, who calculated IRC for the elderly population. These are only slightly different to the general adult population and are one of few sources with IRC for many metrics built from the same method [119], [125], [126], [146].

Table 10.1, Brain injury metrics and their corresponding 80 % likelihoods of AIS 2+ and 4+ injury thresholds.

Metric	Linear or	AIS 2+	AIS 4+
	Angular	Threshold	Threshold
		(source)	(source)
Kinematics			
Peak Linear Acceleration (PLA)	Linear	106 g [116]	300 g [126]
Peak Angular Acceleration (PAA)	Angular	7.9 krad/s² [116]	17.0 krad/s² [126]
Peak Angular Velocity (PAV)	Angular	31.5 rad/s [29]	46.5 rad/s [125], [126]
Injury Criteria (IC)			
Head Injury Criterion $t-t_0$ 15 ms (HIC) [114], [152]	Linear	850 [114], [162]	1800 [114], [162]
Brain Injury Criterion (BrIC) [108]	Angular	0.71 [108]	1.42 [108]
Rotational Velocity Change Index (RVCI) [144]	Angular	42 [161]	57 [161]
Universal Brain Injury Criterion (UBrIC) [157]	Angular	0.5 [161]	0.67 [161]
Diffuse Axonal, Multi-Axis, General Evaluation (DAMAGE) [158]	Angular	0.5 [161]	0.69 [161]
Head Impact Power (HIP) [153]	Linear and Angular	16.5 kW [153]	54 kW [145]

PLA and PAA are common in head impact research as well as test standards, including PSDB 21/04 and NOCSAE ND002-17m21 which have frequently been referenced throughout this programme of work [13], [15]. Peak angular velocity (PAV) is suggested as a slightly better injury predictor than PAA for shorter pulse durations [69], [108], [149]. Although both are still used in head impact research, the automotive industry seems to focus on PAV more than PAA in recent IC and other predictive models [108], [144]. However, some studies highlight that PAV is a poor predictor when the motion of the head is over constrained, thus a neckform or unconstrained headform may be important when measuring PAV [161], [427], [428].

HIC is a measure of the maximum average acceleration (a) over a limited time period $(t-t_0)$, derived from automotive frontal impact recreations [152]. The most appropriate time limit for non-automotive head impacts is up to 15 ms [114]. Up until the last ten years, HIC was the only IC to be used within international automotive safety regulations [429].

$$HIC = \left[(t - t_0) \left\{ \frac{1}{(t - t_0)} \int_{t_0}^{t} a(t) dt \right\}^{2.5} \right]_{max}$$
 (10.1)

BrIC was designed to predict AIS likelihood from rotational kinematics using FE brain strain metrics as the target [108]. The authors of BrIC developed separate IRC for Cumulative Strain Density Measure (CSDM) and Maximum Principal Strain (MPS), though recommend using the latter as it was a stronger correlation. Originally, BrIC included both PAA and PAV (ω) in its formula, although little correlation was found between PAA and CSDM [163]. Sometimes, the former BrIC is still used and termed 'Kinematic Brain Injury Criterion'. BrIC considers PAV by individual headform axes (x, y, and z) because of differing directional injury sensitivities. Critical values (ω_c) for x, y and z are 66.25, 56.45, and 42.87, respectively.

$$BrIC = \sqrt{\left(\frac{\omega_x}{\omega_{xC}}\right)^2 + \left(\frac{\omega_y}{\omega_{yC}}\right)^2 + \left(\frac{\omega_z}{\omega_{zC}}\right)^2}$$
 (10.2)

RVCI also assumes that brain strain correlates with peak angular velocity change and direction has an effect on injury tolerance [144]. This method uses the root sum of weighted (R) directional angular velocities. Similar to HIC, the time window is adjusted to produce a maximum value, though for accuracy this should be capped at 10 ms. The authors demonstrate this method improves predictions of impact-based accidents where BrIC shows little correlation with brain strain, such as automotive pedestrian collisions.

$$\max_{(t_0,t)} \sqrt{\sum_{i} \left[R_i \left(\int_{t_0}^{t} \alpha_i dt \right)^2 \right]}$$
 (10.3)

UBrIC includes both angular acceleration and velocity as a predictor of injury [157]. This demonstrated a better correlate than BrIC for CSDM and MPS at longer durations and similar at shorter durations. Each of the orthogonal axes (x, y, or z) are denoted as 'i' and r = 2 for best performance. α_i^* and ω_i^* are peak magnitudes of angular acceleration and velocity, normalised by critical values (ω_{cx} = 211 rad/s, ω_{cy} = 171 rad/s, ω_{cz} = 115 rad/s, α_{cx} = 20.0 rad/s², α_{cy} = 10.3 rad/s², α_{cz} = 7.76 rad/s²).

$$UBrIC = \left\{ \sum_{i} \left[\omega_{i}^{*} + (\alpha_{i}^{*} - \omega_{i}^{*}) e^{-\frac{\alpha_{i}^{*}}{\omega_{i}^{*}}} \right]^{r} \right\}^{1/2}$$
 (10.4)

DAMAGE is a second-order model to predict injury severity from a scaled (β) time-history of brain displacement (δ), developed by the same authors as UBrIC [158]. This represents brain tissue as a three-dimensional spring-dashpot viscoelastic system with angular acceleration as the input variable. DAMAGE can be calculated using either coupled or uncoupled series of three spring dampers. The authors observed minimal differences in predictive performance between these two methods, therefore this study employed the uncoupled approach for simplicity.

$$DAMAGE = \beta_{max_t}\{|\vec{\delta}(t)|\}$$
 (10.5)

HIP defines that injury is predictable by the rate of energy transfer and sensitive to the direction of motion [153]. The criterion includes mass (m) and directional

moments of inertia (I) of the head, which for the 50^{th} percentile male are: m = 4.5 kg, I_x = 0.016 kg·m², I_y = 0.024 kg·m², I_z = 0.022 kg·m² [150], [180]. Despite combining both linear and angular kinematics within the same criterion, the author of HIP states it is dominated by linear variance.

$$HIP = \sum_{i} \left[4.5 \left(\int_{t_0}^{t} a_i dt \right) \right] + I_x \alpha_x \int_{t_0}^{t} \alpha_x dt + I_y \alpha_y \int_{t_0}^{t} \alpha_y dt + I_z \alpha_z \int_{t_0}^{t} \alpha_z dt \right]$$

$$(10.6)$$

Many sources have been published reviewing peak kinematics, IC, and their geneses, while others have compared their performance [72], [126], [150], [154]. There is little consensus for which are the best predictors and performance is situation specific. This highlights a necessity for evaluating IC with PO representative impacts, rather than taking analogous inspiration.

10.1.2 Implications for a Test Standard

Standardised thresholds should logically be determined from the level of injury they wish to prevent occurring. For example, the current 250 g threshold in PSDB 21/04 is equivalent to a 50 % likelihood of AIS 4+ injury [119]. However, because kinematic metrics are proxies for actual injury occurrence, there will always be differences in their severity predictions [150], [154], [158]. A metric that overpredicts injury would be more scrutinous in a test standard, while this can incentivise innovation it may also set unfeasible requirements. Conversely, if a metric underpredicts injury severity then inadequate designs would be approved. Therefore, this programme of work looks to compare relative injury predictions between metrics to provide baseline for future studies on which should be used in the PO standard.

The chosen metric will become the design focus of manufacturers, thus its selection must reflect the actual injury situation and pathology. The current use of PLA has resulted in a headgear effective at reducing linear force, associated with open form and focal injuries. Should the threshold be changed to an angular

metric then features contributing to the reduction of linear forces may be abandoned. Therefore, the standard must include metrics that force consideration of reducing both linear and angular components simultaneously.

The sensitivity of a metric to the loading conditions, i.e. velocity, location, etc., also affects its suitability. Ideally, variation in the measure should match the corresponding change in injury risk. A metric that is insensitive to loading variations would fail to distinguish between headgear quality, whereas one overly sensitive would lack repeatability and may inadvertently bias helmet design. Being overly sensitive to impact velocity is less of a problem, although passing upper energy thresholds may be more of a challenge. Impact location is a bigger risk; if a metric scores certain impact locations as more severe, a designer would accordingly increase protection in these zones, despite no actual increased injury risk. The standard may wish to include different thresholds to reflect that the brain has different sensitivities depending on impact location [103], [334]. Generally, rotational motion around the longitudinal head axis is suggested to produce greatest brain strain, though not all research has found this to be true and it seems to depend on the impact characteristics [46], [103], [108], [376], [385], [430], [431].

To address these implications, this study evaluates the severity scores for each metric relative to their mTBI and sTBI thresholds and compares linear and angular-based measures as proxy for the breadth of head injury pathologies. While impact velocity variation cannot be assessed with only 5 m/s data in this study, due to limited headgear availability, location differences can be compared. Overall, this work provides a benchmark for future studies to define the most suitable metrics for the PO standard.

10.2 Method

10.2.1 Impact Data

This work used the cradled impact condition from Chapter 9, where the headform affixed with Defender Hybrid PO helmet was dropped onto wooden flat anvils. This included directional (x, y, z) components of linear acceleration and angular velocity from the headform centre of mass (Slice 6DX PRO, DTS). Angular acceleration was

obtained by differentiating angular velocity with the 5-point stencil method [247], [248], [249], [250]. Data were sampled at 100 kHz, with linear and angular signals respectively filtered at CFC 1000 and CFC 180 [28], [244]. Impact velocity was 5 m/s for all conditions, for a total of 12 impacts. More velocities would have improved comparative analysis, although helmet availability was limited at the time of testing (July 2024). Impact locations were the back, front, crown, and side to align with previous chapters. Crown impacts were radial (90° relative to the headform longitudinal axis), whereas the others were oblique (60° relative to the headform longitudinal axis).

10.2.2 Data Processing

Data was entirely processed using MATLAB script (MATLAB 2023b). All impacts were cropped to their initial loading pulses. Angular velocity did not always return to zero because the headform was free to rotate following impact, in this case data was cropped when velocity became constant and a further 15 ms had passed. Peak kinematics (PLA, PAA, and PAV) were the maximum resultant (Pythagorean) across the time series. HIC was calculated from linear acceleration with a maximum 15 ms window [114], [152]. BrIC used the critical values 66.25, 56.45, and 42.87, for x, y, and z, respectively [108]. RVCI was the maximum absolute over a maximum window of 10 ms, with weighting factors $R_x = 1$, $R_v = 2.29$, and $R_z = 1.98$ [144]. UBRIC was similar to BrIC with index r = 2 and critical values of ω_{cx} = 211 rad/s, ω_{cy} = 171 rad/s, ω_{cz} = 115 rad/s, α_{cx} = 20.0 rad/s², α_{cy} = 10.3 rad/s², α_{cz} = 7.76 rad/s^2 [157]. HIP considered the maximum absolute solution for a head mass = 4.5 kg, and directional moments of inertia $I_x = 0.016 \text{ kg} \cdot \text{m}^2$, $I_y = 0.024 \text{ kg} \cdot \text{m}^2$, and $I_z = 0.016 \text{ kg} \cdot \text{m}^2$ 0.022 kg·m² [150], [153]. The score given from DAMAGE will indefinitely increase if the headform remains in prolonged angular motion, which will happen when testing without a neckform [158]. For this reason, duration for the DAMAGE calculation was capped at 12 ms to ensure all angular acceleration pulses completed, but little data was used after (max pulse duration = 11.3 ms).

10.4.3 Statistical Analysis

The nominal scores for each metric were collated and averaged over all trials. Each metric has different scale thus scores were normalised by their respective thresholds for AIS 2+ and 4+ injury for comparison, Table 10.1. AIS 4+ normalised scores were then separated by impact location to assess directional effects.

10.3 Results

10.3.1 Severity Predictions

Table 10.2, Summary of mean (standard deviation) injury metric scores for 5 m/s flat surfaced impacts with a PO helmeted headform. Means include impact locations across the back, crown, front, and side of the headform, hence relatively large standard deviations.

Metric	Linear or Angular	Mean Value (standard	
		deviation)	
Kinematics			
PLA (g)	Linear	162 (± 66.0)	
PAA (krad/s²)	Angular	6.89 (± 3.32)	
PAV (rad/s)	Angular	20.8 (± 6.51)	
Injury Criteria (IC)			
HIC [152]	Linear	581 (± 96.9)	
BrIC [108]	Angular	0.36 (± 0.10)	
RVCI [144]	Angular	25.2 (± 8.55)	
UBrIC [157]	Angular	0.12 (± 0.03)	
DAMAGE [158]	Angular	0.55 (± 0.28)	
HIP [153] (kW)	Linear and Angular	30.5 (± 11.8)	

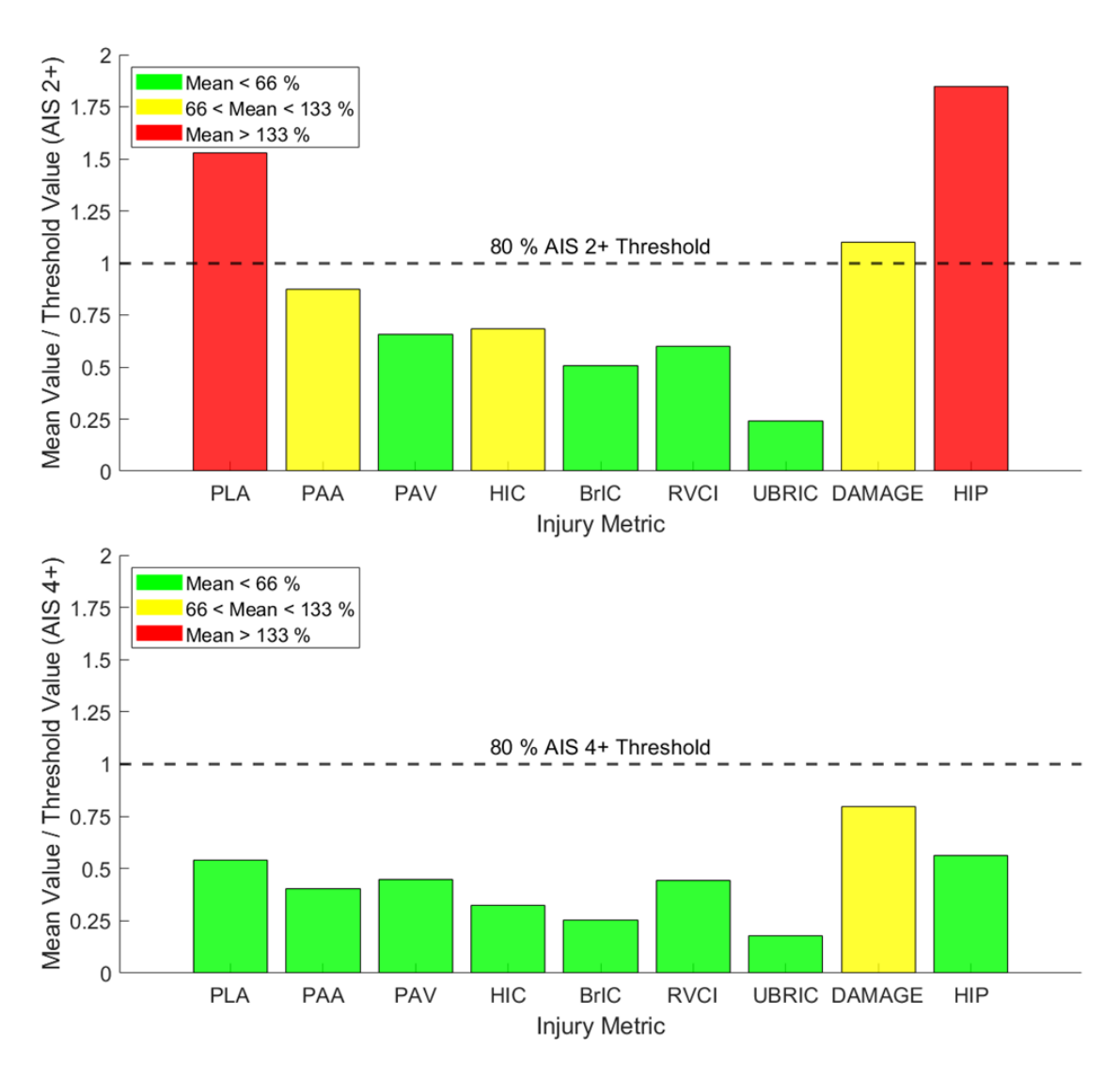


Figure 10.1, Mean injury metric scores, Table 10.2, normalised by their corresponding 80 % likelihood of AIS 2+ and 4+ thresholds, Table 10.1. Bars are coloured according to their proximity to the threshold, where a greater relative score suggests a greater severity of injury.

HIP (185 %), PLA (153 %), and DAMAGE (110 %) exceeded the threshold of 80 % AIS 2+ injury likelihood, Figure 10.1. PAA (87 %) and HIC (68 %) were below the threshold but within ±33 %. No metric exceeded the threshold for AIS 4+ injury and only DAMAGE (80 %) was within ±33 %. All metrics below the 66 % level for AIS 2+ injury are those dependent on angular velocity (PAV = 65, BrIC = 51, RVCI = 60, and UBRIC = 24 %). BrIC (25 %) and UBRIC (17 %) were also the lowest injury likelihood for AIS 4+. HIC, which adds a durational consideration to linear acceleration measures, consistently predicted lower severity than PLA alone (Δ AIS 2+ = -84 %, Δ AIS 4+ = -22 %). HIP, which is derived from linear and angular acceleration, followed a more similar trend to PLA than PAA. PAA was a greater prediction of

AIS2+ injury than PAV (Δ = +21 %), although PAV was slightly greater for sTBI (Δ = -4.0 %).

10.3.2 Impact Location Effects

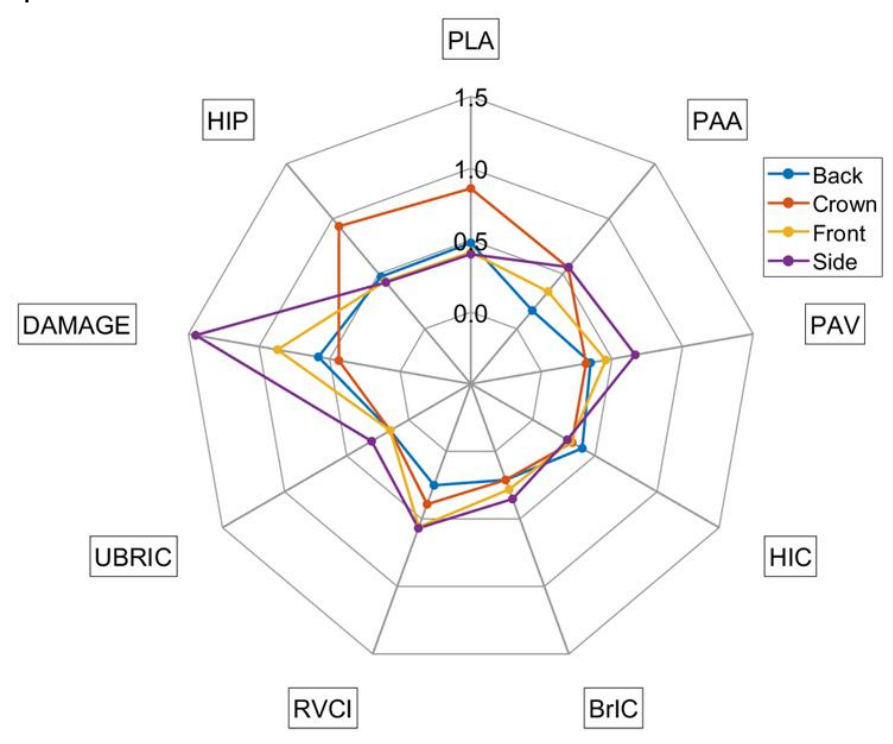


Figure 10.2, Mean injury scores for each impact location, normalised by their corresponding AIS 4+ threshold.

Figure 10.2 shows the spread of injury scores based on location. Crown impacts were the greatest for PLA (86 % of the AIS 4+ threshold) and HIP (93 %), which was expected from the only radial impact condition, although this was not recognised by HIC (32 %). This PLA for crown impacts also exceeds the current PSDB threshold (= 258 g). All angular metrics ranked side impacts as the most severe (mean = 65 %). On average, this was followed by front (44 %), crown (34 %), then back (28 %). The greatest range across locations was for DAMAGE (Δ = 101 %), HIP (Δ = 51 %), and then PLA (Δ = 46 %), while the least were HIC (Δ = 12 %), BrIC (Δ = 14 %), and UBRIC (Δ = 15 %). Considering only oblique loads, PLA (Δ = 8 %) and HIP (Δ = 5 %) had very small ranges, whereas DAMAGE still had the greatest range of all metrics after removing crown impacts (Δ = 87 %). DAMAGE is the only angular metric to show a directional sensitivity near this scale amongst oblique conditions, PAA (Δ = 39 %), RVCI (Δ = 32 %), and PAV (Δ = 32 %) were the closest.

10.4 Discussion

10.4.1 Ranking Injury Metrics

The final decision for the best suited thresholds requires more structured testing to assess metric quality with the finalised test system, anvils, impact velocities, and locations. As discussed, this data is limited to just one velocity and four locations because of little helmet availability. However, the following conclusions have been made that may advise future work to determine the best thresholds for a PO standard:

- The use of a singular metric to capture both linear and angular performance is not better than using two independent metrics. HIP was the only metric to combine the two but was heavily dominated by variation in linear acceleration.
- PLA was the most appropriate performing metric of those that consider linear acceleration in their formulae. PLA predicted much greater injury severity than HIC.
- PAA was the best performing metric of the eight that consider angular kinematics in their formulae. Angular velocity-based metrics generally predicted a less severe injury condition, while DAMAGE varied greatly with impact location.

HIP was the only considered metric to be derived from both linear and angular kinematics, although showed a closer relationship to linear acceleration for all analyses. This attribute was acknowledged by the authors when it was first published [153]. Therefore, there would be concerns for if angular protection is being adequately monitored if it was used on its own. Alternative IC that include linear and angular factors are summarised in Chapter 2: 'GAMBIT', 'PCS', 'KLC', and 'CP'. These may perform differently to HIP, though their injury risk functions were unknown and could not be considered in this study. Of the remaining linear-derived metrics, PLA and HIC, PLA seems the most appropriate for assessing helmet quality as it predicted greater AIS 2+ and 4+ injury severity. HIC also failed to detect the increased impact magnitude for the radial (crown) condition.

All angular velocity-based metrics produced a relatively lower injury prediction than the other metrics for AIS 2+. Irrespective of which are the more accurate proxy for injury, a metric that predicts a lower severity will be easier for headgear to pass, thus encourages less innovation in future designs. BrIC and UBRIC especially, were the lowest predictors of both AIS 2+ and AIS4+ injury occurrence. The remaining angular metrics are based on angular acceleration, PAA and DAMAGE. The latter predicted a greater likelihood of both AIS 2+ (Δ = +23 %) and AIS 4+ injury $(\Delta = +39 \%)$, and the two had similar CV% $(\Delta = 3 \%)$, initially suggesting DAMAGE is the preferred metric. However, DAMAGE was highly sensitive to impact location (Range = 101 % of the AIS 4+ threshold, = 0.7 DAMAGE) and predicted side impacts much greater than any other, the closest being front (Δ min = -58 % of AIS 4+, = 0.4 DAMAGE). Similar directional sensitivity has been seen for DAMAGE with pneumatic ram tests and ice hockey headgear [154]. This would encourage designers to protect the side of the helmet more. Although side impacts have at times shown to be more dangerous [46], [103], [432], others report they require greater loads to achieve equivalent injury [94], [433]. Therefore, although there may be more injury risk to the side for identical impact magnitude, the scale of disparity predicted by DAMAGE seems too large to be truly representative. As a result, PAA was the most appropriate angular based metric from this dataset. Other than DAMAGE, this predicted closest to the AIS 2+ threshold (-13 % compared to PAV = -34 %) and was only marginally less than PAV (Δ = 4 %) and RVCI (Δ = 3 %) for AIS 4+. However, PAA was not perfect, showing higher CV% (48 %) than all metrics except DAMAGE, with relatively large within group variation (mean = 21 %). However, this greatly decreased without radial impacts (mean = 7 %), suggesting PAA may be best used for only oblique loading conditions.

10.4.2 Thresholds Values

PLA: The current PSDB 21/04 threshold of 250 g corresponds with a 50 % likelihood of AIS4+ injury [119]. PLA is a poor predictor of diffuse injuries, thus this threshold should focus on ensuring open form and focal injuries are mitigated [9], [92], [415]. The 250 g threshold is determined from assessment of contusion injuries (focal) so therefore proxies the desired pathology [122]. The question

remains, at what likelihood does the standard wish to reduce sTBI likelihood to, as 50 % is still high. Wu et al's (2021) prediction of 20 % sTBI for an elder population \approx 120 g, which will be slightly lower than the general adult populations tolerance [119], [125], [126], [146], though this may be too difficult for current headgear to achieve. Nevertheless, 250 g is still likely to encourage design innovation with the recommended loading conditions from Chapters 8 and 9, i.e. flat anvils, as the Defender Hybrid already exceeded this limit at 5 m/s crown impacts ($\Delta = +8$ g).

PAA: The 17 krad/s² 80 % AIS 4+ injury threshold from Wu et al (2021) was too high for the current impact setups; only side impacts exceeded this with the absence of a helmet in Chapter 8 (mean = 23 krad/s²). From the same IRC, a 20 % AIS 4+ injury risk occurs at 8 krad/s², which is also correlated with an 80 % risk of AIS 2+ injury [116]. The 6 krad/s² threshold in the NOCSAE ND002-17m21 American Football helmet standard is the equivalent of 50 % AIS 2+ injury likelihood [15], [116]. Should this be the threshold, the current Defender Hybrid helmets would have failed for crown (mean = $9.5 \pm 3.3 \text{ krad/s}^2$) and side ($9.5 \pm 0.6 \text{ krad/s}^2$) locations, front would have been within one standard deviation ($5.8 \pm 0.6 \text{ krad/s}^2$), and back would have passed ($2.8 \pm 0.9 \text{ krad/s}^2$).

Therefore, using limits of 250 g and 6 krad/s² for 120 J impact tests can encourage PO helmet innovation. It is also known that current headgear technology can achieve them, as they are already used in test standards [13], [15], [18], [118]. 250 g reduces likelihood of open and focal injuries to below a 50 % likelihood of severe injury [119], ideally this would be reduced if headgear can achieve it, for which further work could study. The latter reduces to below 50 % likelihood of mild diffuse injury, i.e. concussion, and roughly 10 % likelihood of AIS 4+, which seems a more appropriate severity prediction to use as a failure threshold [116], [126].

10.4.3 Limitations

This work depends on the accuracy of AIS thresholds identified in section 10.1.1 and their relevance for PO specific injury causes. IRC are based on a general population, including many automotive head acceleration events. Further work can explore IRC specific to blunt trauma impact events, for which Finite element

(FE) simulation would be well suited to measure tissue-level brain strains. Moreover, injury thresholds assume equal tolerance for all, whereas age, gender, and a history of previous injuries can affect tolerance [126], [235], [269], [329], [330].

This work highlights how the choice of metric drastically affects the predicted injury severity, Figure 10.1. PLA and PAA seem the superior measures from this small and specific dataset, yet this may differ at other impact velocities and locations. Also, they do not consider how brain injury is susceptible loading direction, although this could be compensated with different threshold limits per location [103], [108], [385]. It is recommended that this work be reassessed with rigid steel anvils, the velocity limits of 2.3 and 6.4 m/s identified in Chapter 8, inclusion of front/rear boss impacts, and a variety of headgear designs with different energy absorbing liners. A greater sample size is also required for improved statistical analyses, ideally with a new helmet per impact zone. This way, variance due to impact velocity and location can be sufficiently assessed using ANOVA and effect size statistics. The kinematics that contribute most variance in the dataset can be identified with Principal Component Analysis (PCA), which would further highlight the proxies that best capture impact mechanics [434]. PCA can also identify how many metrics are needed to capture most of the variance, ideally this will be a minimum of 2, one that best correlates with linear kinematic variance and another for angular.

As mentioned, DAMAGE increases indefinitely for an unconstrained headform. This metric would need a defined time constraint for use in a test standard such as PSDB 21/04. However, selection for this is a challenge because different helmet designs will result in different pulse durations. DAMAGE calculations were repeated with a 20 ms window (Δ = +8 ms), the minimum impact pulse tested by its authors, to highlight how this effects severity prediction. For this scenario, DAMAGE maximised the possible prediction of injury (= 1.0, Δ = 0.45) [158]. Therefore, this metric is not recommended for a drop test standard such as this until further study can advise the most appropriate time windows for realistic injury representation.

10.5 Chapter Conclusion

This chapter has demonstrated preliminary findings for thresholds to be used in the PO headgear standard. Findings highlighted that the choice of metric is crucial, as clear disparities for both mild (AIS 2) and severe (AIS 4) injury predictions were shown. HIP showed to be dominated by linear variation, suggesting a single metric for capturing both linear and angular components is not appropriate. At this stage it is recommended PLA is kept as the metric for assessing linear energy attenuation; PLA had the second greatest AIS 2+ injury prediction and third greatest for AIS 4+, while HIC predicted much milder injuries. Angular velocity-based metrics predicted a lower AIS 2+ injury likelihood more than any other score. DAMAGE had the greater injury predictions though PAA seems more suited for the standards because DAMAGE was overly sensitive to variation in impact location. Within-group variation was high for PAA (CV% = 21 %) unless radial impacts were removed (CV% = 7 %), suggesting it should only be used for oblique load conditions.

Thresholds of PLA = 250 g and PAA = 6 krad/s² correlate to a helmet with less than 50% risk of severe open and focal trauma (linear induced) and mild diffuse trauma (angular induced), respectively. These are within the current capabilities of headgear and also used in the current PO and American Football helmet standard. If possible, the PLA threshold would be lowered to reduce injury risk below 50 % severe, although it is unknown if this is feasible with current headgear technology. Further study is essential to validate these thresholds with the finalised test system, a rigid anvil, impact velocities up to minimum 6.4 m/s (Chapter 8), front/rear boss impact locations, and more headgear designs. Furthermore, more detailed statistical analyses can be made with more repeated measurements, data variation can be better understood with principal component analysis (PCA), and other metrics could be considered if they have corresponding injury risk functions.

11. Discussion

11.1 Introduction

This chapter summarises the contributions in knowledge for improving injury representation in Public Order helmet testing, developed from this project.

Implications, and limitations, of the work are discussed alongside areas identified for further improvement. The structure of the chapter follows that of the original research objectives, that were:

- Identification of events leading to head and brain injuries in Public Order conditions.
- Quantification of blunt trauma head impacts with Public Order representative loading conditions.
- 3. Demonstration for how Public Order representative impacts can be recreated with repeatable helmet impact test methodology.
- Recommendation for how the Public Order helmet test standard can improve situational injury representation and encourage more protective headgear.

This programme of work highlighted that Police Officers are a high-risk sub population for head injury [31], [35], [36], [37], [39], and that the nature of Public Order (PO) events can accentuate violence [32], [33], [34]. However, a review of literature showed there is little knowledge specific to Public Order head injury, despite a prevalence of similar studies for sports and automotive applications [9], [14], [15], [16], [17], [18], [19]. Moreover, the current PO helmet test standard lacks modern considerations for brain injury pathology, such as the effects from angular motion, which could lead to less effective headgear [41], [60], [72], [92]. A plan was devised to monitor head impact events with similar means to what is conducted in sport. However, in this study considerations had to be made due to complications with using instrumentation, and additional ethical concerns, for using live participants in monitoring injurious occurrences. Instead, events and weaponry were recorded from publicly available footage of violent PO events. This revealed the most notable causes of injury were projectile bricks/stones, wielded blunt weaponry, and falling from a height/horseback. Each of these were recreated

in laboratory conditions, with methodology designed to maintain high situational and biomechanical representation. The inbound velocities and headform kinematics were quantified to encapsulate the mechanics of each condition. These were then recreated with a mechanical experimental arrangement comparable to current headgear standards, i.e. a guided rail drop rig, to evaluate the differences between repeatable and representative methodologies. The findings showed that for a guided drop, cradling a headform with no anatomical constraint (i.e. neckform) was most representative of realistic headform mechanics. From this experimentation, recommendations have been made for representative impact velocities, surface properties, and loading angles to use in a revised test standard. These have been evaluated with current-issue PO headgear, which revealed that impact against a flat surface already exceed the current standard threshold, despite the impact being conducted at a lower velocity than currently specified. To assess appropriate thresholds for the standard, different kinematic-based injury metrics were reviewed and applied to the helmeted impact dataset. These showed the choice of metric greatly affects injury severity predictions, while preliminary findings showed peak linear and angular acceleration were the most suited for a standard. This body of research is therefore the first to have quantified PO specific head trauma. The recommendations made for greater representation of situational occurrences, if adopted in future standardised impact tests, would encourage helmet design innovations that hopefully further mitigate head injury risk in PO activity.

11.2 Review of Research Objectives

11.2.1 Identification of Injurious Events

A review of literature (Chapter 2) revealed a gap in knowledge for neurotraumatic injuries specific to PO conditions, despite well-established research within both sports and automotive applications [9], [14], [15], [16], [17], [18], [19]. Police Officers were found more likely to suffer head injuries than the general population, often attributable to strikes, falls, and physical assaults [31], [35], [36], [37], [39]. However, any published data did not differentiate between injurious occurrence attributable to routine police business or PO specific activity. The review also

highlighted that variation in loading conditions, i.e. impact location, angle, and energy, lead to different types of head injuries, thus situational representation is crucial when testing headgear performance [50], [64], [69], [72], [88], [89], [90]. Importantly, consideration for oblique forces and angular head motion is essential to ensure headgear mitigate diffuse injuries, such as concussion or Diffuse Axonal Injury (DAI) [61], [73], [74].

Video content analysis was employed as a non-invasive method to identify injurious events specific to PO activity (Chapter 3). From this projectile bricks/stones were identified as the most frequent threat, accounting for 37 % of all weapon events. This conclusion was further validated by conversation with the Metropolitan Police Physical Protection Group (MPPPG) who supported this element of work. Additionally, wielded objects such as flat-faced wooden beams (24.5%) and non-edged metallic poles (16.3%) were frequently observed.

Occurrences of officers being harassed while mounted on horseback were also notable. Falls from a height such as this seemed likely to cause severe injury thus were worth considering in this programme of work, although at the time it was unknown how the mechanics would compare to that of a projectile missile or wielded weapon.

The chaotic nature of PO activity makes it impossible to represent all injury causes in a single test method, though considerations of projectiles, wielded weapons, and falls capture a broad range of impact mechanisms. There were early indicators that these are not represented in the current PO headgear standard, PSDB 21/04 [13]. For example, flat surfaces, which are features of impact with bricks, wooden beams, and falls to the ground, are not included in the impact criteria, however, sharp and rounded anvils are. This may have detrimental consequences for headgear design; for example, studies using motorcycle helmets with a similar construction to the PO helmets found that impacts onto flat anvils resulted in greater headform kinematics than impacts onto curved or edged anvils [46].

The key findings from meeting objective 1 were:

- Prior knowledge for the causes of neurotrauma specific to PO activity was lacking.
- The chaotic nature of PO activity cannot be fully represented in a single condition, although the mechanisms of projectile bricks/stones, wielded wooden and metallic implements, and falls from horseback encompass a broad range of representative impact mechanics.
- It is essential the test standard encapsulates these in its test criteria to ensure headgear are effective in their application.

11.2.2 Quantification of Head Impact Loading Conditions

Video analysis of probable injurious occurrences in PO situations did not permit capture of kinematic data, such as is common in the sports industry [14], [141], [150], [255], [256]. This was due to the predominantly poor quality of video material in the public domain with no set reference frame for quantifying motion. Instead, head impact mechanics were quantified with experimental means considering impacts attributable to wielded implements (Chapter 4), falling from horseback (Chapter 5), and projectile bricks (Chapter 7). Experimentation was designed to be as situationally representative as possible. A full-body Hybrid III (HIII) Anthropometric Test Device (ATD) was used in the wielded implements, and horseback falls assessments. This was to represent biomechanical fidelity and ensure impacts occurred in similar manner to the in-situ conditions. In addition, impact was imparted with similar means to the in-situ conditions; the metallic and wooden implements were wielded by a human test subject and the ATD was prepositioned at horseback height before falling. It was not possible to project bricks at the ATD in a similar manner to the in-situ without significantly sacrificing accuracy and repeatability. Instead, a mechanical test system was developed to ensure brick impacts were repeatable (Chapter 6).

Headform biomechanics were quantified with linear and angular accelerations.

Peak linear accelerations (PLA) ranged from 126 to 771 g, with pulse durations between 0.75 and 2.79 ms. Mean linear accelerations for each of bricks, wielded

implements, and falling from horseback exceeded the Wayne State Tolerance Curve (WSTC), indicating a universally high-risk of life-threatening injury in PO activity [120]. The greatest PLA was due to projectile bricks thrown at 10.6 m/s. This velocity was calculated from literature on biomechanical throw physics [410] and confirmed with experimental recreation. Experimented head impacts due to bricks and metallic implements showed the greatest injury severity, i.e. PLA relative to the WSTC, occurred when impacting the crown, with mid-coronal side impacts as the second most severe. For wooden implements, these were the opposite (side then crown) and recreating falls from horseback only ever impacted the crown. These suggest the crown and side of the head are high-risk locations where protection is crucial. Impacting the crown is a current requirement in PSDB 21/04, however there is no criteria for mid-coronal side impacts. The inclusion of this location is further supported with angular acceleration measures as impacts from bricks, wooden beams, and metallic poles all displayed the greatest PAA when impacting the mid-coronal side of the headform.

Peak angular accelerations (PAA) ranged from 1.3 to 24.5 krad/s², with durations between 1.37 and 4.71 ms. Similar to PLA, the maximum PAA occurred for 10.6 m/s projectile bricks. The mean values of all experimented conditions were below the Hoshizaki et al (2017) threshold curve for mild traumatic brain injury (mTBI) [109]. At a glance, this suggests a low risk of angular induced neurotrauma, i.e. concussion. However, 24.5 krad/s² far exceeds the failure thresholds in other helmet test standards, such as ND002 (6 krad/s²) [15]. It also exceeds the 80 % mTBI threshold by Zhang et al (2004) (7.9 krad/s²), and the 80 % sTBI threshold for over 60's by Wu et al (2021) (17 krad/ s^2) [116], [126]. The discrepancy with the Hoshizaki curve is a result of the very short pulse durations (< 5 ms). Helmets aim to increase pulse duration when attenuating energy through internal structural deformations [10], [273]. However, this may not reduce PAA if the helmet lacks the appropriate protective components, for example 'MIPS' [287], [288], [289], [290]. Therefore, PSDB 21/04 requires an angular-based failure criterion to ensure headgear are not unwantedly facilitating angular induced neurotrauma and that appropriate protective features are incorporated in future helmet designs.

These findings underscore a requirement for PO helmets to mitigate both linear and angular force components, with linear presenting the greater risk of severe injury. The current PO headgear standard has no considerations for rotational induced injury, nor does it include oblique loads in its test criteria. Oblique impacts can be achieved with angled surfaces; impact angles were measured for wielded implement impacts with a mean of $56 \pm 14^{\circ}$ relative to the headform longitudinal axis. This does not include the crown impacts, which were radial loads $(92 \pm 2^{\circ})$ and are not suitable for angular injury assessment [332]. Impact angles were not recorded for horseback falls because they were always to the crown, similarly for bricks they were determined by the drop rig setup, thus not a reliable source for quantifying situationally representative angles.

The combination of projectile missiles, wielded implements, and falling from height in this programme of work have captured a broad range of loading mechanisms. For example, mean impact velocity for horseback falls was 4.45 ±0.27 m/s whereas the equivalent for wielded wooden implements was 17.1 ±1.2 m/s. Similarly, the full-body mass of the ATD was 78 kg, whereas the brick was 1.9 kg. Despite this, the pulse durations for all conditions were relatively similar to one another when compared to the grander scale of head impacts mechanics [109]. These can be represented with the same test setup and would require rigid impact anvils.

Many research studies include use of more compliant surfaces [15], [21], [336], [391] to produce longer duration impacts in aim to represent in-situ conditions. However, extending duration seems unnecessary for PO representation, as all experimented impacts were below 5 ms. Neckforms are also frequently used in head impact research, to represent biomechanical fidelity [231], [231], [232], [233], [234], [235], [376]. The effects of a neckform were evident during experimental recreations in this programme of work, including secondary loading pulses and directional variations in headform kinematics due to differing directional neck stiffnesses [185], [188], [215], [216], [218], [357]. The inaccuracies of currently available neckforms relative to human-like properties have resulted in debate for whether they are beneficial in head impact testing [221], [222], [223],

[224], [225]. However, work is ongoing to develop neckforms with more realistic stiffness properties, which may benefit future research and test standards [435].

The key findings from meeting objective 2 were:

- PLA ranged from 126 to 771 g with pulse durations between 0.75 and 2.79
 ms.
- PAA ranged from 1.3 to 24.5 krad/s² with pulse durations of 1.37 to 4.71 ms.
 The magnitude of angular acceleration was of significance to suggest chance of angular induced injury in PO activity.
- Pulse durations across all experimented scenarios were similar, despite differing velocity profiles, for example horseback falls at 4.45 ± 0.27 m/s compared to wielded wooden implements at 17.1 ± 1.2 m/s.
- Oblique loads are required for testing angular impact conditions, this can be setup with an angle ≈ 60° relative to the headform to represent wielded weapon impacts.
- Mid-coronal side impacts, which are not a requirement in the current standard, present a high-risk location for both PLA and PAA.

11.2.3 Recreation of Impacts with Repeatable Methodology

Any developed test standard requires a robust, but efficient and economical, methodology that affords repeatable experimentation. In this case, one that ensures repeatability of impact at specific helmet location with precise control over loading conditions. As discussed, the entirety of injurious conditions that can occur in PO activity are impossible to encapsulate with a singular test method. As such, some between group variability, i.e. deviation between different loading conditions, is less of a concern. What is essential is that a standardised method has high within-group repeatability as well as inter-rater repeatability, so the outcome (pass/fail) is reflective of the helmet and not the test system. Methods to achieve objective 2 of this research lacked the repeatability to be appropriate for standardised testing. Currently published helmet test standards favour guided drops as the optimum and most economical method to ensure repeatability,

including PSDB 21/04 [13], [18], [118]. The drop rig from Chapter 6 was used to evaluate how experimental setups compared to representative loading conditions (Chapter 8). These were repeated with current issue PO headgear, 'Defender Hybrid' [294], to assess helmet performance (Chapter 9) and evaluate metrics for injury severity predictions (Chapter 10). Key findings from objective 3 of this work included:

Impact mechanics:

• PLA and PAA should be measured independently for radial and oblique impacts, respectively. PLA followed a predictable power law relationship with velocity for radial impacts (A = 70.9, B = 1.29, RMSE = 0.18), while PAA displayed similar predictability for oblique impacts (A = 1.11, B = 1.34, RMSE = 0.08). The upper limit of representative PLA (range = 126 to 771 g) was achievable with 6.4 m/s radial impacts, whereas 8.4 m/s would be required for oblique. For reference, current non-automotive standardised drop tests do not exceed 7.0 m/s impacts [18], [239].

Neckform effects:

• A cradled setup without a neckform, similar to the current PSDB 21/04 protocol, is recommended for any future PO test standard [13]. Cradled impacts produced more defined loading pulses with less vibration. PAA was greater on average for cradled conditions (Δmean = +86.8 %), with 5 m/s trials near the upper limit for PO activity (limit = 1.3 to 24.5 krad/s², Δ = -1.3 krad/s²). PLA slightly decreased (Δmean = -15.9 %), though this can be offset with greater impact energy. When tested with a helmet, cradled impacts produced greater PLA (Δmin = +20.0 %) and PAA (Δmin = +24.8 %) than all other conditions. The use of a cradled headform is also less system specific, thus improving the inter-rater reliability of the standard.

Anvil properties:

 A flat-surfaced rigid anvil should be added to the test standard, for it improved representativity and showed greater severity. The choice of anvil affected peak kinematics (P < 0.01) although all anvils produced relatively similar pulse durations (Δ max \approx 0.2 ms). The flat wooden anvil produced greater PLA than the curved metallic (Δ = +71 g, P = 0.03), despite it being a more compliant material.

Helmet damage:

• Wear and damage after a single impact caused an increase in PLA for six of eight comparisons and increased PAA in five of eight. However, each of these only had two significant comparisons (P < 0.05) as standard deviations were large due to limited helmet availability. Damage was only visible on the helmet exterior after impacting the metallic cylindrical anvil, as it imparted greater pressure (smaller surface area) and the stress exceeded the failure properties of the glass fibre shell. On internal inspection, the impacts with a cylindrical anvil caused more plastic compression of the energy absorbing liner (EAL), although there was still visible plastic compression due to the flat, despite a seemingly intact shell. This highlights practical limitations for crash style EALs in PO activity, as it is challenging to meticulously ensure helmets are replaced, thus multi-impact systems may need to be incentivised.</p>

Injury metrics:

Initial findings suggest PLA and PAA are the most suited metrics for pass thresholds in the standard with current understanding. The choice of metric is crucial in any future developed standard. For example, 5 m/s helmeted impacts with the cradled setup showed large disparity across nine injury predictor metrics. HIP [153], which combines both linear and angular measures, was dominated by linear components and more ignorant of angular variation. HIC [152], PAV [69], BrIC [108], RVCI [144], and UBRIC [157], predicted relatively lower severity injuries than other metrics and would be easier for headgear to pass. DAMAGE [158] predicted high severity but the performance was largely dependent on impact location, something that has also been found in analogous research [154]. Thresholds of PLA = 250 g and PAA = 6 krad/s² correlate to 50% risk of severe open trauma

(linear induced) and mild diffuse trauma (angular induced), respectively. PLA measures with current PO helmets in this study exceed 250 g during flat anvil tests at only 5 m/s, roughly 42 J below the current standard requirement. If these thresholds were therefore adopted in future standards, they would force design innovation to ensure a helmet was compliant. These thresholds are already adopted in other helmet standards. It is therefore known that modern headgear systems are already able to achieve them [13], [15].

11.2.4 Recommendations for a Revised Public Order Helmet Test Standard The purpose of the energy attenuation test according to PSDB 21/04 is to 'ensure the helmet is capable of attenuating an impact caused by hand thrown and hand wielded blunt weapons' [13]. This work has confirmed the prevalence of such weapons, as well as identifying the additional risk of falling from horseback. Table 11.1 summarises the current protocol for PSDB 21/04, and the recommendations identified from this body of work for improving representativity of injurious conditions that may be anticipated in PO activity. While some existing procedures already align well with PO conditions, such as the use of an unconstrained cradled headform and 120 J maximum impact energy, there is clear need to introduce angular measures and more representative impact surfaces.

Table 11.1, Current energy attenuation test criteria in PSDB 21/04 and the recommended conditions for improving Public Order injury representation.

Criteria	Current	Recommendation
Drop System	Cradled with no	Cradled with no constraint.
	constraint.	
Headform	Tri-axial linear	Tri-axial linear & angular
Data Capture	acceleration.	acceleration.
		 Include tri-axial angular
		acceleration, either direct
		or indirect with angular
		velocity.
Impact	Front, Crown, Front	At least Front, & Crown, and
Locations	Left/Right, and Rear	extend to include mid-coronal
	Left/Right.	side impacts.ª
Impact Anvils	Sharp brick corner	Cylindrical weapon (FPE2/002) of
	(FPE2/001) and	rigid structure.
	cylindrical weapon	Include a flat surface of rigid
	(FPE2/002) of rigid	structure. ^b
Impost	structure. Normal to the direction of	Normal to the direction of fall
Impact Angles	fall (90°).	(90°).
Aligies	iaii (90).	Include 60° to the direction of
		fall.°
Unnar	120 J	120 J. ^d
Upper	120 J	120 J.
Impact		
Energy		
Upper Energy	250 g peak linear	250 g peak linear acceleration (90°
Failure	acceleration.	impact angles). ^e
Threshold		Include 6 krad/s² peak angular
		acceleration (60° impact angles).e

^a Front or Rear Left/Right (boss) impacts were not tested in this study.

^b Sharp anvils were not evaluated in this study, though may still benefit helmet assessment.

 $^{^{\}circ}$ 60° is representative, although 45-30° would produce greater angular force if needed.

^d The recommended velocity of 6.4 m/s is equal to 120 J, assuming mass = 5.8 kg (50^{th} male HIII headform and 1.25 kg helmet).

^e Recommended until metrics can be assessed with finalised test conditions.

Although this research recommends that the current upper impact energy is retained, it also now recommends inclusion of angular considerations. The current upper impact energy condition (120 J) is the same as that required to achieve the upper limit of PO representative headform acceleration (771 g with a bare headform). However, the inclusion of angular considerations, i.e. measurement of PAA and incorporation of oblique impacts, would extend the current criteria considered in helmet design. This will better ensure the mitigation of closed form neurotrauma, such as concussive injuries [61], [73], [74]. In addition, flat impact surfaces better scrutinise helmet protection, as the wider surface area causes less compression for stiffer EALs and reduces energy attenuation [271], [276], [277], [278]. Flat anvit impacts with current PO headgear already exceeded the PSDB 21/04 PLA threshold of 250 g and the recommended PAA threshold of 6 krad/s², despite a lower than maximum test velocity (Δ = -1.4 m/s, -48 J). This underscores their potential to better scrutinise headgear and encourage innovation in future helmet designs.

11.3 Contribution to Knowledge

11.3.1 Understanding PO Injury Risk

This programme of research is the first to directly quantify head injuries encountered in PO activity. It has been identified that despite the form of injurious occurrence, impact mechanics are comparable and could be appropriately mitigated with effective headgear. It has been shown how these injuries can be recreated with a repeatable impact system that is appropriate for standardised testing. Findings highlighted how failure to include consideration of flat impact surfaces with the test standard is a significant oversight. This is impact scenario is omitted despite being a consideration in almost all other helmet standards [18], [118], [170]. Despite impact against flat surfaces being common in PO threat conditions, such as bricks, wielded weapons, and falls, current headgear has been shown less effective at protecting against them. This highlights an urgent need in PO headgear development, as the available models designed to meet the current test standard, afford less than sufficient protection against many impact scenarios to be expected in PO activity.

The comparison of injury metrics underscores the importance of selecting metrics appropriate for that situation, rather than taking inspiration analogous situations. For example, head injury research in sports and for automotive applications has often shown the high predictive performance of angular velocity-based metrics, although for this application they predicted less severe injury than other metrics [69], [108], [129], [130], [131], [163]. If the current trend to adopt Injury Criteria within standards continues, there should be better legislation that advises their selection, thus better ensuring they are suited to the application.

11.3.2 Advising Helmet Test Methodology

The shared design process for a head impact drop rig can accelerate the construction of helmet test systems in both research and industrial test facilities. This work has both emphasised what should be followed as good practice in drop rig development, and also highlighted common oversights during system design [190]. In addition, it highlights the benefit for a singular system that permits rigid, representative, or unconstrained headform motion, while the final design meets the needs of all non-vehicular drop standards [18].

This work highlights the trade-offs between using a neckform or cradling the headform within drop test methods, which is a current topic of debate within head impact research [221], [222], [223], [224], [225]. Findings support the approach of European (CEN) standards that favour cradling headforms [18], showing realistic injury mechanics and greater PAA than equivalent neckform affixed conditions. However, the use of a neckform was found essential when quantifying representative in-field mechanics during earlier chapters, so to maintain a level of biomechanical fidelity. Therefore, while neckforms may not be optimal for standardised drop tests with PO headgear, they have value within injury analysis research.

11.3.3 Implications for Other Head Impact Applications

The focus on in-situ representativity, and the identification of oversights within the test standard, sets a precedent for other headgear applications. A number of other standards for the impact assessment of helmets used within the public sector (fire safety) and construction do not include flat surfaces in their impact criteria [392], [436]. This is despite other public sector occupations being increasingly exposed to similar in-field conditions to PO, and construction workers being at risk or being accidentally struck by similar materials encountered. Standards in these occupations primarily focus on the prevention of penetrative (open) injuries, though the increasing awareness of diffuse injuries may encourage use of flat surface assessments in future revisions. Likewise, the quantified mechanics when falling from height have broad applications across public health, and can advise the development of safety equipment, surfaces, and research for equine-related injury [380].

This projects use of non-invasive video content analysis and laboratory recreations offer practical solutions for monitoring head impacts in other settings where direct instrumentation is challenging, such as military, construction, and other emergency services. Similarly, some of these applications are seeing a lack in helmet innovation compared to the sports industry, which could benefit from improved monitoring of injury causes.

11.3.4 Enabling Computational Research Methods

Lastly, the experimental data from both the representative and repeatable impact methodologies can validate future computational modelling, including Finite Element (FE) models, permitting more detailed tissue-level injury analyses. For example, cumulative strain density measure (CSDM) and maximum principal strain (MPS) can be quantified [107], [108], and strains can be monitored in high-risk locations such as the corpus callosum [437]. These are not limited to PO-specific research, as the impact mechanics are relevant to broad injury causes across sports and public health. FE can also aid equipment designs; a model validated with the drop test study from this body of work can be used with

iterations of EAL structures to best advise performance before creating physical prototypes [438], [439]. Digital prototypes of energy-absorbing liners (EALs) can be iterated and optimised for drop test conditions, meaning their performance is expected before physical testing.

11.4 Limitations

11.4.1 Injury Prediction

The quantification of PO injury conditions with non-invasive means (Chapters 4 through 7) was necessary, although the resulting data is therefore an assumption of the in-vivo conditions. Efforts were made to maintain biomechanical fidelity, however the HIII ATD has limitations. The neckform has different directional stiffnesses to a human neck [185], [188], [215], [216], [217], [218], [219], [220] and the headform skin is a higher than realistic friction [211], [213], [440]. Improvements for these components are currently ongoing, which could benefit future work [118], [213], [435], [440]. Furthermore, the use of a single ATD lacks representation for those outside the 50th percentile male demographic. Research indicates that gender, age, and size affect injury susceptibility [126], [235], [269], [329], [330], thus this oversight may result in headgear that is not suitable for many officers.

Aspects of this work also rely on the accuracy of predictive statistics. For example, study of projectile bricks (Chapter 7) required calculating the upper bound velocity a human can throw, ≈ 13 m/s, which was not achievable with a guided drop. Instead, non-linear regression was used to estimate the resultant headform kinematics [105], [418]. As a result, the measured values of PLA and PAA were greater than those of other experimented conditions. This consequently influenced recommendations for the revision of the current test standard. However, these estimates represent worst-case conditions and scrutinise helmet designs under extreme scenarios. If predicted kinematics were not used then the recommended upper energy condition for the standard (120 J) would have been lower than it is already, which was never the intention of this work.

Severity predictions across different injury metrics (Chapter 10) rely on the accuracy of injury risk curves (IRC) from prior studies. Although selecting AIS 2 and 4 injuries is common practice [108], [116], [126], [161], [162], they are not ideal targets for injury prediction. They are based on a person's loss of consciousness (LOC), for which tolerance varies by individual, location, and the form of injury, and they do not consider that significant injury can occur without LOC [53], [60], [61], [62], [63].

11.4.2 Drop Test Conditions

The primary limitations of Chapters 8 through 10 are a result of limited helmet availability at the time of testing, combined with the limited duration of test window within the project. Consecutive delays in drop rig construction pushed testing to the summer of 2024, within six months of the completion date. At the time, it was not yet known cradled headforms were the most preferred setup, thus headgear were not prioritised for these conditions. Consequently, this limited the ability to investigate effects of more impact locations such as front/rear boss, test steeper impact angles (closer to 30°) for more severe angular conditions, and provide more comprehensive advice for injury thresholds with up to 7 m/s impact velocity.

Cradled tests were also constrained to a maximum velocity of 5 m/s due to the temporary cradle design; there were early signs of damage, for which a higher energy could have caused irreparable damage to the cradle. This prevented regression analyses for cradled setups meaning the neckform condition was used, which had a slightly greater PLA prediction (15 %). If resources had been available sooner, it would have been possible to refine the cradle system and source additional helmets for more extensive testing.

11.5 Future Research

This programme of work has identified several opportunities for further research to improve situational representation in Public Order (PO) helmet standards and benefit helmet design.

Firstly, a 250 g PLA threshold was proposed for assessing helmet performance, while future research should explore if a lower value is achievable with current headgear capabilities. This could be conducted by reviewing and testing helmets designed for similar or greater impact criteria, such as those for snow sports [239], equestrian [375], and automotive [441], [442] applications. For reference, 250 g correlates with a 50 % likelihood of severe neurotrauma [119], which is high for the minimum requirement of a helmet. However, no current guided drop standards have thresholds less than 250 g for similar impact criteria [18].

Expanding on current test conditions with cradled headforms is necessary to address the limitations highlighted in section 11.4.2. Future studies should explore impact velocities up to 7 m/s, which exceed 120 J (assuming a 4.5 kg headform) and surpasses current non-automotive drop test standards. Establishing regression for PLA and PAA over this range could advise how to achieve the upper limit that represents PO activity (771 g). Additional impact locations, including radial and oblique across back, crown, front, side, and front/rear boss areas, should also be investigated to finalise the best locations for the standard. In particular, comparisons should be made between front/rear boss impacts and mid-coronal side impacts to evaluate which can better scrutinise helmet performance by predicting greater accelerations. Furthermore, this programme of work has not considered environmental conditioning, for which the standard requires helmets be tested at -20° and +50°. Test conditions also need to be trialled at these temperatures before recommendations can be finalised.

FE analysis can provide a more comprehensive understanding of impact location, angle, and velocity effects. Although FE would be a valuable extension to this programme of work, the task is a significant undertaking for many institutions due to resource and expertise requirements and would require significant time allocation. Details for tissue strains can advise if different injury thresholds are appropriate and if different thresholds are needed per impact location. FE analysis

can explore cumulative injuries from repeated low-energy impacts, as well as simulate falling from a moving horse, which was too extreme for mechanical experiment. This approach can also extend beyond the 50th percentile male demographic, offering a more cost-effective solution than having multiple ATDs. Collectively, these provide enough detail to improve the representativity of the standard, as best as is possible with current technology.

Finally, further work should assess the predictive performance of injury metrics with cradled headform conditions at 7 m/s impact velocity, using the finalised test setup. Similar to Chapter 10, this should include relevant thresholds for mild and severe injury and evaluate the respective injury predictions. Principal Component Analysis (PCA) could identify the kinematic variables that contribute the most variance in the impact data, thus advising which metrics are best suited for the application. Ideally, these components would separately capture linear and angular variances to provide comprehensive assessment of injury risk. Ultimately, this work would inform how PO head injuries can be represented through headform kinematics, guiding which metrics are most appropriate for the test standard.

11.6 Project Conclusion

This programme of research successfully addressed the aim of improving injury representation within the Public Order helmet test standard, PSDB 21/04. The study identified Public Order specific injury risks, which included projectile bricks, wielded blunt weapons, and falling from horseback height as prominent threats. Experimental recreation of these scenarios produced representative head impact mechanics, which served as target for testing with more repeatable methodology. A test system was designed to accommodate a range of impact conditions and meet the requirements of all current non-vehicular standardised drop tests.

Cradling the headform, similar to CEN standards, achieved the most repeatable and representative head impact kinematics. Testing showed the current upper energy limit of 120 J produces headform kinematics comparable to the most severe in-field conditions. However, the omission of flat impact surfaces in the current standard disregards common in-field characteristics and is easy for helmets to pass. Current Public Order headgear struggled to meet both current and recommended thresholds when tested with flat surfaces, despite greatly reduced energy levels, which highlights the need for design improvement. Key recommendations for the Public Order test standard included oblique loading criteria and angular acceleration measurements, which is in-line with modern strategies to better assess helmet efficacy in mitigating closed-form neurotraumatic injuries.

Overall, this research underscores the severity of head injury risk in Public Order activity and provides the means to encourage effective helmet innovation. The implications of this provide a benchmark for improving helmet quality beyond Public Order, with highlighted potential for construction, fire safety, and military applications.

References

- [1] '16,000 police officers and "swift justice": How to stop a riot', *The Telegraph*, United Kingdom, 2024. Accessed: Jan. 15, 2025. [Online]. Available: https://www.telegraph.co.uk/news/2024/08/05/how-to-stop-a-riot-southport-2024-london-2011/
- [2] Michael Lupton Associates (MLA) Ltd., Unit 2 & 2A Allerthorpe Business Park Pocklington YO42 1NS.
- [3] L. Holm, J. D. Cassidy, L. J. Carroll, and J. Borg, 'Summary of the WHO Collaborating Centre for Neurotrauma Task Force on Mild Traumatic Brain Injury', *Journal of Rehabilitation Medicine*, vol. 37, no. 3. pp. 137–141, 2005. doi: 10.1080/16501970510027321.
- [4] A. A. Hyder, C. A. Wunderlich, P. Puvanachandra, G. Gururaj, and O. C. Kobusingye, 'The impact of traumatic brain injuries: A global perspective', *NeuroRehabilitation*, vol. 22, no. 5. IOS Press, pp. 341–353, 2007. doi: 10.3233/nre-2007-22502.
- [5] M. C. Dewan et al., 'Estimating the global incidence of traumatic brain injury', Journal of Neurosurgery, vol. 130, no. 4, pp. 1080–1097, Apr. 2018, doi: 10.3171/2017.10.JNS17352.
- [6] J. Schulman, J. Sacks, and G. Provenzano, 'State level estimates of the incidence and economic burden of head injuries stemming from non-universal use of bicycle helmets', *Injury Prevention*, vol. 8, no. 1, pp. 47–52, Mar. 2002, doi: 10.1136/ip.8.1.47.
- [7] I. Humphreys, R. L. Wood, C. J. Phillips, and S. Macey, 'The costs of traumatic brain injury: a literature review', *ClinicoEconomics and Outcomes Research*, vol. 5, pp. 281–287, Jun. 2013, doi: 10.2147/CEOR.S44625.
- [8] J. A. Newman, 'The Biomechanics of Head Trauma and the Development of the Modern Helmet. How Far Have We Really Come?', in *IRCOBI Conference*, Prague (Czech Republic), Sep. 2005.
- [9] T. B. Hoshizaki and S. E. Brien, 'The science and design of head protection in sport', Neurosurgery, vol. 55, no. 4, pp. 956–966; discussion 966-967, 2004, doi: 10.1227/01.neu.0000137275.50246.0b.
- [10]T. B. Hoshizaki, A. Post, R. A. Oeur, and S. E. Brien, 'Current and future concepts in helmet and sports injury prevention', *Neurosurgery*, vol. 75, no. 4, pp. 136–148, 2014, doi: 10.1227/NEU.00000000000000496.
- [11] A. Post, C. Karton, T. B. Hoshizaki, and M. D. Gilchrist, 'Analysis of the protective capacity of ice hockey helmets in a concussion injury reconstruction', in *IRCOBI Conference*, 2014, pp. 72–80.

- [12] A. Bartsch, E. Benzel, V. Miele, and V. Prakash, 'Impact test comparisons of 20th and 21st century American football helmets', *Journal of Neurosurgery*, vol. 116, pp. 222–233, 2012, doi: 10.3171/2011.9.jns111059.
- [13] Home Office Police Scientific Development Branch, 'PSDB 21/04 Protective Headwear Standard for UK Police'. 2004.
- [14] E. J. Pellman, D. C. Viano, A. M. Tucker, I. R. Casson, and J. F. Waeckerle, 'Concussion in Professional Football: Reconstruction of Game Impacts and Injuries.', Neurosurgery, vol. 53, no. 4, pp. 799–814, Oct. 2003, doi: 10.1227/01.NEU.0000083559.68424.3F.
- [15] NOCSAE, Standard Performance Specification for Newly Manufactured Football Helmets, ND002-17m21, 2017.
- [16]T. A. Connor *et al.*, 'Current Standards for Sports and Automotive Helmets : A Review', *Ref. Ares 3151745*, no. 2016, pp. 1–42, 2016.
- [17]T. A. Connor, J. M. Clark, P. Brama, M. Stewart, A. Ní Annaidh, and M. D. Gilchrist, 'An Evidence Basis for Future Equestrian Helmet Lateral Crush Certification Tests', Applied Sciences, vol. 10, no. 7, Jan. 2020, doi: 10.3390/app10072623.
- [18]T. Whyte *et al.*, 'A Review of Impact Testing Methods for Headgear in Sports:

 Considerations for Improved Prevention of Head Injury Through Research and

 Standards', *Journal of Biomechanical Engineering*, vol. 141, no. 7, p. 070803, Jul. 2019,

 doi: 10.1115/1.4043140.
- [19] BS EN 1384:2023 Helmets for equestrian activities, 2023.
- [20] D. Haid *et al.*, 'Mechanical metamaterials for sports helmets: structural mechanics, design optimisation, and performance', *Smart Mater. Struct.*, vol. 32, no. 11, p. 113001, Oct. 2023, doi: 10.1088/1361-665X/acfddf.
- [21] D. L. Yount *et al.*, 'Performance of a novel football helmet technology on head impact kinematics', *Sports Eng*, vol. 24, no. 1, p. 18, Aug. 2021, doi: 10.1007/s12283-021-00355-0.
- [22] National Football League (NFL), '2020 HELMET LABORATORY TESTING

 PERFORMANCE RESULTS', 2020. Accessed: Aug 19, 2023. [Online]. Available:

 https://static.www.nfl.com/image/upload/v1601629905/league/awkzblxyzlijm4zud1rp
 .pdf
- [23] National Football League (NFL), '2022 HELMET LABORATORY TESTING

 PERFORMANCE RESULTS', 2022. Accessed: Aug 19, 2023. [Online]. Available:

 https://static.www.nfl.com/image/upload/v1648065981/league/ritzpbkrssxrmdsdcwp

 1.pdf

- [24] National Football League (NFL), '2024 HELMET LABORATORY TESTING PERFORMANCE RESULTS', 2024. Accessed: May 24, 2024. [Online]. Available: https://static.www.nfl.com/image/upload/v1712665965/league/yt3aubz9cjxmg3seascg.pdf
- [25] J. T. Gwin, J. J. Chu, S. G. Diamond, P. D. Halstead, J. J. Crisco, and R. M. Greenwald, 'An Investigation of the NOCSAE Linear Impactor Test Method Based on In Vivo Measures of Head Impact Acceleration in American Football', *Journal of Biomechanical Engineering*, vol. 132, no. 1, p. 011006, Sep. 2010, doi: 10.1115/1.4000249.
- [26] S. Duma, M. Goforth, P. G. Brolinson, R. Greenwald, S. Manoogian, and D. McNeely, 'Analysis of Linear Head Accelerations from Collegiate Football Impacts', *Current Sports Medicine Reports*, 2013, doi: 10.1097/01.csmr.0000306515.87053.fa.
- [27] A. Post, A. Oeur, and M. D. Gilchrist, 'The influence of centric and non-centric impacts to American football helmets on the correlation between commonly used metrics in brain injury research', in *IRCOBI Conference*, 2012, pp. 419–429.
- [28] S. Rowson, G. Brolinson, M. Goforth, D. Dietter, and S. Duma, 'Linear and angular head acceleration measurements in collegiate football', *Journal of Biomechanical Engineering*, vol. 131, no. 6, Jun. 2009, doi: 10.1115/1.3130454.
- [29]S. Rowson *et al.*, 'Rotational head kinematics in football impacts: An injury risk function for concussion', *Annals of Biomedical Engineering*, vol. 40, no. 1, Jan. 2012, doi: 10.1007/s10439-011-0392-4.
- [30] D. F. Meaney, B. Morrison, and C. D. Bass, 'The mechanics of traumatic brain injury: A review of what we know and what we need to know for reducing its societal burden', *Journal of Biomechanical Engineering*, vol. 136, no. 2. Feb. 2014. doi: 10.1115/1.4026364.
- [31] C. K. Crifasi, K. M. Pollack, and D. W. Webster, 'Assaults against U.S. law enforcement officers in the line-of-duty: situational context and predictors of lethality', *Injury Epidemiology*, vol. 3, no. 1, Dec. 2016, doi: 10.1186/s40621-016-0094-3.
- [32] Martin, E. D., 'The Behaviour of Crowds', London: Ernest Benn, 1920.
- [33] S. Reicher, C. Stott, J. Drury, O. Adang, P. Cronin, and A. Livingstone, 'Knowledge-Based Public Order Policing: Principles and Practice', *Policing*, vol. 1, no. 4, pp. 403–415, Nov. 2007, doi: 10.1093/police/pam067.
- [34] J. C. Turner, *Towards a cognitive redefinition of the social group*. in Rediscovering social identity. New York, NY, US: Psychology Press, 2010, p. 234.
- [35] Home Office, 'Statistics on the number of police officers assaulted in 2019 to 2020, England and Wales.', 2020. Accessed: Dec. 16, 2021. [Online]. Available:

- https://assets.publishing.service.gov.uk/media/5f204c60d3bf7f1b164fe006/police-officers-assaulted-201920-england-wales.pdf
- [36] B. Brown, 'Assaults on Police Officers: An examination of the circumstances in which such incidents occur'. Home Office Police Dept, 1994.
- [37] N. I. J. Smith, S. Gilmour, L. Prescott-Mayling, L. Hogarth, J. D. Corrigan, and W. H. Williams, 'A pilot study of brain injury in police officers: A source of mental health problems?', *Journal of Psychiatric and Mental Health Nursing*, pp. 1–13, Jul. 2020, doi: 10.1111/jpm.12676.
- [38] R. B. Frost, T. J. Farrer, M. Primosch, and D. W. Hedges, 'Prevalence of Traumatic Brain Injury in the General Adult Population: A Meta-Analysis', *Neuroepidemiology*, vol. 40, no. 3, pp. 154–159, 2013, doi: 10.1159/000343275.
- [39] R. Orr, E. F. D. Canetti, R. Pope, R. G. Lockie, J. J. Dawes, and B. Schram, 'Characterization of Injuries Suffered by Mounted and Non-Mounted Police Officers', *International Journal of Environmental Research and Public Health*, vol. 20, no. 2, Jan. 2023, doi: 10.3390/ijerph20021144.
- [40] S. Aghili-Mehrizi, E. Williams, S. Yan, M. Willman, J. Willman, and B. Lucke-Wold, 'Secondary Mechanisms of Neurotrauma: A Closer Look at the Evidence', *Diseases*, vol. 10, no. 2, p. 30, May 2022, doi: 10.3390/diseases10020030.
- [41]S. Kleiven, 'Finite element modeling of the human head', KTH, Sweden, 2002. [Online].

 Available: https://www.diva-portal.org/smash/record.jsf?pid=diva2:9137
- [42] D. K. Menon, K. Schwab, D. W. Wright, A. I. Maas, and Demographics and Clinical Assessment Working Group of the International and Interagency Initiative toward Common Data Elements for Research on Traumatic Brain Injury and Psychological Health, 'Position statement: definition of traumatic brain injury', *Arch Phys Med Rehabil*, vol. 91, no. 11, pp. 1637–1640, Nov. 2010, doi: 10.1016/j.apmr.2010.05.017.
- [43] W.-T. W. Chang and N. Badjatia, 'Neurotrauma', *Emerg Med Clin North Am*, vol. 32, no.4, pp. 889–905, Nov. 2014, doi: 10.1016/j.emc.2014.07.008.
- [44] D. Muresanu, S.-A. Dobran, and D. Cretoiu, 'The birth of neurotrauma: a historical perspective from the Academy of Multidisciplinary Neurotraumatology (AMN)', *J Med Life*, vol. 14, no. 6, pp. 737–739, 2021, doi: 10.25122/jml-2021-1006.
- [45] J. W. Bales, R. H. Bonow, and R. G. Ellenbogen, 'Closed Head Injury', in *Principles of Neurological Surgery*, Elsevier, 2018, pp. 366-389.e4. doi: 10.1016/B978-0-323-43140-8.00025-1.
- [46] G. Zheng, X. Zhang, S. Li, T. Pang, Q. Li, and G. Sun, 'Correlation between kinematics and biomechanics of helmeted head under different impact conditions', *Composite Structures*, vol. 291, Jul. 2022, doi: 10.1016/j.compstruct.2022.115514.

- [47] A. Post and T. B. Hoshizaki, 'Mechanisms of brain impact injuries and their prediction: A review', *Trauma*, vol. 14, no. 4. pp. 327–349, 2012. doi: 10.1177/1460408612446573.
- [48] S. G. Piland, T. E. Gould, M. Jesunathadas, J. S. Wiggins, O. McNair, and S. V. Caswell, 'Protective helmets in sports', in *Materials in Sports Equipment*, Elsevier, 2019, pp. 71–121. doi: 10.1016/B978-0-08-102582-6.00003-4.
- [49] E. S. Gurdjian, V. R. Hodgson, W. G. Hardy, L. M. Patrick, and H. R. Lissner, 'Evaluation of the Protective Characteristics of Helmets in Sports', *Journal of Trauma and Acute Care Surgery*, vol. 4, no. 3, p. 309, May 1964.
- [50] C. E. Baker, X. Yu, S. Patel, and M. Ghajari, 'A Review of Cyclist Head Injury, Impact Characteristics and the Implications for Helmet Assessment Methods', *Ann Biomed Eng*, vol. 51, no. 5, pp. 875–904, May 2023, doi: 10.1007/s10439-023-03148-7.
- [51] J. Feler, 'Shifts In Micromobility-Related Trauma In The Age Of Vehicle Sharing: The Epidemiology Of Head Injury', Yale Medicine Thesis Digital Library, Jan. 2020, [Online]. Available: https://elischolar.library.yale.edu/ymtdl/3898
- [52] N. Dodds *et al.*, 'Evaluating the impact of cycle helmet use on severe traumatic brain injury and death in a national cohort of over 11000 pedal cyclists: a retrospective study from the NHS England Trauma Audit and Research Network dataset', *BMJ Open*, vol. 9, no. 9, p. e027845, Sep. 2019, doi: 10.1136/bmjopen-2018-027845.
- [53] S. Kleiven, 'Why Most Traumatic Brain Injuries are Not Caused by Linear Acceleration but Skull Fractures are', *Frontiers in Bioengineering and Biotechnology*, vol. 1, p. 15, 2013, doi: 10.3389/fbioe.2013.00015.
- [54] K. Coburn, 'Traumatic Brain Injury: The Silent Epidemic', *AACN Advanced Critical Care*, vol. 3, no. 1, pp. 9–18, Feb. 1992, doi: 10.4037/15597768-1992-1002.
- [55] S. Fleminger and J. Ponsford, 'Long Term Outcome After Traumatic Brain Injury', *BMJ*, vol. 331, pp. 1419–1420, 2005.
- [56] C. S. Sahler and B. D. Greenwald, 'Traumatic Brain Injury in Sports: A Review', Rehabilitation Research and Practice, vol. 2012, no. 1, p. 659652, 2012, doi: 10.1155/2012/659652.
- [57] M. Faul, M. M. Wald, L. Xu, and V. G. Coronado, 'Traumatic Brain Injury in THE UNITED STATES Emergency Department Visits, Hospitalizations and Deaths 2002-2006'. 2010. [Online]. Available: www.cdc.gov/TraumaticBrainInjury
- [58] I. R. Casson, D. C. Viano, J. W. Powell, and E. J. Pellman, 'Twelve years of national football league concussion data.', *Sports health*, vol. 2, no. 6, pp. 471–83, Nov. 2010, doi: 10.1177/1941738110383963.
- [59] R. J. Rona *et al.*, 'Mild traumatic brain injury in UK military personnel returning from Afghanistan and Iraq: Cohort and cross-sectional analyses', *Journal of Head Trauma*

- Rehabilitation, vol. 27, no. 1, pp. 33–44, Jan. 2012, doi: 10.1097/HTR.0b013e318212f814.
- [60] J. E. Bailes and R. C. Cantu, 'Head Injury in Athletes', *Neurosurgery*, vol. 48, no. 1, Jan. 2001.
- [61]T. A. Gennarelli, L. E. Thibault, J. H. Adams, D. I. Graham, C. J. Thompson, and R. P. Marcincin, 'Diffuse axonal injury and traumatic coma in the primate', *Annals of Neurology*, vol. 12, no. 6, pp. 564–574, 1982, doi: 10.1002/ana.410120611.
- [62]T. A. Gennarelli and E. Wodzin, 'AIS 2005: A contemporary injury scale', *Injury*, vol. 37, no. 12, pp. 1083–1091, Dec. 2006, doi: 10.1016/j.injury.2006.07.009.
- [63] SabinaJ. Strich, 'Shearing of Nerve Fibres As A Cause Of Brain Damage Due To Head Injury: A Pathological Study of Twenty Cases', *The Lancet*, vol. 278, no. 7200, pp. 443–448, Aug. 1961, doi: 10.1016/S0140-6736(61)92426-6.
- [64] R. J. H. Cloots, J. A. W. van Dommelen, T. Nyberg, S. Kleiven, and M. G. D. Geers, 'Micromechanics of diffuse axonal injury: influence of axonal orientation and anisotropy', *Biomech Model Mechanobiol*, vol. 10, no. 3, pp. 413–422, Jun. 2011, doi: 10.1007/s10237-010-0243-5.
- [65] J. Zhang, N. Yoganandan, F. A. Pintar, and T. A. Gennarelli, 'Role of translational and rotational accelerations on brain strain in lateral head impact', *Biomed Sci Instrum*, vol. 42, pp. 501–506, Jan. 2006.
- [66] N. Yoganandan, J. Li, J. Zhang, F. A. Pintar, and T. A. Gennarelli, 'Influence of angular acceleration-deceleration pulse shapes on regional brain strains', *Journal of Biomechanics*, vol. 41, no. 10, pp. 2253–2262, Jul. 2008, doi: 10.1016/j.jbiomech.2008.04.019.
- [67] R. J. Fijalkowski, N. Yoganandan, J. Zhang, and F. A. Pintar, 'A Finite Element Model of Region-Specific Response for Mild Diffuse Brain Injury', presented at the 53rd Stapp Car Crash Conference, Nov. 2009. doi: 10.4271/2009-22-0007.
- [68] D. Bradshaw and C. Morfey, *Pressure And Shear Responses In Brain Injury Models*, 2001.
- [69] A. H. Holbourn, 'Mechanics of Head Injuries', The Lancet, vol. 242, no. 6267, pp. 438–441, 1943, doi: 10.1016/S0140-6736(00)87453-X.
- [70] A. McIntosh et al., 'Sports helmets now and in the future', British Journal of Sports Medicine, vol. 45, no. 16, pp. 1258–1265, 2011, doi: 10.1136/bjsports-2011-090509.
- [71] N. Bourdet, C. Deck, T. Serre, C. Perrin, M. Llari, and R. Willinger, 'In-depth real-world bicycle accident reconstructions', *International Journal of Crashworthiness*, vol. 19, no. 3, pp. 222–232, May 2014, doi: 10.1080/13588265.2013.805293.

- [72] A. Post and T. B. Hoshizaki, 'Mechanisms of brain impact injuries and their prediction: A review', *Trauma*, vol. 14, no. 4, pp. 327–349, Oct. 2012, doi: 10.1177/1460408612446573.
- [73] J. H. Adams, D. I. Graham, and T. A. Gennarelli, 'Head Injury in Man and Experimental Animals: Neuropathology', in *Trauma and Regeneration*, J. H. Adams, Ed., Vienna: Springer, 1983, pp. 15–30. doi: 10.1007/978-3-7091-4147-2_2.
- [74]T. Gennarelli, L. Thibault, and A. Omaya, 'Comparison of translational and rotational accelerations in experimental cerebral concussion.', in *15th Stapp Car Crash Conference*, New York, USA., 1971.
- [75] NOCSAE, Standard Performance Specification for Newly Manufactured Lacrosse Helmets with Faceguard, ND 041-15m18, 2015.
- [76] NOCSAE, Standard Performance Specification for Newly Manufactured Baseball/Softball Batter's Helmets, ND 022-21m24, 2022.
- [77] NOCSAE, Standard Performance Specification for Newly Manufactured Polo Helmets, ND 050–11m19, 2011.
- [78] K. Bian and H. Mao, 'Mechanisms and variances of rotation-induced brain injury: a parametric investigation between head kinematics and brain strain', *Biomechanics and Modeling in Mechanobiology*, vol. 19, no. 6, pp. 2323–2341, Dec. 2020, doi: 10.1007/s10237-020-01341-4.
- [79] A. Post, T. B. Hoshizaki, M. D. Gilchrist, and M. D. Cusimano, 'Peak linear and rotational acceleration magnitude and duration effects on maximum principal strain in the corpus callosum for sport impacts', *Journal of Biomechanics*, vol. 61, pp. 183–192, Aug. 2017, doi: 10.1016/j.jbiomech.2017.07.013.
- [80] B. M. Boggess and G. G. Foreman, 'Mass-Based Considerations for Head Injury Protection Development', Honda R&D Americas, Inc. Paper No. 07-0154, 2005.
- [81] D. J. Searson, 'The influence of test conditions on the results of pedestrian headform impact tests.', 2012. Available: https://www.semanticscholar.org/paper/Theinfluence-of-test-conditions-on-the-results-of-Searson/11358b5c6d2656b83195fe54d819bdbbe5d8cda2
- [82] G. Tierney et al., 'Head Exposure to Acceleration Database in Sport (HEADSport): a kinematic signal processing method to enable instrumented mouthguard (iMG) field-based inter-study comparisons', *BMJ Open Sport Exerc Med*, vol. 10, no. 1, Jan. 2024, doi: 10.1136/bmjsem-2023-001758.
- [83] R. Cross, 'Standing, walking, running, and jumping on a force plate', *American Journal of Physics*, vol. 67, no. 4, pp. 304–309, Apr. 1999, doi: 10.1119/1.19253.

- [84] F. A. Bandak, G. Ling, A. Bandak, and N. C. De Lanerolle, 'Injury biomechanics, neuropathology, and simplified physics of explosive blast and impact mild traumatic brain injury', *Handb Clin Neurol*, vol. 127, pp. 89–104, 2015, doi: 10.1016/B978-0-444-52892-6.00006-4.
- [85] F. A. Bandak, M. J. Vander Vorst, L. M. Stuhmiller, P. F. Mlakar, W. E. Chilton, and J. H. Stuhmiller, 'An imaging-based computational and experimental study of skull fracture: finite element model development', *J Neurotrauma*, vol. 12, no. 4, pp. 679–688, Aug. 1995, doi: 10.1089/neu.1995.12.679.
- [86] J. Ruan and P. Prasad, 'The effects of skull thickness variations on human head dynamic impact responses', *Stapp Car Crash J*, vol. 45, pp. 395–414, Nov. 2001, doi: 10.4271/2001-22-0018.
- [87] A. Hamel, M. Llari, M.-D. Piercecchi-Marti, P. Adalian, G. Leonetti, and L. Thollon, 'Effects of fall conditions and biological variability on the mechanism of skull fractures caused by falls', *Int J Legal Med*, vol. 127, no. 1, pp. 111–118, Jan. 2013, doi: 10.1007/s00414-011-0627-9.
- [88] E. S. Gurdjian, 'Acute Head Injuries', *The Journal of Trauma: Injury, Infection, and Critical Care*, vol. 18, no. 9, pp. 684–670, 1968.
- [89] E. S. Gurdjian, 'Re-evaluation of the biomechanics of blunt impact injury of the head', Surgery, Gynecology and Obstetrics, vol. 140, no. 6, pp. 845–850, 1975.
- [90] E. S. Gurdjian, H. R. Lissner, V. R. Hodgson, and L. M. Patrick, 'Mechanism of head injury', Clin Neurosurg, vol. 12, pp. 112–128, 1964, doi: 10.1093/neurosurgery/12.cn_suppl_1.112.
- [91] S. Kleiven and W. N. Hardy, 'Correlation of an FE Model of the Human Head with Local Brain Motion--Consequences for Injury Prediction', *Stapp Car Crash J*, vol. 46, pp. 123–144, Nov. 2002, doi: 10.4271/2002-22-0007.
- [92] A. I. King, L. Zhang, W. Hardy, and D. C. Viano, 'Is Head Injury Caused by Linear or Angular Acceleration?', in *IRCOBI Conference Lisbon (Portugal)*, 2003.
- [93] S. Kleiven, 'Evaluation of head injury criteria using a finite element model validated against experiments on localized brain motion, intracerebral acceleration, and intracranial pressure', *International Journal of Crashworthiness*, vol. 11, no. 1, pp. 65–79, Jan. 2006, doi: 10.1533/ijcr.2005.0384.
- [94] S. Kleiven, 'Influence of impact direction on the human head in prediction of subdural hematoma', *J Neurotrauma*, vol. 20, no. 4, pp. 365–379, Apr. 2003, doi: 10.1089/089771503765172327.
- [95] D. Denny-Brown and W. R. Russell, 'Experimental Cerebral Concussion', *Brain*, vol. 64, no. 2–3, pp. 93–164, Sep. 1941, doi: 10.1093/brain/64.2-3.93.

- [96] L. M. Thomas, V. L. Roberts, and E. S. Gurdjian, 'Impact-induced pressure gradients along three orthogonal axes in the human skull.', *Journal of neurosurgery*, vol. 26, no. 3, pp. 316–321, Mar. 1966, doi: 10.3171/jns.1967.26.3.0316.
- [97] G. S. Nusholtz, P. S. Kaiker, and W. S. Gould, 'Two factors critical in the pressure response of the impacted head', *Aviat Space Environ Med*, vol. 58, no. 12, pp. 1157–1164, Dec. 1987.
- [98] E. S. Gurdjian, V. L. Roberts, and L. M. Thomas, 'Tolerance Curves of Acceleration and Intracranial Pressure and Protective Index in Experimental Head Injury', *Journal of Trauma and Acute Care Surgery*, vol. 6, no. 5, p. 600, Sep. 1966.
- [99] B. F. Haddad, H. R. Lissner, J. E. Webster, and E. S. Gurdjian, 'Experimental concussion; relation to acceleration to physiologic effect', *Neurology*, vol. 5, no. 11, pp. 798–800, Nov. 1955, doi: 10.1212/wnl.5.11.798.
- [100] F. Unterharnscheidt and L. S. Higgins, 'Neuropathologic effects of translational and rotational acceleration of the head in animal experiments.', in *In: Walker AE, Caveness WF and Critchley M (eds) The Late Effects of Head Injury.*, Illinois: Springfield, 1969, pp. 158–167.
- [101] F. Unterharnscheidt and K. Sellier, 'Closed brain injuries: mechanics and pathomorphology.', in *In: Caveness WF and Walker AE (eds)*, Philadelphia, Lippincott., 1966, pp. 321–341.
- [102] A. K. Ommaya and T. A. Gennarelli, 'Cerebral concussion and traumatic unconsciousness. Correlation of experimental and clinical observations of blunt head injuries', *Brain*, vol. 97, no. 4, pp. 633–654, Dec. 1974, doi: 10.1093/brain/97.1.633.
- [103] V. R. Hodgson, L. M. Thomas, and T. B. Khalil, 'The Role of Impact Location in Reversible Cerebral Concussion', presented at the 27th Stapp Car Crash Conference with IRCOBI and Child Injury and Restraint Conference with IRCOBI (1983), Oct. 1983, p. 831618. doi: 10.4271/831618.
- [104] W. N. Hardy et al., 'A Study of the Response of the Human Cadaver Head to Impact', Stapp Car Crash J, vol. 51, pp. 17–80, Oct. 2007.
- [105] D. Stitt, N. Kabaliuk, K. Alexander, and N. Draper, 'Drop Test Kinematics Using Varied Impact Surfaces and Head/Neck Configurations for Rugby Headgear Testing', *Annals of Biomedical Engineering*, vol. 50, no. 11, pp. 1633–1647, Nov. 2022, doi: 10.1007/s10439-022-03045-5.
- [106] S. Meng, M. Fahlstedt, and P. Halldin, 'The Effect of Impact Velocity Angle on Helmeted Head Impact Severity: A Rationale for Motorcycle Helmet Impact Test Design', 2018.

- [107] E. G. Takhounts *et al.*, 'Investigation of Traumatic Brain Injuries Using the Next Generation of Simulated Injury Monitor (SIMon) Finite Element Head Model', in *SAE Technical Papers*, SAE International, Nov. 2008. doi: 10.4271/2008-22-0001.
- [108] E. G. Takhounts, M. J. Craig, K. Moorhouse, J. McFadden, and V. Hasija, 'Development of Brain Injury Criteria (BrIC)', Stapp Car Crash, vol. 57, pp. 243–266, 2013, doi: 10.4271/2013-22-0010.
- [109] T. B. Hoshizaki *et al.*, 'The development of a threshold curve for the understanding of concussion in sport', *Trauma*, vol. 19, no. 3, pp. 196–206, Jul. 2017, doi: 10.1177/1460408616676503.
- [110] S. Edberg, J. Rieker, and A. Angrist, 'Study of impact pressure and acceleration in plastic skull models', *Lab Invest*, vol. 12, pp. 1305–1311, Dec. 1963.
- [111] R. Lindenberg and E. Freytag, 'The mechanism of cerebral contusions. A pathologic-anatomic study', *Arch Pathol*, vol. 69, pp. 440–469, Apr. 1960.
- [112] V. H. Kenner and W. Goldsmith, 'Dynamic loading of a fluid-filled spherical shell', *International Journal of Mechanical Sciences*, vol. 14, no. 9, pp. 557–568, Sep. 1972, doi: 10.1016/0020-7403(72)90056-2.
- [113] J. A. Kopecky and E. A. Ripperger, 'Closed brain injuries: An engineering analysis', Journal of Biomechanics, vol. 2, no. 1, pp. 29–34, Mar. 1969, doi: 10.1016/0021-9290(69)90039-6.
- [114] P. Prasad and H. J. Mertz, 'The Position of the United States Delegation to the ISO Working Group 6 on the Use of HIC in the Automotive Environment', *Transactions*, vol. 94. pp. 106–116, 1985.
- [115] H. Mertz, P. Prasad, and G. Nusholtz, 'Head injury risk assessment for forehead impacts', *Journal of Passenger Cars*, vol. 105, no. 6, pp. 26–46, 1996.
- [116] L. Zhang, K. H. Yang, and A. I. King, 'A Proposed Injury Threshold for Mild Traumatic Brain Injury', *Journal of Biomechanical Engineering*, vol. 126, no. 2, pp. 226–236, Apr. 2004, doi: 10.1115/1.1691446.
- [117] S. Ji *et al.*, 'Use of Brain Biomechanical Models for Monitoring Impact Exposure in Contact Sports', *Annals of Biomedical Engineering*, vol. 50, no. 11, pp. 1389–1408, Nov. 2022, doi: 10.1007/s10439-022-02999-w.
- [118] B. Emsley, J. Farmer, P. Sherratt, P. Goodall, T. Jackson, and A. West, 'An overview of the test methodology used in current cycling helmet standards and literature', *International Journal of Impact Engineering*, vol. 188, p. 104928, Jun. 2024, doi: 10.1016/j.ijimpeng.2024.104928.

- [119] J. A. Newman, 'A Generalized Acceleration Model For Brain Injury Threshold (GAMBIT)', in *International Conference on the Biomechanics of Impact IRCOBI*, 1986, pp. 121–131.
- [120] H. R. Lissner, M. Lebow, and F. G. Evans, 'Experimental studies on the relation between acceleration and intracranial pressure changes in man', *Surg Gynecol Obstet*, vol. 111, pp. 329–338, Sep. 1960.
- [121] M. Hajiaghamemar, M. Seidi, and S. S. Margulies, 'Head Rotational Kinematics, Tissue Deformations, and Their Relationships to the Acute Traumatic Axonal Injury', *Journal of Biomechanical Engineering*, vol. 142, no. 3, Mar. 2020, doi: 10.1115/1.4046393.
- [122] T. A. Gennarelli, J. M. Abel, H. Adams, and D. Graham, 'Differential tolerance of frontal and temporal lobes to contusion induced by angular acceleration', *Proceedings: Stapp Car Crash Conference*, vol. 23, pp. 563–586, 1979.
- [123] K. Ono, K. Kikuchi, M. Nakamura, H. Kobayashi, and N. Nakamura, 'Human head tolerance to sagittal impact reliable estimation deduced from experimental head injury using subhuman primates and human cadaver skulls.', presented at the 24th STAPP Car Crash Conference, Troy, MI, USA: SAE paper 801303., 1980.
- [124] A. K. Ommaya, P. Yarnell, A. E. Hirsch, and E. H. Harris, 'Scaling of Experimental Data on Cerebral Concussion in Sub-Human Primates to Concussion Threshold for Man', presented at the 11th Stapp Car Crash Conference, Feb. 1967. doi: 10.4271/670906.
- [125] S. S. Margulies and L. E. Thibault, 'A proposed tolerance criterion for diffuse axonal injury in man', *J Biomech*, vol. 25, no. 8, pp. 917–923, Aug. 1992, doi: 10.1016/0021-9290(92)90231-o.
- [126] H. Wu *et al.*, 'The Head AIS 4+ Injury Thresholds for the Elderly Vulnerable Road User Based on Detailed Accident Reconstructions', *Frontiers in Bioengineering and Biotechnology*, vol. 9, Jun. 2021, doi: 10.3389/fbioe.2021.682015.
- [127] A. Post, K. Taylor, T. B. Hoshizaki, S. Brien, M. D. Cusimano, and S. Marshall, 'A biomechanical analysis of traumatic brain injury for slips and falls from height', *Trauma (United Kingdom)*, vol. 21, no. 1, pp. 27–34, Jan. 2019, doi: 10.1177/1460408617721564.
- [128] C. Van Lierde, 'Biomechanics of head injury damage criteria for skull and brain lesions.', KU Leuven, 2005.
- [129] X. Zhan *et al.*, 'The relationship between brain injury criteria and brain strain across different types of head impacts can be different', *JR Soc Interface*, vol. 18, no. 179, p. 20210260, doi: 10.1098/rsif.2021.0260.

- [130] S. Kleiven, 'Predictors for traumatic brain injuries evaluated through accident reconstructions', *Stapp Car Crash J*, vol. 51, pp. 81–114, Oct. 2007, doi: 10.4271/2007-22-0003.
- [131] S. Kleiven, 'Influence of Direction and Duration of Impacts to the Human Head Evaluated Using the Finite Element Method', in *Proceedings of International Research Council on the Biomechanics of Injury*, Prague, Czech Republic, 2005, pp. 41–57.
- [132] A. Madhukar and M. Ostoja-Starzewski, 'Finite Element Methods in Human Head Impact Simulations: A Review', *Ann Biomed Eng*, vol. 47, no. 9, pp. 1832–1854, Sep. 2019, doi: 10.1007/s10439-019-02205-4.
- [133] K. Tse, S. Lim, V. Tan, and H. Lee, 'A Review of Head Injury and Finite Element Head Models', American Journal of Engineering, Technology and Society. 1. 28-52., Dec. 2014,
- [134] A. Alshareef, T. Wu, J. S. Giudice, and M. B. Panzer, 'Toward subject-specific evaluation: methods of evaluating finite element brain models using experimental high-rate rotational brain motion', *Biomech Model Mechanobiol*, vol. 20, no. 6, pp. 2301–2317, Dec. 2021, doi: 10.1007/s10237-021-01508-7.
- [135] K. O'Riordain, P. M. Thomas, J. P. Phillips, and M. D. Gilchrist, 'Reconstruction of real world head injury accidents resulting from falls using multibody dynamics', *Clin Biomech*, vol. 18, no. 7, pp. 590–600, Aug. 2003, doi: 10.1016/s0268-0033(03)00111-6.
- [136] N. Fahse, M. Millard, F. Kempter, S. Maier, M. Roller, and J. Fehr, 'Dynamic human body models in vehicle safety: An overview', *GAMM Mitteilungen*, vol. 46, no. 2, Jun. 2023, doi: 10.1002/gamm.202300007.
- [137] H. Mao et al., 'Development of a finite element human head model partially validated with thirty five experimental cases', *J Biomech Eng*, vol. 135, no. 11, p. 111002, Nov. 2013, doi: 10.1115/1.4025101.
- [138] H. Mao, H. Gao, L. Cao, V. V. Genthikatti, and K. H. Yang, 'Development of high-quality hexahedral human brain meshes using feature-based multi-block approach', *Comput Methods Biomech Biomed Engin*, vol. 16, no. 3, pp. 271–279, 2013, doi: 10.1080/10255842.2011.617005.
- [139] R. Happee *et al.*, 'Mathematical Human Body Models Representing A Mid Size Male And A Small Female For Frontal, Lateral And Rearward Impact Loading'. IRCOBI Conference. 28, pp. 67-84, 2000.
- [140] K. M. Tse and D. Holder, 'A Biomechanical Evaluation of a Novel Airbag Bicycle Helmet Concept for Traumatic Brain Injury Mitigation', *Bioengineering*, vol. 8, no. 11, Nov. 2021, doi: 10.3390/bioengineering8110173.

- [141] G. Tierney, 'Concussion biomechanics, head acceleration exposure and brain injury criteria in sport: a review', *Sports Biomechanics*, vol. 23, no. 11, pp. 1888–1916, Nov. 2021, doi: 10.1080/14763141.2021.2016929.
- [142] L. F. Gabler, J. R. Crandall, and M. B. Panzer, 'Assessment of Kinematic Brain Injury Metrics for Predicting Strain Responses in Diverse Automotive Impact Conditions', *Annals of Biomedical Engineering*, vol. 44, no. 12, pp. 3705–3718, Dec. 2016, doi: 10.1007/s10439-016-1697-0.
- [143] Y. Takahashi and T. Yanaoka, 'A STUDY OF INJURY CRITERIA FOR BRAIN INJURIES IN TRAFFIC ACCIDENTS'.
- [144] T. Yanaoka, Y. Dokko, and Y. Takahashi, 'Investigation on an Injury Criterion Related to Traumatic Brain Injury Primarily Induced by Head Rotation', in *SAE Technical Papers*, SAE International, Apr. 2015. doi: 10.4271/2015-01-1439.
- [145] D. Marjoux, D. Baumgartner, C. Deck, and R. Willinger, 'Head injury prediction capability of the HIC, HIP, SIMon and ULP criteria', *Accident Analysis and Prevention*, vol. 40, pp. 1135–1148, 2008.
- [146] E. J. Sanchez *et al.*, 'Evaluation of Head and Brain Injury Risk Functions Using Sub-Injurious Human Volunteer Data', *Journal of Neurotrauma*, vol. 34, no. 16, pp. 2410–2424, Aug. 2017, doi: 10.1089/neu.2016.4681.
- [147] J. S. Giudice, W. Zeng, T. Wu, A. Alshareef, D. F. Shedd, and M. B. Panzer, 'An Analytical Review of the Numerical Methods used for Finite Element Modeling of Traumatic Brain Injury', *Ann Biomed Eng*, vol. 47, no. 9, pp. 1855–1872, Sep. 2019, doi: 10.1007/s10439-018-02161-5.
- [148] M. Fahlstedt *et al.*, 'Ranking and Rating Bicycle Helmet Safety Performance in Oblique Impacts Using Eight Different Brain Injury Models', *Ann Biomed Eng*, vol. 49, no. 3, pp. 1097–1109, Mar. 2021, doi: 10.1007/s10439-020-02703-w.
- [149] X. Zhan et al., 'The relationship between brain injury criteria and brain strain across different types of head impacts can be different', *JR Soc Interface*, vol. 18, no. 179, p. 20210260, Jun. 2021, doi: 10.1098/rsif.2021.0260.
- [150] F. Hernandez *et al.*, 'Six Degree-of-Freedom Measurements of Human Mild Traumatic Brain Injury', *Annals of Biomedical Engineering*, vol. 43, no. 8, pp. 1918–1934, 2015, doi: 10.1007/s10439-014-1212-4.
- [151] C. W. Gadd, 'Use of a Weighted-Impulse Criterion for Estimating Injury Hazard'. 1966.
- [152] J. Versace, 'A Review of the Severity Index'. 1971.

- [153] J. A. Newman, N. Shewchenko, and E. Welbourne, 'A Proposed New Biomechanical Head Injury Assessment Function-The Maximum Power Index', *Stapp Car Crash Journal*, vol. 44, 2000, [Online]. Available: http://www.stapp.org
- [154] Y. Levy, K. Bian, L. Patterson, R. Ouckama, and H. Mao, 'Head Kinematics and Injury Metrics for Laboratory Hockey-Relevant Head Impact Experiments', *Annals of Biomedical Engineering*, vol. 49, no. 10, pp. 2914–2923, Oct. 2021, doi: 10.1007/s10439-021-02855-3.
- [155] H. Kimpara and M. Iwamoto, 'Mild traumatic brain injury predictors based on angular accelerations during impacts', *Annals of Biomedical Engineering*, vol. 40, no. 1, pp. 114–126, Jan. 2012, doi: 10.1007/s10439-011-0414-2.
- [156] H. Kimpara, Y. Nakahira, M. Iwamoto, S. Rowson, and S. Duma, 'Head Injury Prediction Methods Based on 6 Degree of Freedom Head Acceleration Measurements during Impact'. 2011.
- [157] L. F. Gabler, J. R. Crandall, and M. B. Panzer, 'Development of a Metric for Predicting Brain Strain Responses Using Head Kinematics', *Annals of Biomedical Engineering*, vol. 46, no. 7, pp. 972–985, Jul. 2018, doi: 10.1007/s10439-018-2015-9.
- [158] L. F. Gabler, J. R. Crandall, and M. B. Panzer, 'Development of a Second-Order System for Rapid Estimation of Maximum Brain Strain', *Annals of Biomedical Engineering*, vol. 47, no. 9, pp. 1971–1981, Sep. 2019, doi: 10.1007/s10439-018-02179-9.
- [159] R. M. Greenwald, J. T. Gwin, J. J. Chu, and J. J. Crisco, 'Head Impact Severity Measures for Evaluating Mild Traumatic Brain Injury Risk Exposure', *Neurosurgery*, vol. 62, pp. 789–798, 2008, doi: 10.1227/01.NEU.0000311244.05104.96.
- [160] S. Rowson and S. M. Duma, 'Brain injury prediction: assessing the combined probability of concussion using linear and rotational head acceleration', *Ann Biomed Eng*, vol. 41, no. 5, pp. 873–882, May 2013, doi: 10.1007/s10439-012-0731-0.
- [161] Road vehicles Injury risk curves for the THOR dummy, ISO/TR 19222:2021, 2021.
 Accessed: Jan. 18, 2024. [Online]. Available:
 https://www.iso.org/standard/64046.html
- [162] NHTSA, 'FMVSS No. 208 Final Economic Assessment'. 2000. [Online]. Available: www.nhtsa.dot.gov
- [163] E. G. Takhounts, S. A. Ridella, S. Rowson, and S. M. Duma, 'Kinematic Rotational Brain Injury Criterion (BRIC)', 22nd Enhanced Safety of Vehicles Conference Proceedings, p. Paper No. 11-0263, 2011.

- [164] M. L. Levy, B. M. Ozgur, C. Berry, H. E. Aryan, and M. L. J. Apuzzo, 'Birth and Evolution of the Football Helmet', *Neurosurgery*, vol. 55, no. 3, p. 656, Sep. 2004, doi: 10.1227/01.NEU.0000134599.01917.AA.
- [165] D. H. Daneshvar, C. M. Baugh, C. J. Nowinski, A. C. McKee, R. A. Stern, and R. C. Cantu, 'Helmets and Mouth Guards: The Role of Personal Equipment in Preventing Sport-Related Concussions', *Clinics in Sports Medicine*, vol. 30, no. 1, pp. 145–163, Jan. 2011, doi: 10.1016/j.csm.2010.09.006.
- [166] N. Yoganandan, Frontiers in Head and Neck Trauma: Clinical and Biomechanical, vol. 21. IOS Press, 1998.
- [167] A. Post, T. B. Hoshizaki, M. Gilchrist, and S. Brien, 'Analysis of the influence of independent variables used for reconstruction of a traumatic brain injury incident', in Proceedings of the Institution of Mechanical Engineers, Part P: Journal of Sports Engineering and Technology, Sep. 2012, pp. 290–298. doi: 10.1177/1754337112436629.
- [168] L. Zhang, K. H. Yang, and A. I. King, 'Biomechanics of neurotrauma', *Neurol Res*, vol. 23, no. 2–3, pp. 144–156, 2001, doi: 10.1179/016164101101198488.
- [169] J. S. Delaney, V. Puni, and F. Rouah, 'Mechanisms of injury for concussions in university football, ice hockey, and soccer: a pilot study', *Clin J Sport Med*, vol. 16, no. 2, pp. 162–165, Mar. 2006, doi: 10.1097/00042752-200603000-00013.
- [170] Equipment and Procedures Used in Evaluating the Performance Characteristics of Protective Headgear, F1446-15b, 2015. doi: 10.1520/F1446-15.
- [171] Uniform provisions concerning the approval of protective helmets and of their visors for drivers and passengers of motor cycles and mopeds, 22.05, Geneva., 2017.
- [172] D. Abram, A. Wikarna, F. Golnaraghi, and G. Wang, 'A Novel Oblique Impact Test Rig for Testing Helmet', *International Journal of Sports and Exercise Medicine*, vol. 6, no. 1, Feb. 2020, doi: 10.23937/2469-5718/1510158.
- [173] E. S. Walsh, M. Kendall, A. Post, A. Meehan, and T. B. Hoshizaki, 'Comparative analysis of Hybrid III neckform and an unbiased neckform', *Sports Eng*, vol. 21, no. 4, pp. 479–485, Dec. 2018, doi: 10.1007/s12283-018-0286-x.
- [174] E. S. Walsh, M. Kendall, T. B. Hoshizaki, and M. D. Gilchrist, 'Dynamic Impact Response and Predicted Brain Tissue Deformation Comparisons for an Impacted Hybrid III Headform With and Without a Neckform and Torso Masses', 2014.
- [175] ASTM International, *Standard Specification for Protective Headgear Used in Martial Arts*, ASTM F2397-09(2015), 2015.
- [176] ASTM International, *Standard Specification for Headgear Used in Soccer*, ASTM F2439-06(2016), 2016. Available: https://www.astm.org/f2439-06r16.html

- [177] L. Jeffries, C. Zerpa, E. Przysucha, P. Sanzo, and S. Carlson, 'The Use of a Pneumatic Horizontal Impact System for Helmet Testing', *Journal of Safety Engineering*, vol. 6, no. 1, pp. 8–13, 2017.
- [178] D. C. Viano, C. Withnall, and D. Halstead, 'Impact Performance of Modern Football Helmets', *Ann Biomed Eng*, vol. 40, no. 1, pp. 160–174, Jan. 2012, doi: 10.1007/s10439-011-0384-4.
- [179] E. D. Edwards *et al.*, 'Kinematic assessment of the NOCSAE headform during blunt impacts with a pneumatic linear impactor', *Sports Engineering*, vol. 26, no. 1, Dec. 2023, doi: 10.1007/s12283-023-00403-x.
- [180] D. B. Camarillo, P. B. Shull, J. Mattson, R. Shultz, and D. Garza, 'An Instrumented Mouthguard for Measuring Linear and Angular Head Impact Kinematics in American Football', *Ann Biomed Eng*, vol. 41, no. 9, pp. 1939–1949, Sep. 2013, doi: 10.1007/s10439-013-0801-y.
- [181] F. Hernandez, P. B. Shull, and D. B. Camarillo, 'Evaluation of a laboratory model of human head impact biomechanics', *Journal of Biomechanics*, vol. 48, no. 12, pp. 3469–3477, Sep. 2015, doi: 10.1016/j.jbiomech.2015.05.034.
- [182] M. Jesunathadas, T. E. Gould, T. A. Plaisted, E. D. Edwards, and S. G. Piland, 'Describing headform pose and impact location for blunt impact testing', *Journal of Biomechanics*, vol. 109, p. 109923, Aug. 2020, doi: 10.1016/j.jbiomech.2020.109923.
- [183] F. Hernandez et al., 'Comparing In Vivo Head Impact Kinematics From American Football With Laboratory Drop and Linear Impactors', presented at the ASME 2013 Summer Bioengineering Conference, American Society of Mechanical Engineers Digital Collection, 2013. doi: 10.1115/SBC2013-14680.
- [184] S. Rowson and S. M. Duma, 'Development of the STAR Evaluation System for Football Helmets: Integrating Player Head Impact Exposure and Risk of Concussion', *Ann Biomed Eng*, vol. 39, no. 8, pp. 2130–2140, Aug. 2011, doi: 10.1007/s10439-011-0322-5.
- [185] B. R. Cobb, A. MacAlister, T. J. Young, A. R. Kemper, S. Rowson, and S. M. Duma, 'Quantitative comparison of Hybrid III and National Operating Committee on Standards for Athletic Equipment headform shape characteristics and implications on football helmet fit', *Proceedings of the Institution of Mechanical Engineers, Part P: Journal of Sports Engineering and Technology*, vol. 229, no. 1, pp. 39–46, Mar. 2015, doi: 10.1177/1754337114548245.
- [186] A. S. McIntosh and P. McCrory, 'Impact energy attenuation performance of football headgear', *British Journal of Sports Medicine*, vol. 34, pp. 337-341., 2000, doi: 10.1136/bjsm.34.5.337.

- [187] A. Post, A. Oeur, B. Hoshizaki, and M. D. Gilchrist, 'An examination of American football helmets using brain deformation metrics associated with concussion', *Materials & Design*, vol. 45, pp. 653–662, Mar. 2013, doi: 10.1016/j.matdes.2012.09.017.
- [188] E. J. Pellman, D. C. Viano, C. Withnall, N. Shewchenko, C. A. Bir, and P. D. Halstead, 'Concussion in professional football: Helmet testing to assess impact performance Part 11', *Neurosurgery*, vol. 58, no. 1, pp. 78–95, 2006, doi: 10.1227/01.NEU.0000196265.35238.7C.
- [189] B. Rowson, S. Rowson, and S. M. Duma, 'Hockey STAR: A Methodology for
 Assessing the Biomechanical Performance of Hockey Helmets', *Ann Biomed Eng*, vol.
 43, no. 10, pp. 2429–2443, Oct. 2015, doi: 10.1007/s10439-015-1278-7.
- [190] W. Dawber, L. Foster, T. Senior, and J. Hart, 'Design Development of a Repeatable Helmet Test System for Public Order Threat Recreations', in *Design Tools and Methods* in *Industrial Engineering III*, M. Carfagni, R. Furferi, P. Di Stefano, L. Governi, and F. Gherardini, Eds., Cham: Springer Nature Switzerland, 2024, pp. 169–176. doi: 10.1007/978-3-031-58094-9_20.
- [191] S. Carlson *et al.*, 'EVIDENCE OF RELIABILITY AND VALIDITY FOR THE USE OF A HELMET IMPACT DROP SYSTEM', in *34th international Conference on Biomechanics in Sports*, 2016, pp. 391–394.
- [192] E. Bliven *et al.*, 'Evaluation of a novel bicycle helmet concept in oblique impact testing', *Accident Analysis and Prevention*, vol. 124, pp. 58–65, Mar. 2019, doi: 10.1016/j.aap.2018.12.017.
- [193] J. M. Clark, A. Post, T. B. Hoshizaki, and M. D. Gilchrist, 'Protective Capacity of Ice Hockey Helmets against Different Impact Events', *Annals of Biomedical Engineering*, vol. 44, no. 12, pp. 3693–3704, Dec. 2016, doi: 10.1007/s10439-016-1686-3.
- [194] M. Jesunathadas *et al.*, 'Headform Kinematic Comparison Across Three Blunt Impact Testing Modes', DEVCOM Army Research Laboratory, Aberdeen Proving Ground, MD, Nov. 2021. doi: 10.21236/AD1154202.
- [195] N. Petrone, G. Carraro, S. D. Castello, L. Broggio, A. Koptyug, and M. Bäckström, 'A Novel Instrumented Human Head Surrogate for the Impact Evaluation of Helmets', *Proceedings*, vol. 2, no. 6, Art. no. 6, 2018, doi: 10.3390/proceedings2060269.
- [196] E. T. Campolettano, R. A. Gellner, D. W. Sproule, M. T. Begonia, and S. Rowson, 'Quantifying Youth Football Helmet Performance: Assessing Linear and Rotational Head Acceleration', *Ann Biomed Eng*, vol. 48, no. 6, pp. 1640–1650, Jun. 2020, doi: 10.1007/s10439-020-02505-0.

- [197] L. Gabler *et al.*, 'Consensus Head Acceleration Measurement Practices (CHAMP): Laboratory Validation of Wearable Head Kinematic Devices', *Annals of Biomedical Engineering*, Nov. 2022, doi: 10.1007/s10439-022-03066-0.
- [198] R. P. Hubbard and D. G. McLeod, 'Definition and Development of A Crash Dummy Head', *SAE Transactions*, vol. 83, pp. 3836–3851, 1974.
- [199] V. R. Hodgson, 'National Operating Committee on Standards for Athletic Equipment football helmet certification program', *Med Sci Sports*, vol. 7, no. 3, pp. 225–232, 1975.
- [200] N. E.-P. Stark, M. Begonia, L. Viano, and S. Rowson, 'The Influence of Headform Friction and Inertial Properties on Oblique Impact Helmet Testing', *Ann Biomed Eng*, vol. 52, no. 10, pp. 2803–2811, Oct. 2024, doi: 10.1007/s10439-024-03460-w.
- [201] 'BS EN 960-2006–[2021-11-16–02-19-37 PM]'.
- [202] M. L. Bland, D. S. Zuby, B. C. Mueller, and S. Rowson, 'Differences in the protective capabilities of bicycle helmets in real-world and standard-specified impact scenarios', *Traffic Inj Prev*, vol. 19, no. sup1, pp. S158–S163, Feb. 2018, doi: 10.1080/15389588.2017.1388915.
- [203] J. R. Funk, R. E. Quesada, A. M. Miles, and J. R. Crandall, 'Inertial Properties of Football Helmets', *Journal of Biomechanical Engineering*, vol. 140, no. 064501, Apr. 2018, doi: 10.1115/1.4039673.
- [204] T. A. Connor, N. Colgan, M. Stewart, A. Ní Annaidh, and M. D. Gilchrist, 'Inertial properties of a living population for the development of biofidelic headforms', Proceedings of the Institution of Mechanical Engineers, Part P: Journal of Sports Engineering and Technology, vol. 237, no. 1, pp. 52–62, Mar. 2023, doi: 10.1177/1754337120921646.
- [205] T. A. Connor, M. Stewart, R. Burek, and M. D. Gilchrist, 'Influence of headform mass and inertia on the response to oblique impacts', *International Journal of Crashworthiness*, vol. 24, no. 6, pp. 677–698, Nov. 2019, doi: 10.1080/13588265.2018.1525859.
- [206] M. Kendall, E. S. Walsh, and T. B. Hoshizaki, 'Comparison between Hybrid III and Hodgson–WSU headforms by linear and angular dynamic impact response', Proceedings of the Institution of Mechanical Engineers, Part P: Journal of Sports Engineering and Technology, vol. 226, no. 3–4, pp. 260–265, Sep. 2012, doi: 10.1177/1754337112436901.
- [207] A. MacAlister and V. Tech, 'Surrogate Head Forms for the Evaluation of Head Injury Risk', in *Brain Injuries and Biomechanics Symposium*, 2013.

- [208] G. W. Wood, M. B. Panzer, C. R. Bass, and B. S. Myers, 'Viscoelastic Properties of Hybrid III Head Skin', SAE Int. J. Mater. Manuf., vol. 3, no. 1, Art. no. 2010-01-0383, Apr. 2010, doi: 10.4271/2010-01-0383.
- [209] S. York *et al.*, 'Influence of Friction at the Head–Helmet Interface on Advanced Combat Helmet (ACH) Blunt Impact Kinematic Performance', *Military Medicine*, vol. 188, no. 7–8, pp. e1918–e1925, Jul. 2023, doi: 10.1093/milmed/usab547.
- [210] B. L. Suderman, R. W. Hoover, R. P. Ching, and I. S. Scher, 'The effect of hardhats on head and neck response to vertical impacts from large construction objects', *Accid Anal Prev*, vol. 73, pp. 116–124, Dec. 2014, doi: 10.1016/j.aap.2014.08.011.
- [211] A. Trotta, D. Zouzias, G. D. Bruyne, and A. N. Annaidh, 'The Importance of the Scalp in Head Impact Kinematics', *Annals of Biomedical Engineering*, vol. 46, no. 6, pp. 831–840, 2018, doi: 10.1007/s10439-018-2003-0.
- [212] H. J. Mertz, 'Biofidelity of the Hybrid III Head', *Transactions*, vol. 94. pp. 97–105, 1985. [Online]. Available: https://www.jstor.org/stable/44724008
- [213] X. Yu, P. Halldin, and M. Ghajari, 'Oblique impact responses of Hybrid III and a new headform with more biofidelic coefficient of friction and moments of inertia', *Frontiers in Bioengineering and Biotechnology*, vol. 10, Sep. 2022, doi: 10.3389/fbioe.2022.860435.
- [214] NHTSA and Office of Crashworthiness Standards, 'Parts List and Drawings, Hybrid III 50th Percentile Male'. 1997.
- [215] K. Hansen *et al.*, 'Angular Impact Mitigation System for Bicycle Helmets to Reduce Head Acceleration and Risk of Traumatic Brain Injury', *Accid Anal Prev*, vol. 59, pp. 109–117, Oct. 2013, doi: 10.1016/j.aap.2013.05.019.
- [216] T. Y. Pang et al., 'Head and neck responses in oblique motorcycle helmet impacts: a novel laboratory test method', *International Journal of Crashworthiness*, vol. 16, no. 3, pp. 297–307, Jun. 2011, doi: 10.1080/13588265.2011.559799.
- [217] A. S. Mcintosh, A. Lai, and E. Schilter, 'Bicycle Helmets: Head Impact Dynamics in Helmeted and Unhelmeted Oblique Impact Tests', *Traffic Injruy Prevention*, vol. 14, pp. 501–508, 2013, doi: 10.1080/15389588.2012.727217.
- [218] J. R. Funk, J. M. Cormier, C. E. Bain, H. Guzman, and E. Bonugli, 'Validation and Application of a Methodology to Calculate Head Accelerations and Neck Loading in Soccer Ball Impacts', *SAE Technical Paper*, 2009.
- [219] J. G. Beckwith, J. J. Chu, and R. M. Greenwald, 'Validation of a noninvasive system for measuring head acceleration for use during boxing competition', *Journal of Applied Biomechanics*, vol. 23, no. 3, pp. 238–244, 2007, doi: 10.1123/jab.23.3.238.

- [220] D. C. Viano, C. Withnall, and M. Wonnacott, 'Football helmet drop tests on different fields using an instrumented Hybrid III head', *Ann Biomed Eng*, vol. 40, no. 1, pp. 97–105, Jan. 2012, doi: 10.1007/s10439-011-0377-3.
- [221] A. Bartsch, E. Benzel, V. Miele, D. Morr, and V. Prakash, 'Hybrid III anthropomorphic test device (ATD) response to head impacts and potential implications for athletic headgear testing', *Accid Anal Prev*, vol. 48, pp. 285–291, Sep. 2012, doi: 10.1016/j.aap.2012.01.032.
- [222] A. Hering and S. Derler, 'Motorcycle Helmet Drop Tests Using a Hybrid III Dummy', presented at the IRCOBI Conference, Montpellier (France), 2000.
- [223] A. Gilchrist and N. J. Mills, 'Protection of the side of the head', *Accid Anal Prev*, vol. 28, no. 4, pp. 525–535, Jul. 1996, doi: 10.1016/0001-4575(96)00030-9.
- [224] N. J. Mills and A. Gilchrist, 'Oblique impact testing of bicycle helmets', International Journal of Impact Engineering, vol. 35, pp. 1075–1086, 2008, doi: 10.1016/j.ijimpeng.2007.05.005.
- [225] A. Post, L. Dawson, T. B. Hoshizaki, M. D. Gilchrist, and M. D. Cusimano, 'Development of a test method for adult ice hockey helmet evaluation', *Comput Methods Biomech Biomed Engin*, pp. 1–13, Apr. 2020, doi: 10.1080/10255842.2020.1758680.
- [226] D. C. Viano, I. R. Casson, and E. J. Pellman, 'Concussion in professional football: biomechanics of the struck player--part 14', *Neurosurgery*, vol. 61, no. 2, pp. 313–327; discussion 327-328, Aug. 2007, doi: 10.1227/01.NEU.0000279969.02685.D0.
- [227] M. Fahlstedt, P. Halldin, V. Alvarez, and S. Kleiven, 'Influence of the Body and Neck on Head Kinematics and Brain Injury Risk in Bicycle Accident Situations', in *IRCOBI* Conference, Malaga, Spain, 2016, pp. 459–478.
- [228] M. Ghajari, S. Peldschus, U. Galvanetto, and L. Iannucci, 'Effects of the presence of the body in helmet oblique impacts', *Accid Anal Prev*, vol. 50, pp. 263–271, Jan. 2013, doi: 10.1016/j.aap.2012.04.016.
- [229] P. Rousseau, T. B. Hoshizaki, M. D. Gilchrist, and A. Post, 'Estimating the influence of neckform compliance on brain tissue strain during a Helmeted impact', *Stapp Car Crash J*, vol. 54, pp. 37–48, Nov. 2010, doi: 10.4271/2010-22-0003.
- [230] C. Klug, F. Feist, and E. Tomasch, 'Testing of bicycle helmets for preadolescents', presented at the IRCOBI Conference, Lyon, France, 2015, pp. 136–155.
- [231] M. Ghajari, S. Peldschus, U. Galvanetto, and L. Iannucci, 'Evaluation of the effective mass of the body for helmet impacts', *International Journal of Crashworthiness*, vol. 16, no. 6, pp. 621–631, Dec. 2011, doi: 10.1080/13588265.2011.616078.

- [232] M. Homayounpour, N. G. Gomez, A. N. Vasavada, and A. S. Merryweather, 'The role of neck muscle co-contraction and postural changes in head kinematics after safe head impacts: Investigation of head/neck injury reduction', *Journal of Biomechanics*, vol. 128, p. 110732, Nov. 2021, doi: 10.1016/j.jbiomech.2021.110732.
- [233] K. A. Reynier *et al.*, 'The Effect of Muscle Activation on Head Kinematics During Non-injurious Head Impacts in Human Subjects', *Ann Biomed Eng*, vol. 48, no. 12, pp. 2751–2762, Dec. 2020, doi: 10.1007/s10439-020-02609-7.
- [234] M. Ghajari, U. Galvanetto, L. Iannucci, and R. Willinger, 'Influence of the body on the response of the helmeted head during impact', *International Journal of Crashworthiness*, vol. 16, no. 3, pp. 285–295, Jun. 2011, doi: 10.1080/13588265.2011.559798.
- [235] E. M. P. Williams et al., 'Sex differences in neck strength and head impact kinematics in university rugby union players', European Journal of Sport Science, vol. 22, no. 11, pp. 1649–1658, 2022, doi: 10.1080/17461391.2021.1973573.
- [236] Specification for protective helmets for vehicle users, BS 6658:1985, 1985.
- [237] Standard for Protective Headgear for Use With Motorcycles and Other Motorized Vehicles, SNELL M2000, 2000.
- [238] D. R. Thom, 'Comparison Tests of Motorcycle Helmets qualified to international standards.', in *International Motorcycle Safety Conference*., 2006.
- [239] Standard for Protective Headgear for Skiing and Other Winter Activities, S-98, 1998. Available: https://smf.org/standards/pdf/S98STD.pdf
- [240] Test Methods for Nonballistic-resistant Helmets Worn by Law Enforcement and Corrections, ASTM E3343/E3343M-23, 2023. Available: https://www.astmonline.com/standards/ASTM-E3343-E3343M-23/
- [241] N. I. for Justice, 'NIJ Standard for Riot Helmets and Face Shields', no. August 1980. pp. 2–6, 1984.
- [242] G. DiGiacomo, S. Tsai, and M. Bottlang, 'Impact Performance Comparison of Advanced Snow Sport Helmets with Dedicated Rotation-Damping Systems', *Ann Biomed Eng*, vol. 49, no. 10, pp. 2805–2813, 2021, doi: 10.1007/s10439-021-02723-0.
- [243] E. Bonugli, J. Cormier, M. Reilly, and L. Reinhart, 'Replicating Real-World Friction of Motorcycle Helmet Impacts and Its Effects on Head Injury Metrics', presented at the SAE World Congress Experience, Mar. 2017, pp. 2017-01–1433. doi: 10.4271/2017-01-1433.
- [244] Instrumentation for Impact Test Part 1 Electronic Instrumentation, J211/1, 2022.
- [245] J. R. Funk, A. S. McIntosh, C. Withnall, M. Wonnacott, and R. Jadischke, 'Best Practices for Conducting Physical Reconstructions of Head Impacts in Sport', *Ann*

- *Biomed Eng*, vol. 50, no. 11, pp. 1409–1422, Nov. 2022, doi: 10.1007/s10439-022-03024-w.
- [246] J. R. W. Morris, 'ACCELEROMETRY- A TECHNIQUE FOR THE MEASUREMENT OF HUMAN BODY MOVEMENTS', J. Biomechanics, vol. 6, pp. 729–736, 1973.
- [247] T. Sauer, Numerical analysis, 2nd ed. Boston: Pearson, 2012.
- [248] D. Nevins, L. Smith, and P. Petersen, 'An improved method for obtaining rotational accelerations from instrumented headforms', *Sports Engineering*, 2019, doi: 10.1007/s12283-019-0312-7.
- [249] G. A. Wood, 'DATA SMOOTHING AND DIFFERENTIATION PROCEDURES IN BIOMECHANICS', *Exercise and Sport Sciences Reviews*, vol. 10, no. 1, p. 308, Jan. 1982.
- [250] Calculation Guidelines for Impact Testing, J1727, 2015. [Online]. Available: https://www.sae.org/standards/content/j1727_201502/
- [251] W. R. Bussone, J. Olberding, and M. Prange, 'Six-Degree-of-Freedom Accelerations: Linear Arrays Compared with Angular Rate Sensors in Impact Events', *SAE International Journal of Transportation Safety*, vol. 5, no. 2, pp. 194–207, 2017, doi: 10.4271/2017-01-1465.
- [252] J. J. Crisco, J. J. Chu, and R. M. Greenwald, 'An algorithm for estimating acceleration magnitude and impact location using multiple nonorthogonal single-axis accelerometers', *Journal of Biomechanical Engineering*, vol. 126, no. 6, pp. 849–854, Dec. 2004, doi: 10.1115/1.1824135.
- [253] F. DiMasi, Transformation of Nine-Accelerometer-Package (NAP) Data for Replicating Headpart Kinematics and Dynamic Loading, DOT HS 808 282;DOT-VNTSC-NHTSA-94-5, 1995. [Online]. Available: https://rosap.ntl.bts.gov/view/dot/11564
- [254] A. Post, J. M. Clark, D. G. E. Robertson, T. B. Hoshizaki, and M. D. Gilchrist, 'The effect of acceleration signal processing for head impact numeric simulations', *Sports Eng*, vol. 20, no. 2, pp. 111–119, Jun. 2017, doi: 10.1007/s12283-016-0219-5.
- [255] J. J. Crisco *et al.*, 'Head Impact Exposure in Collegiate Football Players', *J Biomech*, vol. 44, no. 15, pp. 2673–2678, Oct. 2011, doi: 10.1016/j.jbiomech.2011.08.003.
- [256] J. G. Beckwith *et al.*, 'Head impact exposure sustained by football players on days of diagnosed concussion', *Med Sci Sports Exerc*, vol. 45, no. 4, pp. 737–746, Apr. 2013, doi: 10.1249/MSS.0b013e3182792ed7.
- [257] D. A. Patton, 'A Review of Instrumented Equipment to Investigate Head Impacts in Sport', *Appl Bionics Biomech*, vol. 2016, p. 7049743, 2016, doi: 10.1155/2016/7049743.

- [258] R. M. Greenwald, J. J. Chu, J. J. Crisco, and J. A. Finkelstein, 'Head Impact Telemetry System (HITS) for measurement of head acceleration in the field', presented at the American Society of Biomechanics Annual Meeting, Toledo, USA, 2003.
- [259] M. Panzer, C. Bass, R. Salzar, J. Pellettiere, and B. Myers, 'EVALUATION OF EAR-MOUNTED SENSORS FOR DETERMINING IMPACT HEAD ACCELERATION', in *IRCOBI Conference*, York (UK), 2009, pp. 319–322.
- [260] L. C. Wu et al., 'In Vivo Evaluation of Wearable Head Impact Sensors', *Ann Biomed Eng*, vol. 44, no. 4, pp. 1234–1245, Apr. 2016, doi: 10.1007/s10439-015-1423-3.
- [261] C. M. Huber, D. A. Patton, K. L. Wofford, S. S. Margulies, D. K. Cullen, and K. B. Arbogast, 'Laboratory Assessment of a Headband-Mounted Sensor for Measurement of Head Impact Rotational Kinematics', *Journal of Biomechanical Engineering*, vol. 143, no. 024502, Nov. 2020, doi: 10.1115/1.4048574.
- [262] M. Higgins, P. D. Halstead, L. Snyder-Mackler, and D. Barlow, 'Measurement of impact acceleration: Mouthpiece accelerometer versus helmet accelerometer', *Journal of Athletic Training*, vol. 42, no. 1, pp. 5–10, 2007.
- [263] A. Bartsch, S. Samorezov, E. Benzel, V. Miele, and D. Brett, 'Validation of an "Intelligent Mouthguard" Single Event Head Impact Dosimeter', *Stapp Car Crash J*, vol. 58, pp. 1–27, Nov. 2014, doi: 10.4271/2014-22-0001.
- [264] G. J. Tierney, C. Kuo, L. Wu, D. Weaving, and D. Camarillo, 'Analysis of head acceleration events in collegiate-level American football: A combination of qualitative video analysis and in-vivo head kinematic measurement', *J Biomech*, vol. 110, p. 109969, Sep. 2020, doi: 10.1016/j.jbiomech.2020.109969.
- [265] D. A. Patton et al., 'Head Impact Sensor Studies In Sports: A Systematic Review Of Exposure Confirmation Methods', Ann Biomed Eng, vol. 48, no. 11, pp. 2497–2507, Nov. 2020, doi: 10.1007/s10439-020-02642-6.
- [266] A. Post *et al.*, 'Analysis of speed accuracy using video analysis software', *Sports Eng*, vol. 21, no. 3, pp. 235–241, Sep. 2018, doi: 10.1007/s12283-018-0263-4.
- [267] J. Newman et al., 'A NEW BIOMECHANICAL ASSESSMENT OF MILD TRAUMA TIC BRAIN INJURY PART 1-METHODOLOGY', in *IRCOBI Conference*, 1999, pp. 17–36.
- [268] D. A. Patton, C. M. Huber, C. C. McDonald, S. S. Margulies, C. L. Master, and K. B. Arbogast, 'Video Confirmation of Head Impact Sensor Data From High School Soccer Players', *Am J Sports Med*, vol. 48, no. 5, pp. 1246–1253, Apr. 2020, doi: 10.1177/0363546520906406.
- [269] D. R. L. Powell, F. J. Petrie, P. D. Docherty, H. Arora, and E. M. P. Williams, 'Development of a Head Acceleration Event Classification Algorithm for Female Rugby

- Union', *Ann Biomed Eng*, vol. 51, no. 6, pp. 1322–1330, Jun. 2023, doi: 10.1007/s10439-023-03138-9.
- [270] N. Cortes *et al.*, 'Video Analysis Verification of Head Impact Events Measured by Wearable Sensors', *Am J Sports Med*, vol. 45, no. 10, pp. 2379–2387, Aug. 2017, doi: 10.1177/0363546517706703.
- [271] L. J. Gibson and M. F. Ashby, Eds., 'Energy absorption in cellular materials', in Cellular Solids: Structure and Properties, 2nd ed., in Cambridge Solid State Science Series., Cambridge: Cambridge University Press, 1997, pp. 309–344. doi: 10.1017/CBO9781139878326.010.
- [272] S. Ankrah and N. J. Mills, 'Analysis Of Ankle Protection In Association Football', Sports Engineering, vol. 7, pp. 41–52, 2004.
- [273] L. Di Landro, G. Sala, and D. Olivieri, 'Deformation mechanisms and energy absorption of polystyrene foams for protective helmets', *Polymer Testing*, vol. 21, no. 2, pp. 217–228, Jan. 2002, doi: 10.1016/S0142-9418(01)00073-3.
- [274] S. R. G. Bates, I. R. Farrow, and R. S. Trask, '3D printed elastic honeycombs with graded density for tailorable energy absorption', in *Society of PhotoOptical Instrumentation Engineers (SPIE)*, G. Park, Ed., Las Vegas, Nevada, United States, Apr. 2016. doi: 10.1117/12.2219322.
- [275] I. S. Scher, L. L. Stepan, J. E. Shealy, and R. W. Hoover, 'Examining ski area padding for head and neck injury mitigation', *Journal of Science and Medicine in Sport*, vol. 24, no. 10, pp. 1010–1014, Oct. 2021, doi: 10.1016/j.jsams.2020.04.019.
- [276] O. Duncan, 'Fast optimisation of honeycombs for impact protection', *International Journal of Impact Engineering*, vol. 189, p. 104973, Jul. 2024, doi: 10.1016/j.ijimpeng.2024.104973.
- [277] J. A. Newman, 'Biomechanics of Human Trauma: Head Protection', in *Accidental Injury: Biomechanics and Prevention*, A. M. Nahum and J. W. Melvin, Eds., New York, NY: Springer, 1993, pp. 292–310. doi: 10.1007/978-1-4757-2264-2_13.
- [278] M. A. Forero Rueda, L. Cui, and M. D. Gilchrist, 'Optimisation of energy absorbing liner for equestrian helmets. Part I: Layered foam liner', *Materials & Design*, vol. 30, no. 9, pp. 3405–3413, Oct. 2009, doi: 10.1016/j.matdes.2009.03.037.
- [279] S. Janbaz, K. Narooei, T. Van Manen, and A. A. Zadpoor, 'Strain rate-dependent mechanical metamaterials', *Sci. Adv.*, vol. 6, no. 25, p. eaba0616, Jun. 2020, doi: 10.1126/sciadv.aba0616.
- [280] A. Post, T. B. Hoshizaki, and S. Brien, 'Head Injuries, Measurement Criteria, and Helmet Design', in *Handbook of Ergonomics in Sport and Exercise*, New York: Routledge Publishers, 2013.

- [281] E. Spyrou and T. B. Hoshizaki, 'Shock absorbing effectiveness of hockey helmet liner foams after exposure to repeated impacts', in *Materials and Science in Sports.*, F. H. Froes and S. J. Haake, Eds., Warrendale, Minerals, Metals, & Materials Society, 2001, pp. 199–209.
- [282] N. Bailly, Y. Petit, J.-M. Desrosier, O. Laperriere, S. Langlois, and E. Wagnac, 'Strain Rate Dependent Behavior of Vinyl Nitrile Helmet Foam in Compression and Combined Compression and Shear', *Applied Sciences*, vol. 10, no. 22, Art. no. 22, Jan. 2020, doi: 10.3390/app10228286.
- [283] E. S. Walsh *et al.*, 'Dynamic impact response characteristics of a helmeted Hybrid III headform using a centric and non-centric impact protocol', *Proceedings of the Institution of Mechanical Engineers, Part P: Journal of Sports Engineering and Technology*, vol. 226, no. 3–4, pp. 220–225, Sep. 2012, doi: 10.1177/1754337112442299.
- [284] A. Post, A. Oeur, B. Hoshizaki, and M. D. Gilchrist, 'Examination of the relationship between peak linear and angular accelerations to brain deformation metrics in hockey helmet impacts', *Comput Methods Biomech Biomed Engin*, vol. 16, no. 5, pp. 511–519, 2013, doi: 10.1080/10255842.2011.627559.
- [285] M. Bottlang, A. Rouhier, S. Tsai, J. Gregoire, and S. M. Madey, 'Impact Performance Comparison of Advanced Bicycle Helmets with Dedicated Rotation-Damping Systems', *Ann Biomed Eng*, vol. 48, no. 1, pp. 68–78, 2020, doi: 10.1007/s10439-019-02328-8.
- [286] A. J. Roseveare, D. J. Plant, and M. Ghajari, 'A New Helmet-liner Design for Improved Survivability', presented at the IRCOBI Conference, Malaga, Spain, 2016.
- [287] 'MIPS(TM)'. [Online]. Available: https://mipsprotection.com/
- [288] H. von Holst and P. Halldin, 'Protective helmet', US6658671B1, Dec. 09, 2003
- [289] P. Halldin, M. Aare, S. Kleiven, and H. Holst, 'Improved helmet design and test methods to reduce rotational induced brain injuries', in RTO Specialist Meeting, the NATO's Research and Technology Organization (RTO). 2003.
- [290] P. Halldin, A. Gilchrist, and N. J. Mills, 'A new oblique impact test for motorcycle helmets', *International Journal of Crashworthiness*, vol. 6, no. 1, pp. 53–64, Jan. 2001, doi: 10.1533/cras.2001.0162.
- [291] A. Post and T. Blaine Hoshizaki, 'Rotational Acceleration, Brain Tissue Strain, and the Relationship to Concussion', *Journal of Biomechanical Engineering*, vol. 137, no. 030801, Mar. 2015, doi: 10.1115/1.4028983.

- [292] P. Rousseau, E. Walsh, S. Foreman, and T. B. Hoshizaki, 'The Effect of Impact Condition on the Relationship Between Linear and Angular Acceleration', presented at the ISBS-Conference, 2009.
- [293] T. A. Smith, P. D. Halstead, E. McCalley, S. A. Kebschull, S. Halstead, and J. Killeffer, 'Angular head motion with and without head contact: implications for brain injury', *Sports Eng*, vol. 18, no. 3, pp. 165–175, Sep. 2015, doi: 10.1007/s12283-015-0175-5.
- [294] MLA Ltd., '2022 Defender Hybrid Public Order Helmet Specification'. 2022.
 Accessed: Nov. 05, 2022. [Online]. Available:
 https://www.mlaltd.co.uk/storage/app/uploads/public/621/cd8/1d7/621cd81d77e8f8
 43980584.pdf
- [295] I. Khan, A. Shinde, S. Khandelwal, V. Sah, and B. Narendiranath, 'FINITE ELEMENT Analysis On Different Materials For Motorcycle Helmet Shell.', *International Research Journal of Engineering and Technology*, vol. 6, no. 5, pp. 4581–4586, 2019.
- [296] C. Elanchezhian, B. V. Ramnath, and J. Hemalatha, 'Mechanical Behaviour of Glass and Carbon Fibre Reinforced Composites at Varying Strain Rates and Temperatures', Procedia Materials Science, vol. 6, pp. 1405–1418, Jan. 2014, doi: 10.1016/j.mspro.2014.07.120.
- [297] O. Buzzi, S. Fityus, Y. Sasaki, and S. Sloan, 'Structure and properties of expanding polyurethane foam in the context of foundation remediation in expansive soil', Mechanics of Materials, vol. 40, no. 12, pp. 1012–1021, Dec. 2008, doi: 10.1016/j.mechmat.2008.07.002.
- [298] B.K. Hwang, S.K. Kim, J.H. Kim, J.D. Kim, and J.M. Lee, 'Dynamic compressive behavior of rigid polyurethane foam with various densities under different temperatures', *International Journal of Mechanical Sciences*, vol. 180, p. 105657, Aug. 2020, doi: 10.1016/j.ijmecsci.2020.105657.
- [299] M. K. Neilsen, R. D. Krieg, and H. L. Schreyer, 'A constitutive theory for rigid polyurethane foam', *Polymer Engineering & Science*, vol. 35, no. 5, pp. 387–394, 1995, doi: 10.1002/pen.760350503.
- [300] W. Chen, F. Lu, and N. Winfree, 'High-strain-rate compressive behavior of a rigid polyurethane foam with various densities', *Experimental Mechanics*, vol. 42, no. 1, pp. 65–73, Mar. 2002, doi: 10.1007/BF02411053.
- [301] 'GENTEX Corp.' 600 N. Centennial St., Zeeland, MI,. USA. https://gentexcorp.com/.
- [302] K. A. Stokes *et al.*, 'Does reducing the height of the tackle through law change in elite men's rugby union (The Championship, England) reduce the incidence of

- concussion? A controlled study in 126 games', *Br J Sports Med*, vol. 55, no. 4, pp. 220–225, Feb. 2021, doi: 10.1136/bjsports-2019-101557.
- [303] S. Hendricks *et al.*, "Tackling" rugby safety through a collective approach', *Br J Sports Med*, vol. 57, no. 10, pp. 562–563, May 2023, doi: 10.1136/bjsports-2023-107020.
- [304] M. G. Tawell, 'Kinetic energy less lethal weapons and their associated blunt trauma injuries', Cranfield University, 2010. [Online]. Available: http://dspace.lib.cranfield.ac.uk/handle/1826/4655
- [305] M. Aare and S. Kleiven, 'Evaluation of head response to ballistic helmet impacts using the finite element method', *International Journal of Impact Engineering*, vol. 34, no. 3, pp. 596–608, Mar. 2007, doi: 10.1016/j.ijimpeng.2005.08.001.
- [306] R. L. Stalnaker, J. W. Melvin, G. S. Nusholtz, N. M. Alem, and J. B. Benson, 'Head Impact Response', *Transactions*, vol. 86. pp. 3156–3170, 1977. [Online]. Available: https://about.jstor.org/terms
- [307] H.-C. Shih, 'A Survey of Content-Aware Video Analysis for Sports', *IEEE Transactions on Circuits and Systems for Video Technology*, vol. 28, no. 5, pp. 1212–1231, May 2018, doi: 10.1109/TCSVT.2017.2655624.
- [308] P. N. Carter, E. E. Hall, C. J. Ketcham, and O. H. Ahmed, 'Not Just for Dancing? A Content Analysis of Concussion and Head Injury Videos on TikTok', *Front. Sports Act. Living*, vol. 3, Oct. 2021, doi: 10.3389/fspor.2021.692613.
- [309] M. Makdissi and G. Davis, 'Using video analysis for concussion surveillance in Australian football', *J Sci Med Sport*, vol. 19, no. 12, pp. 958–963, Dec. 2016, doi: 10.1016/j.jsams.2016.02.014.
- [310] S. W. West *et al.*, 'Caught on camera: a video assessment of suspected concussion and other injury events in women's rugby union', *J Sci Med Sport*, vol. 25, no. 10, pp. 805–809, Oct. 2022, doi: 10.1016/j.jsams.2022.07.008.
- [311] 'RIOT Footage of Riots from Around the World', youtube.com/@Heikki.M. Accessed: Feb. 24, 2022. [Online]. Available: https://www.youtube.com/watch?v=a5d3tEdnv_U&ab_channel=HeikkiM
- [312] Buzzfeed News, "You Are Not Losing The US Capitol!": What An Hour Looked Like For Police On Jan. 6'. Accessed: Feb. 24, 2022. [Online]. Available: https://www.buzzfeednews.com/article/zoetillman/capitol-riot-police-body-cam-footage
- [313] S. W. West *et al.*, 'Same name, same game, but is it different? An investigation of female rugby union match events in Canadian Varsity players', *International Journal of*

- Sports Science & Coaching, vol. 17, no. 5, pp. 1119–1127, Oct. 2022, doi: 10.1177/17479541211051961.
- [314] M. L. McHugh, 'Interrater reliability: the kappa statistic', *Biochemia Medica*, vol. 22, no. 3, pp. 276–282, 2012.
- [315] On Demand News, *Police Officer Knocked Off Horse in Shocking Incident at London Protest*, (Jun. 07, 2020). Accessed: Feb. 24, 2022. [Online Video]. Available: https://www.youtube.com/watch?v=89diMZg-uCA
- [316] P. Gervais, P. Baudin, B. Cruikshank, and D. L. Dahlstedt, 'Comparative analysis between police batons', *Forensic Science International*, vol. 91, no. 1, pp. 7–17, Jan. 1998, doi: 10.1016/S0379-0738(97)00177-1.
- [317] A. Roberts, L. Nokes, S. Leadbeatter, and H. Pike, 'Impact characteristics of two types of police baton', *Forensic Sci Int*, vol. 67, no. 1, pp. 49–53, Jun. 1994, doi: 10.1016/0379-0738(94)90411-1.
- [318] A. R. MacIntosh and G. T. Desmoulin, 'Police Officer performance and perception using light, medium and heavy weight tactical batons', *Applied Ergonomics*, vol. 75, pp. 178–183, Feb. 2019, doi: 10.1016/j.apergo.2018.10.004.
- [319] J. M. Clark, T. B. Hoshizaki, A. N. Annaidh, and M. D. Gilchrist, 'Equestrian Helmet Standards: Do They Represent Real-World Accident Conditions?', *Annals of Biomedical Engineering*, vol. 48, no. 8, pp. 2247–2267, Aug. 2020, doi: 10.1007/s10439-020-02531-y.
- [320] J. M. Clark *et al.*, 'Proposed injury thresholds for concussion in equestrian sports', *Journal of Science and Medicine in Sport*, vol. 23, no. 3, pp. 222–236, Mar. 2020, doi: 10.1016/j.jsams.2019.10.006.
- [321] T. B. VanItallie, 'Traumatic brain injury (TBI) in collision sports: Possible mechanisms of transformation into chronic traumatic encephalopathy (CTE)', *Metabolism*, vol. 100, p. 153943, Nov. 2019, doi: 10.1016/j.metabol.2019.07.007.
- [322] E. L. Abner *et al.*, 'Self-Reported Head Injury and Risk of Late-Life Impairment and AD Pathology in an AD Center Cohort', *Dementia and Geriatric Cognitive Disorders*, vol. 37, no. 5–6, pp. 294–306, Dec. 2013, doi: 10.1159/000355478.
- [323] M. Hajiaghamemar, M. Seidi, J. R. Ferguson, and V. Caccese, 'Measurement of Head Impact Due to Standing Fall in Adults Using Anthropomorphic Test Dummies', *Annals of Biomedical Engineering*, vol. 43, no. 9, pp. 2143–2152, Sep. 2015, doi: 10.1007/s10439-015-1255-1.
- [324] E. G. Takhounts, R. H. Eppinger, J. Q. Campbell, R. E. Tannous, E. D. Power, and L. S. Shook, 'On the Development of the SIMon Finite Element Head Model', *Stapp Car Crash Journal*, vol. 47, pp. 107–133, 2003.

- [325] H. Mao *et al.*, 'Development of a finite element human head model partially validated with thirty five experimental cases', *Journal of Biomechanical Engineering*, vol. 135, no. 11, 2013, doi: 10.1115/1.4025101.
- [326] S. Ji *et al.*, 'Parametric Comparisons of Intracranial Mechanical Responses from Three Validated Finite Element Models of the Human Head', *Ann Biomed Eng*, vol. 42, no. 1, pp. 11–24, Jan. 2014, doi: 10.1007/s10439-013-0907-2.
- [327] D. Bruneau, D. Cronin, M. Panzer, S. Giudice, and R. Kent, 'Comparison of the hybrid III head and neck to a detailed head and neck finite element model with active musculature', in *IRCOBI Conference*, Athens, Greece, 2018, pp. 322–323.
- [328] Z. J. Wang, B. Loeber, A. Tesny, G. Hu, and Y. S. Kang, 'Neck Biofidelity Comparison of THOR-AV, THOR and Hybrid III 50th Dummies', in *IRCOBI Conference*, 2021, pp. 136–156.
- [329] K. Upadhyay *et al.*, 'Effect of Human Head Shape on the Risk of Traumatic Brain Injury: A Gaussian Process Regression-Based Machine Learning Approach', *Military Medicine*, vol. 189, no. Supplement_3, pp. 608–617, Aug. 2024, doi: 10.1093/milmed/usae199.
- [330] R. A. Oeur, M. D. Gilchrist, and T. B. Hoshizaki, 'Interaction of impact parameters for simulated falls in sport using three different sized Hybrid III headforms', International Journal of Crashworthiness, vol. 24, no. 3, pp. 326–335, May 2019, doi: 10.1080/13588265.2018.1441617.
- [331] K. Brolin, 'Human Body Models', in *Transport Planning and Traffic Safety: Making Cities, Roads, and Vehicles Safer*, 1st ed., G. Tiwari and D. Mohan, Eds., Boca Raton: CRC Press, 2016, pp. 175–186. doi: 10.1201/b19737.
- [332] X. Li, A. von Schantz, M. Fahlstedt, and P. Halldin, 'Evaluating child helmet protection and testing standards: A study using PIPER child head models aged 1.5, 3, 6, and 18 years', *PLOS ONE*, vol. 19, no. 1, p. e0286827, Jan. 2024, doi: 10.1371/journal.pone.0286827.
- [333] M. Hajiaghamemar, M. Seidi, V. Caccese, and M. Shahinpoor, 'CHARACTERISTICS OF FALLING IMPACT OF HEAD USING A TEST DUMMY', in *International Mechanical Engineering Congress & Exposition IMECE*, 2013.
- [334] E. S. Walsh, P. Rousseau, and T. B. Hoshizaki, 'The influence of impact location and angle on the dynamic impact response of a Hybrid III headform', *Sports Engineering*, vol. 13, no. 3, pp. 135–143, Mar. 2011, doi: 10.1007/s12283-011-0060-9.
- [335] R. A. Oeur, M. D. Gilchrist, and T. B. Hoshizaki, 'Parametric study of impact parameters on peak head acceleration and strain for collision impacts in sport',

- International Journal of Crashworthiness, vol. 26, no. 1, pp. 16–25, 2021, doi: 10.1080/13588265.2019.1634336.
- [336] D. Haid, O. Duncan, J. Hart, and L. Foster, 'Free-fall drop test with interchangeable surfaces to recreate concussive ice hockey head impacts', *Sports Engineering*, vol. 26, no. 1, Dec. 2023, doi: 10.1007/s12283-023-00416-6.
- [337] S. de Grau, A. Post, A. Meehan, L. Champoux, T. B. Hoshizaki, and M. D. Gilchrist, 'Protective capacity of ice hockey helmets at different levels of striking compliance', Sports Eng, vol. 23, no. 1, p. 11, Jun. 2020, doi: 10.1007/s12283-020-00325-y.
- [338] S. de Grau, A. Post, T. B. Hoshizaki, and M. D. Gilchrist, 'Effects of surface compliance on the dynamic response and strains sustained by a player's helmeted head during ice hockey impacts', *Journal of Sports Engineering and Technology*, vol. 234, no. 1, pp. 98–106, Mar. 2020, doi: 10.1177/1754337119871866.
- [339] J. M. Clark, K. Taylor, A. Post, T. B. Hoshizaki, and M. D. Gilchrist, 'Comparison of Ice Hockey Goaltender Helmets for Concussion Type Impacts', *Ann Biomed Eng*, vol. 46, no. 7, pp. 986–1000, Jul. 2018, doi: 10.1007/s10439-018-2017-7.
- [340] D. Schorah, S. Choppin, and D. James, 'Effects of moment of inertia on restricted motion swing speed', *Sports Biomech*, vol. 14, no. 2, pp. 157–167, Jun. 2015, doi: 10.1080/14763141.2015.1027949.
- [341] R. Cross, 'Impact of sports balls with striking implements', *Sports Eng*, vol. 17, no. 1, pp. 3–22, Mar. 2014, doi: 10.1007/s12283-013-0132-0.
- [342] R. Cross and R. Bower, 'Effects of swing-weight on swing speed and racket power', *J Sports Sci*, vol. 24, no. 1, pp. 23–30, Jan. 2006, doi: 10.1080/02640410500127876.
- [343] A. M. Nathan, J. J. Crisco, R. M. Greenwald, D. A. Russell, and L. V. Smith, 'A comparative study of baseball bat performance', *Sports Engineering*, vol. 13, no. 4, pp. 153–162, Jul. 2011, doi: 10.1007/s12283-011-0065-4.
- [344] L. Smith, J. Broker, and A. M. Nathan, 'A study of softball player swing speed', in *Sports Dynamics: Discovery and application*, A. Subic, P. Travailo, and F. Alam, Eds., Melbourne, VIC: RMIT University., 2003, pp. 12–17.
- [345] J. B. Morgan and C. B. Daish, 'The Physics of Ball Games', *The Mathematical Gazette*, vol. 57, no. 401. p. 233, 1973. doi: 10.2307/3615603.
- [346] A. A. Shabana, 'Equations of Motion of Rigid Body Systems', in *Dynamics of Multibody Systems*, 4th ed., R. Schwertassek and R. E. Roberson, Eds., Cambridge University Press, 1988, pp. 145–147.
- [347] R. Gellner, M. Begonia, S. Gagliardi, G. Tierney, and S. Rowson, 'Optimal Cutoff Frequencies for Filtering Linear Acceleration and Angular Velocity Signals Associated

- with Laboratory Head Impacts Measured with Externally Mounted Sensors'. pp. 332–342, 2023.
- [348] H. W. Sampson, J. L. Montgomery, and G. L. Henryson, *Atlas of the Human Skull*. Texas A&M University Press, 1991.
- [349] Loose steel tubes for tube and coupler scaffolds. Technical delivery conditions, BS EN 39:2001, 2001. [Online]. Available: https://knowledge.bsigroup.com/products/loose-steel-tubes-for-tube-and-coupler-scaffolds-technical-delivery-conditions?version=standard
- [350] *MATLAB*. (2023). The MathWorks Inc., Natick, Massachusetts. [Online]. Available: https://www.mathworks.com
- [351] S. Urban, J. Leitloff, and S. Hinz, 'Improved wide-angle, fisheye and omnidirectional camera calibration', *ISPRS Journal of Photogrammetry and Remote Sensing*, vol. 108, pp. 72–79, Oct. 2015, doi: 10.1016/j.isprsjprs.2015.06.005.
- [352] D. Scaramuzza, A. Martinelli, and R. Siegwart, 'A Toolbox for Easily Calibrating Omnidirectional Cameras', in *Proceedings of IEEE International Workshop on Intelligent Robots and Systems*, Beijing, China: IEEE, 2006, pp. 5695–5701. doi: 10.1109/IROS.2006.282372.
- [353] J. Heikkila and O. Silven, 'A four-step camera calibration procedure with implicit image correction', in *Proceedings of IEEE Computer Society Conference on Computer Vision and Pattern Recognition*, Jun. 1997, pp. 1106–1112. doi: 10.1109/CVPR.1997.609468.
- [354] Z. Zhang, 'A flexible new technique for camera calibration', *IEEE Transactions on Pattern Analysis and Machine Intelligence*, vol. 22, no. 11, pp. 1330–1334, Nov. 2000, doi: 10.1109/34.888718.
- [355] Y. S. Kang, K. Moorhouse, and J. H. B. IV, 'Measurement of Six degrees of freedom head kinematics in impact conditions employing six accelerometers and three angular rate sensors (6aω configuration)', *Journal of Biomechanical Engineering*, vol. 133, no. 11, 2011, doi: 10.1115/1.4005427.
- [356] X. Yu, I. Logan, I. de Pedro Sarasola, A. Dasaratha, and M. Ghajari, 'The Protective Performance of Modern Motorcycle Helmets Under Oblique Impacts', *Ann Biomed Eng*, vol. 50, no. 11, pp. 1674–1688, Nov. 2022, doi: 10.1007/s10439-022-02963-8.
- [357] M. L. Bland, C. McNally, and S. Rowson, 'Headform and Neck Effects on Dynamic Response in Bicycle Helmet Oblique Impact Testing', in *IRCOBI conference*, 2018, pp. 413–423.
- [358] Y. Peng, J. Yang, C. Deck, D. Otte, and R. Willinger, 'Development of head injury risk functions based on real-world accident reconstruction', *International Journal of*

- *Crashworthiness*, vol. 19, no. 2, pp. 105–114, Mar. 2014, doi: 10.1080/13588265.2013.805290.
- [359] G. M. Watt and C. F. Finch, 'Preventing equestrian injuries. Locking the stable door', Sports Med, vol. 22, no. 3, pp. 187–197, Sep. 1996, doi: 10.2165/00007256-199622030-00005.
- [360] 'YouTube.com/@LondonCityWalks'. Accessed: Feb. 25, 2022. [Online]. Available: https://www.youtube.com/channel/UClTrXkVGaaLOywnISCYqVmQ
- [361] S. L. Zuckerman *et al.*, 'Functional and Structural Traumatic Brain Injury in Equestrian Sports: A Review of the Literature', *World Neurosurgery*, vol. 83, no. 6. Elsevier Inc., pp. 1098–1113, Jun. 2015. doi: 10.1016/j.wneu.2014.12.030.
- [362] R. T. Loder, 'The demographics of equestrian-related injuries in the United States: injury patterns, orthopedic specific injuries, and avenues for injury prevention', *J Trauma*, vol. 65, no. 2, pp. 447–460, Aug. 2008, doi: 10.1097/TA.0b013e31817dac43.
- [363] M. F. Hoffmann, M. Bernstorff, N. Kreitz, B. Roetman, T. A. Schildhauer, and K. E. Wenning, 'Horse-related injury patterns: a single center report', *J Orthop Surg Res*, vol. 18, no. 1, p. 83, Feb. 2023, doi: 10.1186/s13018-023-03549-3.
- [364] L. Meredith, R. Ekman, and R. Thomson, 'Horse-related incidents and factors for predicting injuries to the head', *BMJ Open Sport Exerc Med*, vol. 4, no. 1, Aug. 2018, doi: 10.1136/bmjsem-2018-000398.
- [365] F. M. Abu-Zidan and S. Rao, 'Factors affecting the severity of horse-related injuries', Injury, vol. 34, no. 12, pp. 897–900, Dec. 2003, doi: 10.1016/s0020-1383(03)00054-8.
- [366] S. B. Davidson, P. A. Blostein, A. Schrotenboer, C. A. Sloffer, and S. L. VandenBerg, 'Ten Years of Equine-related Injuries: Severity and Implications for Emergency Physicians', *J Emerg Med*, vol. 49, no. 5, pp. 605–612, Nov. 2015, doi: 10.1016/j.jemermed.2015.03.025.
- [367] T. Gibson, K. Thai, J. Saxon, and R. Pollock, 'The effectiveness of safety equipment in horse racing falls', presented at the IRCOBI Conference, Bern, Switzerland, 2008, pp. 453–456. doi: 10.1016/s0021-9290(07)70129-x.
- [368] C. N. J. McGhee, R. W. Gullan, and J. D. Miller, 'Horse Riding and Head Injury:

 Admissions to a Regional Head Injury Unit', *British Journal of Neurosurgery*, vol. 1, no.

 1, pp. 131–135, Jan. 1987, doi: 10.3109/02688698709034348.
- [369] P. R. Fleming, J. L. Crompton, and D. A. Simpson, 'Neuro-ophthalmological sequelae of horse-related accidents', Clin Exp Ophthalmol, vol. 29, no. 4, pp. 208–212, Aug. 2001, doi: 10.1046/j.1442-9071.2001.00430.x.
- [370] M. A. F. Rueda and M. D. Gilchrist, 'Equestrian Helmet Design: A Computational and Head Impact Biomechanics Simulation Approach', in *6th World Congress of*

- *Biomechanics (WCB)*, C. T. Lim and J. C. H. Goh, Eds., Singapore: Springer, 2010, pp. 205–208. doi: 10.1007/978-3-642-14515-5_53.
- [371] T. A. Connor *et al.*, 'Do equestrian helmets prevent concussion? A retrospective analysis of head injuries and helmet damage from real-world equestrian accidents', *Sports Med Open*, vol. 5, no. 1, p. 19, May 2019, doi: 10.1186/s40798-019-0193-0.
- [372] J. M. Clark *et al.*, 'Analysis of Helmet Damage and Associated Head Injuries Arising from Real-World Equestrian Fall Accidents', *Journal of Testing and Evaluation*, vol. 48, no. 3, pp. 2185–2195, May 2020, doi: 10.1520/JTE20190513.
- [373] K. Mutore, J. Lim, D. Fofana, A. Torres-Reveron, and J. J. Skubic, 'Hearing hoofbeats? Think head and neck trauma: a 10-year NTDB analysis of equestrian-related trauma in the USA', *Trauma Surg Acute Care Open*, vol. 6, no. 1, p. e000728, Sep. 2021, doi: 10.1136/tsaco-2021-000728.
- [374] N. Bourdet and R. Willinger, 'Head impact conditions in case of equestrian accident', in *IRCOBI Conference*, 2015, pp. 156–167.
- [375] Standard Specification for Protective Headgear Used in Horse Sports and Horseback Riding, ASTM F1163-15, 2015. [Online]. Available: https://www.astm.org/f1163-15.html
- [376] A. Post, T. B. Hoshizaki, M. D. Gilchrist, S. Brien, M. Cusimano, and S. Marshall, 'The dynamic response characteristics of traumatic brain injury', *Accident Analysis and Prevention*, vol. 79, pp. 33–40, 2015, doi: 10.1016/j.aap.2015.03.017.
- [377] X. Yu, C. E. Baker, and M. Ghajari, 'Head Impact Location, Speed and Angle from Falls and Trips in the Workplace', *Annals of Biomedical Engineering*, 2023, doi: 10.1007/s10439-023-03146-9.
- [378] A. Post *et al.*, 'Characterization of persistent concussive syndrome using injury reconstruction and finite element modelling', *Journal of the Mechanical Behavior of Biomedical Materials*, vol. 41, pp. 325–335, Jan. 2015, doi: 10.1016/j.jmbbm.2014.07.034.
- [379] M. C. Doorly and M. D. Gilchrist, 'The use of accident reconstruction for the analysis of traumatic brain injury due to head impacts arising from falls', *Comput Methods Biomech Biomed Engin*, vol. 9, no. 6, pp. 371–377, Dec. 2006, doi: 10.1080/10255840601003551.
- [380] W. Dawber, L. Foster, T. Senior, and J. Hart, 'Traumatic Brain Injury Predictions Amid Equestrian Activity With Realistic Biomechanical Constraints.', in *IRCOBI Conference Proceedings*, Cambridge, UK, 2023, pp. 637–638.
- [381] B. M. Potvin, O. M. G. Aguiar, V. Komisar, A. Sidhu, K. Elabd, and S. N. Robinovitch, 'A comparison of the magnitude and duration of linear and rotational head

- accelerations generated during hand-, elbow- and shoulder-to-head checks delivered by hockey players', *Journal of Biomechanics*, vol. 91, pp. 43–50, Jun. 2019, doi: 10.1016/j.jbiomech.2019.05.002.
- [382] N. G. Ibrahim and S. S. Margulies, 'Biomechanics of the toddler head during low-height falls: an anthropomorphic dummy analysis', *J Neurosurg Pediatr*, vol. 6, no. 1, pp. 57–68, Jul. 2010, doi: 10.3171/2010.3.PEDS09357.
- [383] A. Kaul, A. Abbas, G. Smith, S. Manjila, J. Pace, and M. Steinmetz, 'A revolution in preventing fatal craniovertebral junction injuries: lessons learned from the Head and Neck Support device in professional auto racing', *Journal of Neurosurgery: Spine*, vol. 25, no. 6, pp. 756–761, Dec. 2016, doi: 10.3171/2015.10.SPINE15337.
- [384] B. W. Schulz, W. E. Lee, and J. D. Lloyd, 'Estimation, simulation, and experimentation of a fall from bed', *JRRD*, vol. 45, no. 8, pp. 1227–1236, 2008, doi: 10.1682/JRRD.2007.06.0092.
- [385] A. Post, T. B. Hoshizaki, M. D. Gilchrist, S. Brien, M. Cusimano, and S. Marshall, 'Traumatic brain injuries: the influence of the direction of impact', *Neurosurgery*, vol. 76, no. 1, pp. 81–91, Jan. 2015, doi: 10.1227/NEU.000000000000554.
- [386] B. Hoshizaki, A. Post, M. Kendall, C. Karton, and S. Brien, 'The Relationship between Head Impact Characteristics and Brain Trauma', *J Neurol Neurophysiol*, vol. 05, no. 01, 2013, doi: 10.4172/2155-9562.1000181.
- [387] P. A. Cripton, D. M. Dressler, C. A. Stuart, C. R. Dennison, and D. Richards, 'Bicycle helmets are highly effective at preventing head injury during head impact: Head-form accelerations and injury criteria for helmeted and unhelmeted impacts', *Accident Analysis and Prevention*, vol. 70, pp. 1–7, 2014, doi: 10.1016/j.aap.2014.02.016.
- [388] B. Fréchède, A. McIntosh, R. Grzebieta, and M. Bambach, 'Hybrid III ATD in inverted impacts: Influence of impact angle on neck injury risk assessment', *Annals of Biomedical Engineering*, vol. 37, no. 7, pp. 1403–1414, Jul. 2009, doi: 10.1007/s10439-009-9711-4.
- [389] D. M. Brouwer, J. Bennik, J. Leideman, H. M. J. R. Soemers, and S. Stramigioli, 'Mechatronic design of a fast and long range 4 degrees of freedom humanoid neck', Proceedings - IEEE International Conference on Robotics and Automation, pp. 574– 579, 2009, doi: 10.1109/ROBOT.2009.5152585.
- [390] J. Lloyd and F. Conidi, 'Brain injury in sports', *Journal of Neurosurgery*, vol. 124, no.3, pp. 667–674, Mar. 2016, doi: 10.3171/2014.11.JNS141742.
- [391] NOCSAE, Standard Performance Specification for Newly Manufactured Ice Hockey Helmets, ND 030, 2016. [Online]. Available: https://nocsae.org/wp-

- content/uploads/2018/05/ND030-
- 11m16MfrdIceHockeyHelmetsStandardPerformance.pdf
- [392] Industrial safety helmets, BS EN 397:2012, 2012. [Online]. Available: https://knowledge.bsigroup.com/products/industrial-safety-helmets?version=standard
- [393] HIWIN Technologies Corp., 'Linear Guideways Technical Information', 2019. Accessed: Mar. 05, 2022. [Online]. Available: www.hiwin.tw
- [394] Aalco Metals Ltd., 'General Material Datasheet'. 2011. [Online]. Available: aalco.co.uk
- [395] Norgren, 'ISOLine(TM) 15552 ctlinder, double acting shock absorbers technical datsheet'. 2016.
- [396] V. W. J. Chung, L. Dias, G. Booth, and P. A. Cripton, 'Incorporating neck biomechanics in helmet testing: Evaluation of commercially available WaveCel helmets', *Clin Biomech (Bristol)*, vol. 94, p. 105628, Apr. 2022, doi: 10.1016/j.clinbiomech.2022.105628.
- [397] Ansys Academic Research Mechanical. (2018).
- [398] D. M. Elsherif, A. A. Abd El-Wahab, and M. H. Abdellatif, 'Factors affecting stress distribution in wind turbine blade', *IOP Conf. Ser.: Mater. Sci. Eng.*, vol. 610, no. 1, p. 012020, Sep. 2019, doi: 10.1088/1757-899X/610/1/012020.
- [399] W. Zhang, X. Yuan, C. Chen, and L. Yang, 'Finite element analysis of steel wire ropes considering creep and analysis of influencing factors of creep', *Engineering Structures*, vol. 229, Feb. 2021, doi: 10.1016/j.engstruct.2020.111665.
- [400] W. Morgan, 'Rioter hit by two bricks in 10 seconds and the second is a low blow', Birmingham Live. Accessed: Nov. 09, 2024. [Online]. Available: https://www.birminghammail.co.uk/news/uk-news/southport-rioter-hit-two-bricks-29646532
- [401] O. N. Aneziris *et al.*, 'Occupational risk quantification owing to falling objects', *Safety Science*, vol. 69, pp. 57–70, Nov. 2014, doi: 10.1016/j.ssci.2014.02.017.
- [402] M. Ptak, M. Dymek, D. Wdowicz, A. Szumiejko, and A. Kwiatkowski, 'Energy-absorbing limitations of hard hat safety helmets in mitigating trauma from falling objects', *Arch. Civ. Mech. Eng.*, vol. 24, no. 4, p. 199, Jul. 2024, doi: 10.1007/s43452-024-01012-6.
- [403] E. Khashaba, M. El-Helaly, A. H. El-Gilany, S. M. Motawei, and S. Foda, 'Risk factors for non-fatal occupational injuries among construction workers: A case-control study', *Toxicol Ind Health*, vol. 34, no. 2, pp. 83–90, Feb. 2018, doi: 10.1177/0748233717733853.

- [404] H. Kim, A. Colantonio, and M. Chipman, 'Traumatic brain injury occurring at work', *NeuroRehabilitation*, vol. 21, no. 4, pp. 269–278, 2006.
- [405] B. Haseltine, 'Bricks and Brickwork', in *Construction Materials Reference Book*, 2nd ed., Routledge, 2013, pp. 125–134.
- [406] Specification for clay bricks, BS 3921:1985, 1985.
- [407] Specification for masonry units Manufactured stone masonry units, BS EN 771-5:2011+A1:2015, 2011.
- [408] The Building Regulations 2C: Thickness of walls in small buildings., 2010.
 Accessed: Nov. 11, 2024. [Online]. Available:
 https://assets.publishing.service.gov.uk/media/5a80437640f0b623026927b2/BR_PDF
 _AD_A_2013.pdf
- [409] A. Burden, 'Uniform acceleration and projectile motion', in *Instant Notes in Sport and Exercise Biomechanics*, 2nd ed., London, UK: Routledge, 2019, pp. 44–55.
- [410] R. Cross, 'Physics of overarm throwing', *American Journal of Physics*, vol. 72, no. 3, pp. 305–312, Mar. 2004, doi: 10.1119/1.1634964.
- [411] Tracker: Video Analysis and Modelling Tool. Open Source Physics. Accessed: Mar. 09, 2024. [Online]. Available: https://www.compadre.org/OSP/items/detail.cfm?ID=7365
- [412] D. Brown and A. J. Cox, 'Innovative Uses of Video Analysis', *Physics Education*, vol.47, no. 4, pp. 145–150, Mar. 2009, doi: 10.1119/1.3081296.
- [413] L. K. Wee, C. Chew, G. H. Goh, S. Tan, and T. L. Lee, 'Using Tracker as a pedagogical tool for understanding projectile motion', *Phys. Educ.*, vol. 47, no. 4, p. 448, Jul. 2012, doi: 10.1088/0031-9120/47/4/448.
- [414] *Matlab: 'Curve Fitting Toolbox'*. (2020). MathWorks, Natick, Massachusetts. [Online]. Available: https://www.mathworks.com/products/curvefitting.html.
- [415] N. Yoganandan and F. A. Pintar, 'Biomechanics of temporo-parietal skull fracture', Clin Biomech (Bristol), vol. 19, no. 3, pp. 225–239, Mar. 2004, doi: 10.1016/j.clinbiomech.2003.12.014.
- [416] M. Hitosugi, H. Murayama, Y. Motozawa, K. Ishii, M. Ogino, and K. Koyama, 'Biomechanical analysis of acute subdural hematoma resulting from judo', *Biomed Res*, vol. 35, no. 5, pp. 339–344, 2014, doi: 10.2220/biomedres.35.339.
- [417] B. Fréchède and A. S. McIntosh, 'Numerical reconstruction of real-life concussive football impacts', *Med Sci Sports Exerc*, vol. 41, no. 2, pp. 390–398, Feb. 2009, doi: 10.1249/MSS.0b013e318186b1c5.

- [418] M. Fahlstedt, K. Baeck, P. Halldin, J. V. Sloten, J. Goffin, and B. Depreitere, 'Influence of Impact Velocity and Angle in a Detailed Reconstruction of a Bicycle Accident', presented at the IRCOBI Conference, Dublin, Ireland, 2012, pp. 787–799.
- [419] P. G. Petersen, L. V. Smith, and D. Nevins, 'The effect of surface roughness on oblique bicycle helmet impact tests', *Proceedings of the Institution of Mechanical Engineers, Part P: Journal of Sports Engineering and Technology*, vol. 234, no. 4, pp. 320–327, Dec. 2020, doi: 10.1177/1754337120917809.
- [420] M. L. Bland, C. McNally, and S. Rowson, 'Differences in Impact Performance of Bicycle Helmets during Oblique Impacts', *Journal of Biomechanical Engineering*, vol. 140, no. 9, Sep. 2018, doi: 10.1115/1.4040019.
- [421] N. J. Mills, S. Wilkes, S. Derler, and A. Flisch, 'FEA of oblique impact tests on a motorcycle helmet', *International Journal of Impact Engineering*, vol. 36, no. 7, pp. 913–925, Jul. 2009, doi: 10.1016/j.ijimpeng.2008.12.011.
- [422] C. Harrison and K. Robinette, 'Principles of Fit to Optimize Helmet Sizing', NATO Air Force Research Laboratory, 2005. [Online]. Available: http://www.rto.nato.int/abstracts.asp.
- [423] A. Gilchrist, N. J. Mills, and T. Khan, 'Survey of head, helmet and headform sizes related to motorcycle helmet design', *Ergonomics*, vol. 31, no. 10, pp. 1395–1412, 1988, doi: 10.1080/00140138808966784.
- [424] K. T. Thai, A. S. McIntosh, and T. Y. Pang, 'Bicycle helmet size, adjustment, and stability', *Traffic Inj Prev*, vol. 16, pp. 268–275, 2015, doi: 10.1080/15389588.2014.931948.
- [425] Protective helmets. Test methods Shock absorption, BS EN 13087-2:2012, 2012.
- [426] A. Gilchrist and N. Mills, 'Dynamic Testing of the Strength of Helmet Chin Straps', Journal of Testing and Evaluation, vol. 21, no. 6, pp. 488–493, Nov. 1993, doi: 10.1520/JTE11796J.
- [427] L. Shi, Y. Han, H. Huang, J. Davidsson, and R. Thomson, 'Evaluation of injury thresholds for predicting severe head injuries in vulnerable road users resulting from ground impact via detailed accident reconstructions', *Biomech Model Mechanobiol*, vol. 19, no. 5, pp. 1845–1863, Oct. 2020, doi: 10.1007/s10237-020-01312-9.
- [428] E. NCAP, 'TB035: Brain Injury Calculation'. 2023.
- [429] F. Wang, Z. Wang, L. Hu, H. Xu, C. Yu, and F. Li, 'Evaluation of Head Injury Criteria for Injury Prediction Effectiveness: Computational Reconstruction of Real-World Vulnerable Road User Impact Accidents', *Frontiers in Bioengineering and Biotechnology*, vol. 9, Jun. 2021, doi: 10.3389/fbioe.2021.677982.

- [430] M. A. Forero Rueda and M. D. Gilchrist, 'Comparative multibody dynamics analysis of falls from playground climbing frames', *Forensic Science International*, vol. 191, no. 1, pp. 52–57, Oct. 2009, doi: 10.1016/j.forsciint.2009.06.007.
- [431] A. A. Weaver, K. A. Danelson, and J. D. Stitzel, 'Modeling Brain Injury Response for Rotational Velocities of Varying Directions and Magnitudes', *Ann Biomed Eng*, vol. 40, no. 9, pp. 2005–2018, Sep. 2012, doi: 10.1007/s10439-012-0553-0.
- [432] J. Usman, A. S. McIntosh, K. Quarrie, and S. Targett, 'Shoulder injuries in elite rugby union football matches: Epidemiology and mechanisms', *Journal of Science and Medicine in Sport*, vol. 18, no. 5, pp. 529–533, Sep. 2015, doi: 10.1016/j.jsams.2014.07.020.
- [433] C. Zhou, T. B. Khalil, and A. I. King, 'A New Model Comparing Impact Responses of the Homogeneous and Inhomogeneous Human Brain', *SAE Transactions Section* 6: *Journal of Passenger Cars, Part 2*, vol. 104, pp. 2999–3015, 1995.
- [434] P. Arrué, N. Toosizadeh, H. Babaee, and K. Laksari, 'Low-Rank Representation of Head Impact Kinematics: A Data-Driven Emulator', *Front. Bioeng. Biotechnol.*, vol. 8, p. 555493, Sep. 2020, doi: 10.3389/fbioe.2020.555493.
- [435] J. Farmer, S. Mitchell, P. Sherratt, and Y. Miyazaki, 'A human surrogate neck for traumatic brain injury research', *Front. Bioeng. Biotechnol.*, vol. 10, Dec. 2022, doi: 10.3389/fbioe.2022.854405.
- [436] Helmets for fire fighting in buildings and other structures, BS EN 443:2008, 2008.
- [437] C. K. Donat *et al.*, 'From biomechanics to pathology: predicting axonal injury from patterns of strain after traumatic brain injury', *Brain*, vol. 144, no. 1, pp. 70–91, Jan. 2021, doi: 10.1093/brain/awaa336.
- [438] M. N. Abdullah, F. Mustapha, M. K. H. Muda, M. K. A. Arrifin, A. S. M. Rafie, and M. A. Shamsudin, 'SIMULATING BIO-COMPOSITE CYCLING HELMET PERFORMANCE THROUGH FEA AND CFD APPROACHES', Movement, Health & Exercise, vol. 4, no. 1, pp. 77–91, 2015.
- [439] N. J. Cecchi, H. V. Alizadeh, Y. Liu, and D. B. Camarillo, 'Finite element evaluation of an American football helmet featuring liquid shock absorbers for protecting against concussive and subconcussive head impacts', *Frontiers in Bioengineering and Biotechnology*, vol. 11, Jun. 2023, doi: 10.3389/fbioe.2023.1160387.
- [440] C. E. Baker, X. Yu, B. Lovell, R. Tan, S. Patel, and M. Ghajari, 'How Well Do Popular Bicycle Helmets Protect from Different Types of Head Injury?', *Ann Biomed Eng*, vol. 52, no. 12, pp. 3326–3364, Dec. 2024, doi: 10.1007/s10439-024-03589-8.
- [441] Standard for Protective Headgear for Use in Competitive Automotive Sports, SA2015, 2014.

[442] Standard for Protective Headgear for Use in Elite Automotive Sports, EA2016, 2016. [Online]. Available: https://smf.org/standards/EA/EA2016/EA2016.pdf

Appendix

Ethics Approval

A.E.1 Developing an Improved Methodology for the Assessment of Public Order

Helmet Efficacy - Lab Impact Testing.

Ethics Review ID: ER40381534.

Workflow Status: Application Approved

Type of Ethics Review Template: No human participants, human tissue or personal

data.

Q1. General overview of study: Making recommendations of how to improve the

energy attenuation test standard for public order helmets. The research will

include laboratory-based equipment testing using instrumented anthropometric

test 'dummy' (ATD) body segments. ATDs will be subject to impacts to simulate

real world collisions using drop test methods. Data collected from the ATDs will be

kinematic data such as force, acceleration and impact duration which will be used

to understand the impact scenario and help advise recommendations to improve

the test standard with the primary goal of reducing concussion diagnosis rates in

public order officers.

Date of submission and supervisor sign-off: 31/01/2022

A.E.2 Developing an Improved Methodology for the Assessment of Public Order

Helmet Efficacy - Understanding Threats of Brain Injury Within Public Order

Situations

Ethics Review ID: ER44721174

Workflow Status: Application Approved

Type of Ethics Review Template: No human participants, human tissue or personal

data.

Q1. General overview of study: This study aims to improve our understanding of

the conditions within Public Order operations by studying media available within

the public domain. Specifically, news reels and YouTube clips of Public Order

251

operations found from internet search engines. Media will only be accessed through public web links and therefore, not stored. Clips will be monitored by the primary researcher (PhD Student) and incidents of blunt weaponry and scenarios where head injury is high-risk will be coded for content analysis. Weapons present within threatening scenarios will be categorised on how they are being used and their physical properties i.e., wielded wooden implements, metallic implements, thrown glass projectiles etc. This process will be repeated by another member of staff to assess inter-rater reliability of the method. The most prevalent and dangerous threats of head injury will be considered for use within a lab test that measures the injury characteristics, should a head impact occur. This test will utilise the Anthropometric Test Device (ATD, often referred to as a 'Crash Test Dummy') which is owned by SHU Sports Engineering Research Group. The ATD will be equipped with a UK Public Order standard helmet and impacts will simulate what occurs within analysed videos. The impacts will only be administered by the primary researcher. The kinematics of the head will be captured using the inertial sensors within the ATD and validated alongside high-speed video motion tracking. Data will be stored on the University networked storage platform. This data will advise test methodology that represents the threatening conditions faced within Public Order as closely as possible and in a repeatable manner.

Date of submission and supervisor sign-off: 08/08/2022

A.3 Causes of Head Injury in Public Order Conditions
A.3.1 Videos used for content analysis of head injury risk in PO activity.

Video ID	Durati on (s)	Web Link		
1	54	https://www.buzzfeednews.com/article/zoetillman/capitol-riot-police-		
	7	<u>body-cam-footage</u>		
2	223	https://www.buzzfeednews.com/article/zoetillman/capitol-riot-police-		
	223	<u>body-cam-footage</u>		
3	236	https://www.youtube.com/watch?v=a5d3tEdnv_U		
4	818	https://www.youtube.com/watch?v=Go3VBpMDCpA		
5	751	https://www.youtube.com/watch?v=Go3VBpMDCpA		
6	1798	https://www.youtube.com/watch?v=Go3VBpMDCpA		
7	357	https://www.youtube.com/watch?v=Go3VBpMDCpA		
8	97	https://www.youtube.com/watch?v=Go3VBpMDCpA		
9	276	https://www.youtube.com/watch?v=Go3VBpMDCpA		
10	183	https://www.youtube.com/watch?v=Go3VBpMDCpA		

11	212	https://www.youtube.com/watch?v=Go3VBpMDCpA
12	34	https://www.youtube.com/watch?v=Go3VBpMDCpA
13	76	https://www.youtube.com/watch?v=Go3VBpMDCpA
14	254	https://www.youtube.com/watch?v=Go3VBpMDCpA
15	60	https://www.youtube.com/watch?v=Go3VBpMDCpA
16	158	https://www.youtube.com/watch?v=Go3VBpMDCpA
17	83	https://www.youtube.com/watch?v=Go3VBpMDCpA
18	164	https://www.youtube.com/watch?v=Go3VBpMDCpA
19	266	https://www.youtube.com/watch?v=Go3VBpMDCpA
20	164	https://www.youtube.com/watch?v=Go3VBpMDCpA
21	336	https://www.youtube.com/watch?v=Go3VBpMDCpA
22	104	https://www.youtube.com/watch?v=Go3VBpMDCpA
23	150	https://www.youtube.com/watch?v=Go3VBpMDCpA
24	184	
25	431	https://www.youtube.com/watch?v=Go3VBpMDCpA https://www.youtube.com/watch?v=Go3VBpMDCpA
26	409	
27	80	https://www.youtube.com/watch?v=Go3VBpMDCpA https://www.youtube.com/watch?v=Go3VBpMDCpA
28	82	https://www.youtube.com/watch?v=Go3VBpMDCpA
29	123	https://www.youtube.com/watch?v=KeGFP4ZQWJA
30	317	https://www.youtube.com/watch?v=ZcFjRA6trVs
31	344	https://www.youtube.com/watch?v=CFfc4UWzVB8
32	255	https://www.youtube.com/watch?v=Lbd-ezFKd5g
33	173	https://www.youtube.com/watch?v=DmtevA2oe5k
34	699	https://www.youtube.com/watch?v=S 4FluN2Wsk
35	141	https://www.youtube.com/watch?v=xitBNZH0LFM&t=1s
36	117	https://www.youtube.com/watch?v=eTD_3v6Wk-g
37	392	https://www.youtube.com/watch?v=en5DZgJTWZ8
38	219	https://www.youtube.com/watch?v=q2L-8-rUM7s
39	72	https://www.youtube.com/watch?v=ErV_UPJr8Oc
40	131	https://www.youtube.com/watch?v=bNUjT9aSO30
41	173	https://www.youtube.com/watch?v=6igzuRGc10E
42	204	https://www.youtube.com/watch?v=LRXTFuzBclY
43	115	https://www.youtube.com/watch?v=j6m0X8FcKf0
44	1728	https://www.youtube.com/watch?v=zNGo3GLFrg8&t=507s
45	207	https://www.youtube.com/watch?v=73BUxt-YRX0
46	24	https://www.youtube.com/watch?v=-uaaOVNBQJI
47	76	https://www.youtube.com/watch?v=KlghWXwEQ2c
48	164	https://www.youtube.com/watch?v=IU9UBzxqbWg
49	141	https://www.youtube.com/watch?v=8aONGnwjOcE
50	53	https://www.youtube.com/watch?v=0J7I718Gs9A
51	102	https://www.youtube.com/watch?v=dQI5JG4q7vY&t=2s
52	69	https://www.youtube.com/watch?v=Beo2Cl6IXsU
53	180	https://www.youtube.com/watch?v=akFdxftvWTA
54	37	https://www.youtube.com/watch?v=uLsEAvo1VtI
55	135	https://www.youtube.com/watch?v=LQ62gtUARBI
56	133	https://www.youtube.com/watch?v=BVyI-TQHbUE&t=1s
57	84	https://www.youtube.com/watch?v=BqGbQJ5B8Q0
58	108	https://www.youtube.com/watch?v=foW_9Nu8xzU
		The state of the s

59	171	https://www.youtube.com/watch?v=dtZt-fT1peo
60	238	https://www.youtube.com/watch?v=7isLhaNYgkU&t=2s
61	196	https://www.youtube.com/watch?v=6PJDF5Ne1nc
62	59	https://www.youtube.com/watch?v=hLWm60hEgRU
63	161	https://www.youtube.com/watch?v=czkMLNpuGh4
64	482	https://www.youtube.com/watch?v=2jx8ZxV7ZKw
65	70	https://www.youtube.com/watch?v=GoYsIcWXi2w
66	84	https://www.youtube.com/watch?v=CH71Jp0P1Z8
67	76	https://www.youtube.com/watch?v=mt6yvsrI260
68	166	https://www.youtube.com/watch?v=aOB1dxXtoRA&t=73s
69	301	https://www.youtube.com/watch?v=xgiAXvSlgJE&t=70s
70	693	https://www.youtube.com/watch?v=z3aFZ50MDzs&t=207s
71	194	https://www.theguardian.com/world/2014/feb/20/ukraine-dead-
/1	154	<u>protesters-police</u>
72	94	https://www.theguardian.com/world/video/2014/jun/23/violence-
/ 2	J4	<u>kosovo-mitrovica-serbs-albanians-video</u>
73 87		https://www.theguardian.com/football/video/2016/jun/11/french-
/5		<u>riot-police-march-england-fans-euro-2016-marseille-video</u>
/4 140 -		https://edition.cnn.com/2021/11/21/europe/europe-lockdown-
protests-violence-intl/index.html		protests-violence-intl/index.html
75	53	https://www.theguardian.com/world/video/2017/oct/01/riot-police-
		attack-protesters-as-violence-breaks-out-in-barcelona-video
76	100	https://www.dailymail.co.uk/video/news/video-2438807/Video-Riot-
		police-march-crowd-shields-batons-South-Bank.html
77	55	https://www.dailymail.co.uk/video/news/video-2541197/Video-Riot-
		police-march-Parliament-Square-fireworks-set-off.html
78	114	https://edition.cnn.com/videos/us/2021/06/17/capitol-riot-police-
		officer-assault-patrick-mccaughey-eg-orig.cnn
79	225	https://www.dailymail.co.uk/news/article-9152791/DC-cop-says-
	454	police-didnt-shoot-MAGA-mob-guns-won-firefight.html
80	151	https://www.youtube.com/watch?v=Wtc_SHSFa_0
81	42	https://www.youtube.com/watch?v=4q2dGw1kmBU

A.3.2 Identified incidents summary table

Video	Head impact	Dangerous situation	High threat wielded	High threat projectile	Dangerous scenario
ID			weapon	weapon	involving horseback
3			Man wields metal flagpole		
			and swings at officer.		
4		Man jumps onto a crowd of	Numerous members of a		
		officers and causes some to fall	crowd wielding poles/sticks		
		over which may have resulted in	and swinging at officers.		
		a head collision with the floor.			
5	Officer hit with a	Crowd pushing officers riot	Man wielding a skateboard	Glass bottle thrown at	Police surrounded by
	skateboard on the top of	shields into them which is likely	and swings at officers.	officers.	rioters on horseback
	the head.	to result in collisions to the	Man wielding a bike and	Rioter throwing rocks down	and losing control of
	Crowd pushing officers'	head. X3	barging officers riot shields.	towards police	horses which may
	riot shields into them	Rioters throw big log of wood at	Rioters take riot shield.	Rioters throw big log of wood	result in falling off
	which makes a collision	police officers		at police officers	horse and hitting
	with their head. X2	Group wielding poles and			head.
	Crowd throw riot shields	attacking officers.			
	at head of police.	Rioter throwing rocks down			
	Officers hit with metal	towards police			
	fence that rioters are	Man throwing rocks into a crowd			
	pushing against them.	of police			
6	Traffic cone thrown at	Crowd pushing officers riot		Traffic cone thrown at	Police surrounded by
	the heads of officers	shields into them which is likely		officers	rioters on horseback
		to result in collisions to the		Large rock thrown at police.	and losing control of
		head.			horses which may
					result in falling off
					horse and hitting
					head.

7	Horse lost control and ran officer into a pole				Horses were surrounded and losing control which may result in officers falling off the horse and hitting their head
8	Police officer hit in head and knocked to floor by a rock		Rioters wielding sticks	Rioters throwing sticks Rioters throwing rocks	
9	Rioter swings metal pole down onto an officer's helmet Officer is knocked out unconscious by a barrage of head strikes with poles	Rioters pushing against riot shields potentially causing head collisions Rioters drag an officer down to the floor and down steps	Rioter wielding a pole and swinging at officers		
10	Protestors hit officers on the head with banner signs (wooden plank)		Protestors wield banner signs		
11	Rioters throw metal bin lid at officer's head and knocked to the ground			Rioters throw metal bin lid at officer	
12		Officer is knocked unconscious to the floor	Rioters wield wood banner signs		
13	Crowd pushing officers' riot shields into them which makes a collision with their head.	Officer is knocked to the floor and hit with a metal pole Numerous objects including metal poles are thrown at officers which is likely to hit their head	Rioters wield metal flagpoles and attack officers		

14	Officer barged against a wall by rioters and hits his head on the wall	Officers attacked by various weapons and punches by rioters			
15	Rioters throw large rocks at officer's heads	Rioters throw large rocks at officers	Rioters wield metal poles and attack officers	Rioters throw large rocks at officers	
16	Rioters wield rocks and hit officers on the head with the rock Rioter throws bin at head of an officer	Rioters throw several rocks at officers Rioters attack officers with metal poles	Rioters wield metal poles and attack officers Rioters wield rocks and hit officers with the rock Rioters wield stadium seats and attack officers.	Rioters throw rocks at officers. Rioter throws bin at officer Rioters throw stadium seats at officers	
17		Rioters throw numerous cones at a group of officers	Rioters wield planks of wood.	Rioter throws metal road sign towards officers Rioters throw traffic cones at officers Rioters throw planks of wood at officers	
18		Crowd pushing officers riot shields into them which is likely to result in collisions to the head.			Horses running through crowds, officers could fall off and hit their head.
19		Crowd pushing officers riot shields into them which is likely to result in collisions to the head.			Horses running through crowds, officers could fall off and hit their head.
20	Crowd pushing officers' riot shields into them which makes a collision with their head.				Horses running through crowds, officers could fall off and hit their head.

21		Rioters throw several rocks at		Rioters throw rocks at	
00		officers	Di	officers.	
22		Rioters throwing rocks at officers	Rioters wielding metal	Rioters throwing rocks at	
		Rioters swinging metal poles at officers	poles	officers	
23	Rioter throws rock at an	Rioters wielding wooden planks	Rioters wielding wooden	Rioters throwing planks of	
	officer's head	and swinging downwards at	planks	wood	
	Rioter hits officer on	officers	Rioter wields metal ladder	Rioters throwing rocks	
	head with plank of wood	Rioter wields metal ladder and	and barges it into them		
	numerous times	barges it into a group of officers	_		
		Rioters throwing planks of wood			
		at a group of officers			
		Rioters throwing rocks at officers			
24		Rioters throwing rocks at officers		Rioters throwing rocks	
25		Rioters throwing rocks at officers		Rioters throwing rocks	Rocks thrown towards
					horses; horses
					become uncontrolled
26	Officer hit on back of			Rioters throw foldable chair	
	head with glass bottle			Rioter throws glass bottle	
27		Rioters barge metal fence into		Rioters throwing rocks	Horses running
		officers		Rioter throws large cement	through crowds,
		Rioters throwing rocks at officers		brick	officers could fall off
		Rioter throws large cement brick		Rioters throw glass bottles	and hit their head
		into a group of officers		_	
28	Glass bottle hits an	Glass bottles thrown into a		Rioters throw glass bottles	
	officer on the head	crowd of officers			
29		Rioters throwing rocks at officers		Rioters throwing rocks	
30					Horses running
					through crowds,

					officers could fall off
					and hit their head
34				Rioter throws rock at officers	
Total	23	35	18	31	10

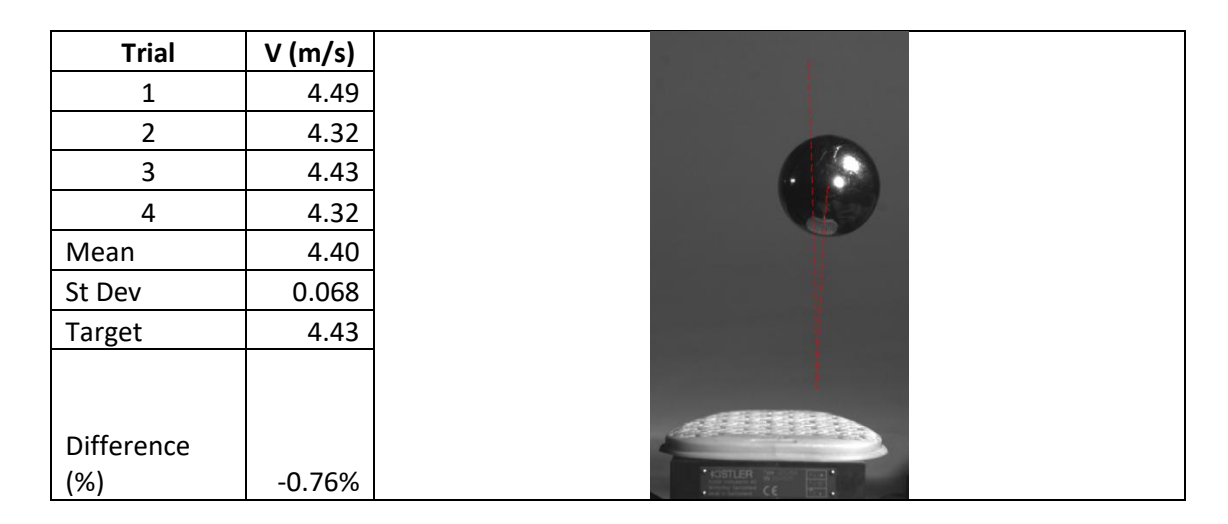
A.3.3 Cohens kappa calculation for inter-rater reliability

			Researcher		
		0	1		
Research	0	57	7	64	59%
Assistant	1	1	43	44	41%
		58	50	108	
		54%	46%		<u>-</u> "

P(a)	0.93
P(e)	0.51
k	0.85

A.4 Injury due to Wielded Blunt Implements

A.4.1 Mean impact velocity validation of the HSV tracking algorithm. Data is from four trials at a fall height of 1 m (4.43 m/s). $\Delta V = -0.76$ %, std dev = 1.5 %. Image is the tracked path of the ball centroid before and after impact.



A.4.2 Mean (± one standard deviation) absolute angles for wooden and metallic implements at the point of impact, taken relative to a global horizontal plane.

		Mean absolu	ıte impact an	gle (degrees)	
Implement					All
	Back	Crown	Front	Side	locations
Wooden	28.1 ± 0.77	27.1 ± 0.96	30.5 ± 1.39	31.6 ± 1.81	29.3 ± 2.19
Metallic	34.4 ±	31.3 ± 1.42	32.5 ± 1.46	37.3 ± 2.02	33.9 ± 2.70
_	0.18)				

A.4.3 Tukey's post-hoc ANOVA results for PLA from swung wielded weaponry trials.

(PLA Impact location)

Location	Mean (g)
Back	287.29
Crown	508.71
Front	316.50
Side	433.20

Pairwise cor	mparisons				
Α	В	Low CI (g)	A-B (g)	Upper CI (g)	P-value
Back	Crown	-284.33	-221.42	-158.50	0.000
Back	Front	-87.16	-29.21	28.75	0.551
Back	Side	-207.61	-145.91	-84.21	0.000
Crown	Front	129.29	192.21	255.12	0.000
Crown	Side	9.13	75.51	141.89	0.019
Front	Side	-178.40	-116.70	-55.00	0.000

(PLA Weapon type)

Location	Mean (g)
Wooden	314.43
Metallic	458.42

Pairwise comparisons							
Α	В	Low CI (g)	A-B (g)	Upper CI (g)	P-value		
Wooden	Metallic	-177.40	-143.98	-110.57	0.000		

(PLA Impact location: Weapon type)

, F	
Location	Mean (g)
W Back	210.4
W Crown	377.4
W Front	258.5
W Side	411.4
M Back	364.2
M Crown	640.0
M Front	374.5

Pairwise con	Pairwise comparisons						
Α	В	Low CI (g)	A-B (g)	Upper CI (g)	P-value		
W Back	W Crown	-264.24	-167.00	-69.76	0.000		
W Back	W Front	-145.32	-48.08	49.16	0.783		
W Back	W Side	-302.97	-200.98	-99.00	0.000		
W Back	M Back	-250.99	-153.75	-56.51	0.000		
W Back	M Crown	-542.86	-429.58	-316.30	0.000		
W Back	M Front	-261.32	-164.08	-66.84	0.000		

M Side 455.0

W Back	M Side	-349.61	-244.58	-139.55	0.000
W Crown	W Front	21.68	118.92	216.16	0.006
W Crown	W Side	-135.97	-33.98	68.00	0.967
W Crown	M Back	-83.99	13.25	110.49	1.000
W Crown	M Crown	-375.86	-262.58	-149.30	0.000
W Crown	M Front	-94.32	2.92	100.16	1.000
W Crown	M Side	-182.61	-77.58	27.45	0.307
W Front	W Side	-254.89	-152.90	-50.91	0.000
W Front	M Back	-202.91	-105.67	-8.43	0.024
W Front	M Crown	-494.78	-381.50	-268.22	0.000
W Front	M Front	-213.24	-116.00	-18.76	0.009
W Front	M Side	-301.53	-196.50	-91.47	0.000
W Side	M Back	-54.75	47.23	149.22	0.835
W Side	M Crown	-345.98	-228.60	-111.22	0.000
W Side	M Front	-65.09	36.90	138.89	0.949
W Side	M Side	-153.04	-43.60	65.84	0.917
M Back	M Crown	-389.11	-275.83	-162.55	0.000
M Back	M Front	-107.57	-10.33	86.91	1.000
M Back	M Side	-195.86	-90.83	14.20	0.140
M Crown	M Front	152.22	265.50	378.78	0.000
M Crown	M Side	64.96	185.00	305.04	0.000
M Front	M Side	-185.53	-80.50	24.53	0.262

A.4.4 Tukey's post-hoc ANOVA results for PAA from swung wielded weaponry trials.

(PAA Impact location)

Location	Mean (krad.s²)
Back	3.20
Crown	7.16
Front	3.45
Side	12.85

Pairwise comparisons					
Α	В	Low CI (krad.s ²)	A-B (krad.s ²)	Upper CI (krad.s²)	P-value
Back	Crown	-6.01	-3.96	-1.92	0.000
Back	Front	-2.13	-0.25	1.64	0.986
Back	Side	-11.65	-9.64	-7.64	0.000
Crown	Front	1.67	3.72	5.76	0.000
Crown	Side	-7.84	-5.68	-3.53	0.000
Front	Side	-11.40	-9.40	-7.40	0.000

(PAA Weapon type)

Location	Mean (g)
Wooden	4.72
Metallic	8.61

Pairwise comparisons					
Α	В	Low CI (g)	A-B (g)	Upper CI (g)	P-value
Wooden	Metallic	-4.97	-3.88	-2.80	0.000

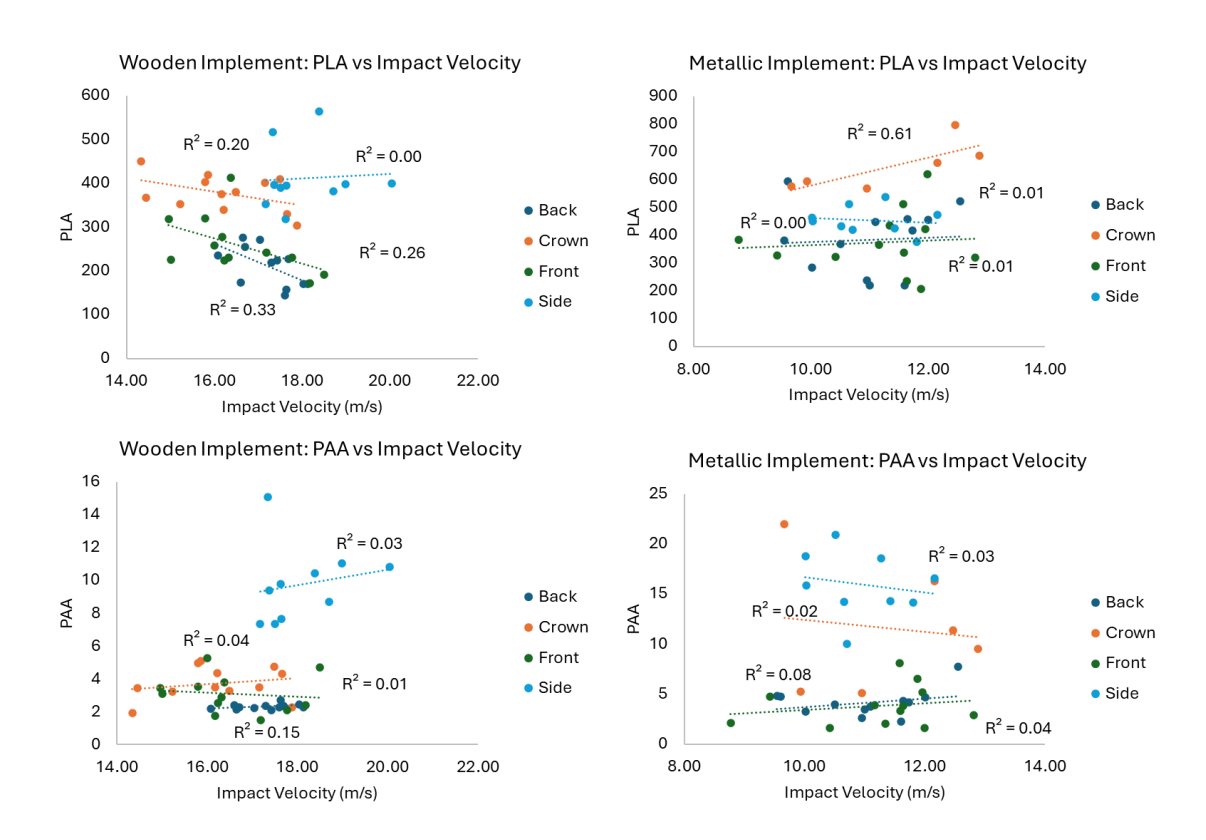
(PAA Impact location:Weapon type)

` '	
Location	Mean (g)
W Back	2.32
W Crown	3.72
W Front	3.09
W Side	9.77
M Back	4.09
M Crown	10.61
M Front	3.80
M Side	15.92

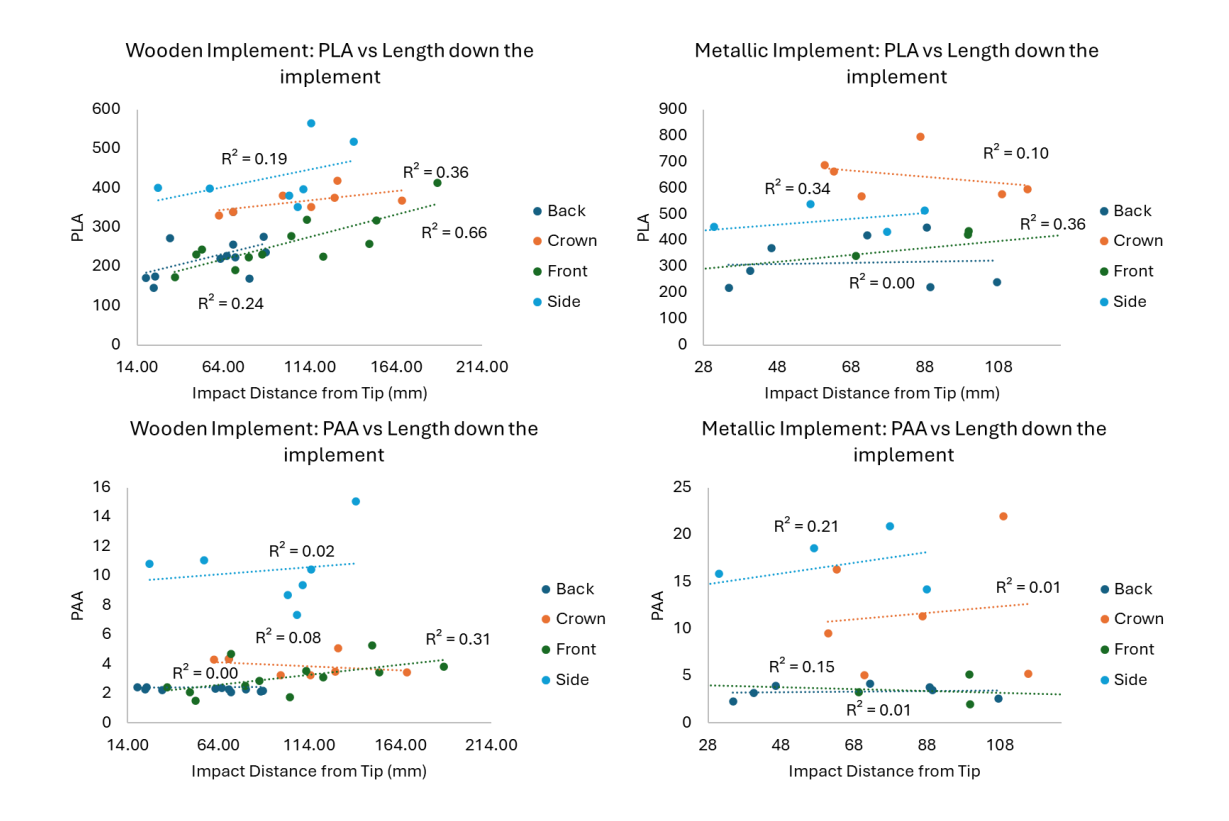
Pairwise comparisons					
A	В	Low CI (g)	A-B (g)	Upper CI (g)	P-value
W Back	W Crown	-4.56	-1.40	1.76	0.863
W Back	W Front	-3.93	-0.77	2.38	0.995
W Back	W Side	-10.76	-7.45	-4.14	0.000
W Back	M Back	-4.93	-1.77	1.39	0.658
W Back	M Crown	-11.97	-8.30	-4.62	0.000
W Back	M Front	-4.64	-1.49	1.67	0.823
W Back	M Side	-17.02	-13.61	-10.20	0.000

W Crown	W Front	-2.53	0.63	3.78	0.999
W Crown	W Side	-9.36	-6.05	-2.74	0.000
W Crown	M Back	-3.53	-0.37	2.79	1.000
W Crown	M Crown	-10.57	-6.90	-3.22	0.000
W Crown	M Front	-3.24	-0.09	3.07	1.000
W Crown	M Side	-15.62	-12.21	-8.80	0.000
W Front	W Side	-9.99	-6.68	-3.36	0.000
W Front	M Back	-4.15	-1.00	2.16	0.976
W Front	M Crown	-11.20	-7.52	-3.84	0.000
W Front	M Front	-3.87	-0.71	2.44	0.997
W Front	M Side	-16.24	-12.83	-9.42	0.000
W Side	M Back	2.37	5.68	8.99	0.000
W Side	M Crown	-4.66	-0.84	2.97	0.997
W Side	M Front	2.65	5.96	9.28	0.000
W Side	M Side	-9.71	-6.16	-2.60	0.000
M Back	M Crown	-10.20	-6.53	-2.85	0.000
M Back	M Front	-2.87	0.28	3.44	1.000
M Back	M Side	-15.25	-11.84	-8.43	0.000
M Crown	M Front	3.13	6.81	10.49	0.000
M Crown	M Side	-9.21	-5.31	-1.41	0.002
M Front	M Side	-15.53	-12.12	-8.71	0.000

A.4.5 R² correlations between peak headform linear and angular accelerations and impact velocity for both wooden (left) and metallic (right) implements.

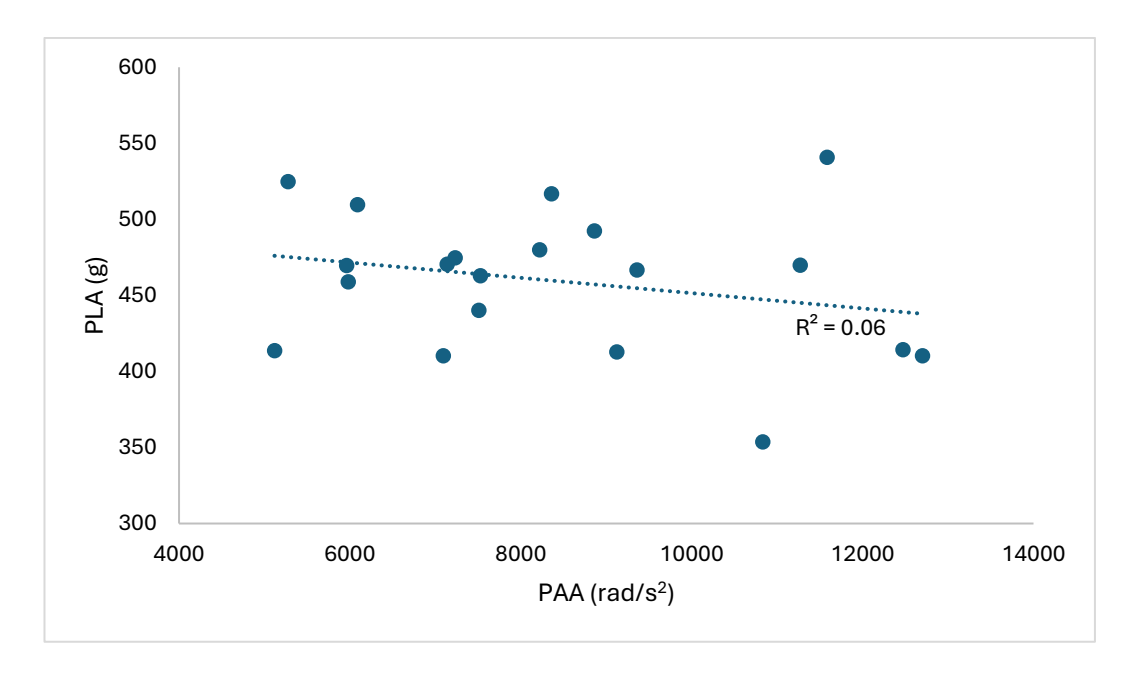


A.4.6 R² correlations between peak headform linear and angular accelerations and the impact distance from the tip for both wooden (left) and metallic (right) implements.



A.5 Injury due to Falling from Horseback

A.5.1 R² correlations between PLA and PAA for all falling from horseback recreations. Results show no significant correlation between the two.



A.6 Development of a Helmet Impact Test System

A.6.1 Product Design Specification for bespoke helmet drop rig to achieve PO representative impact recreations.

	SPECIFICATION FOR: Bespoke PO Helmet Impact Test Rig				
D/W	Requirement	Comments			
	Function(s):				
D	Produce repeatable impacts between fixed anvils and helmeted/bare headforms.	Impact location, velocity, and energy must be consistent between repeat rials.			
D	Permit adjustable impact velocities within a minimum range of 3.4 - 6.9 m/s.	Velocity ranges for none-vehicular helmet standards are 3.4 - 6.9 m/s (30 – 120 J with 5 kg mass).			
D	Compatible with anthropometric representative headforms.	Examples include the Hybrid III, EN 960, and NOCASE headforms.			
D	Can cradle headforms and manually adjust them to define impact location.	Some test standards, such as PSDB 21/04, require a cradled headform with no motion constrains after impact.			
D	Can affix headforms with a neckform and constrain to realistic biomechanical motion.	Neck-like degrees of freedom permit biomechanically representative rotational inertial measurements. Neckforms such as the Hybrid III are common practice.			
D	Can impact all non-facial locations on headforms.	Reference areas for headgear impact attenuation do not include the face, they typically impact a region above the transverse plane of the head (PSDB 21/04 reference line AA').			
D	Combined mass of drop assembly, including head and neckform, must not exceed 15 kg.	Limit to ensure structural calculations can be safely assumed at 15 kg and to have impact mass similar to other systems using head and neckforms.			

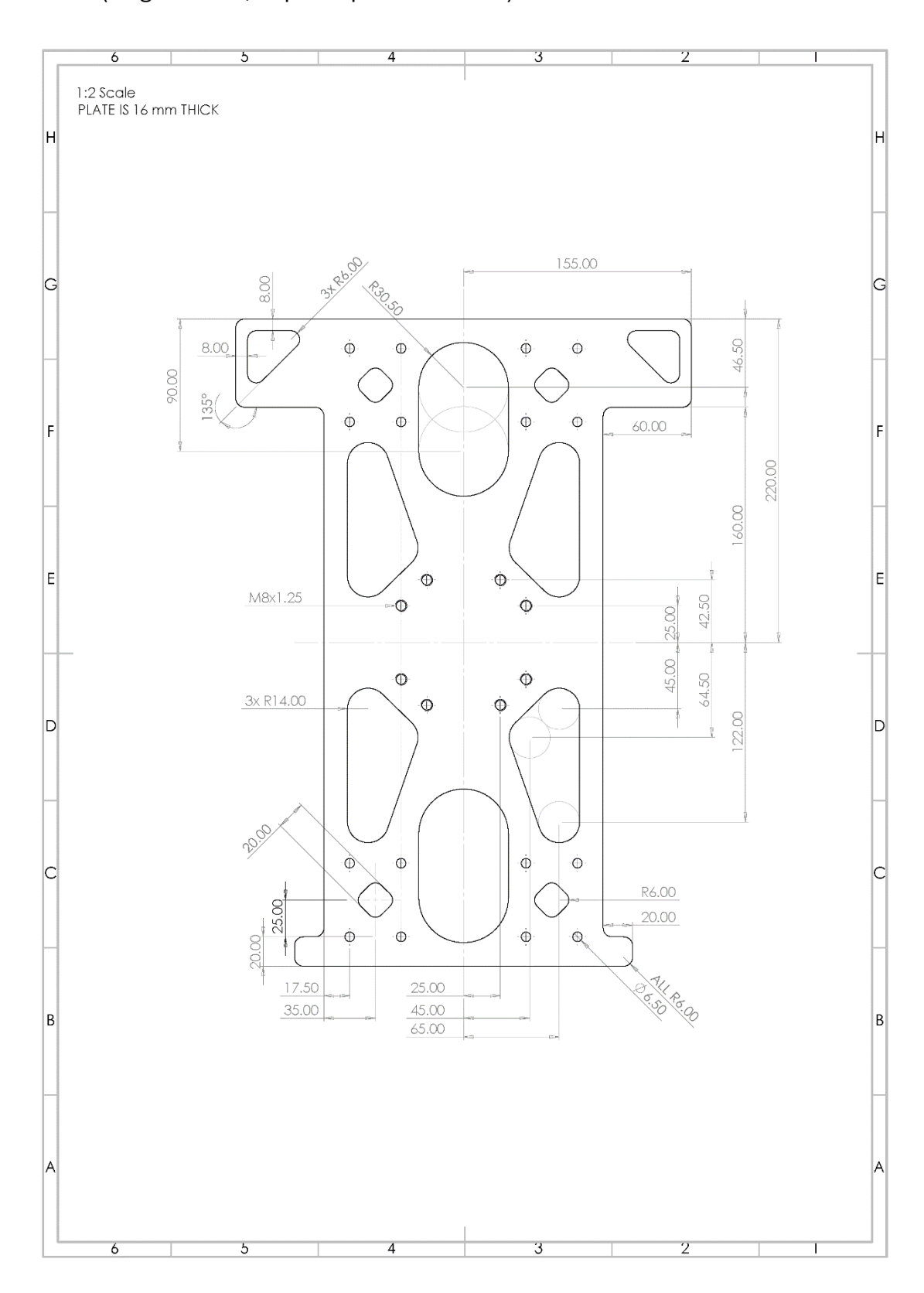
D	Can swap head/neckform and impact anvils so to make the head stationary at impact instead.	Impact anvils or other representative objects can then be used to represent more realistic conditions and maintain their representative inertia, i.e. a projectile brick can hit a stationary headform.
D	Interchangeable impact surfaces between trials.	Standards include different anvil geometries to represent different loading scenarios (e.g. ASTM F1446-20).
D	Capable of damping the impacting system automatically/mechanically. Expected impact energies up to 450 J.	Impact energy assumes a 20 kg drop assembly at 6.6 m/s impact velocity.
W	Permit repeat testing within 90 s time intervals.	Standards can have maximum time intervals between repeated tests, particularly when they include environmental conditioning. Ice hockey is an example (ASTM F1045-16).
W	Integrated sensors for immediate impact condition measurements.	Velocity measurements can confirm impact conditions are as desired and are common in test standard methods (PSDB 21/04).
W	Permits impacts while headform accelerometers are wired to the data acquisition system.	This allows for faster data logging and instant feedback for headform kinematics.
W	Includes workable/non-obtrusive work area for video equipment	High-speed video benefits the understanding and comparison of head impact conditions, work should consider cameras will be used and make efforts to not obstruct view/positioning.
		Operation:
D	System must be operable by one person at a time.	Reduces labour intensity and training requirements. Also, should an accident happen then one person is needed to support.
D	Arming the system (i.e. raising to drop height) and release must be controllable away from the impact zone.	Prioritises safety, making sure the user is absent from the drop zone when the system is armed.
D	System control must not involve high technical skill.	No use of complex control systems i.e. coding, intricate gearings, etc. that limit who can use it.

D	A safety catch mechanism must be present to stop the	Prevents unintended drops that could endanger the operator or damage equipment.	
D	system falling if released on accident.	revents unintended drops that could endanger the operator of damage equipment.	
D	Instrumentation or control interfaces must be accessible away from the impact zone.	e accessible Ensures operators can access/see what is required while staying away from the impact area.	
D	Prevention of entry/egress from the test area once armed.	Ensures personnel cannot enter the test area once armed. Also prevents any components or impacted equipment escaping the test area.	
W	System arming and release should require minimal manual effort.	Mechanical advantage could be used, i.e. pulleys, to make lifting less effort.	
W	Means for swapping impact equipment (headgear, anvils, headforms, etc.) should require minimal manual effort.	Minimal manual effort for this makes testing more efficient reduces the risk of musculoskeletal strain during setup and testing.	
W	Operating, arming, and release systems should not be entirely electrical.	Electrical failures could result in unwanted release or dangers in the event of power loss or damage.	
W	System should have clear visual or audible indicators to show when armed and not to approach.	Lights or alarms provide clear warnings to personnel in the area and signal danger when the system in operation.	
W	A lockout mechanism should be available to prevent use of the system.	Prevents unauthorised personnel from operating the system.	
W	Interfaces and controls should be ergonomically designed.	This supports prolonged use with less risk of musculoskeletal damage or strain.	
		Materials and construction:	
D	Components experiencing impact or lifting must be rated to minimum working load of 25 kN (or relative if torque induced).	Reduces risk of damage. Force calculation assumes 6.6 m/s drop, 20 kg mass, and contact time of 5 ms.	
D	A minimum safety factor of 3 must be applied to all components subject to impact load.	Safety factor of 3 significantly reduces likelihood of damage or accident by ensuring all components can withstand minimum 3 times the maximum anticipated impact load.	
D	Components must be wear-resistant with at least 200 hours between servicing.	Improves the rigidity and efficiency of the system while minimising labour demand.	

	Low friction guidance must be used for the drop.	Provides the maximum possible velocity for available drop height as well as improving repeatability and predictability while reducing wear on the guidance components.
C	High-strength, low-corrosion metallic components should be prioritised where possible. Use of aluminium should be used for high strength/low weight desirability.	Bosch Rexroth struts are an example of low weight high strength structural components. Recommended corrosion-resistant metals are aluminium or stainless steel.
	Drop system should be supported by a rigid member or frame.	Provides rigid strength to maintain an upright position and reduce likelihood of warping or damage with prolonged use.
	Impact surface must be completely rigid.	Prevents energy loss from permanent damage of components. Surfaces can be deformable if realistic representation of in-field materials is compulsory.
	Base of the system must be completely flat.	A warped or curved surface permits deformation in anvil components and prevents a rigid structure.
	Mechanical properties of materials must not show significant change across temperatures of -10 to 50 °C	Temperature changes can be expected with ambient testing and laboratory conditioning, parts must remain to specification.
	Shielding or protective components around the impact zone must be transparent.	Allows vision of the impact zone and system while in operation. Also allows the use of cameras outside the test zone.
V	Precise components should be CNC machined.	CNC provides accuracy and repeatability if components need replacing.
٧	Interchangeable components should be made from lightweight materials	Makes transporting, removal, and installation easier for the operator.
V	Components should avoid having sharp edges.	Reduces likelihood of injurious cuts and lacerations.
V	Modular construction with standard components, i.e. Bosch Rexroth struts, should be incorporated where possible.	Modular and standard components make maintenance and replacement simpler. They also make it easier to amend the system for future test requirements.
V	Consumable components should be recyclable/reuseable.	Sustainable materials should be considered if the system involves consumable items, this ensures end of life disposable is eco-friendly.

	Size and lab integration:					
D	Floor to ceiling height must accommodate for the impact velocity range (4.4 - 6.6 m/s) considering the expected friction of the guide system, though not exceed 4 m.	This ensures the rig can achieve impact conditions using gravitational acceleration and not artificial mechanical acceleration. 4 m is the floor to ceiling height available in the lab.				
D	Impact zone must be minimum 0.5 x 0.5 m footprint to accommodate impact components.	Head and neckforms have combined lengths of up to 0.45 m. Impact anvils for most standards are commonly less than 0.25 m in any direction (ASTM F1446-20).				
D	Systems must not be in the way of common footfall areas in the lab.	Avoiding such areas reduces the risk of accidental interference/danger from unaware personnel entering the test area. Also improves the efficiency of the system if testing is not inhibited by passing personnel.				
D	The area around the head and neckform must allow for full motion following impact.	Nothing should restrict the motion of head/neckform after impact so to not disturb impact data.				
D	Excessive cabling must be avoided and protruding cables should be manageable to reduce trip hazards or accidents.	Minimises clutter as well as trip risks.				
W	A maximum lab footprint of 2 x 2 m.	The lab is a shared space and limiting footprint ensures the system does not interfere with other resources in the area.				

A.6.2 Detailed engineering drawing of the drop plate for affixing a neckform or cradle (singular view, depth of plate is 16 mm).



A.6.3 Detailed breakdown of the individual components of the drop rig, their supply, and safety features.

Tower	Description
Brand	Bosch Rexroth
Material	EN AW – Al MgSi Material designation according to DIN EN 573 for
	Rexroth strut profiles.
	EN AW – 6060 Material number according to DIN EN 573.
	E (elastic modulus) = 70,000 N/mm ²
Dimensions	160 x 80 x 4000 mm (x, y, z)
Wall	Description
Brackets	
Material	5 mm Stainless steel
Dimensions	6 brackets
	290 x 170 x 100 mm
Fixings per	To wall (breeze block):
bracket	1 x M6 x 70L stainless steel anchor bolt.
	Hole for anchor is drilled to manufacturers recommendation at 10 mm.
	For breeze block, bolts should be torqued to 8 Nm.
	To tower:
	8 x M5 x 10L stainless steel Allen bolts into stainless steel Bosch T
	sockets.
	Spacers:
	4 x M5 x 55L Allen bolts for the adjustable alignment of brackets to
	maintain a vertical tower.
Rails and	Description
Bearings	
Brand	HIWIN Technologies
Material	Rails: Stainless steel
Specification	HGH® 25HA Series.
Load Rating	69.07 kN in each orthogonal axis.
Fixings	Rail-> Tower:
	32 M6x20L top mounted capped bolts per rail.
	Bearings-> Drop Plat:
	4 M6x20L capped bolts per bearing.
Drop Plate	Description
Supplier	Premier Aerospace, Derby
Material	6082 Aluminium. Hard anodised to BS EN 12373-1AA25.
External	190 x 440 x 16 mm
Dimensions	
Mass	2.7 kg
Fixings	Plate-> Bearings:
	4 M6x20L head capped Allen bolts per bearing.
	ATD-> Plate
	4 M8x20L head capped Allen bolts.
Rope	Description

revention of falls of falls from a 121, last issued	
et falls from a	
/s - Safety	
5). UIAA 127.	
Aluminium exterior plates. Stainless steel cam and friction plate.	
·	
between 8.9	
s between 8.9	
s between 8.9	
s between 8.9	
s between 8.9	
,	

A.6.4 Cost breakdown for each key component of the drop tower system.

Purchases were mostly made Summer 2022 with some in Spring 2024. *Estimated totals where detail was not available.

Feature	Item	Unit Price (£)	Quantity	Total (£)
Base	Steel Plate	200*	1	200.00*
Drop Guide	Rails	384.06	2	768.12
	Bearings	69.44	4	277.76
	Strut (Tower)	265.8	2	531.60
	Wall Brackets	200*	1	200.00*
Drop	Struts (Cradle)	18.42	2	36.84
Assembly	Aluminium plate	536	1	536.00
Release	Locking pin	14.33	1	14.33
and Lifting	Eye bolt	3.15	1	3.15
	Rope	25	1	25.00
	Pulleys	16.5	3	49.50
	Ratchet stop	60.84	1	60.84
	Carabiners	7.65	3	22.95
All	Fixings	50*	1	50*
Total sum (£) 292			2926.09	

A.6.5 Estimated cost breakdown for a pneumatic linear ram and pendulum system, as of spring 2022.

Pendulum estimate	Estimated Price (£)
Lever Arm + Steel Structure	3000
Electric Motor	1200
Carriage System	1500
Impact head	100
Release Mechanism	100
Sum	£ 5,900.00
Pneumatic ram estimate	Price
Pressure cylinder	1200
Pump	500
System structure	2500
Impactor Ram	800
Impactor surface	100
Carriage System	1500
Electronic Release	100
Sum	£ 6,700.00

A.7 Injury due to Projectile Bricks

A.7.1 Tukey's post-hoc ANOVA results for PLA from projectile brick impact trials.

(PLA Impact location)

Location	Mean (g)
Back	224.9
Crown	239.3
Front	167.9
Side	255.8

Pairwise comparisons					
Α	В	Low CI (g)	A-B (g)	Upper CI (g)	P-value
Back	Crown	-22.59	-14.39	-6.18	0.000
Back	Front	49.29	57.07	64.85	0.000
Back	Side	-38.82	-30.88	-22.93	0.000
Crown	Front	63.25	71.46	79.66	0.000
Crown	Side	-24.85	-16.49	-8.13	0.000
Front	Side	-95.89	-87.95	-80.00	0.000

(PLA Impact Velocity)

Location	Mean (g)
3	124
5	208
6.5	334

Pairwise comparisons						
Α	В		Low CI (g)	A-B (g)	Upper CI (g)	P-value
	3	5	-89.79	-83.57	-77.35	0.000
	3	6.5	-215.56	-209.09	-202.62	0.000
	5	6.5	-131.89	-125.52	-119.14	0.000

(PLA Impact location:Impact Velocity)

Location	Mean (g)
3 Back	134
3 Crown	114
3 Front	88
3 Side	161
5 Back	206

Pairwise comparisons					
Α	В	Low CI (g)	A-B (g)	Upper CI (g)	P-value
3 Back	3 Crown	2.21	19.62	37.03	0.016
3 Back	3 Front	28.44	45.85	63.26	0.000
3 Back	3 Side	-45.33	-26.86	-8.40	0.000
3 Back	5 Back	-89.18	-71.77	-54.36	0.000

5 Crown	230
5 Front	162
5 Side	235
6.5 Back	335
6.5 Crown	374
6.5 Front	254
6.5 Side	372

3 Back	5 Crown	-113.03	-95.62	-78.21	0.000
3 Back	5 Front	-45.08	-27.67	-10.26	0.000
3 Back	5 Side	-118.03	-100.62	-83.21	0.000
3 Back	6.5 Back	-218.20	-200.79	-183.38	0.000
3 Back	6.5 Crown	-259.82	-239.72	-219.61	0.000
3 Back	6.5 Front	-136.94	-119.53	-102.12	0.000
3 Back	6.5 Side	-255.13	-237.72	-220.31	0.000
3 Crown	3 Front	8.82	26.23	43.64	0.000
3 Crown	3 Side	-64.94	-46.48	-28.01	0.000
3 Crown	5 Back	-108.80	-91.39	-73.98	0.000
3 Crown	5 Crown	-132.65	-115.24	-97.83	0.000
3 Crown	5 Front	-64.70	-47.29	-29.88	0.000
3 Crown	5 Side	-137.65	-120.24	-102.83	0.000
3 Crown	6.5 Back	-237.82	-220.41	-203.00	0.000
3 Crown	6.5 Crown	-279.44	-259.33	-239.23	0.000
3 Crown	6.5 Front	-156.56	-139.15	-121.74	0.000
3 Crown	6.5 Side	-274.74	-257.33	-239.92	0.000
3 Front	3 Side	-91.18	-72.71	-54.25	0.000
3 Front	5 Back	-135.03	-117.62	-100.21	0.000
3 Front	5 Crown	-158.88	-141.47	-124.06	0.000
3 Front	5 Front	-90.93	-73.52	-56.11	0.000
3 Front	5 Side	-163.88	-146.47	-129.06	0.000
3 Front	6.5 Back	-264.05	-246.64	-229.23	0.000
3 Front	6.5 Crown	-305.67	-285.57	-265.46	0.000
3 Front	6.5 Front	-182.7908	-165.381	-147.9711	0.00E+00
3 Front	6.5 Side	-300.9742	-283.5644	-266.1545	0
3 Side	5 Back	-63.37499	-44.90907	-26.44316	6.16E-09
3 Side	5 Crown	-87.22609	-68.76017	-50.29426	7.40E-15

3 Side	5 Front	-19.27564	-0.809729	17.656185	1
3 Side	5 Side	-92.22545	-73.75954	-55.29362	5.67E-16
3 Side	6.5 Back	-192.3962	-173.9302	-155.4643	0
3 Side	6.5 Crown	-233.8795	-212.8552	-191.8308	0
3 Side	6.5 Front	-111.1351	-92.66917	-74.20325	4.71E-20
3 Side	6.5 Side	-229.3185	-210.8526	-192.3867	0.00E+00
5 Back	5 Crown	-41.26093	-23.8511	-6.441271	1.26E-03
5 Back	5 Front	26.68951	44.09934	61.509174	1.95E-09
5 Back	5 Side	-46.26029	-28.85046	-11.44063	5.01E-05
5 Back	6.5 Back	-146.431	-129.0212	-111.6113	4.28E-32
5 Back	6.5 Crown	-188.0492	-167.9461	-147.8429	0.00E+00
5 Back	6.5 Front	-65.16993	-47.7601	-30.35027	1.86E-10
5 Back	6.5 Side	-183.3533	-165.9435	-148.5337	0.00E+00
5 Crown	5 Front	50.54061	67.95044	85.360275	1.34E-15
5 Crown	5 Side	-22.40919	-4.999362	12.410468	0.997218
5 Crown	6.5 Back	-122.5799	-105.1701	-87.76024	1.68E-24
5 Crown	6.5 Crown	-164.1981	-144.095	-123.9918	1.53E-30
5 Crown	6.5 Front	-41.31882	-23.90899	-6.499164	0.001218
5 Crown	6.5 Side	-159.5022	-142.0924	-124.6826	0
5 Front	5 Side	-90.35964	-72.94981	-55.53998	9.24E-17
5 Front	6.5 Back	-190.5303	-173.1205	-155.7107	0
5 Front	6.5 Crown	-232.1486	-212.0454	-191.9423	0.00E+00
5 Front	6.5 Front	-109.2693	-91.85944	-74.44961	4.11E-21
5 Front	6.5 Side	-227.4527	-210.0429	-192.633	0
5 Side	6.5 Back	-117.5805	-100.1707	-82.76088	3.56E-23
5 Side	6.5 Crown	-159.1988	-139.0956	-118.9925	4.42E-29
5 Side	6.5 Front	-36.31946	-18.90963	-1.499802	2.29E-02
5 Side	6.5 Side	-154.5029	-137.093	-119.6832	0.00E+00

6.5 Back	6.5 Crown	-59.02805	-38.92491	-18.82177	1.94E-06
6.5 Back	6.5 Front	63.85125	81.26108	98.67091	1.19E-18
6.5 Back	6.5 Side	-54.33217	-36.92234	-19.51251	2.25E-07
6.5 Crown	6.5 Front	100.0829	120.186	140.28913	3.30E-24
6.5 Crown	6.5 Side	-18.10056	2.002576	22.105716	1
6.5 Front	6.5 Side	-135.5932	-118.1834	-100.7736	2.42E-28

A.7.2 Tukey's post-hoc ANOVA results for PAA from projectile brick impact trials.

(PAA Impact location)

Location	Mean (krad/s^2)
Back	90.9
Crown	3.0
Front	5.3
Side	8.9

Pairwise comparisons					
Α	В	Low CI (g)	A-B (g)	Upper CI (g)	P-value
Back	Crown	73.40	87.91	102.43	0.000
Back	Front	71.77	85.54	99.32	0.000
Back	Side	67.93	81.98	96.04	0.000
Crown	Front	-16.89	-2.37	12.15	0.972
Crown	Side	-20.72	-5.93	8.86	0.710
Front	Side	-17.62	-3.56	10.50	0.906

(PAA Impact Velocity)

7.4
23.1
50.5

Pairwise comparisons					
Α	В	Low CI (g)	A-B (g)	Upper CI (g)	P-value
3	5	-26.67	-15.67	-4.67	0.003
3	6.5	-54.50	-43.06	-31.62	0.000
5	6.5	-38.67	-27.39	-16.11	0.000

(PAA Impact location:Impact Velocity)

<u> </u>	•
Location	Mean (krad/s^2)
3 Back	19.5
3 Crown	1.3
3 Front	2.7
3 Side	6.2
5 Back	77.8
5 Crown	2.9
5 Front	5.2
5 Side	6.5
6.5 Back	175.3
6.5 Crown	4.7
6.5 Front	8.0
6.5 Side	14.0

Pairwise comparisons					
Α	В	Low CI (g)	A-B (g)	Upper CI (g)	P-value
3 Back	3 Crown	-12.56	18.25	49.05	0.665
3 Back	3 Front	-14.01	16.79	47.60	0.766
3 Back	3 Side	-19.29	13.38	46.05	0.955
3 Back	5 Back	-89.07	-58.27	-27.46	0.000
3 Back	5 Crown	-14.13	16.68	47.48	0.774
3 Back	5 Front	-16.51	14.30	45.10	0.900
3 Back	5 Side	-17.77	13.03	43.84	0.944
3 Back	6.5 Back	-186.54	-155.73	-124.93	0.000
3 Back	6.5 Crown	-20.75	14.82	50.39	0.950
3 Back	6.5 Front	-19.26	11.54	42.35	0.976
3 Back	6.5 Side	-25.26	5.54	36.35	1.000
3 Crown	3 Front	-32.26	-1.46	29.35	1.000
3 Crown	3 Side	-37.54	-4.87	27.81	1.000
3 Crown	5 Back	-107.32	-76.51	-45.71	0.000
3 Crown	5 Crown	-32.38	-1.57	29.23	1.000
3 Crown	5 Front	-34.75	-3.95	26.86	1.000
3 Crown	5 Side	-36.02	-5.21	25.59	1.000
3 Crown	6.5 Back	-204.78	-173.98	-143.17	0.000
3 Crown	6.5 Crown	-39.00	-3.43	32.14	1.000
3 Crown	6.5 Front	-37.51	-6.70	24.10	1.000
3 Crown	6.5 Side	-43.51	-12.70	18.10	0.953
3 Front	3 Side	-36.08	-3.41	29.26	1.000
3 Front	5 Back	-105.86	-75.06	-44.25	0.000
3 Front	5 Crown	-30.92	-0.12	30.69	1.000

3 Front 6.5 Back -203.33 -172.52 -14 3 Front 6.5 Crown -37.54 -1.97 3 3 Front 6.5 Front -36.05415 -5.248813 25.556 3 Front 6.5 Side -42.05333 -11.248 19.55 3 Side 5 Back -104.321 -71.64699 -38 3 Side 5 Crown -29.3788 3.295192 35.96 3 Side 5 Front -31.75444 0.919547 33.59 3 Side 5 Side -33.02278 -0.348787 32.32 3 Side 6.5 Back -201.7861 -169.1121 -136.4 3 Side 6.5 Crown -35.76129 1.439685 38.644 3 Side 6.5 Front -34.51189 -1.837893 30.83 3 Side 6.5 Side -40.51107 -7.837079 24.83 5 Back 5 Crown 44.13685 74.94219 105.74 5 Back 5 Front 41.7612 72.56654 103.3 5 Back 5 Side 40.49287 71.29821 102.10 5 Bac	0.9803 8.973 9.72E- 9184 03539 25205 1.00E+
3 Front 6.5 Crown -37.54 -1.97 3 3 Front 6.5 Front -36.05415 -5.248813 25.556 3 Front 6.5 Side -42.05333 -11.248 19.557 3 Side 5 Back -104.321 -71.64699 -38 3 Side 5 Crown -29.3788 3.295192 35.96 3 Side 5 Front -31.75444 0.919547 33.59 3 Side 5 Side -33.02278 -0.348787 32.32 3 Side 6.5 Back -201.7861 -169.1121 -136.4 3 Side 6.5 Crown -35.76129 1.439685 38.64 3 Side 6.5 Front -34.51189 -1.837893 30.83 3 Side 6.5 Side -40.51107 -7.837079 24.83 5 Back 5 Crown 44.13685 74.94219 105.74 5 Back 5 Front 41.7612 72.56654 103.33 5 Back 5 Side 40.49287 71.29821 102.10 5 Back 6.5 Back -128.2704 -97.46507 -66.61 <t< td=""><td>33.60 1.00 66522 1.00E+1 67336 0.9803 8.973 9.72E-1 69184 93539 25205 1.00E+1</td></t<>	33.60 1.00 66522 1.00E+1 67336 0.9803 8.973 9.72E-1 69184 93539 25205 1.00E+1
3 Front 6.5 Front -36.05415 -5.248813 25.55 3 Front 6.5 Side -42.05333 -11.248 19.55 3 Side 5 Back -104.321 -71.64699 -38 3 Side 5 Crown -29.3788 3.295192 35.96 3 Side 5 Front -31.75444 0.919547 33.59 3 Side 5 Side -33.02278 -0.348787 32.32 3 Side 6.5 Back -201.7861 -169.1121 -136.4 3 Side 6.5 Crown -35.76129 1.439685 38.64 3 Side 6.5 Front -34.51189 -1.837893 30.836 3 Side 6.5 Side -40.51107 -7.837079 24.836 5 Back 5 Crown 44.13685 74.94219 105.76 5 Back 5 Side 40.49287 71.29821 102.10 5 Back 5 Side 40.49287 71.29821 102.10 5 Back 6.5 Back -128.2704 -97.46507 -66.61 5 Back 6.5 Front 39.00376 69.8091 100.61 <td>1.00E+1 1.00E+1 1.00E+1 1.00E+1 1.00E+1 1.00E+1 1.00E+1</td>	1.00E+1 1.00E+1 1.00E+1 1.00E+1 1.00E+1 1.00E+1 1.00E+1
3 Front 6.5 Side -42.05333 -11.248 19.55 3 Side 5 Back -104.321 -71.64699 -38 3 Side 5 Crown -29.3788 3.295192 35.96 3 Side 5 Front -31.75444 0.919547 33.59 3 Side 5 Side -33.02278 -0.348787 32.32 3 Side 6.5 Back -201.7861 -169.1121 -136.4 3 Side 6.5 Crown -35.76129 1.439685 38.644 3 Side 6.5 Front -34.51189 -1.837893 30.836 3 Side 6.5 Side -40.51107 -7.837079 24.836 5 Back 5 Crown 44.13685 74.94219 105.74 5 Back 5 Side 40.49287 71.29821 102.10 5 Back 5 Side 40.49287 71.29821 102.10 5 Back 6.5 Back -128.2704 -97.46507 -66.60 5 Back 6.5 Front 39.00376 69.8091 100.60	0.9803 8.973 9.72E- 9184 03539 25205 1.00E+
3 Side 5 Back -104.321 -71.64699 -38 3 Side 5 Crown -29.3788 3.295192 35.96 3 Side 5 Front -31.75444 0.919547 33.59 3 Side 5 Side -33.02278 -0.348787 32.32 3 Side 6.5 Back -201.7861 -169.1121 -136.4 3 Side 6.5 Crown -35.76129 1.439685 38.640 3 Side 6.5 Front -34.51189 -1.837893 30.836 3 Side 6.5 Side -40.51107 -7.837079 24.836 5 Back 5 Crown 44.13685 74.94219 105.74 5 Back 5 Front 41.7612 72.56654 103.3 5 Back 5 Side 40.49287 71.29821 102.10 5 Back 6.5 Back -128.2704 -97.46507 -66.60 5 Back 6.5 Crown 37.51574 73.08668 108.60 5 Back 6.5 Front 39.00376 69.8091 100.60	8.973 9.72E-69184 93539 25205 1.00E+1
3 Side 5 Crown -29.3788 3.295192 35.969 3 Side 5 Front -31.75444 0.919547 33.599 3 Side 5 Side -33.02278 -0.348787 32.329 3 Side 6.5 Back -201.7861 -169.1121 -136.4 3 Side 6.5 Crown -35.76129 1.439685 38.644 3 Side 6.5 Front -34.51189 -1.837893 30.836 3 Side 6.5 Side -40.51107 -7.837079 24.836 5 Back 5 Crown 44.13685 74.94219 105.74 5 Back 5 Front 41.7612 72.56654 103.3 5 Back 5 Side 40.49287 71.29821 102.10 5 Back 6.5 Back -128.2704 -97.46507 -66.60 5 Back 6.5 Crown 37.51574 73.08668 108.60 5 Back 6.5 Front 39.00376 69.8091 100.60	9184 93539 25205 1.00E+
3 Side 5 Front -31.75444 0.919547 33.593 3 Side 5 Side -33.02278 -0.348787 32.323 3 Side 6.5 Back -201.7861 -169.1121 -136.4 3 Side 6.5 Crown -35.76129 1.439685 38.644 3 Side 6.5 Front -34.51189 -1.837893 30.83 3 Side 6.5 Side -40.51107 -7.837079 24.83 5 Back 5 Crown 44.13685 74.94219 105.74 5 Back 5 Front 41.7612 72.56654 103.3 5 Back 5 Side 40.49287 71.29821 102.10 5 Back 6.5 Back -128.2704 -97.46507 -66.60 5 Back 6.5 Crown 37.51574 73.08668 108.60 5 Back 6.5 Front 39.00376 69.8091 100.60	25205 1.00E+
3 Side 5 Side -33.02278 -0.348787 32.325 3 Side 6.5 Back -201.7861 -169.1121 -136.4 3 Side 6.5 Crown -35.76129 1.439685 38.640 3 Side 6.5 Front -34.51189 -1.837893 30.830 3 Side 6.5 Side -40.51107 -7.837079 24.830 5 Back 5 Crown 44.13685 74.94219 105.74 5 Back 5 Front 41.7612 72.56654 103.3 5 Back 5 Side 40.49287 71.29821 102.10 5 Back 6.5 Back -128.2704 -97.46507 -66.60 5 Back 6.5 Crown 37.51574 73.08668 108.60 5 Back 6.5 Front 39.00376 69.8091 100.60	25205 1.00E+
3 Side 6.5 Back -201.7861 -169.1121 -136.4 3 Side 6.5 Crown -35.76129 1.439685 38.640 3 Side 6.5 Front -34.51189 -1.837893 30.830 3 Side 6.5 Side -40.51107 -7.837079 24.830 5 Back 5 Crown 44.13685 74.94219 105.74 5 Back 5 Front 41.7612 72.56654 103.33 5 Back 5 Side 40.49287 71.29821 102.10 5 Back 6.5 Back -128.2704 -97.46507 -66.60 5 Back 6.5 Crown 37.51574 73.08668 108.60 5 Back 6.5 Front 39.00376 69.8091 100.60	
3 Side 6.5 Crown -35.76129 1.439685 38.640 3 Side 6.5 Front -34.51189 -1.837893 30.830 3 Side 6.5 Side -40.51107 -7.837079 24.830 5 Back 5 Crown 44.13685 74.94219 105.74 5 Back 5 Front 41.7612 72.56654 103.3 5 Back 5 Side 40.49287 71.29821 102.10 5 Back 6.5 Back -128.2704 -97.46507 -66.60 5 Back 6.5 Crown 37.51574 73.08668 108.60 5 Back 6.5 Front 39.00376 69.8091 100.60	4381 1.07E-
3 Side 6.5 Front -34.51189 -1.837893 30.836 3 Side 6.5 Side -40.51107 -7.837079 24.836 5 Back 5 Crown 44.13685 74.94219 105.74 5 Back 5 Front 41.7612 72.56654 103.33 5 Back 5 Side 40.49287 71.29821 102.10 5 Back 6.5 Back -128.2704 -97.46507 -66.60 5 Back 6.5 Crown 37.51574 73.08668 108.60 5 Back 6.5 Front 39.00376 69.8091 100.60	
3 Side 6.5 Side -40.51107 -7.837079 24.836 5 Back 5 Crown 44.13685 74.94219 105.74 5 Back 5 Front 41.7612 72.56654 103.3 5 Back 5 Side 40.49287 71.29821 102.10 5 Back 6.5 Back -128.2704 -97.46507 -66.60 5 Back 6.5 Crown 37.51574 73.08668 108.60 5 Back 6.5 Front 39.00376 69.8091 100.60	0662
5 Back 5 Crown 44.13685 74.94219 105.74 5 Back 5 Front 41.7612 72.56654 103.3 5 Back 5 Side 40.49287 71.29821 102.10 5 Back 6.5 Back -128.2704 -97.46507 -66.60 5 Back 6.5 Crown 37.51574 73.08668 108.60 5 Back 6.5 Front 39.00376 69.8091 100.60	36099 1.00E+
5 Back 5 Front 41.7612 72.56654 103.3 5 Back 5 Side 40.49287 71.29821 102.10 5 Back 6.5 Back -128.2704 -97.46507 -66.60 5 Back 6.5 Crown 37.51574 73.08668 108.60 5 Back 6.5 Front 39.00376 69.8091 100.60	6913 9.99E-
5 Back 5 Side 40.49287 71.29821 102.10 5 Back 6.5 Back -128.2704 -97.46507 -66.60 5 Back 6.5 Crown 37.51574 73.08668 108.60 5 Back 6.5 Front 39.00376 69.8091 100.60	4752 6.10E-
5 Back 6.5 Back -128.2704 -97.46507 -66.60 5 Back 6.5 Crown 37.51574 73.08668 108.60 5 Back 6.5 Front 39.00376 69.8091 100.60	37187 1.48E-
5 Back 6.5 Crown 37.51574 73.08668 108.69 5 Back 6.5 Front 39.00376 69.8091 100.69	.0354 2.37E-
5 Back 6.5 Front 39.00376 69.8091 100.63	55974 2.03E-
	55762 4.86E-
	61443 4.15E-
5 Back 63.80991 94.61	.5249 4.00E-
5 Crown 5 Front -33.18098 -2.375645 28.4	1.00E+
5 Crown 5 Side -34.44931 -3.64398 27.16	0.9999
5 Crown 6.5 Back -203.2126 -172.4073 -141.	.6019 1.77E-
5 Crown 6.5 Crown -37.42644 -1.855507 33.7	1.00E+
5 Crown 6.5 Front -35.93842 -5.133086 25.672	2249 0.9999
5 Crown 6.5 Side -41.93761 -11.13227 19.673	3064 0.9818
5 Front 5 Side -32.07367 -1.268334 29.53	

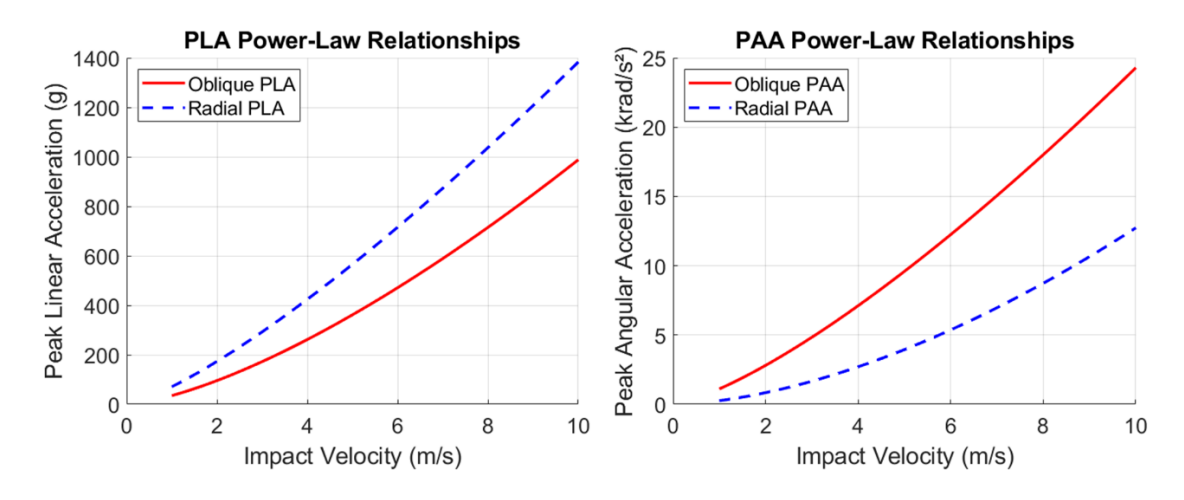
5 Front	6.5 Back	-200.8369	-170.0316	-139.2263	3.83E-22
5 Front	6.5 Crown	-35.0508	0.520138	36.091075	1.00E+00
5 Front	6.5 Front	-33.56278	-2.75744	28.047895	1.00E+00
5 Front	6.5 Side	-39.56196	-8.756626	22.048709	0.997454
5 Side	6.5 Back	-199.5686	-168.7633	-137.9579	5.76E-22
5 Side	6.5 Crown	-33.78246	1.788473	37.35941	1.00E+00
5 Side	6.5 Front	-32.29444	-1.489106	29.316229	1.00E+00
5 Side	6.5 Side	-38.29363	-7.488292	23.317044	9.99E-01
6.5 Back	6.5 Crown	134.9808	170.5518	206.12269	3.71E-19
6.5 Back	6.5 Front	136.4688	167.2742	198.07951	9.26E-22
6.5 Back	6.5 Side	130.4697	161.275	192.08032	6.09E-21
6.5 Crown	6.5 Front	-38.84852	-3.277579	32.293358	1
6.5 Crown	6.5 Side	-44.8477	-9.276764	26.294173	0.998817
6.5 Front	6.5 Side	-36.80452	-5.999186	24.80615	0.999926

A.8 Recreating Public Order Impact Mechanics with a Drop Rig

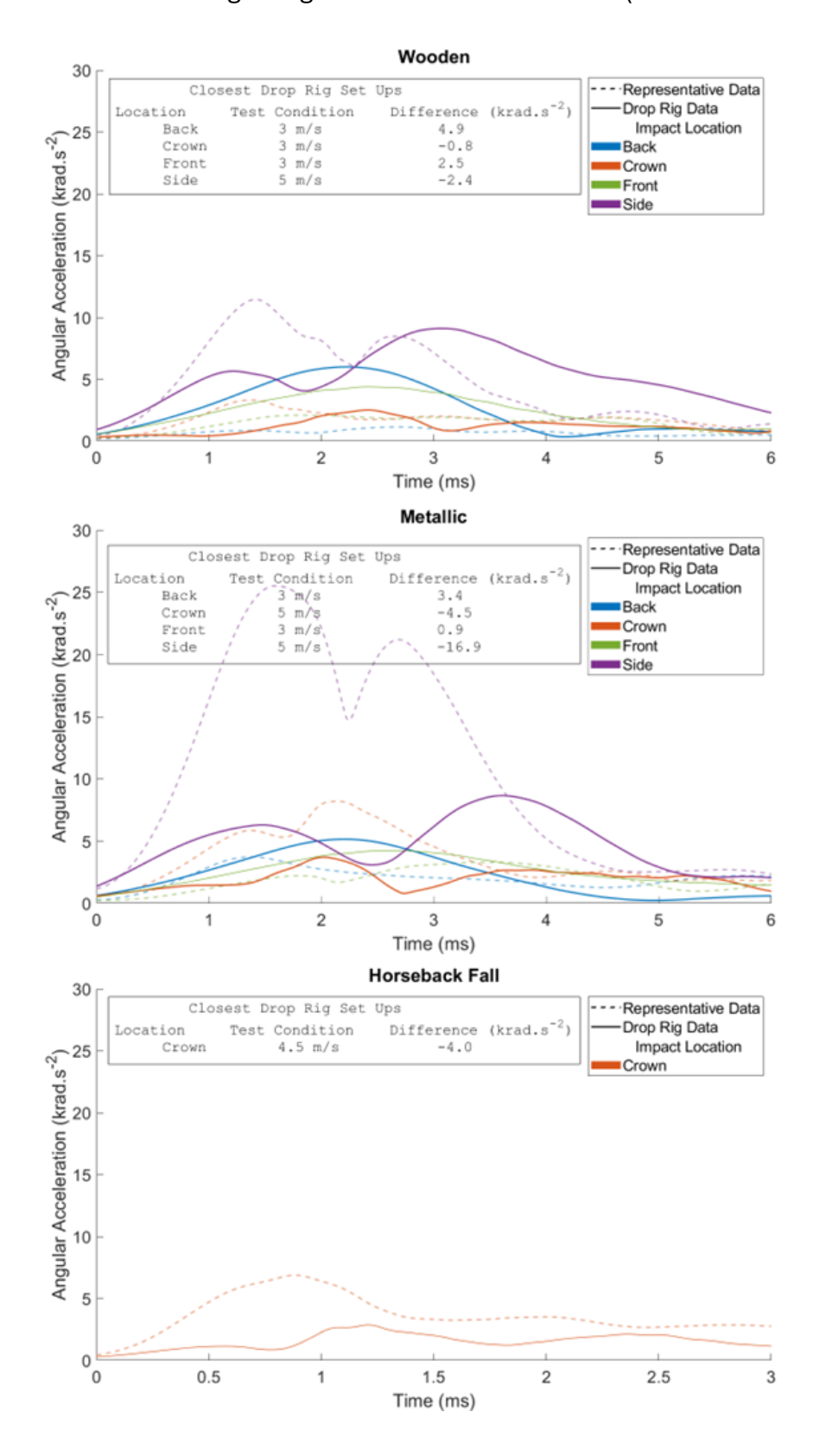
A.8.1 Details for the mean peak accelerations (linear and angular) across all experimented PO represented impact conditions. Distances are the vertical difference between mean peaks and the respective linear (WSTC) and angular (Hoshizaki) tolerance curves.

Condition	Location	PLA	DLin	Distance To Tolerance	PAA	DAng	Distance To Tolerance
				(g)			(krad/s²)
Brick 10.6 m/s	Back	612	0.76	258	-	-	-
Brick 10.6 m/s	Crown	814	1.08	535	11.0	1.32	-37.9
Brick 10.6 m/s	Front	505	1.53	284	15.9	1.89	-18.8
Brick 10.6 m/s	Side	639	0.95	334	25.1	1.92	-9.06
Brick 6.5 m/s	Back	335	1.00	40.7	-	-	-
Brick 6.5 m/s	Crown	374	1.30	127	4.70	2.50	-21.8
Brick 6.5 m/s	Front	254	1.80	55.8	8.00	2.90	-15.0
Brick 6.5 m/s	Side	372	1.00	77.7	14.0	2.40	-13.6
Horseback Fall	Crown	460	2.64	307	8.39	3.76	-9.53
Metallic	Back	364	2.26	194	4.09	4.20	-12.0
Metallic	Crown	640	1.73	436	10.6	3.44	-8.91
Metallic	Front	375	1.91	185	3.80	4.01	-13.0
Metallic	Side	455	1.68	247	15.9	2.59	-9.71
Wooden	Back	210	1.74	7.25	2.32	4.19	-13.8
Wooden	Crown	377	1.36	138	3.72	2.81	-20.0
Wooden	Front	259	1.52	36.9	3.09	4.16	-13.2
Wooden	Side	411	1.31	166	9.77	2.52	-16.5

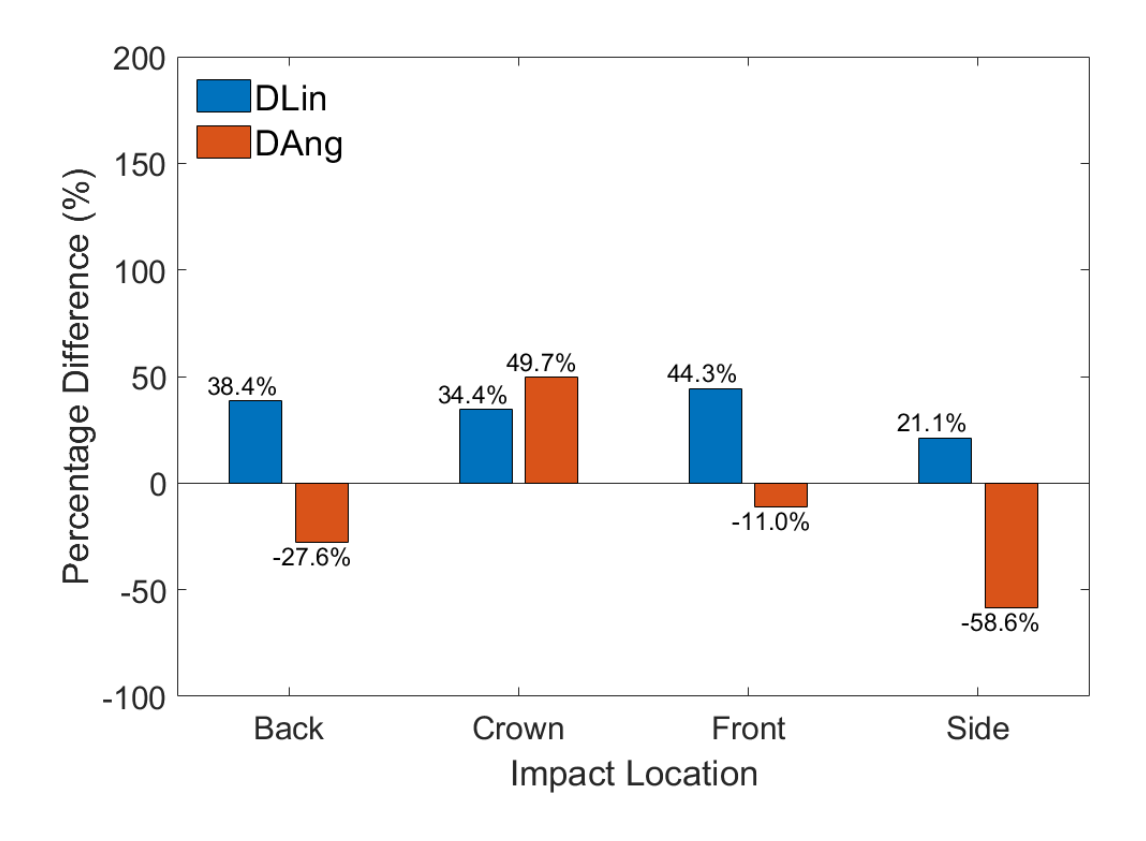
A.8.2 Power law relationships for both PLA and PAA with increasing velocity using the coefficients from Table 8.4. These curves are calculated for oblique and linear conditions respectively, using the neckform affixed drops across all anvil surfaces.



A.8.3 Transient pulse comparisons for the angular dynamics of drop rig impacts compared to the more representative experimentation of chapters 4, 5, and 7. There is little to compare with these curves relative to the pulses for the linear dynamics because the target angular accelerations are low (less than 5 krad/s²).



A.8.4 Bar chart for the % change in duration when removing a neckform and cradling the headform as per current PSDB 21/04 requirements. % = (cradled-neckform)/neckform. Overall, there is a consistent increase in duration for linear mechanics though mostly a reduction in duration for angular. An increased duration for angular crown impacts is not of concern, for these loads are radial and should not be used for angular measurements.



A.8.5 Tukey's post-hoc ANOVA results for PLA from drop recreations of PO representative impact scenarios.

Anvil Type

One-way ANOVA Results.

There was a significant effect due to anvil type P = 0.00020374

Weapon type	Mean PLA (g)
Horseback Fall	528
Metallic	331
Wooden	402

Α	В	Low CI (g)	A-B (g)	Upper CI (g)	Р
Horseback Fall	Metallic	91.03687	197.4347	303.8325	0.000
Horseback Fall	Wooden	21.58406	126.0986	230.6131	0.015
Metallic	Wooden	-137.437	-71.3361	-5.23532	0.032

Impact Location

One-way ANOVA Results.

There was significant effect due to location: p-value: 7.5621e-10

Location	Mean PLA (g)
Back	311.4
Crown	544.1
Front	345.3
Side	362.3

Α	В	Low CI (g)	A-B (g)	Upper CI (g)	Р
Back	Crown	-295.963	-232.679	-169.395	0.000
Back	Front	-87.0087	-33.9218	19.1652	0.322
Back	Side	-104.017	-50.9304	2.156571	0.064
Crown	Front	134.3122	198.7573	263.2025	0.000
Crown	Side	117.3035	181.7487	246.1938	0.000
Front	Side	-71.4747	-17.0086	37.45745	0.830

Impact velocity

One-way ANOVA Results.

There was a significant effect due to velocity P = 1.6325e-18

Velocity		Mean PLA (g)
	3	196
	5	402
	7	627

Α	В	Low CI (g)	A-B (g)	Upper CI (g)	Р
3	5	-271.236	-206.262	-141.289	0.000
3	7	-502.412	-431.165	-359.918	0.000
5	7	-297.692	-224.903	-152.113	0.000

A.8.6 Tukey's post-hoc ANOVA results for PAA from drop recreations of PO representative impact scenarios.

Anvil Type

One-way ANOVA Results.

There was a significant effect due to weapon type P = 0.0035055

Weapon type	Mean PAA (krad/s^2)
Horseback Fall	2.36
Metallic	4.13
Wooden	2.88

Α	В	Low CI (g)	A-B (g)	Upper CI (g)	Р
Horseback Fall	Metallic	-2.70986	-1.77024	-0.83062	0.003
Horseback Fall	Wooden	-1.34712	-0.51845	0.310216	0.213
Metallic	Wooden	0.261336	1.251786	2.242236	0.019

Impact Location

One-way ANOVA Results.

There was significant effect due to location: p-value: 1.1255e-08

Location	Mean PAA (krad/s^2)
Back	13.3
Crown	3.4
Front	8.9
Side	9.1

Α	В	Low CI (g)	A-B (g)	Upper CI (g)	Р
Back	Crown	7.684456	9.936397	12.18834	0.000
Back	Front	2.497354	4.386441	6.275528	0.000
Back	Side	2.30062	4.189707	6.078794	0.000
Crown	Front	-7.84322	-5.54996	-3.25669	0.000
Crown	Side	-8.03995	-5.74669	-3.45343	0.000
Front	Side	-2.1349	-0.19673	1.741428	0.992

Impact velocity

One-way ANOVA Results.

There was a significant effect due to velocity P = 3.9924e-14

Velocity	Mean PAA (krad/s^2)	
3	4.27	
5	8.60	
7	13.92	

Α	В	Low CI (g)	A-B (g)	Upper CI (g)	Р
3	5	-6.2255	-4.32308	-2.42067	0.000
3	7	-11.7316	-9.6455	-7.5594	0.000
5	7	-7.45368	-5.32241	-3.19115	0.000

A.9.1 The percentage change in duration between bare and helmeted head impacts for drop rig recreations of wooden, metallic, brick, and cradled headform conditions. The headform was fitted with a 'Defender Hybrid' PO helmet for all conditions.

